DISCLAIMER NOTICE

THIS DOCUMENT IS THE BEST QUALITY AVAILABLE.

COPY FURNISHED CONTAINED A SIGNIFICANT NUMBER OF PAGES WHICH DO NOT REPRODUCE LEGIBLY.

FUEL CELL
RESEARCH & DEVELOPMENT

HYDROCARBON – AIR FUEL CELLS

Semi-Annual

Technical Summary Report No. 10

1 July – 31 December 1966

ARPA ORDER: Number 247
CONTRACT : Number DA44-009-AMC-479 (T)

U.S. ARMY
ENGINEER RESEARCH AND DEVELOPMENT LABORATORIES
FT. BELVOIR, VIRGINIA

DIRECT ENERGY CONVERSION OPERATION
GENERAL ELECTRIC
930 WESTERN AVE., LYNN, MASS

BLANK PAGE

FOREWORD

This is Technical Summary Report Number 10 of a research program conducted by the General Electric Company under contract with the U. S. Army Engineer Research and Development Laboratories. The purpose of this program is to investigate hydrocarbon-air fuel cells for military applications. This program continues the research effort on the direct oxidation of hydrocarbon fuels first undertaken by General Electric Company in November 1960, under contract DA 44-009-ENG-3771. Investigation has continued under contracts DA 44-009-ENG-4853, DA 44-009-ENG-4909 and DA 44-009-AMC-479 (T). This work is conducted at the Company's Research and Development Center in Schenectady, New York, and at the Direct Energy Conversion Operation's Research and Development Laboratory in Lynn, Massachusetts. Program management is the responsibility of the Direct Energy Conversion Operation.

These technical summary reports are issued on a semi-annual basis. The technical content is reviewed by ERDL prior to publication. The Contracting Officer's Technical Representative is Dr. Maxine Savitz.

This work is made possible by the support of the Advanced Research Projects Agency (Order No. 247) under Project Lorraine through the U. S. Army Engineer Research and Development Laboratories, Fort Belvoir, Virginia.

TABLE OF CONTENTS

TABLE OF CONTENTS (CONT'D)

BLANK PAGE

1.0 GENERAL SUMMARY

1.1 PROGRAM SUMMARY

The work reported herein is a continuation of the tasks discussed in Semi-Annual Technical Summary Report No. 9, covering the reporting period of 1 January - 30 June 1966, with the addition of a system study for a direct oxidation hydrocarbon-air fuel cell system for liquid fuels. Effective 15 August 1966, Tasks III and IV, covering multi-component fuel studies and investigations with alternate acid electrolytes, were discontinued and the remaining technical and engineering effort re-directed toward the selection of an optimum direct hydrocarbon-air fuel cell system for use with liquid hydrocarbon fuel. By agreement with ERDL personnel, the report on this system study, included herein, is submitted in lieu of, and fulfills the requirement for a final report under this contract.

The objective of this program still remains to develop a technology which will facilitate the design and fabrication of practical military fuel cell power sources for operation with ambient air and conventional hydrocarbon fuels. The system study represents a preliminary analytical evaluation of the technological results achieved to date when applied to a complete fuel cell power source.

As redirected by Modification No. 4 to Contract DA44-009-AMC-479(T), the revised task definitions as of 15 August 1966 are as follows:

Task I - Optimum Direct Oxidation Hydrocarbon-Air Fuel Cell System for Liquid Fuels

The experimental information obtained to date on this program will be reviewed and the optimum direct hydrocarbon-air fuel cell system for use with liquid hydrocarbon fuel will be selected. This will include:

a. Choice of electrolyte
b. Choice of cell operating temperature
c. Choice of fuel vaporization or injection procedure
d. Choice of electrolyte containment method
e. Choice of electrical composition

Based on these prime choices of approach and operating conditions an analysis of the total system will be made which will include detailed heat, water, and mass balance calculations. Major components will be described in terms of the functions they perform and approximate sizings, and a preliminary conceptual layout of a 0.5 KW direct hydrocarbon fuel cell system will be prepared.

Task II - Carbon Monoxide and Hydrogen Adsorption on Platinum-Rhodium Alloys

The rate of adsorption and the steady-state coverage of carbon monoxide and hydrogen will be studied as a function of potential at 80°C in 4N sulfuric acid using multipulse potentiodynamic methods for rhodium metal and platinum-rhodium alloys.

Task III - Study of Refractory Compounds as Catalyst Supports

Refractory compounds made up of elements from Groups III and IV of the periodic table compounded with carbon will be studied to determine their suitability as substrates for electrocatalysts in fuel cell electrodes. These materials will be processed into fuel cell electrodes and evaluated in fuel cells in their catalyzed and uncatalyzed form.

Task IV - Alloy Electrocatalysts

Methods will be developed for dispersing selected alloy compositions on suitable supports, including refractory carbides, semi-conducting oxides and carbons. Electrode fabrication procedures will be devised for these composite electrocatalysts and the experimental electrodes obtained will be evaluated in fuel cells.

These last three tasks are essentially a continuation of Tasks I and II as described in the last summary report.

1.2 RESEARCH SUMMARY

1.2.1 Electrocatalyst Research

Studies with unsupported noble metals as catalysts for hydrogen-carbon monoxide anodes have been brought to a conclusion with the completion of work with platinum-rhodium and platinum-iridium. The behavior of these materials appears to parallel that of platinum-ruthenium which was found to be the superior composite catalyst among the group.

As a result of the encouraging performance obtained with platinum-ruthenium, platinum-rhodium and platinum-iridium electrocatalysts with hydrogen-carbon monoxide fuel mixtures, attempts have been made to prepare active electrodes by supporting small amounts of these metal combinations on substrates. Excellent performance has been observed with platinum-ruthenium dispersed on boron carbide and other supports with noble metal loadings of less than 3 mg/cm^2. Somewhat inferior performance was observed with supported platinum-rhodium and platinum-iridium catalysts, but this may be due to incomplete reduction of the metal halides on the substrates.

Selected metal borides and silicides appear to be potentially useful catalyst supports which offer advantages over boron carbide.

Work is also continuing on the use of stabilized tungsten oxides as catalyst supports and promoters. Emphasis during the period has been placed upon improving corrosion resistance and reducing platinum loadings in preparation for future work with hydrocarbon fuels. Fuel cell performance data obtained during the period with hydrogen-carbon monoxide fuels and 2 to 5 mg Pt/cm^2 loadings were similar to previous results obtained with 34 mg Pt/cm^2. Admixture of such an oxide with platinum-ruthenium alloy catalyst resulted in exceptionally good performance with a hydrogen-carbon monoxide fuel at 25°C. Parallel runs with Pt-Rh and Pt-Ir alloys admixed with the oxide did not show this effect.

Improvements have been made in electrodes prepared by spreading a platinum-boron carbide Teflon mix on a foamed nickel base which is leached out after curing to give an electrode with an interconnecting system of macropores. The leakage problem has been markedly improved. Current density at load voltages of interest has been increased by another factor of 1.6 for cathode operation. This was accomplished by incorporating a second leachable additive into the electrode. The second leachable additive preferably has an elongated particle shape so that it forms small pores branching out from the macropore system. Control of both total porosity and the ratio of large to small pore volume is possible with this method of preparation. It appears that the structure contains interface between micro and macropores distributed throughout the volume of the electrode.

A sensitive method for determining platinum in phosphoric acid by ultraviolet adsorption has been devised. It has been used to show that unreduced platinum (from diammine dinitrite decomposition) on boron carbide dissolves slowly in phosphoric acid at elevated temperatures around 150°C. After reduction, the dissolution stops. Some loss of Pt has taken place in past experiments. Steps to minimize this loss and measure it can now be taken.

Teflon-bonded tungsten carbide electrodes have been investigated. They show high activity with hydrogen at 145°C. One electrode sustained 150 ma/cm^2 only 100 millivolts from the reversible hydrogen potential. Propane still showed no activity on this electrode. Some of the evidence suggests that tungsten carbide acts as an electronically conducting support for a surface layer of tungsten oxide.

Hydrogen fuel cell anodes of the noble metals show varying sensitivity to the presence of CO in the gas feed. Studies of the mixed adsorption of CO and hydrogen on microelectrodes of these metals provide insight into the mechanistic details of electrode "poisoning." While the adsorption of CO on Pt has received considerable attention, similar studies on Rh electrodes have been lacking. On the other hand, considerable background information has been provided as a result of various voltammetric studies of the adsorption of oxygen and hydrogen on Rh. The voltammetric approach followed in these studies is similar to that used in previous studies of Pt electrodes.

It was shown that CO adsorption on rhodium may be studied in a quantitative manner (by anodic stripping) if a "multipulse potentiodynamic" sequence is used to establish reproducible initial conditions. Additionally, comparisons have been made between the amount of CO and of hydrogen atoms co-adsorbed under dynamic conditions.

Up to 0.5 v the CO coverage on Rh electrodes is essentially constant over the entire range of CO concentrations and independent of whether or not CO was pre-adsorbed on the electrode at 0.12 v. Above 0.5 v, the results do depend on the concentration of CO and steady-state is somewhat sluggishly established (the mean of the value achieved with and without pre-adsorption at 0.12 v). It seems reasonable to conclude that for this highly irreversible chemisorption, there is the tendency for full monolayer coverage over the entire range of concentrations and potentials, and that only the opposing rate of oxidation of CO to CO_2 tends to drive the coverage down at high potentials.

The adsorption isotherm for hydrogen on Rh retains its original form when CO adsorbs, i.e. that there does not appear to be preferential CO adsorption on sites with the highest heats for hydrogen. This may be interpreted in two different ways. One possibility is that "original" heterogeneity leads to no significant differences in the heats of adsorption of CO on various sites. A surface partially covered with CO simply acts as if the effective area had been decreased and retains the same adsorption isotherm. The alternative is that heats of adsorption do vary over the surface due to

original heterogeneity, but under conditions of mass-transport controlled adsorption there is a completely random distribution of CO molecules over the various sites. Due to immobile adsorption, there is no subsequent re-distribution of adsorbed CO according to the heats of adsorption of the surface sites. Hence, a random distribution of CO molecules is retained as is the form of the original hydrogen adsorption isotherm.

1.2.2 Multi-Component Fuels

Work previously reported in this area has been continued and two main aspects were covered:

1. The question of relative reactivity of various hydrocarbon additives in a multi-component mixture. Here, it was shown that aromatics, olefins, and to a certain extent, naphthenes, but not sulfur compounds that are basic in character, are preferentially adsorbed and oxidized at the conditions prevailing at the anode. An attempt was made to explain this behavior in terms of kinetic theory.

2. The aspect of extended tests for given multi-component mixtures. This investigation revealed that a great variety of types and concentrations of additives to a paraffinic fuel can be tolerated at anode conditions involving high potentials (of the order of 600-700 mv DC vs. H_2/H^+) and no cycling. Methylcyclopentane was shown to be a particularly interesting constituent, in that it can be tolerated at high concentrations (50 mole % or more) with no harmful effect on anode performance, as compared to pure octane. Furthermore, no performance cycling was observed.

1.2.3 Investigations with Alternate Electrolytes

The previous work with carbon-supported electrocatalysts using liquid octane fuel and hydrofluoric acid electrolyte at 105°C has been extended to include higher area graphitic and non-graphitic substrates. The specific performance of the electrocatalysts increases with increasing substrate specific area up to at least 212 and 350 m^2/g for the graphitic and non-graphitic substrates, respectively (the highest areas tested). Based on an average standard cathode performance, an anode performance level of 0.83 watt/g Pt at an I-R free cell voltage of 0.4V, or 0.69 watt/g Pt at 0.4V I-R included for an 1/8 inch electrolyte spacer, was achieved using a 212 m^2/g graphite supported electrocatalyst at a loading of 10.3 mg Pt/cm^2. Further improvements are likely through the use of higher area substrates in an optimized electrode structure.

1.3 ANALYSIS OF DIRECT HYDROCARBON/AIR FUEL CELL SYSTEM FOR LIQUID FUELS

Based on the data assembled under previous contracts, certain choices of components which seemed logical from the standpoint of high performance were chosen. Phosphoric acid seemed to be the best electrolyte in spite of the anodic cycling which has been observed in single cells. Teflon-bonded platinum electrodes supported on tantalum screens were chosen in spite of their limited life and high cost. Normal octane was chosen as the fuel, even though it also is expensive. The result of the system study was, therefore, a view of the upper limit in performance attainable today, even though the system is expensive.

The system analysis of a direct liquid hydrocarbon system showed the optimum components and conditions to be:

Phosphoric acid electrolyte, about 96 w/o at 150°C, with a 1/16 inch electrolyte.

Platinum electrodes of active area 10 by 15 inches.

Normal octane as the fuel and air as the oxidant.

Three times stoichiometric reaction air.

Such a system is capable of delivering 540 watts net at an overall efficiency of 20% based on higher heating value. The system is water conservative at ambients of 85°F or lower. About 60 watts is needed for parasitic power if free convection cooling is used. Not much system weight reduction could be obtained by decreasing the electrolyte gap by half, but the weight could be reduced by 40% by designing for an operating temperature of 180°C. The high concentration of acid needed at 180°C poses a problem of electrolyte solidification upon cooling after shutdown of the unit. Free convection cooled auxiliaries were favored for system simplicity and higher efficiency. A conceptual layout of a 0.5 KW system for the free convection configuration operating at 150°C is presented.

1.4 PERSONNEL

Research and Development Center, Schenectady, N.Y.

Supervision - Dr. H. A. Liebhafsky

Mr. I.F. Danzig

Dr. S. Gilman*

Dr. W.T. Grubb*

Mr. G.J. Haworth

Mr. L.H. King

Dr. D.W. McKee*

Mr. J.R. Morgan

Dr. L.W. Niedrach*

Dr. J. Paynter*

Mr. A.J. Scarpellino

Research and Development Laboratory, Lynn, Mass.

Supervision - Dr. H.J.R. Maget, Dr. E.Y. Weissman

Mr. P.J. Chludzinski*

Mr. J.B. Lennon*

Dr. E. Luksha*

Mr. D.C. Shah

---

* Principal Investigators

1.5 REPORTS AND PUBLICATIONS

1.5.1 Previous Reports

Semi-Annual Technical Summary Report No. 9, Hydrocarbon-Air Fuel Cells, 1 January - 30 June 1966, ARPA Order No. 247, Contract DA-44-009-AMC-479(T)

1.5.2 Publications

a) "Fuel Cells" Chapter in "Direct Energy Conversion," W. T. Grubb and L. W. Niedrach, ed. by G. Sutton, McGraw-Hill Book Co., Inc., New York, N.Y. (1966).

b) "Carbon Dioxide Determination During the Galvanostatic Oxidation of Adsorbed Propane Intermediates," W. T Grubb and M. E. Lazarus, submitted.

c) "Electrocatalysts for Hydrogen/Carbon Monoxide Fuel Cell Anodes. I. The Platinum-Ruthenium System," L. W. Niedrach, D. W. McKee, J. Paynter and I. F. Danzig, Electrochem. Tech., In Press.

d) "Electrocatalysts for Hydrogen/Carbon Monoxide Fuel Cell Anodes. II. The Platinum-Rhodium and Platinum-Iridium Systems," D. W. McKee, L. W. Niedrach, J. Paynter and I. F. Danzig, Electrochem. Tech., In Press.

e) "Interaction of Hydrogen and Carbon Monoxide on Noble Metals," D. W. McKee, J. Catalysis, In Press.

f) "Studies of Hydrocarbon Fuel Cell Anodes by the Multipulse Potentiodynamic Method II. Behavior of Methane on Conducting Porous Teflon Electrodes," L. W. Niedrach, J. Electrochem. Soc., 113, 645 (1966).

g) "Fuel Cells," W. T. Grubb and L. W. Niedrach, Chapter in Advanced Energy Conversion Systems, G. Sutton, ed., McGraw-Hill, New York, 1966.

1.5.3 Talks

a) W. T. Grubb, "Voltammetry and Product Analysis at High-Area Platinum Hydrocarbon Anodes." Presented at the Philadelphia meeting of the Electrochemical Society, October 1966.

b) L. W. Niedrach, D. W. McKee, J. Paynter and I. F. Danzig, "Electrocatalysts for Hydrogen/Carbon Monoxide Fuel Cell Anodes. I. The Platinum-Ruthenium System." Presented at the Philadelphia meeting of the Electrochemical Society, October 1966.

c) E.J. Cairns, A.M. Breitensteln, and A.J. Scarpellino, "Kinetics of Adsorption and Surface Reaction of Propane on Platinum in Hydrofluoric Acid." Presented at the Philadelphia meeting of the Electrochemical Society, October 1966.

d) S. Gilman, "A Multipulse Potentiodynamic Study of the Competitive Adsorption of Ethane and Chloride Ions on Platinum." Presented at the Philadelphia meeting of the Electrochemical Society, October 1966.

e) E.J. Cairns and E.J. McInerney, "Electrocatalysts for the Direct Electrochemical Oxidation of n-Octane in Fuel Cells." Presented at the Philadelphia meeting of the Electrochemical Society, October 1966.

f) H.J.R. Maget, R. Roethlein, and E.Y. Weissman, "The Electrochemical Reduction of Oxygen in Controlled Pore Geometries." Presented at the Philadelphia meeting of the Electrochemical Society, October 1966.

g) E.Y. Weissman, "Structural Studies on Porous Gas Diffusion Electrodes." Presented at the Philadelphia meeting of the Electrochemical Society, October 1966.

BLANK PAGE

2.0 DETAILS OF INVESTIGATIONS

2.1 ELECTROCATALYST RESEARCH

2.1.1 Alloy Electrocatalysts Compatible with H_2-CO Mixtures (D.W. McKee, L.W. Niedrach, I.F. Danzig, and A.J. Scarpellino)

Work with fuel mixtures containing hydrogen-carbon monoxide has been continued. Studies of unsupported noble metals were brought to a conclusion during the period, while work with supported systems was accelerated. Boron carbide, metal borides, and metal silicides were among the supports considered.

In all of the fuel cell work, Teflon-bonded electrodes having the structure described by Niedrach and Alford (2.1-1) were employed. These were mounted in circular cells of conventional design. A hydrogen reference electrode was employed, and all measurements were made with a Kordesch-Marko bridge.

The electrodes were normally evaluated with 5N sulfuric acid as the electrolyte at 25 and 85°C. Electrolytic hydrogen and the synthetic mixtures in Table 2.1-1 were employed as fuels. For continuity with the earlier work, mixture C was used as the general reference fuel. Purified oxygen was used as the oxidant.

Table 2.1-1

Synthetic Fuel Mixtures

	% H_2	% CO	% CO_2	% CH_4
A	69.6	0.2	14.9	15.3
B	71.4	1.0	14.4	14.2
C	77.8	2.0	20	0.25
D	71.3	5.0	12.5	12.2
E	65.3	9.8	12.7	12.2
F	45.6	29.9	12.2	12.3

2.1.1.1 Unsupported Noble Metal Alloy Electrocatalysts

The survey of the Pt-Rh and Pt-Ir systems was completed with investigations of the effect of CO concentration in the fuel gas on the performance and studies of CO utilization. Data showing the effect of CO content are summarized in Figure 2.1-1 and 2.1-2 in the form of anode vs reference

(2.1-1) L.W. Niedrach and H.R. Alford, J. Electrochem. Soc., 112, 117 (1965).

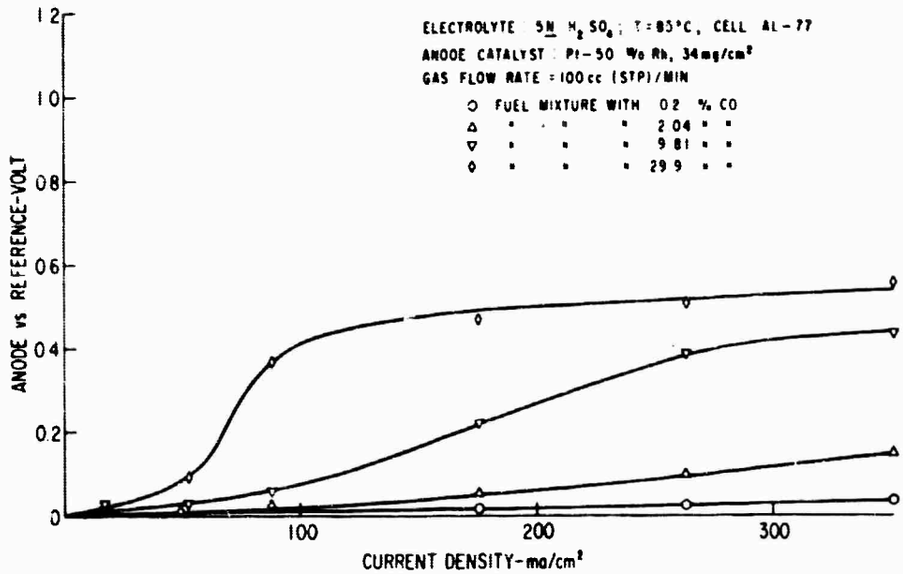

Figure 2.1-1. Effect of CO Content on Performance of Impure H_2 on Pt-Rh Electrodes at 85°C

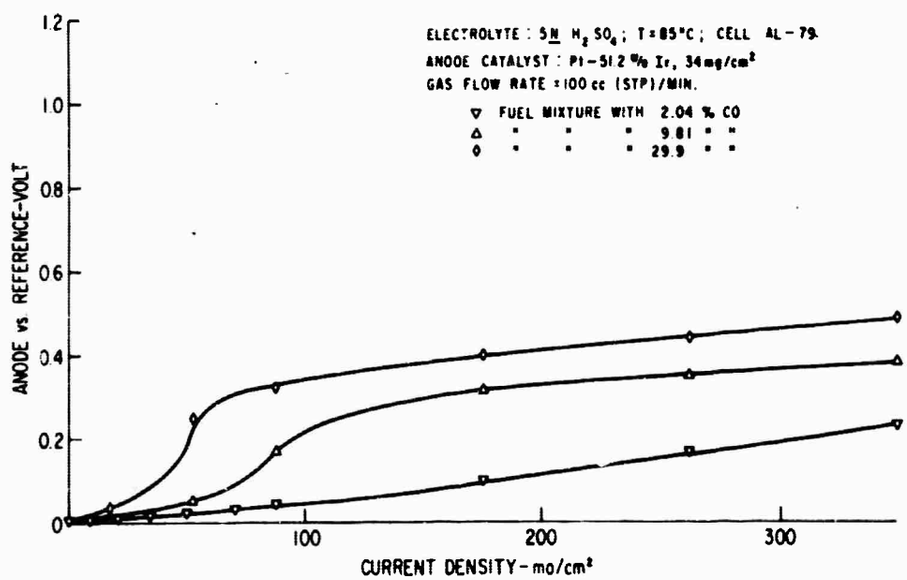

Figure 2.1-2. Effect of CO Content on Performance of Impure H_2 on Pt-Ir Electrodes at 85°C

polarization curves. As in the case of Pt-Ru (2.1-2) the performance declines considerably as the carbon monoxide content is increased.

The fate of the carbon monoxide in the fuel was investigated under various load conditions by analyzing the effluent gases from working fuel cells with a mass spectrometer. The fuel in each case was a H_2-5% CO mixture and the operating temperature was 85°C. Results obtained with typical anodes of platinum-rhodium and platinum-iridium are summarized in Table 2.1-2 and Figure 2.1-3. This figure which shows the apparent percent of the current carried by carbon monoxide oxidation as a function of current density, also includes similar data for platinum and platinum-ruthenium electrodes for comparison purposes. All of these data were obtained with a constant fuel flow rate that corresponded to about twice the stoichiometric rate at 250 ma/cm^2.

In all cases, a small amount of carbon dioxide was formed at open circuit, probably through the water gas shift reaction. Because this is included in the calculation of the current carried by carbon monoxide oxidation, a minimum occurs in all of the plots of Figure 2.1-3.

Related data showing the anode vs reference voltage plotted against the hydrogen and carbon monoxide oxidation currents for the four catalysts appear in Figure 2.1-4. The performance curve shown for pure hydrogen is representative of that for all four electrodes.

From these data it is evident that the behavior of all of the composite catalysts is similar in that little oxidation of carbon monoxide occurs at the low polarizations encountered over a wide range of current densities. The platinum stands out in that extensive carbon monoxide oxidation begins at relatively low current densities and a steep rise in the polarization simultaneously occurs.

As noted previously (2.1-2), the improved performance of the composite catalysts therefore appears to relate to the availability of a larger number of sites for hydrogen oxidation with these materials. Because of this, limiting hydrogen oxidation currents are not encountered in the operating range of interest. A transition from a potential region controlled by hydrogen oxidation kinetics to one dominated by carbon monoxide oxidation kinetics is therefore avoided. That the differences in behavior do not specifically reflect the differences in the overvoltage associated with carbon monoxide oxidation is indicated by the curves for this reaction to the left in Figure 2.1-4. The plots for the three composites fall on both sides of that for platinum, yet all three show similar improvements in performance.

(2.1-2) D.W. McKee, L.W. Niedrach, I.F. Danzig, and H.I. Feliger, Technical Summary Report No. 9, Hydrocarbon Air Fuel Cells, 1 January - 30 June 1966, ARPA Order No. 247, Contract No. DA 44-009-AMC-479 (T), p. 2-4.

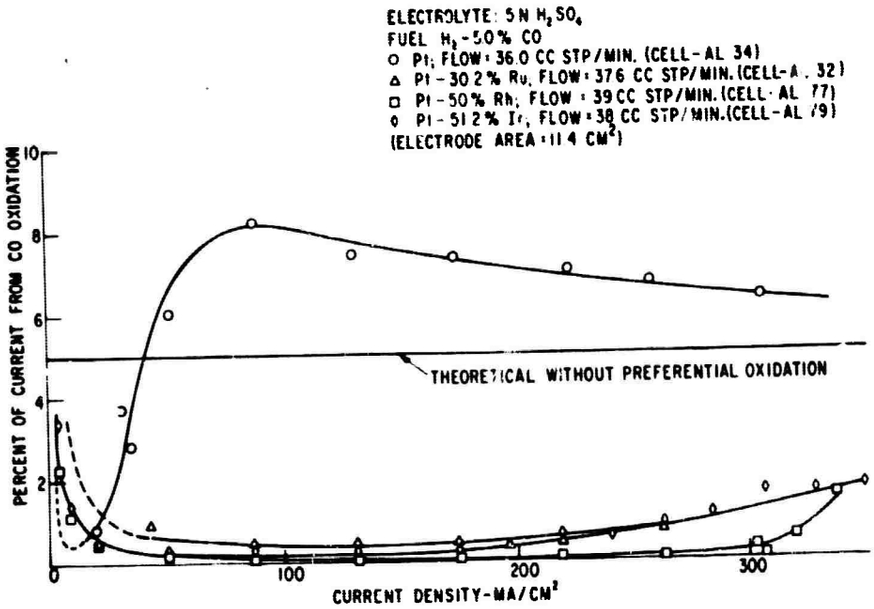

Figure 2.1-3. Effect of Current Density on Percent of Total Current Associated with CO Oxidation

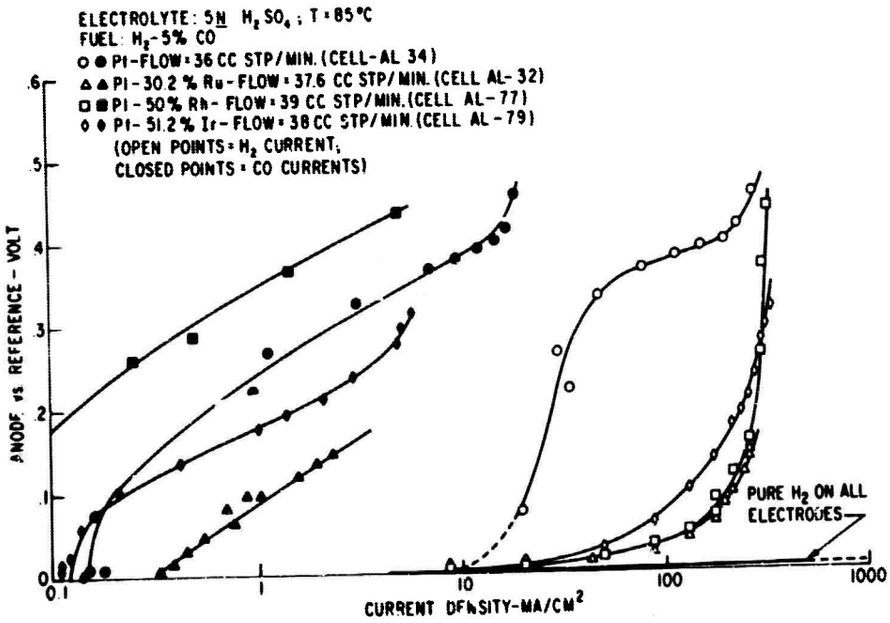

Figure 2.1-4. Relationships Between Anode Potential and Oxidation Currents

Table 2.1-2

Behavior of Carbon Monoxide on Pt-50% Rh and Pt-51.2% Ir Electrodes
Cells AL-77 and 79

Temp. 85°C, 5N H_2SO_4, Fuel H_2-5% CO, Electrode Area 11.4 cm^2.

Sample No.	i, ma/cm^2	Anode vs Ref, volt	CO Oxidized %	CO Oxidized cc(STP)/min.	i_{CO}, %	i_{CO}, ma/cm^2
(Pt - 50% Rh Electrode Fuel Flow Rate = 39 cc(STP)/min.)						
1	0	0.002	0.52	0.010	-	(0.12)
2	0	.002	.48	.0094	-	(0.12)
3	50	.019	.41	.0080	0.20	0.10
4	88	.033	.36	.0070	.10	.088
5	132	.050	.33	.0064	.062	.082
6	176	087	.31	.0060	.043	.076
7	219	.115	.29	.0057	.033	.072
8	263	.155	.30	.0058	.028	.074
9	307	.260	1.00	.0195	.080	.25
10	50	.021	.46	.0090	.23	.12
11	20	.010	.43	.0084	.52	.10
12	8.8	.005	.40	.0078	1.13	.098
13	4.4	.000	.40	.0078	2.24	.098
14	338	.434	20.7	.40	1.50	5.1
15	301	.287	1.63	.032	.13	.39
16	320	.368	6.12	.119	.47	1.50
17	176	.065	.32	.0062	.045	.079
(Pt - 51.2% Ir Electrode Fuel Flow Rate = 38 cc(STP/min.)						
1	0	-0.001	0.56	0.011	-	(0.14)
2	4.4	.000	.62	.012	3.4	0.15
3	8.8	.004	.48	.0091	1.3	.11
4	20	.011	.44	.0084	.53	.11
5	50	.025	.51	.0097	.24	.12
6	88	.060	.58	.011	.16	.14
7	132	.100	.89	.017	.16	.21
8	176	.135	1.73	.033	.24	.42
9	219	.175	4.20	.080	.46	1.01
10	241	.191	5.82	.111	.58	1.40
11	263	.210	9.12	.173	.83	2.18
12	285	.235	12.7	.241	1.06	3.02
13	307	.279	20.8	.39	1.62	5.0
14	329	.295	21.8	.41	1.59	5.2
15	350	.316	24.6	.47	1.67	5.9

With regard to the final sharp rise in potential at 300 ma/cm^2 for all of the catalysts, this appears to be associated with mass transport effects in the boundary layer at the electrode-gas interface. It has been found previously (2.1-2) that at these relatively high current densities, fuel flow rates in excess of two times the stoichiometric rate are required to avoid these effects.

At present, it is not clear whether the additional hydrogen oxidation sites available on the composite catalysts result from differences in surface areas, intrinsic differences in the extent of carbon monoxide adsorption, or differences in morphology and structure, e.g., pore size and distribution. The data for specific surface areas would tend to preclude the former, but either of the two remaining alternatives are attractive. Additional work will be required to resolve this point. In this connection, direct measurements of adlayer composition in the presence of mixtures of CO and H_2 and relative heats of adsorption of these adsorbates on the various noble metals and alloys would be of considerable interest.

2.1.1.2 Supported Alloy Electrocatalysts

A. New Supports for Electrocatalysts

One practical approach to the problem of cost reduction in fuel cells is the use of a support to attenuate the noble metal electrocatalyst. The support stabilizes the active metal phase in a high degree of dispersion and thereby enhances the activity per unit weight of the costly noble metal. In fuel cell applications, catalyst supports must meet certain stringent requirements which do not arise in conventional catalysts. Thus, the substrate material must be of low electrical resistivity, of moderately high surface area and small particle size, and resistant to the corrosive environment of the hot acid electrolyte. So far, very few materials have been found which meet these requirements and only boron carbide and graphite have been found satisfactory for fuel cell use.

Preliminary studies have indicated that certain refractory metal compounds, in particular metallic borides and silicides, are potentially useful support materials for platinum metals and alloys as fuel cell electrocatalysts. Tests are being carried out in fuel cells using hydrogen and hydrogen-carbon monoxide mixed fuels and anodes containing platinum and platinum group metal alloys dispersed on tantalum boride and tungsten, molybdenum and titanium silicides. Some typical physical properties of these materials and of boron carbide are given in Table 2.1-3.

Table 2.1-3

Physical Properties of Electrocatalyst Supports

Compound	Density, g/cm^3	Knoop Hardness, kg/mm^2	Electrical Resistivity, ohm-cm	Cost, $/lb	Surface Area, m^2/g
TaB_2	11.0	2600	68×10^{-6}	56 (high purity)	7.5
$TiSi_2$	4.4	870	123×10^{-6}	10	7.2
WSi_2	9.3	1090	33×10^{-6}	10	4
$MoSi_2$	6.2	1290	21×10^{-6}	10	
B_4C	2.5	2800	variable 0.3	25	11

Although high purity TaB_2 is at present considerably more expensive than commercial boron carbide, the silicides are much cheaper and are obtainable in pure form and of uniform particle size. Boron carbide has the disadvantage that the commercial product varies considerably in composition and frequently contains iron impurity and free graphite which affects its physical properties and performance in the fuel cell. It is also very hard and reduction in particle size to a useful level is a very tedious operation. On the other hand, very satisfactory electrodes have been made from commercial powdered silicides with no further treatment or processing.

The performance of these support materials in H_2-CO fuel cells is discussed below.

As described in the previous section, certain metal combinations, notably Pt-Ru, Pt-Rh and Pt-Ir, have shown markedly greater tolerance for carbon monoxide in mixed H_2-CO fuels than has been observed for platinum alone. The electrodes tested in this work all contained massive quantities of noble metal, generally around 34 mg/cm^2 of electrode surface. For economic and practical reasons it is, therefore, desirable to reduce this platinoid metal content without undue sacrifice of performance. A desirable loading of noble metal would be in the range of 1 to 5 mg/cm^2.

The metal powders previously used have been found to possess high surface areas (exceeding 100 m^2/g in some cases) and a well developed pore structure. It is, therefore, possible that the observed behavior towards H_2-CO fuels arises from mass transport effects in the narrow pores of the catalysts. Such diffusion effects would not be likely to occur with supported catalysts containing only small amounts of the active metal phase and it is not, therefore, obvious that such supported catalysts will show the same tolerance for CO exhibited by the alloy blacks. Encouraging performance has, however, been observed for binary metal catalysts, especially those containing Pt-Ru, supported

on a variety of substrates. These results have given rise to the hope that satisfactory catalysts for synthetic reformer gas can be prepared using very small loadings of platinum group metals.

B. Preparation of Supported Catalysts

Noble metals were generally deposited on the substrate materials by thermal decomposition and reduction of suitable complex salts. For example, platinum and ruthenium were co-deposited by a variety of methods, including: evaporation of mixed solutions of platinum "P" salt $\left(\text{Dinitrito-diammino platinum, } Pt(NH_3)_2(NO_2)_2\right)$ and ruthenium nitrosohydroxide, $RuNO(OH)_3 \cdot H_2O$; platinum "P" salt and ruthenium nitrate; and platinum "P" salt and ruthenium chloride and chloroplatinic acid and ruthenium chloride. A final metal composition of Pt-20%Ru was initially chosen as this was within the optimum composition range observed with the unsupported metal catalysts. The samples were generally reduced at 150°C in flowing hydrogen, ground and screened to 400 mesh before fabrication into electrodes by the "painted screen" technique.

Platinum and rhodium were co-deposited from mixed solutions of platinum "P" salt and ammonium rhodium nitrite, $(NH_4)_2NaRh(NO_2)_6$, evaporated to dryness, then reduced in hydrogen. Platinum-iridium catalysts were prepared from platinum "P" salt and iridium chloride solutions and platinum-palladium catalysts from the mixed "P" salt solutions.

Details regarding preparation of a typical supported Pt/Ru electrode are given in Appendix 4.1.2.

C. Performance of Pt-Ru Supported Catalysts

Typical data for a catalyst preparation containing 2.6 mg noble metal (N.M.)/cm^2 $\left(\text{Pt-20\%Ru}\right) - B_4C$ are shown in Figure 2.1-5. Anode vs reference data for a standard Pt black are also shown for comparison purposes. The test cells used 5N sulfuric acid at 85°C and synthetic gas mixtures containing 2, 5 and 10% CO in H_2. All measurements were made with a Kordesch-Marko bridge in the usual way. It is evident that, in spite of the low noble metal loading, the performance of the supported catalyst is considerably improved over that of the standard platinum electrode and a $Pt-B_4C$ electrode under the same conditions. A comparison of the performance of this electrode with a Pt-29%Ru unsupported alloy electrode is shown in Figure 2.1-6 for a 5% $CO-H_2$ mixture. Figure 2.1-7 shows anode vs reference data for a $\left(\text{Pt-20\%Ru}\right) - B_4C$ electrode containing the very low loading of 1.6 mg N.M./cm^2 which still shows an improvement over the standard Pt electrode over a wide range of current density.

The performance of electrodes incorporating borides and silicides as supporting materials for the Pt/Ru are shown in Figures 2.1-8 thru 2.1-10. Uniformly good performance was found in each case, suggesting that the improved tolerance for carbon monoxide is due neither to some effect of the substrate nor to the pore structure of the catalyst but rather to some intrinsic property of ruthenium.

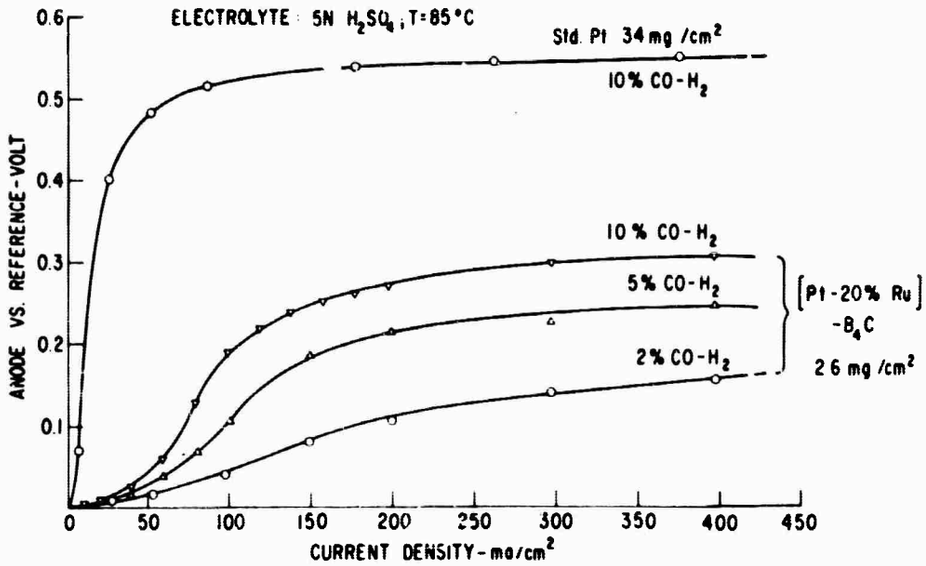

Figure 2.1-5. Performance of 10% (Pt - 20%Ru) - B_4C (2.6 mg N. M. /cm^2) Anode with H_2 - CO Mixtures at 85°C

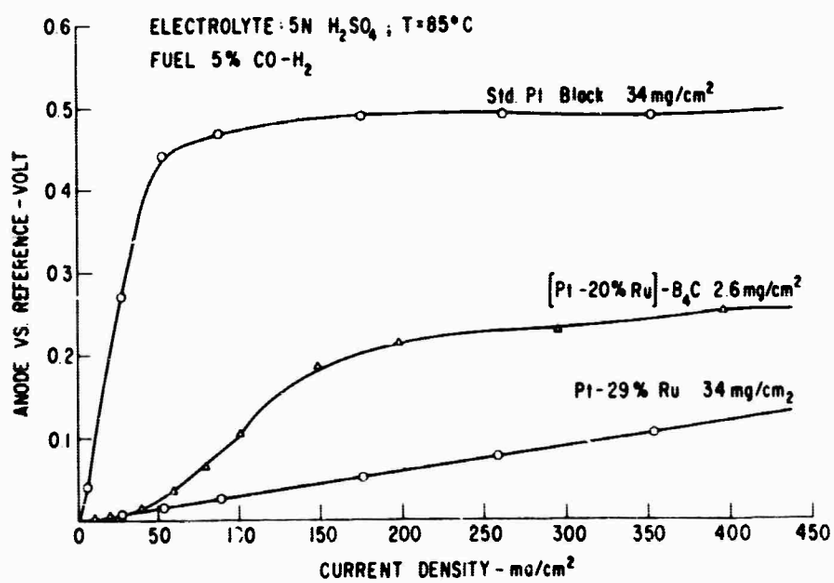

Figure 2.1-6. Comparison of Performance of Pt Black, 10% (Pt - 20%Ru) - B_4C and Pt - 29%Ru Alloy Electrodes with 5%CO - H_2 at 85°C

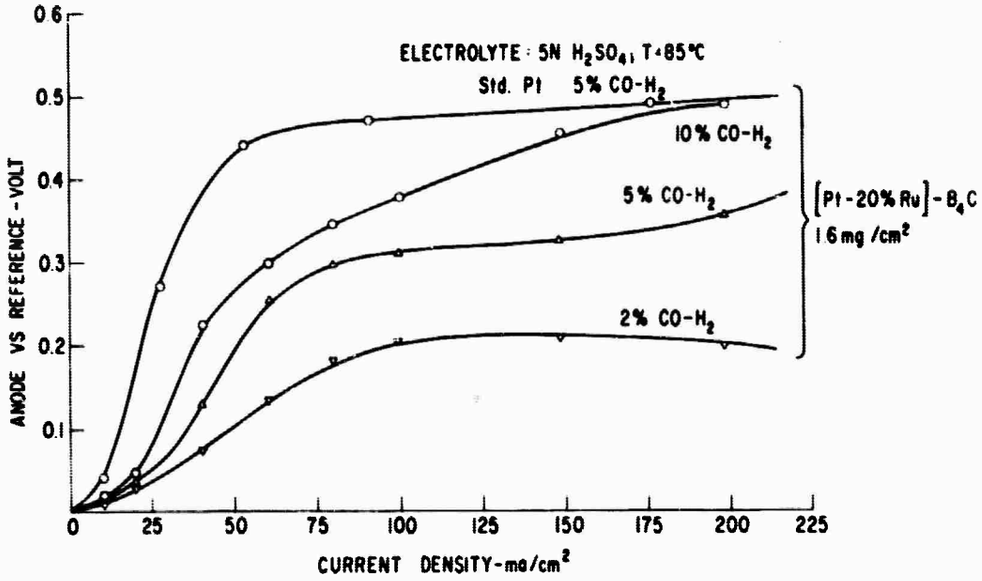

Figure 2.1-7. Performance of 5% (Pt - 20%Ru) - B_4C (1.6 mg N.M./cm^2) Anode with H_2-CO Mixtures at 85°C

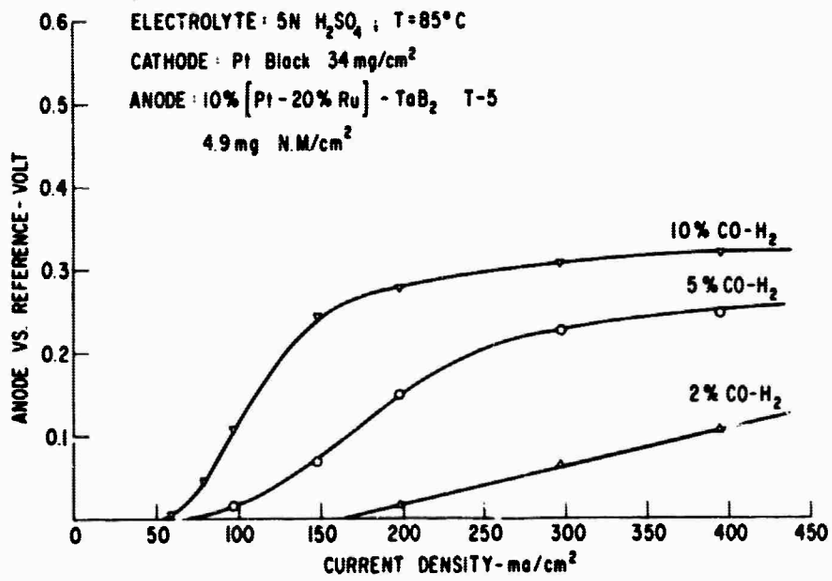

Figure 2.1-8. Performance of 10% (Pt - 20%Ru) - TaB_2 (4.9 mg N.M./cm^2) Anode with H_2-CO Mixtures at 85°C

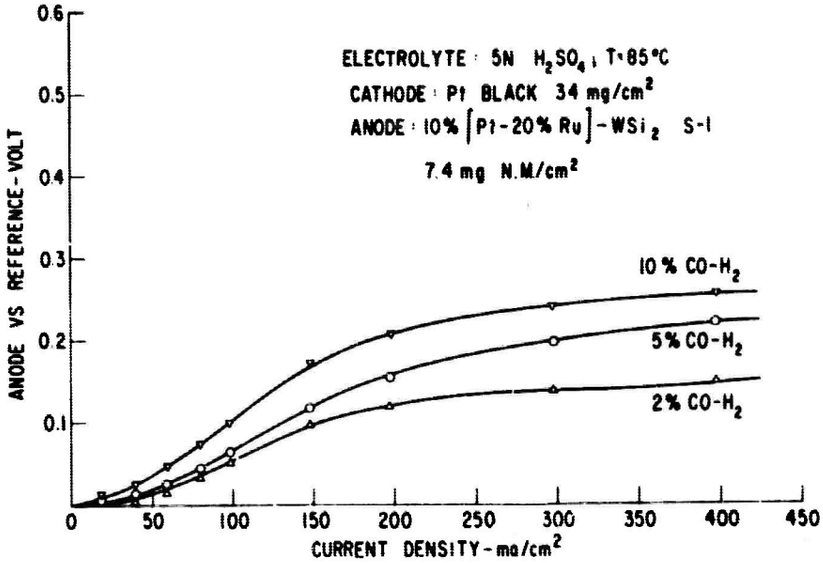

Figure 2.1-9. Performance of 10% (Pt - 20%Ru) - WSi_2 (7.4 mg N.M./cm^2) Anode with H_2-CO Mixtures at 85°C

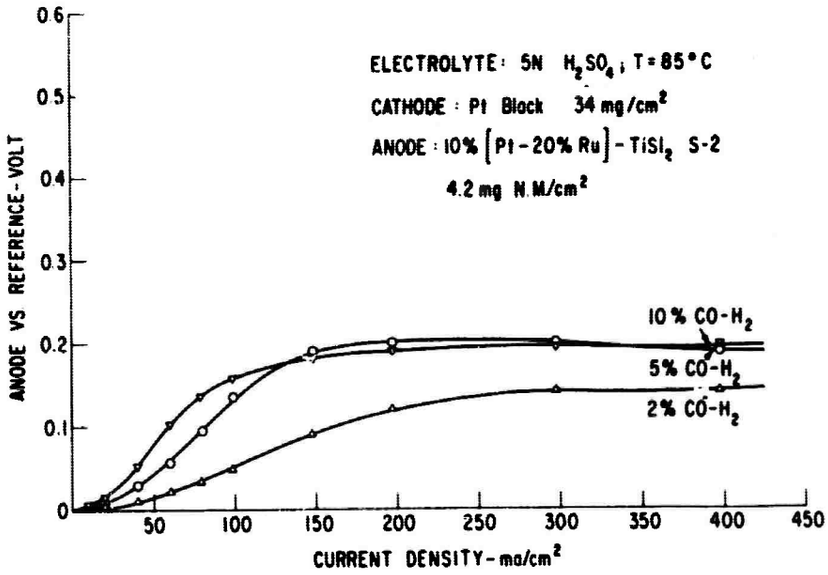

Figure 2.1-10. Performance of 10% (Pt - 20%Ru) - $TiSi_2$ (4.2 mg N.M./cm^2) Anode with H_2-CO Mixtures at 85°C

Generally, the best catalysts were prepared from mixed solutions of Pt "P" salt and $Ru(OH)_3(NO)$ or $Ru(NO_3)_3$, chloride salts giving somewhat inferior performance with the mixed fuels but not with pure hydrogen. It is uncertain whether this reduced activity is due to poisoning of the electrode by halide or as a result of incomplete reduction of ruthenium chloride to the metal. The effect of variation in the Ru/Pt ratio on the support and the influence of initial reduction temperature on the catalyst activity is currently being studied.

D. Behavior of Other Bi-Metallic Supported Catalysts

The high level of performance towards H_2-CO mixed fuels found for unsupported Pt-Rh and Pt-Ir blacks has not generally been maintained in supported catalysts containing these metal combinations. Typical data for a 10% (Pt-50% Rh) - TaB_2 electrode and for a 20% (Pt - 50% Ir) - B_4C electrode are shown in Figures 2.1-11 and 2.1-12. Some improvement over the behavior of pure platinum is indicated, but the electrodes were generally inferior to those containing supported Pt-Ru. This somewhat unexpected result may be due to the difficulty of finding suitable thermally unstable salts of rhodium and iridium which can be used to deposit these metals on the supports. There is evidence that the halides are not completely reduced under the conditions used. Alternatively, the improved tolerance for CO shown by the unsupported Pt-Rh and Pt-Ir blacks may be related to the surface morphology of these catalysts, rather than to some intrinsic property of Rh or Ir. Additional methods of depositing these metals on substrates are at present being investigated.

2.1.1.3 Conclusions

Platinum-rhodium and platinum-iridium catalysts, like platinum-ruthenium, show an exceptional tolerance for carbon monoxide in hydrogen. In the platinum-iridium system, maximum activity is obtained with a Pt-50% Ir catalyst. In the rhodium system, high activity is evident over the range from about 10 to 100% rhodium. The experimental results suggest that the excellent performance of all these catalysts results from the availability of a larger number of sites for preferential hydrogen adsorption and oxidation than in the case of platinum. Promotion of the oxidation of carbon monoxide does not appear to be the determining factor.

The exceptional tolerance for carbon monoxide exhibited by platinum-ruthenium blacks has been found also with supported Pt-Ru catalysts containing very low concentrations of noble metal. On the other hand, the performance of Pt-Rh and Pt-Ir combinations is reduced when these metals are deposited on a substrate. Preliminary results indicate that selected metal borides and silicides are potentially useful materials for catalyst supports.

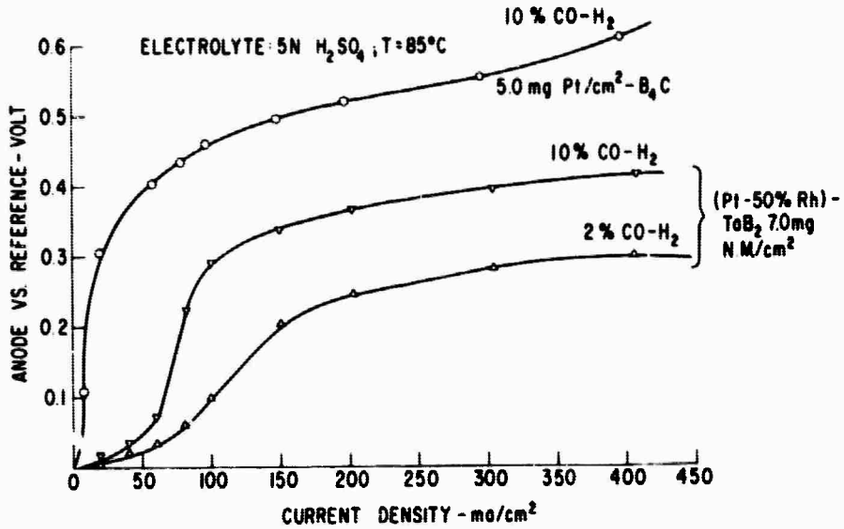

Figure 2.1-11. Performance of 10% (Pt - 50%Rh) - TaB_2 (7.0 mg N.M./cm^2) Anode with H_2-CO Mixtures at 85°C

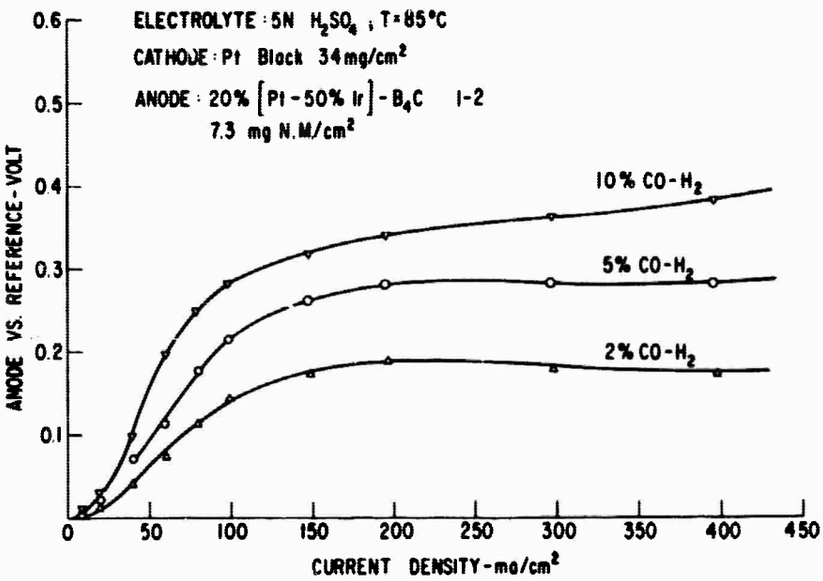

Figure 2.1-12. Performance of 20% (Pt - 50%Ir) - B_4C (7.3 mg N.M./cm^2) Anode with H_2-CO Mixtures at 85°C

2.1.2 Metal Oxide - Noble Metal Catalysts (L. W. Niedrach, J. Haworth)

Work has been continuing on the promotion of platinum catalysts with metal oxides, particularly those based upon the lower oxides of tungsten. In the past, these oxides have shown exceptional activity in promoting the electro-oxidation of carbon monoxide and impure hydrogen on platinum when the noble metal was present in high concentration in simple admixture with the oxide. It is anticipated that these and related oxides will serve as useful supports and promoters for hydrocarbon oxidation reactions. Before this application can be evaluated it is felt desirable to develop suitable materials and procedures for the purpose. This includes improved corrosion resistance, methods of incorporating the noble metal catalyst into the structure, and methods of preparing satisfactory electrodes. For these purposes it has been considered advantageous to perform evaluation work with impure hydrogen as the fuel.

During the present reporting period, effort has been concentrated on reducing platinum loadings from 34 mg/cm^2 to the range of 1 to 5 mg/cm^2 and to examine the corrosion resistance of oxides in the chromia-tungsten oxide system. This system has proven to be the most attractive one to date. During the present period, electrode compositional variables have been examined and attention has been given to the optimum distribution of the platinum catalyst, i.e., direct support on the oxide, support on another substrate such as graphite or boron carbide, or a combination of both. In addition, a very preliminary look has been taken at the behavior of the oxides mixed with composite noble metal catalysts, Pt-Ru, Pt-Rh and Pt-Ir.

2.1.2.1 Procedures

A. Preparation of Materials

In order to obtain highly dispersed oxides as the base materials, a precipitation method was employed for their preparation. The general approach involved precipitation of hydroxides of chromium, titanium or niobium from solutions of their chlorides with ammonium hydroxide. These precipitates were wet-blended with tungstic acid, H_2WO_4, having a surface area of about 12 m^2/gm. After air drying at 150°C, the mixes were reduced at 600-800°C in flowing hydrogen for periods of 4 hours. After cooling in argon the materials were ready for use. In a few cases, alternative treatments were employed in an effort to induce further activity. One of these variations involved the use of nitrate solutions to avoid contamination with chlorides. In another approach the starting materials, air dried chromium hydroxide-tungstic acid mixtures, were heated in air at 600°C prior to reduction at 600°C in hydrogen. Another set of chromium hydroxide-tungstic acid mixtures was cycled through a hydrogen reduction, an air oxidation and a second hydrogen reduction, all at 600°C. It was hoped through these treatments to obtain more uniform products that would show enchanced activity.

A number of platinized oxides were also prepared for use in electrodes or in corrosion tests. One method of platinization involved treating the reduced oxide with a solution of chloroplatinic acid in water. The amount of water was limited to that required for thorough mixing with the solid. After drying at ambient temperature in a vacuum desiccator, the catalyst was treated for two hours with hydrogen at 150°C. Alternatively, samples were treated with "P" salt ($Pt(NH_3)_2(NO_2)_2$), dried in air at 105°C for one hour, and oven dried for an additional hour at 150°C in air. This procedure was adapted from that previously described (2.1-3) for the platinization of boron carbide.

A number of samples were platinized by treating the unreduced chromium hydroxide-tungstic acid with a platinum salt solution, air drying at 105-150°C, and subsequently reducing at 600°C in hydrogen for 4 hours. Several platinum salts were used in these preparations, H_2PtCl_6, $Pt(NH_3)_4Cl_2$ and $Pt(NH_3)_2(NO_2)_2$.

Properties of the oxides used during this period are summarized in Table 4.1-1 of Appendix 4.1. Included are preparational variables, X-ray diffraction data, resistivities and surface areas as determined with a Perkin-Elmer-Shell Sorptometer using nitrogen as the adsorbate.

Platinized boron carbide samples were prepared by the method of Grubb (2.1-3) using "P" salt. Platinized graphite used in some of the work was commercially available material (American Cyanamid - Improved 25% Pt on Graphite, Lot No. S-7547-49).

B. Preparation of Electrodes

Early work with supported catalysts indicated that the conventional composition and preparation procedures for Teflon-bonded electrodes would have to be modified. In a number of cases delamination of the electrode was encountered. Comparisons of performance for variable pressure conditions, as well as variable Teflon content, indicated that considerable effort would be required to optimize any one catalyst system and that this would not necessarily optimize another. On the other hand, early work with the "painted screen" method indicated good performance but at some possible sacrifice in structural strength.

The "painted screen" method differs from the "pasted screen" method of Grubb in a number of respects. A "catalyst paint" is prepared in a polyethylene dish with the catalyst powder in the Teflon T-30 and water mixture. This is then painted onto the clean 40 mesh platinum screen with a

(2.1-3) W. T. Grubb and J. G. Lucas, Technical Summary Report No. 6, Hydrocarbon - Air Fuel Cells, July 1, 1964 - December 31, 1964, ARPA Order No. 247, Contract Nos. DA44-009-ENO-4909 and DA44-009-AMC-479(T), p. 4-143.

camel's hair brush in layers until all of the catalyst paint is used. Each coat is cured over a hotplate at 225°C and then the electrode is allowed to cool before the next coat is applied. A half-hour cure on the hotplate is followed by spraying of the Teflon film in a manner previously described. The electrode is finally cured between the platens of the 350°C hot press but with no pressure or contact to the Teflon side of the electrode.

In order to obtain a good smooth paint and have a good electrode structure, finely ground powders must be used. The electrode structure has been found adequate for the current studies of catalyst behavior. They normally are used in a cell for approximately a day with polarization data being taken for various fuel mixtures. When more of the catalyst variables have been optimized it will be necessary to optimize the electrode structure. This will be approached by varying temperature and pressure as well as the binder concentration.

C. Fuel Cell Tests

The electrodes were mounted in cells of conventional design with a hydrogen electrode serving as a reference. Tests were run at 85°C with a 5N sulfuric acid electrolyte. Electrolytic hydrogen and synthetic mixtures C, D and E of Table 2.1-1 were employed as fuels. The latter contained 2, 5 and 10% CO and varying amounts of CO_2 and CH_4 in hydrogen. Mixture C was used in most of the work. Purified oxygen was used as the oxidant at the counter electrode.

D. Resistivity Measurements

Resistivity measurements were made on the powdered samples with a 1 Kc General Radio bridge using a procedure previously described (2.1-4). The powders were compressed in a 1/4 inch diameter die of heavy wall glass tubing. Brass plungers were employed and a standard torque of 5 in.-lb was applied to the screw drive for compression. It is estimated that the compression force was about 10,000 psi. The thickness of the pressed pellets was between 0.03 and 0.10 cm. While the resistivities have little significance in an absolute sense, they do permit comparisons among samples and they were found useful in following gross resistance changes that occur during corrosion tests.

E. Corrosion Tests

Apart from preliminary runs with 85% phosphoric acid at 150°C in preparation for future work with hydrocarbons, all corrosion tests were run with 5N sulfuric acid at 85°C. The tests were conducted under reflux in air and in an atmosphere of nitrogen containing 0.5% hydrogen. It had

(2.1-4) W.T. Grubb, Ref. 2.1-3, p. 5 - 4 ff.

previously been found that this nitrogen-hydrogen mixture poised the system at a potential of about 0.075 V positive with respect to pure hydrogen in the same system (2.1-5). This potential is in the normal range of anodic polarization in a desirable fuel cell.

In most cases the oxide samples were platinized at the 9% level prior to test. This was accomplished using chloroplatinic acid as previously described. For comparison purposes, a few samples were exposed in the absence of platinum. The exposure time was 9 days (about 216 hours).

Upon completion of the tests the samples were recovered by filteration. After washing they were dried overnight in a vacuum dessicator and their resistivities were measured. Portions were also submitted for X-ray diffraction analysis. The filtrates were analyzed for tungsten and the added metal.

2.1.2.2 Chromia Stabilized Oxides with Low Platinum Loadings

A. Effect of Type of Support, Teflon-loading and Composition

It was felt that the most attractive approach to lower platinum loadings would be through the use of supports. Three directions were considered: 1) direct support on the oxide; 2) support on B_4C; and 3) support on graphite. In the latter two cases, oxides were physically admixed with the platinized supports during electrode fabrication, just as had been previously done with platinum black catalysts.

An initial comparison of the performance of platinized boron carbide and graphite in the presence and absence of 0.1 Cr_2O_3. WO_x is shown in Figure 2.1-13. Detailed data concerning electrode composition are given in Tables 4.1-2A thru 4.1-2C of Appendix 4.1. While it is clear that the addition of the oxide results in beneficial effects in both cases, it was not certain that optimum electrode compositions were employed, particularly with regard to the Teflon content.

In a subsequent series of experiments, the Teflon content was varied with both types of electrodes. Performance data showing the effect of Teflon content are summarized in Figures 2.1-14 and 2.1-15. It is clear that the range of Teflon contents permissible with the two supports are quite different, and that the most satisfactory performances were obtained with the boron carbide support. In the latter case, a fairly wide range of Teflon contents may be used without great variations in performances. Amounts less than 10% seem to result in some additional improvement in performance

(2.1-5) L.W. Niedrach, Technical Summary Report No. 9 Hydrocarbon-Air Fuel Cells, January 1 - June 30, 1966, ARPA Order No. 247, Contract No. DA44-009-AMC-479(T) p. 2-29.

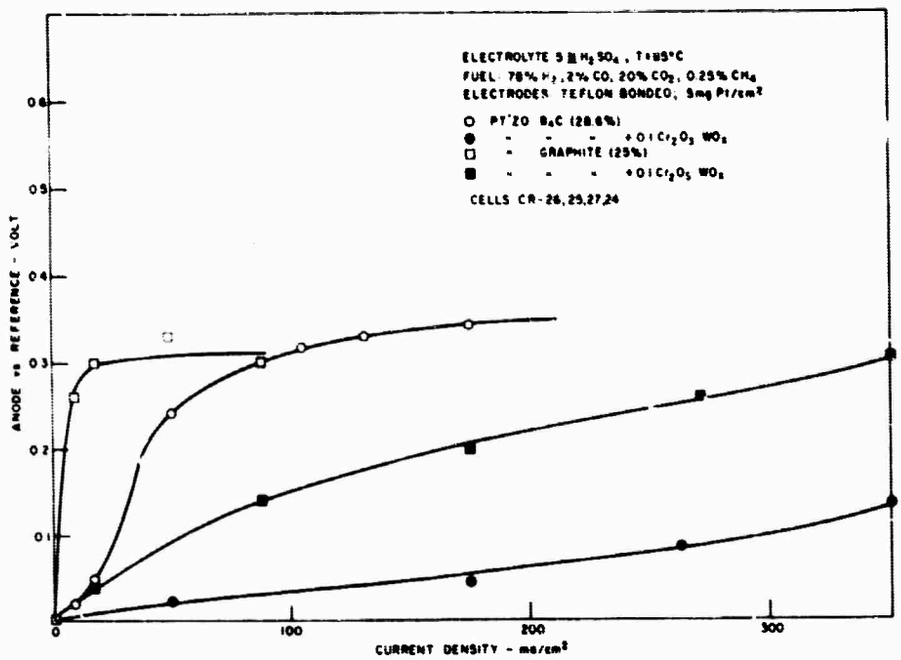

Figure 2.1-13. Effect of 0.1 $Cr_2O_3 \cdot WO_x$ On Performance of Platinized Graphite and B_4C Electrodes

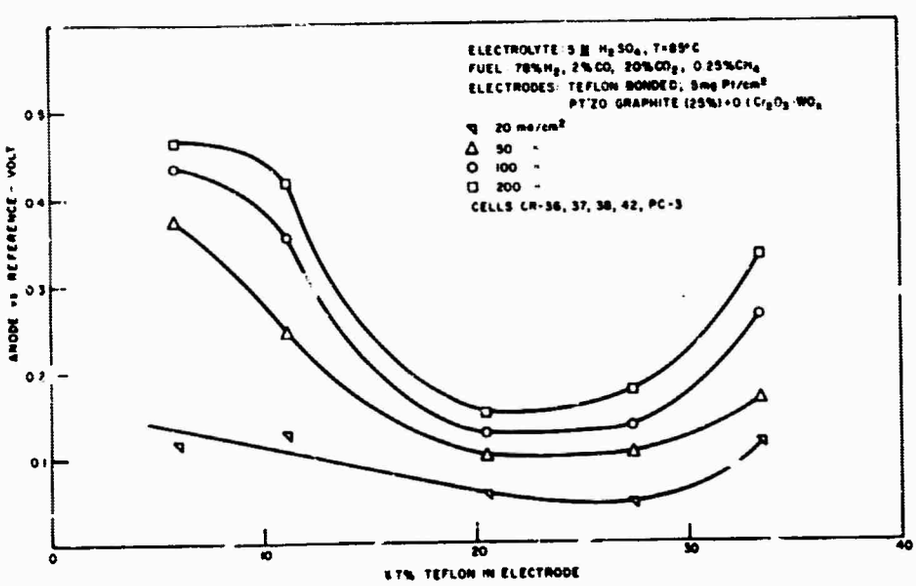

Figure 2.1-14. Effect of Teflon Content on Performance of Platinized Graphite - 0.1 $Cr_2O_3 \cdot WO_x$ Electrodes

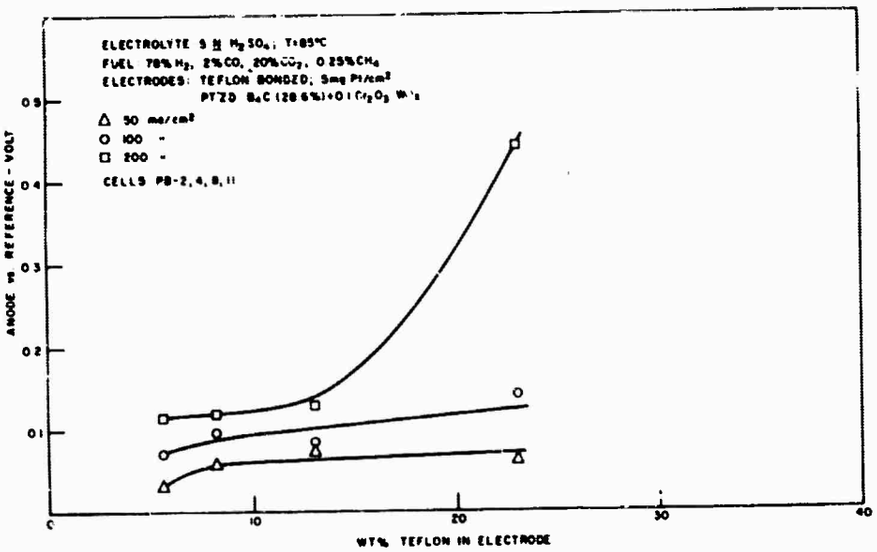

Figure 2.1-15. Effect of Teflon Content on Performance of Platinized B_4C - 0.8 $Cr_2O_3 \cdot WO_x$ Electrodes

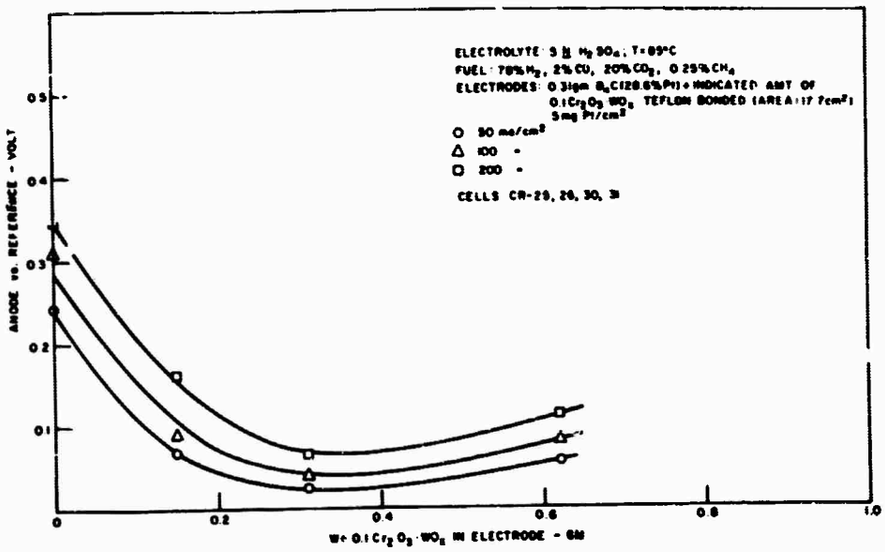

Figure 2.1-16. Effect of Oxide Content on Performance of Platinized B_4C - 0.1 $Cr_2O_3 \cdot WO_x$ Electrodes

but this range has not been investigated further to date, partly because it is suspected that the structures may be lacking in strength.

An additional variable that was examined with the boron carbide support was the effect of the amount of added oxide. The data summarized in Figure 2.1-16 indicate that a 1:1 ratio of the carbide to the oxide is in a satisfactory range in that moderate deviations in either direction cause little change in electrode performance.

Additional exploratory work also indicated that platinization of the oxides themselves is feasible. As illustrated by the data in Figures 2.1-17 and 2.1-18, these materials perform satisfactorily in admixture with unplatinized B_4C or when used alone. It is felt that with some of the oxides having higher electrical resistivities, performance may benefit from adding a conductor such as boron carbide to the electrode structure. This point has not been fully resolved.

On the basis of this work, boron carbide was adapted as a standard material for use as a support or as a conducting diluent in preparing electrodes for the work that follows. A ratio of 0.310 gm oxide to 0.310 gm boron carbide was also used and Teflon contents in the range of 8 to 13% (0.06 to 0.10 cc of T-30 suspension) were used. Since it is possible that optimum electrode composition may change from oxide to oxide, further investigation of these variables will be in order at a later date when other system variables have been settled.

B. Effect of Cr:W Ratio in the Oxide

While the previous work with the chromia-stabilized oxides and high platinum loadings indicated some decline in activity with increasing chromium content (2.1-5), the superior corrosion resistance of the high-chromia oxides justified additional work with these materials. The performance of a series of catalysts covering the range from 0.1 to 1.0 Cr_2O_3 per WO_x has been re-examined in admixture with platinized boron carbide (5 mg Pt/cm^2 of electrode area). Data are summarized in Figure 2.1-19. A small increase in anode polarization again appears to be evident as the chromia content is increased. The penalty associated with chromia additions is not considered severe, however, in the light of the corrosion data given in Section 2.1.2.5.

In part, the effect of increasing the chromia content may result from the associated increases in electrical resistivity of the oxide. It is anticipated that this may be circumvented by suitable "doping" of the material.

On the basis of these results, most of the subsequent work was performed with oxides containing 0.8 to 1.0 Cr_2O_3 per WO_x.

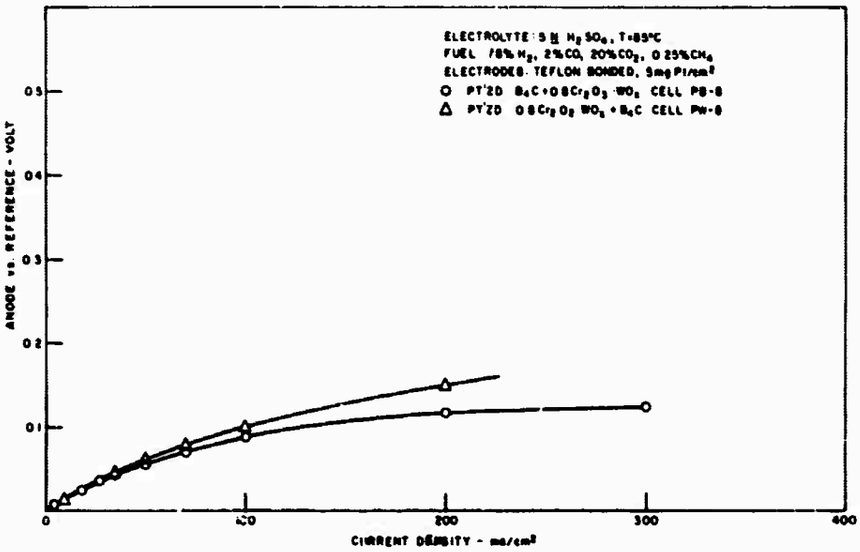

Figure 2.1-17. Comparison of B_4C - 0.8 $Cr_2O_3 \cdot WO_x$ Electrodes with Different Platinum Distributions

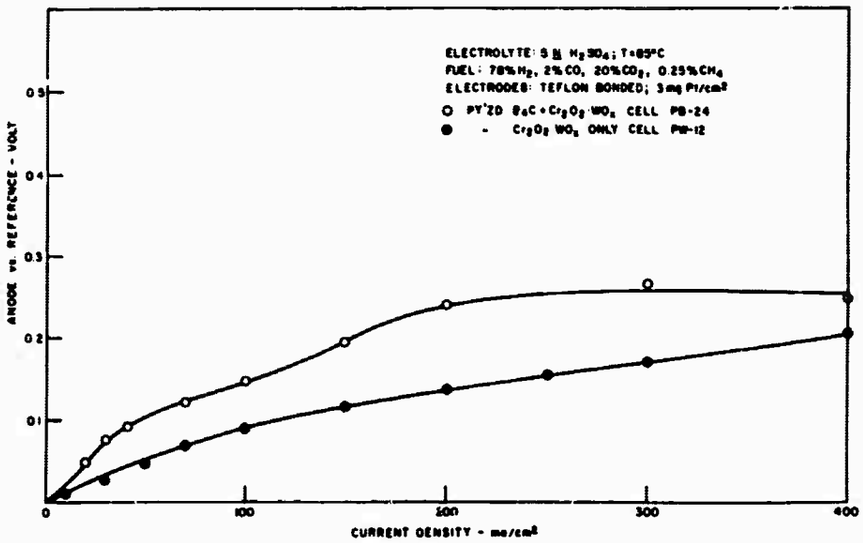

Figure 2.1-18. Comparison of Platinized $Cr_2O_3 \cdot WO_x$ Electrode with Platinized B_4C - $Cr_2O_3 \cdot WO_x$ Electrode

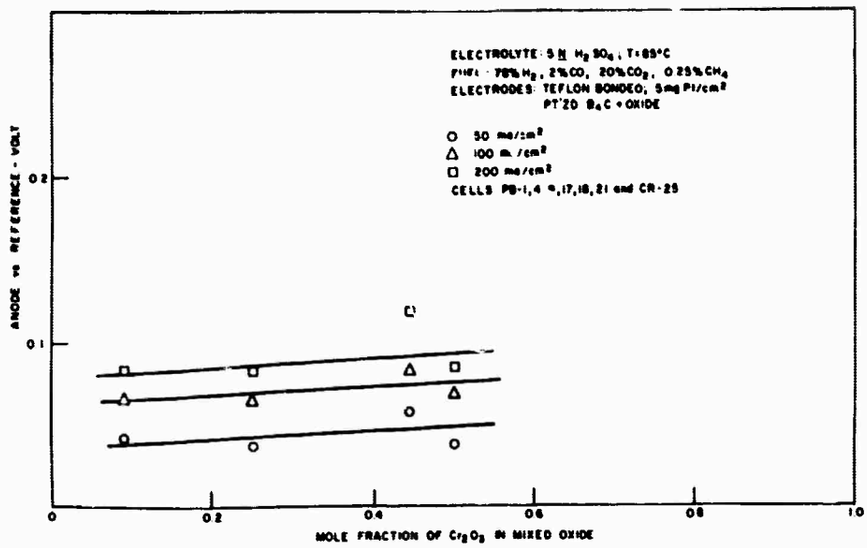

Figure 2.1-19. Effect of Chromium Content on Performance of Platinized B_4C - Mixed Oxide Electrodes

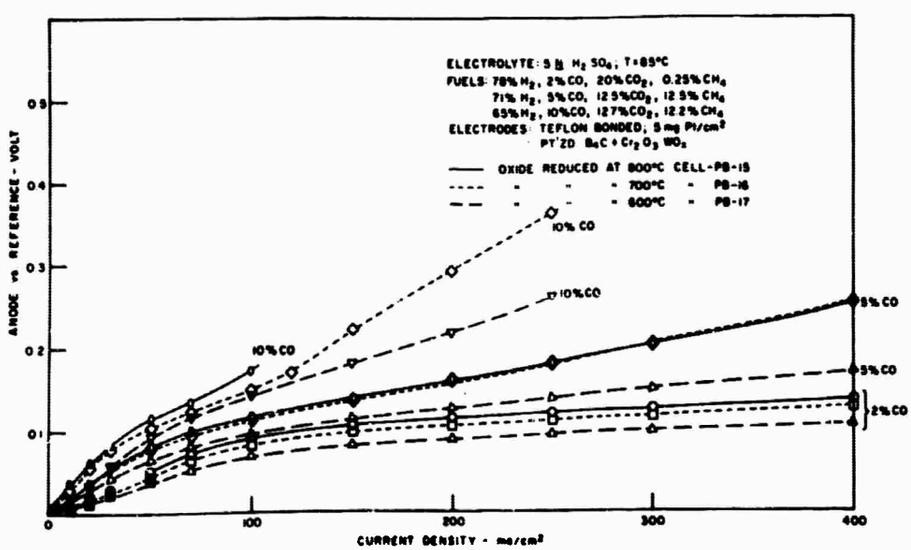

Figure 2.1-20. Effect of Reduction Temperature On Performance of $Cr_2O_3 \cdot WO_x$ in Electrodes with Platinized B_4C

C. Effect of Conditions of Preparation of Oxides

Two variables were examined, the reduction temperature and the effect of pre-treatments prior to a final reduction step at 600°C. For the former, reduction temperatures of 600°C, 700°C and 800°C were used. It was hoped that the higher temperatures would result in improved conductivity and, therefore, improved performance. The results with 0.8 Cr_2O_3, WO_x and 1.0 Cr_2O_3, WO_x in Figures 2.1-20 and 2.1-21 indicate only minor effects from changing the reduction temperature. The meaning is somewhat obscured, however, because of the compositional changes that occurred in the catalysts with temperature (see Table 4.1-1 of Appendix 4.1). Because of this, the effect of reduction temperature will be investigated further by performing the reductions in controlled atmospheres. In this way the final product will be determined by equilibrium rather than kinetic factors.

With regard to pretreatments, two were considered. In the first, the starting mixture, air dried precipitated chromium hydroxide mixed with tungstic acid, was heated in air at 600°C prior to reduction at 600°C in hydrogen. In the second, the starting mixture was reduced in hydrogen at 600°C, re-oxidized in air at 600°C, and then reduced in hydrogen at 600°C. While slight differences in appearance, X-ray diffraction pattern, and surface area resulted from these treatments, no significant improvements in performance resulted from these more involved preparation procedures. The materials were tested only with gross loadings of platinum black (34 mg/cm^2 of electrode area) and the data are summarized in Table 4.1-2C of Appendix 4.1.

D. Effect of Platinum Loading

A few attempts were made to reduce the platinum loadings below 5 mg/cm^2 of electrode area. In most of these experiments the platinum was supported on boron carbide with the amount adjusted to give the desired electrode loading while retaining the amount of platinized carbide constant at 0.31 gm. Performance data obtained with fuels containing 2 and 5% carbon monoxide are summarized in Figures 2.1-22 and 2.1-23. An additional performance curve obtained with an electrode containing platinized Cr_2O_3, WO_x at the 3 mg Pt/cm^2 level but in the absence of boron carbide was presented in Figure 2.1-18.

While the results showed the anticipated trend towards poorer performance with lower platinum loadings, it is felt that loadings below 5 mg Pt/cm^2 are within grasp as other variables are optimized.

E. Alternative Routes to Platinized Oxides

As an alternative to platinization of the reduced oxides, some attention was given to introducing the platinum before the reduction step. Three different salts were employed, H_2PtCl_6,

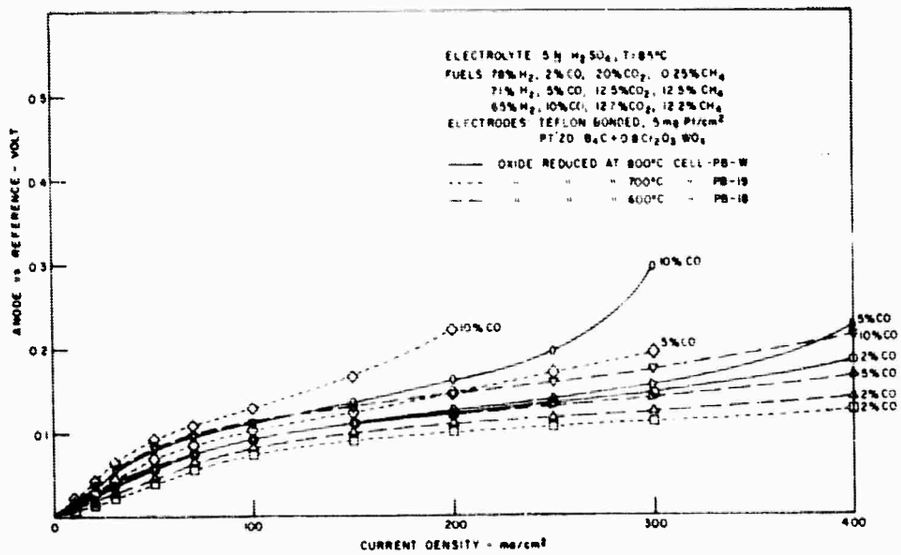

Figure 2.1-21. Effect of Reduction Temperature on Performance of $0.8\ Cr_2O_3 \cdot WO_x$ in Electrodes with Platinized B_4C

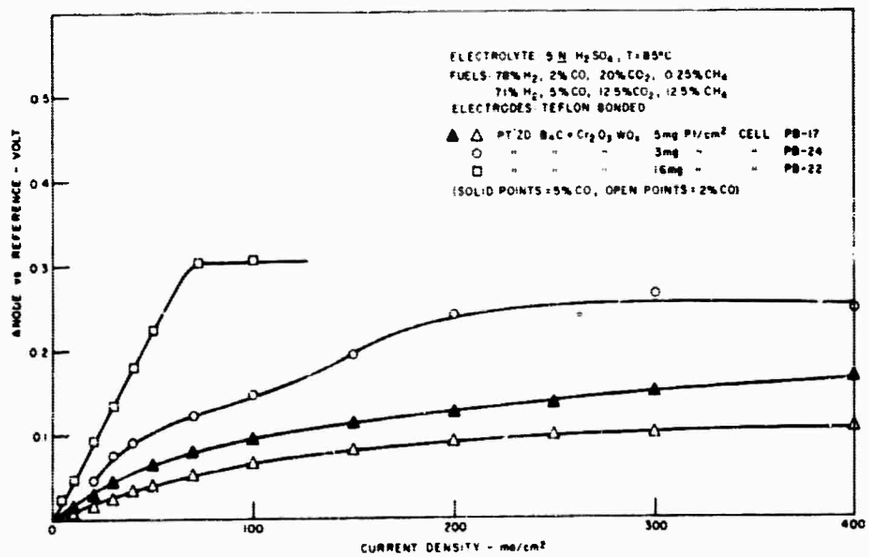

Figure 2.1-22. Effect of Platinum Loading On Performance of Platinized $B_4C - Cr_2O_3 \cdot WO_x$ Electrodes

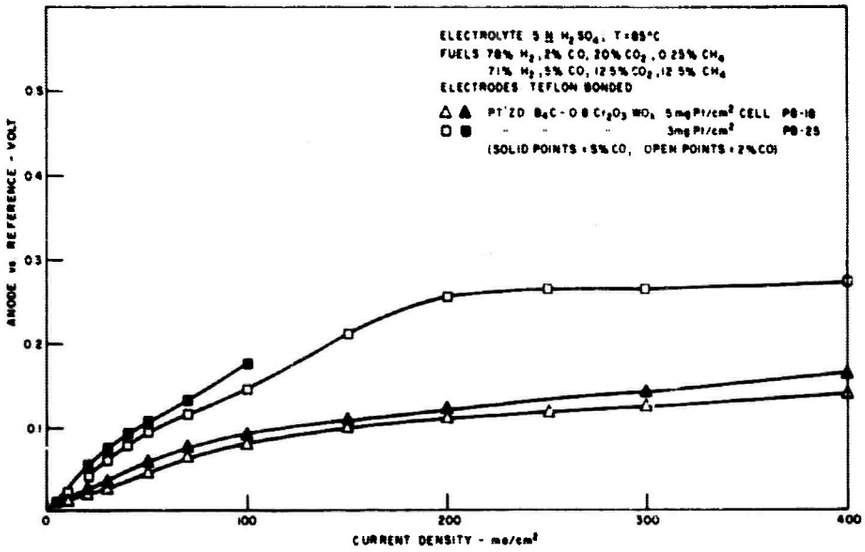

Figure 2.1-23. Effect of Platinum Loading On Performance of Platinized $B_4C \cdot 0.8\ Cr_2O_3 \cdot WO_x$ Electrodes

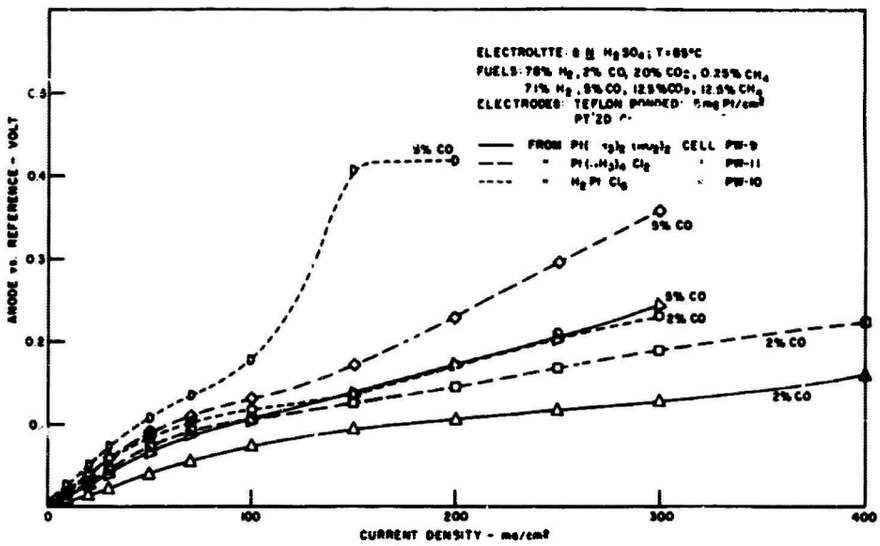

Figure 2.1-24. Effect of Platinization Procedure On Performance of Platinized $Cr_2O_3 \cdot WO_x$ - B_4C Electrodes

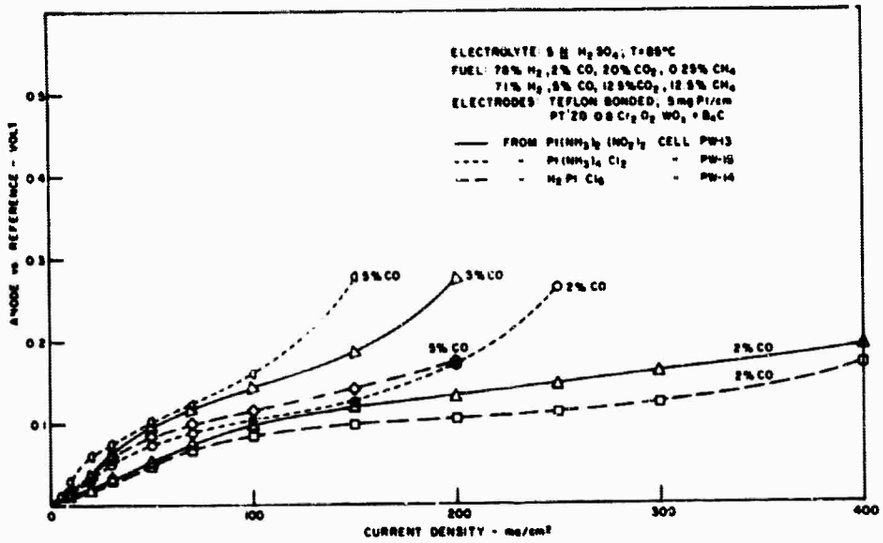

Figure 2.1-25. Effect of Platinization Procedure On Performance of Platinized 0.8 $Cr_2O_3 \cdot WO_x$ - B_4C Electrodes

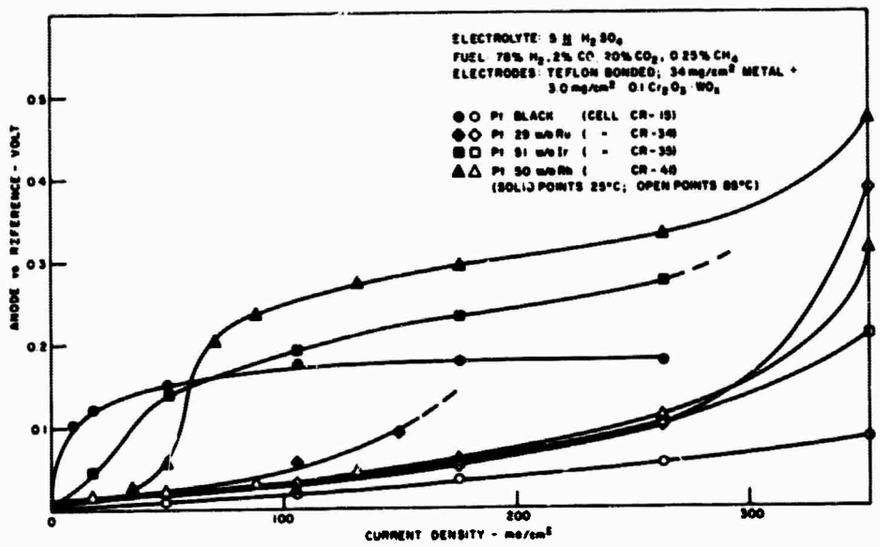

Figure 2.1-26. Performance of Noble Metal Alloys with 0.1 $Cr_2O_3 \cdot WO_x$

$Pt(NH_3)_4Cl_2$, and $Pt(NH_3)_2(NO_2)_2$. The preparation procedure is previously described. The product materials were then admixed with platinized boron carbide and Teflon in the usual fashion to prepare electrodes. Performance data obtained with these materials are summarized in Figures 2.1-24 and 2.1-25. Considerable scatter is evident and no definite trends are evident. In no case, however, did the performance exceed that previously obtained with earlier electrodes.

2.1.2.3 Chromia Stabilized Oxides with Noble Metal Alloy Catalysts

In view of the improved performance of impure hydrogen with noble metal alloys as well as tungsten oxides, it was felt desirable to determine whether additional advantages would accrue from combining the two types of catalysts. Preliminary experiments have been performed with such combinations, and results are summarized in Figure 2.1-26. In this figure anodic polarization curves are shown for electrodes containing the following catalyst loadings:

No. 902 34 mg/cm^2 Pt black + 3.0 mg/cm^2 0.1 $Cr_2O_3 \cdot WO_x$

No. 937 34 mg/cm^2 Pt-29 w/o Ru alloy + 3.0 mg/cm^2 0.1 $Cr_2O_3 \cdot WO_x$

No. 938 34 mg/cm^2 Pt-51 w/o Ir alloy + 3.0 mg/cm^2 0.1 $Cr_2O_3 \cdot WO_x$

No. 950 34 mg/cm^2 Pt-50 w/o Rh alloy + 3.0 mg/cm^2 0.1 $Cr_2O_3 \cdot WO_x$

In all cases, 3.0 mg/cm^2 Teflon was used as a binder and 1.6 mg/cm^2 Teflon was used in the hydrophobic film. The electrolyte was 5N H_2SO_4. The fuel mixture consisted of 78% H_2, 2.0% CO, 20% CO_2, and 0.25% CH_4. Operation was at 25 and 85°C.

At the relatively high catalyst loadings employed, little advantage was seen for the alloys over straight platinum at 85°C. At room temperature the system based upon the platinum-ruthenium alloy combined with the tungsten oxide performed unusually well.

Additional work is planned in this area, although emphasis will be placed on studies of oxides combined with supported alloys.

2.1.2.4 Other Stabilizing Agents

In the previous report some work was discussed in which other oxides than chromia were employed in an effort to stabilize the tungsten oxide. This work was continued with titanium oxide and niobium oxide.

In the case of titanium oxide, the previous work was extended to $3TiO_2 \cdot WO_x$ and pure TiO_2. (Previously, $0.1TiO_2 \cdot WO_x$, $0.3\ TiO_2 \cdot WO_x$ and $TiO_2 \cdot WO_x$ had been examined.) In addition to pure TiO_2, two other oxides were prepared in which the conductors B_4C and graphite were mixed with the titanium hydroxide precipitate before the material was fired in hydrogen at 650°C. The three samples

were prepared without tungsten because it had previously been felt that the earlier data may have indicated some activity from hydrogen-fired titania itself. All of the results obtained with titanium-containing oxides are summarized in Figure 2.1-27 and in Table 4.1-2 of Appendix 4.1. While the performance of $TiO_2 \cdot WO_x$ is slightly better than that of the chromia stabilized oxides, this material has not been found as resistant to corrosion. None of the tungsten-free oxides showed promise. Further work with titania-containing systems is not planned.

Performance data for the niobium oxide system are summarized in Figure 2.1-28. These materials all show moderate performance, however, preliminary corrosion data are not encouraging. A decision with regard to further work with this system will await the results of corrosion tests which have not yet been completed.

2.1.2.5 Corrosion Studies

Results showing the resistance of chromia stabilized oxides towards corrosion by 5N H_2SO_4 at 85°C are summarized in Table 4.1-3 of Appendix 4.1 and Figures 2.1-29 and 2.1-30. Interpretation is complicated by several factors: 1) much of the attack results in the formation of insoluble WO_3 and its hydrates; 2) the resistivity of the starting materials, both platinized and unplatinized, changes as the chromium content is varied; 3) the resistivity measurements on the pressed powders are not highly precise; and 4) surface areas have not yet been determined for all of the powders. Nevertheless, a definite indication of increasing corrosion resistance with increasing chromium content is evident. This trend is supported most strongly by the resistivity data for the samples corroded in air, the X-ray diffraction results for the corroded samples, and the analytical data for chromium in the filtrates.

The results of the chromium analyses in Figure 2.1-29 indicate that the potential of the system is quite important and that attack is markedly greater at high potentials (under air), particularly at low chromium contents. In Figure 2.1-29 the data are plotted in two ways: 1) in terms of total chromium lost to the filtrate from a 500 mg sample; and 2) in terms of the percent of the oxide attacked. The latter data were derived on the assumption that attack of the tungsten and chromium in the samples was directly proportional to the amounts of the two metals in the oxides. The fact that the attack in the air and nitrogen (hydrogen) atmospheres is essentially identical for the 1:1 oxide ($Cr_2O_3 \cdot WO_x$) is particularly significant since it indicates that overpolarization of an electrode containing this oxide should not lead to degradation. Similarly, such an electrode could be exposed to air without concern.

It is clear from the data of Figure 2.1-30 that serious changes in the properties of the WO_2 and low chromium oxide catalysts result even from the relatively small attack that occurs at low

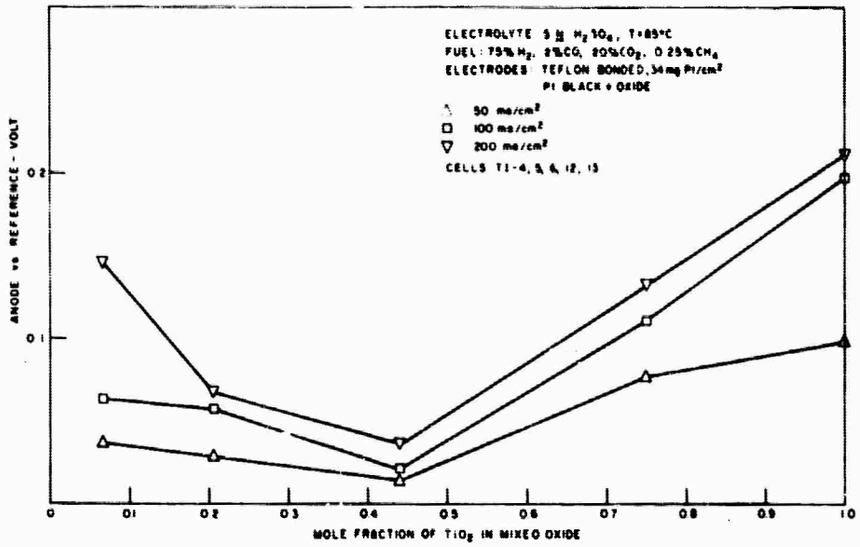

Figure 2.1-27. Effect of Titanium Content On Performance of Titania Stabilized Oxides Mixed with Platinum Black

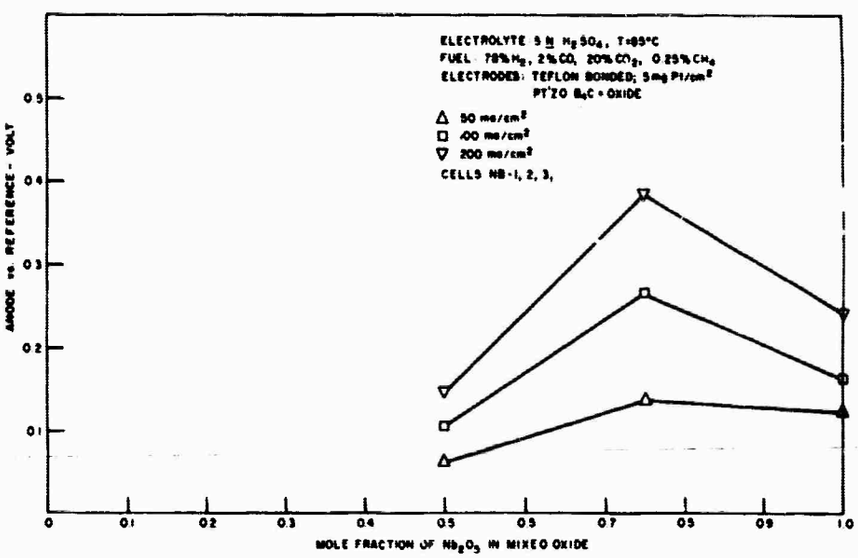

Figure 2.1-28. Effect of Niobium Content On Performance of Niobia Stabilized Oxides Mixed with Platinized B_4C

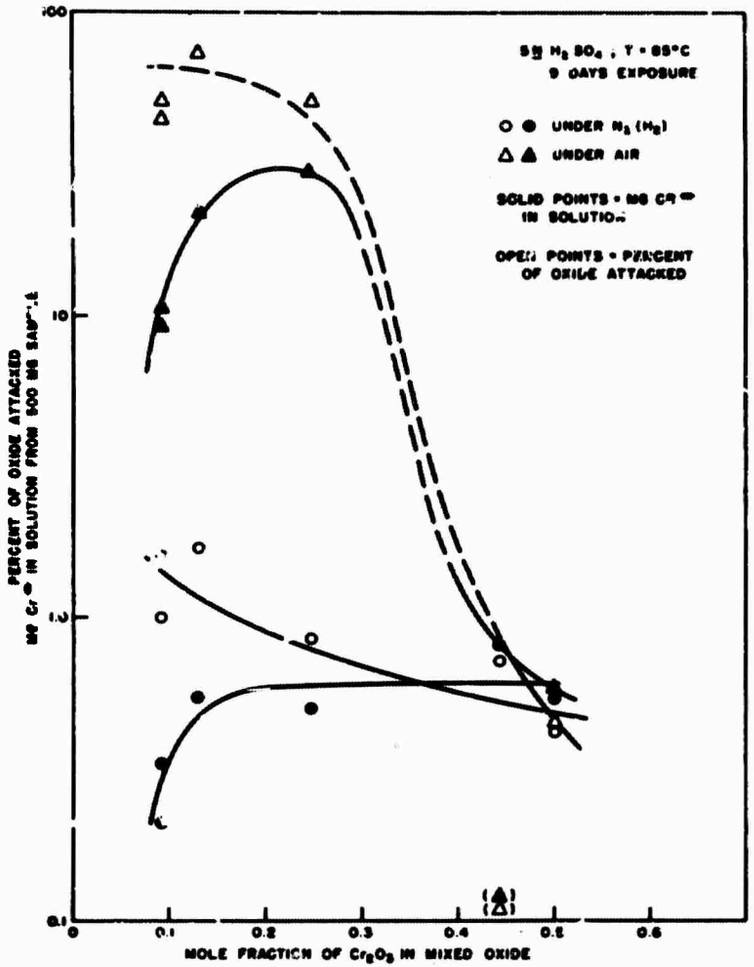

Figure 2.1-29. Corrosion Losses from Chromia Stabilized Oxides in 5 $\underline{N}$ H_2SO_4 at 85°C.

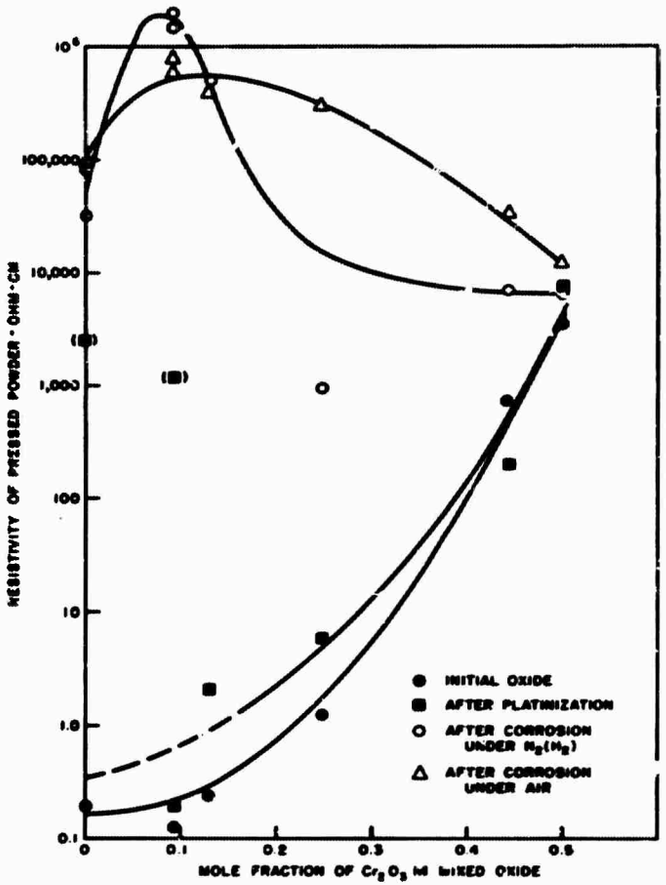

Figure 2.1-30. Resistivities of Chromia Stabilized Oxides Before and After Corrosion Tests

potentials under the nitrogen-hydrogen atmosphere. Much smaller effects are observed as the chromium content increases, and the resistivity data are in agreement with the chromium analyses in indicating that little attack of the 1:1 oxide occurs even in air.

Related tests have also been run with TiO_2 and Nb_2O_5 "stabilized" tungsten oxides. The results tend to confirm observations of the previous report (2.1-5) that chromium oxide is the most effective additive. Additional tests are required, however, to confirm that the resistance of catalytic activity towards decay parallels the corrosion resistance. It would also appear desirable to investigate means of reducing the electronic resistivity of this oxide since this may well lead to improved catalyst performance.

2.1.2.6 Conclusions

Considerable success has been realized in improving the corrosion resistance of tungsten oxide towards acid electrolytes. Chromium additions have been most effective in this regard, and reduced oxides containing Cr : W ratios close to one appear to be most desirable. Such oxides appear to be promising catalyst supports. When used in conjunction with impure hydrogen fuels containing carbon monoxide, they effectively promote anodic oxidation with 2 to 5 mg/cm^2 platinum loadings. The systems are reaching a stage of development that should warrant investigations with hydrocarbons.

2.1.3 Activated Boron Carbide Electrodes (W. T. Grubb, L. H. King)

2.1.3.1 Platinum-Activated Boron Carbide Electrodes on Hydrocarbon Fuels

A. General

During the present reporting period some studies have been carried out concerning the effect of conditions on the reduction of platinum supported in oxidized form on boron carbide. It has been found desirable in the past to prepare electrodes from electrocatalyst containing unreduced platinum and reduce it in situ after the finished electrode has been assembled into a fuel cell. An especially convenient way to do this is to reduce the electrode with a hydrocarbon fuel. Propane is especially convenient as both a reducing agent and a test fuel for evaluating the effectiveness of an electrode or electrocatalyst variation being tested. In the current experiments, it has been found that propane reduction at several temperatures showed a wide range of rate. It was also found that the heat treatment of the electrode during its fabrication had a pronounced effect upon the rate of reduction of the platinum by propane at a given temperature. In cases in which the reduction of platinum was very slow at 150°C, it was found that the oxidized form of platinum dissolved slowly in the phosphoric acid and could be detected in the effluent from the cell by taking the ultraviolet spectrum of a complex

of platinum formed by the addition of hydrochloric acid to the solution. It became evident that the amount of platinum dissolved before reduction could represent a significant fraction of the total platinum present. Subsequent to this, analysis for platinum in a nitric acid leach employed during the preparation of the electrode revealed that some platinum was also present in this solution. It is evident that significant losses of platinum have occurred in the past with electrodes of this type. Future work will aim to prevent such loss. In particular, conditions which promote rapid reduction of the supported platinum "oxide" at as low a temperature as possible (to reduce dissolution before reduction) are indicated. No platinum dissolution was detected after reduction. In addition to this, elimination of the nitric acid leaching step in preparing electrodes will be evaluated. Some of the conclusions reached in this part of the work will be valuable for future experiments using other refractory carbides as supports.

B. Effect of Temperature upon Reduction of Supported Platinum "Oxide"

Three similar electrodes were prepared using standard procedures previously described (2.1-6), but without nickel foam and not pressed. These were heated in assembled fuel cells to a given temperature and propane supplied to the anode (oxygen to the standard platinum black cathode). Cell voltage was monitored continuously with a recording voltmeter and at selected times with a potentiometer. The cell was kept on open circuit. A typical voltage vs time plot is shown in Figure 2.1-31. The reduction was considered complete at a cell voltage of 0.6V. The time for reduction varied from about 5 hours at 100°C down to about 2 minutes at 150°C, see Table 2.1-4.

Table 2.1-4

Electrode Reduction Times and Temperatures

Reduction Temperature, °C	Reduction Time, min.	Platinum Loading, mg/cm^2
100	308	4.8
125	67	4.2
150	2.0	5.2

(2.1-6) W. T. Grubb and L. H. King, Technical Summary Report No. 9, Hydrocarbon-Air Fuel Cells, ARPA Order No. 247, Contract No. DA44-009-AMC-479(T) p. 2-1 (1966).

C. Effect of Electrode Heat Treatment Variable Upon the Reduction of Supported Platinum "Oxide" by Propane

In the preparation of Teflon-bonded platinum black or other electrodes it is standard practice to heat the electrode containing uncured Teflon binder and electrocatalyst to about 250°C to decompose wetting agent present in the T-30 suspension used as a source of Teflon (2.1-7). This is normally carried out on a hot plate starting from room temperature and holding at 250°C for about 30 minutes including heat-up time. Such a method was also used in preparing platinum-activated boron carbide electrodes. It was discovered that electrodes prepared during this and the previous reporting period were actually receiving the above heat treatment at 260°C due to calibration changes in the hot plate used. This was not thought to be significant since the electrode was subsequently cured at 350°C. However, it has been found that this has a distinct effect upon the rate of reduction of the electrode with propane.

Using the method described above, the reduction times of different electrodes by propane gas at 145°C were determined. These values are given in Table 2.1-5 for electrodes with platinum loading of 5 ± 0.5 mg/cm^2.

Table 2.1-5

Electrode (5 ± 0.5 mg Pt/cm^2) Reduction Times with Propane

Heat Treatment Temp, °C	Pt Reduction Time at 145°C, min.
260 (Electrode No. 427)	120
280	5
305	5

The results of Table 2.1-5 indicate that the platinum diammine dinitrite salt used to activate the boron carbide substrate in these electrodes is not converted into a form readily reduced to platinum when the electrode is heat-treated at 260°C for 30 minutes followed by a short, 2 minute cure at 350°C. Tightly complexed residual oxides of nitrogen may remain at 260°C and be removed only at higher temperature. The slow reduction might not of itself be a disadvantage, except that such slow reduction adds to the aforementioned platinum dissolution problem.

D. Analysis for Platinum in Cell Electrolyte Effluent

The first electrode of Table 2.1-5 spent some two hours at 145°C in unreduced condition with electrolyte flowing through the cell. It was noted that the effluent electrolyte was slightly colored and began to emerge water-white after reduction had taken place. Suspecting that the form of

(2.1-7) L.W. Niedrach and H.R. Alford, J. Electrochem. Soc. 112 117 (1965).

platinum which was hard to reduce also might be that which was dissolving in the phosphoric acid electrolyte, a portion of the electrolyte was measured for ultraviolet absorption and no bands were found. Addition of some HCl to this sample caused little change. However, after standing for 72 hours at room temperature, bands developed which were identical to those obtained from a dilute solution of chloroplatinic acid in concentrated phosphoric acid. The electrolyte collected after reduction showed no absorption bands under the same conditions.

The ultraviolet spectra were obtained with a Perkin-Elmer Model 202 Spectrometer using automatic scanning from 200 to 390 millimicrons. The other conditions and solutions compositions are indicated in Figures 2.1-32 thru 2.1-34. Figure 2.1-32 shows the absorption spectrum of chloroplatinic acid. Figure 2.1-33 is the absorption spectrum of the electrolyte from the first cell of Table 2.1-5 after the addition of HCl and after 72 hours standing at room temperature. Figure 2.1-34 shows the absorption spectrum of a second sample of the cell electrolyte (with HCl added) after several different time intervals at room temperature. The slow formation of the absorbing complex is characteristic of a number of noble metal complexes (2.1-8). The zero has been shifted in all curves by 0.2 absorbance units and is actually near 0 at 390 millimicrons. The effluent from the cell contains platinum in an amount which can be detected by ultraviolet absorption of the chloride complex and can be estimated quantitatively by comparison with known solutions of chloroplatinic acid in phosphoric acid-hydrochloric acid solvent of the same composition. For quantitative estimation of the platinum concentration, the absorption peak at about 260 millimicrons is the more reproducible and useful of the two peaks and is found to obey Beer's law as shown in Figure 2.1-35.

Quantitative estimate of a few milligrams of Pt per liter of phosphoric acid is easily made. However, it was found that below about 0.3 mg/l the band is lost in a background absorption and estimates below this point cannot be made by the method described.

The first electrode of Table 2.1-5 was found to have lost 18.5 mg of platinum out of a total of 102 mg, which lowered its platinum loading from 5.7_2 to 4.6_8 mg/cm^2.

As noted earlier, electrodes during preparation are leached in 50 vol % nitric acid for 1 hour at about 100°C. An analysis of this leachant for platinum by a different method (see Appendix 4.2-1) showed that from an electrode similar to the above, 8.5 mg of platinum were removed during this step (in 130 ml of leachant solution). This loss of platinum will further reduce the platinum loading of electrode No. 427 to 4.2_0 mg/cm^2.

(2.1-8) L. E. Orgel "An Introduction to Transition Metal Chemistry," John Wiley and Sons, Inc. New York, N.Y., 1960, pp. 103 ff.

(2.1-9) H. Taube, Chem. Rev. 50 69 (1952).

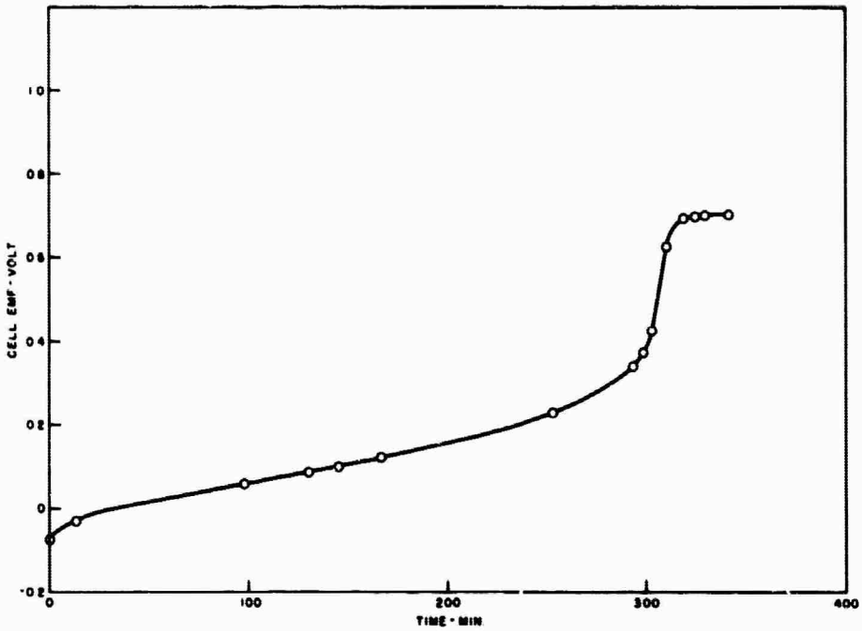

Figure 2.1-31. Reduction of Platinum "Oxide" on Boron Carbide by Propane at 100°C as Measured by Propane-Oxygen Cell Voltage vs Time

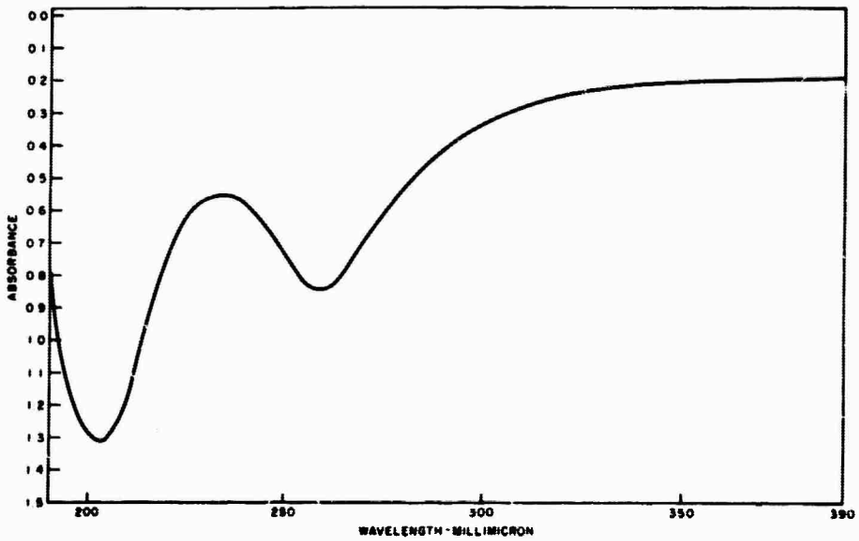

Figure 2.1-32. Ultraviolet Absorption of H_2PtCl_6 in 14.4 M H_3PO_4, 0.2 M HCl Concentration 0.731 mg/100 ml Pt as H_2PtCl_6. Cell Path Length 1.000 cm, Slit Setting 25, Scan Speed Fast. Reference Cell Path Length 1.000 cm, Ref. Solution 14.7 M H_3PO_4.

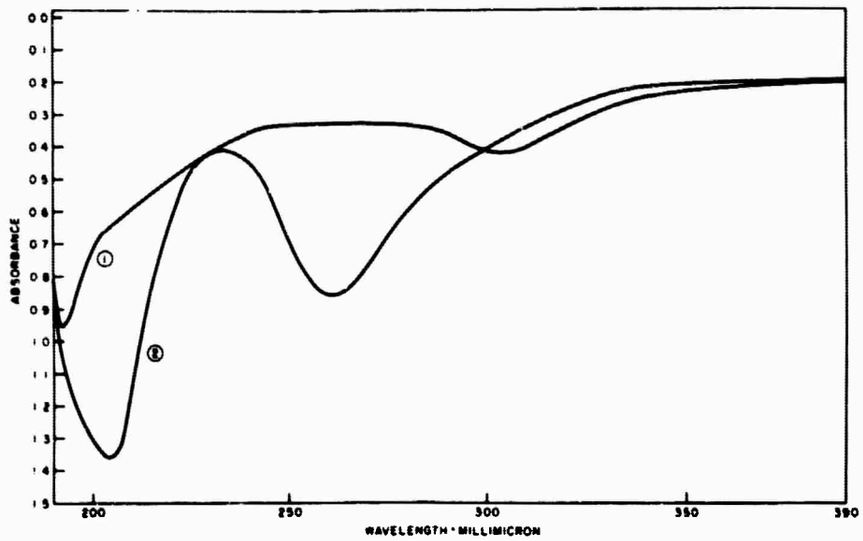

Figure 2.1-33. Ultraviolet Absorption of Phosphoric Acid Electrolyte from Cell No. 427. HCl Added to Give 0.2 HCl, Other Conditions as in Figure 2.1-32. Curve 1, 0 Hrs and Curve 2, 72 Hrs After HCl Addition.

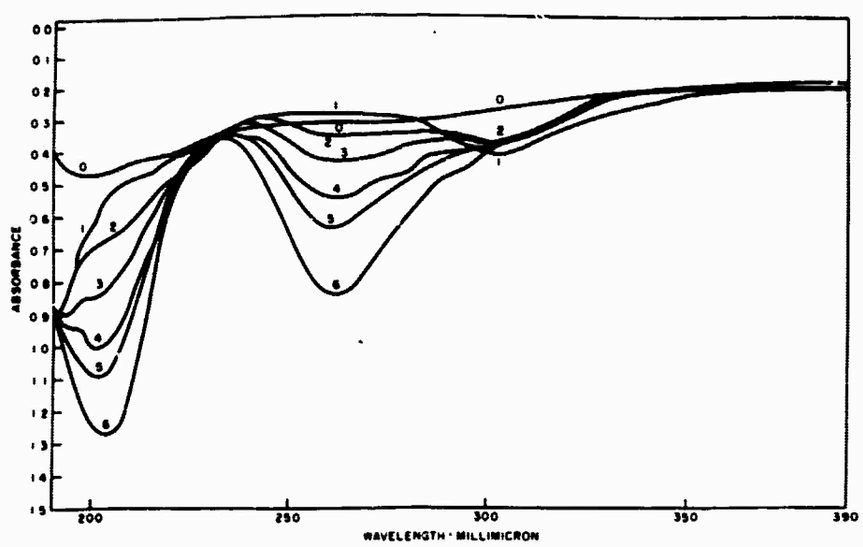

Figure 2.1-34. Ultraviolet Absorption of Electrolyte from Cell No. 427. Curve O, Before HCl addition; Curve 1, Just After HCl Addition; Curve 2, After 4 Hr; Curve 3, After 12 Hr; Curve 4, After 23 Hr; Curve 5, After 31 Hr; and Curve 6, After 59 Hr.

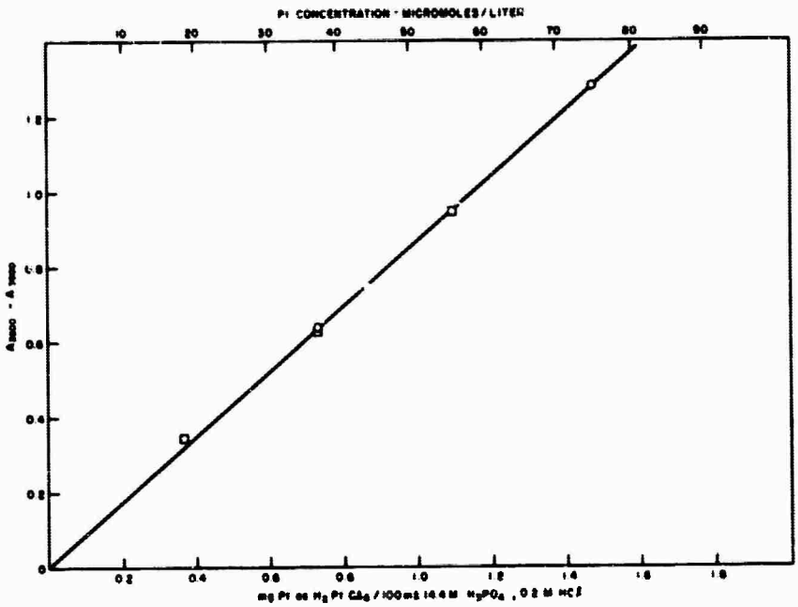

Figure 2.1-35. Beer's Law Plot for H_2PtCl_6 in Concentrated H_3PO_4 with Excess HCl Present, Using Peak Absorbance Near 260 Millimicrons.

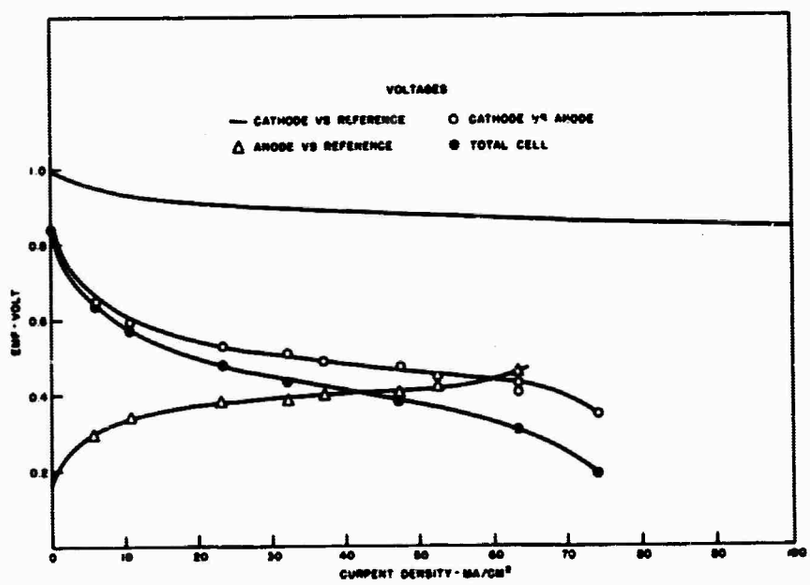

Figure 2.1-36. Performance Curve for Platinized Boron Carbide Anode No. 427 Against Standard Pt Black Cathode with Propane Fuel, Oxygen Oxidant, Electrolyte 14.7 M H_3PO_4 at 150°C.

E. Performance of Electrodes on Propane

Electrode No. 427 was operated on propane fuel at 150°C using 14.7 M H_3PO_4 as electrolyte. The performance curves are shown in Figure 2.1-36. This electrode is considerably short of the performance of the best electrodes at its calculated platinum loading of 5.7_2 mg/cm^2 but it is not bad based on the corrected value of 4.2_0 mg/cm^2.

F. Conclusions

It has been sometimes thought that the slowest practicable rate of reduction of supported platinum "oxide" will give the best results. This will not be true at elevated temperatures unless the particular oxidized form of platinum is resistant to dissolution in the electrolyte. In the present case it has been found that platinum daimmine dinitrite should be decomposed at a temperature greater than 260°C and preferably at about 280°C in order to facilitate its reduction. The less completely decomposed platinum diammine dinitrite is probably more readily dissolved in phosphoric acid at elevated temperatures. In the future, electrodes of this type will be heat-treated at 280°C or higher and their reduction with propane in the cell will be carried out during the heat-up period beginning at about 100°C. The effectiveness of these measures will be monitored by platinum analysis of the electrolyte from the cell.

2.1.3.2 Platinum-Activated Boron Carbide Electrodes of the Leached Nickel Foam (V.C.) Structure

A. General

The previous work has been extended during this period with the exploration of new variables and some optimization of those already identified as important. Air performance at room temperature and at 80°C with 6N sulfuric acid electrolyte was taken as the standard performance test for these electrodes. The method of preparation gives a high degree of porosity concentrated in the large pores formed from leaching out the strands of nickel foam and leaving active material between these large pores which is probably rather highly compressed and not very porous.

The concept of producing an electrode in which small pores branch out from the large pores has been explored. This has been achieved by incorporating a second leachable additive into the mixture of activated boron carbide and Teflon. This technique gave a considerable improvement in air cathode performance (relative to platinum loading). The better of two second additives tried was the one which has elongated, needle-like particles and would be expected to form a larger number of small pore-large pore intersections. An electrode of this structure produced the highest ratio of performance to platinum loading so far achieved. In wet-proofed electrodes, electrolyte will tend to fill the large pores preferentially while the small tributary pores remain filled with gas. A

particularly large amount of electrocatalyst surface covered with electrolyte film and still possessing good access to the bulk gas phase and low electroiytic resistance to the bulk electrolyte phase is probably achieved by this structure. It may be considered a dual porosity electrode in which the interface between large and small pores wanders throughout the volume of the electrode in three dimensions.

B. Electrodes Prepared Using a Second Leachable Additive

The most effective electrode structure produced in the current series was achieved by combining two approaches already described:

1. The leaching out of nickel foam of extremely high porosity to form a pore system of interconnected tunnels in a Teflon-bonded electrode.
2. The simultaneous leaching out of a particulate additive to form smaller pores intersecting with these larger pores.

In compilation of Appendix 4.2.2, electrodes No. 436, 444, 446, 461, and 473 were prepared in this manner using either a silica gel, Cab-O-Sil*, or a calcium metasilicate, Cab-O-Lite*, as the second leachable additive. The current density at 0.7 volt iR-free obtained from a cell with a standard platinum black anode supplied with pure hydrogen and the test cathode supplied with ambient air (no forced circulation) was used as an index of performance. This was divided by the platinum loading of the cathode to get a performance index in ma/mg of Pt. By this criterion, the two 5% Cab-O-Lite electrodes produced $68._6$ and $72._6$ ma/mg, a 20% Cab-O-Lite electrode $50._4$ ma/mg, a 5.6% Cab-O-Sil electrode $58._5$, and a 5% Cab-O-Sil electrode $33._4$ ma/mg. The best electrode without a second leachable additive produced $59._4$ ma/mg.

The best electrode prepared with Cab-O-Lite as the second leachable additive exceeded the best of all the other electrodes of the leached nickel foam structure by about 22%. The better of the two Cab-O-Lite electrodes gave the performance shown in Figure 2.1-37. For comparison, a standard platinum black cathode of high (45.5 mg/cm^2) platinum loading is included. By the criterion of ma/mg at 0.7 volt the new electrode is about 9 times as good as the standard platinum black electrode. The new electrode achieved a much higher limiting current and was better than the Pt black electrode at current densities above approximately 450 ma/cm^2.

It is somewhat surprising that the total % void volume of the dual porosity electrodes is not generally greater than the leached nickel foam electrodes. This is caused either by the approximate nature of % void volume calculation or the fact that the total porosity really is about the same but has

* Godfrey L. Cabot Co., Boston, Mass.

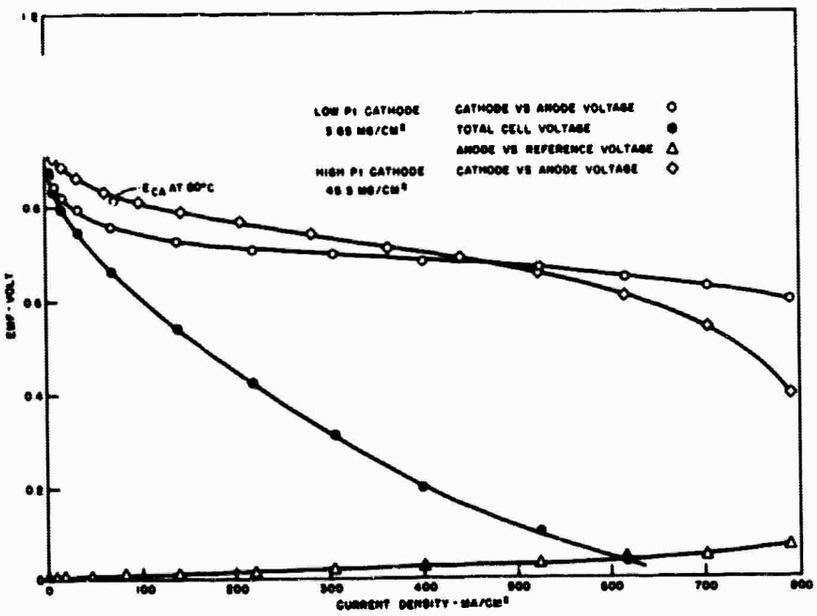

Figure 2.1-37. Air Performance of Electrode No. 473 at 3.65 mg/cm^2 Platinum Loading vs H_2 Pt Black Anode 45.5 mg/cm^2. Comparison Air Cathode Pt Black, 45.5 mg/cm^2. Electrolyte 6N H_2SO_4 Room Temperature.

a more favorable distribution with respect to pore size.

Optimization of the percentage of particulate additive needs to be carried out, in addition to testing of the dual porosity electrodes on air and other reactants at high temperature.

It was planned to test electrode No. 473 on hydrocarbons and air at elevated temperature in phosphoric acid. Unfortunately, it was damaged in removal from the low temperature air housing. A similar electrode will be evaluated in the future.

In general, the many variables involved in preparation of these electrodes have been adjusted to more nearly optimal values and performance has improved considerably. The ma/mg at 0.7 volt had an average value during the current reporting period of $44._5$ compared with $30._3$ during the preceding period. The last electrode of this period produced $72._6$ ma/mg.

The shape of particles in the second leachable additive appears to be important. The more effective calcium metasilicate additive possesses elongated particles as shown in Figure 2.1-38. The less effective silica additive has rather spherical particles as shown in Figure 2.1-39. (These are agglomerates of much smaller particles of silica.) On geometric grounds, it might be expected that the elongated particles would produce more small pores intersecting the tunnel-like macropores.

Some simple computer programs were written for the purpose of calculating percent void volume and other electrode parameters of leached nickel foam electrodes. This eliminated many straightforward but tedious calculations especially the void volume calculation. Appendix 4.2.2 contains a table of all the electrodes prepared and tested during the last two contract periods and includes a complete set of parameters, some of which were obtained from the computer calculations not included in the previous report.

C. Leakage Prevention with Leached Nickel Foam Electrodes

This electrode structure is easier to make than a standard pasted electrode with no nickel foam pressed into the current collecting screen because the screen-foam aggregate presents a means of holding the activated boron carbide-aqueous Teflon dispersion slurry in a uniform layer. For this reason, adventitious pinhcles as such can be all but eliminated. However, the pores formed by removal of the nickel foam can be large enough to leak under some head of electrolyte. That is, a good electrode tends to be entirely leak-tight, but electrolyte may begin to go through the largest of the macropores under a head of only a few centimeters. Some means of overcoming this defect is needed.

Figure 2.1-38. Particles of Calcium Metasilicate (Cab-O-Lite) Photographed at 58X

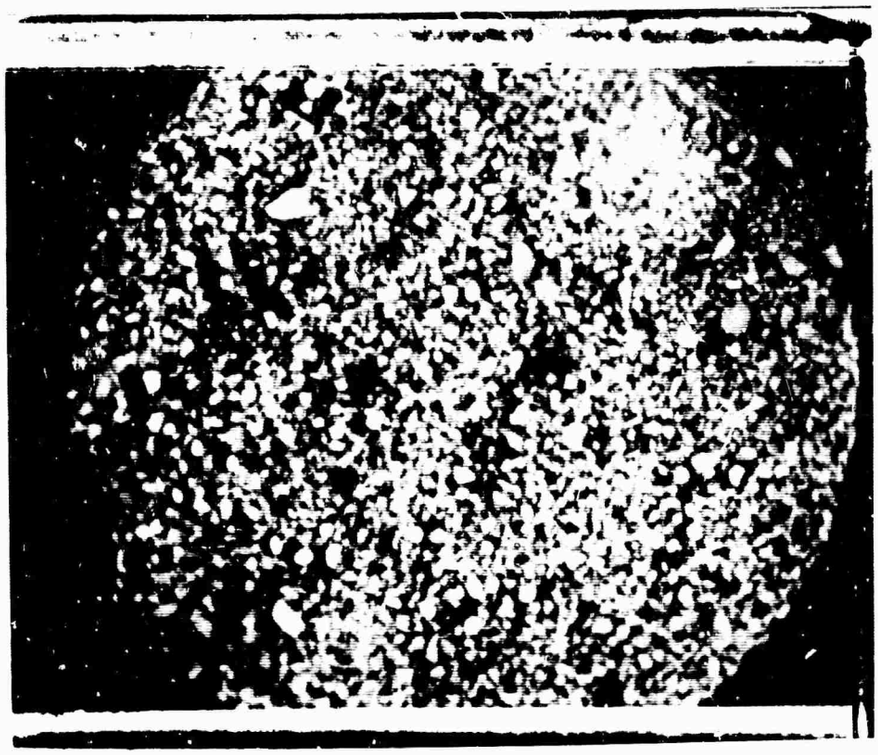

Figure 2.1-39. Particles of Silica Gel (Cab-O-Sil) Photographed at 58X

Some initial experiments have been performed which show promise that a hydrophilic layer next to the electrode on the electrolyte side strongly reduces the leaking tendency. To test this idea, a Millipore* filter of 0.3 micron average pore diameter was mounted in a cell and held against the electrolyte side of the electrode by a platinum screen.

This had the effect of increasing the electrolyte head which could be tolerated without leakage and, in fact, at an electrolyte head of a few centimeters this barrier completely stopped the electrolyte from leaking through the electrode. This test was performed on an electrode which in the absence of the Millipore filter was one of the leakiest electrodes made in this series.

It is, of course, undesirable to have to hold a barrier against the electrode mechanically. It is planned to investigate some bonded barrier layers.

D. Conclusions

Activated boron carbide electrodes continue to show promise for both anode and cathode structures of low platinum content. Great interest attaches to determining if the improvements in heat treatment and reduction procedures can be combined with the structure improvements to yield better phosphoric acid cathodes and better performance on hydrocarbon fuels than previously observed. The attainment of controlled porosity of nickel foam removal has produced much more consistent limiting current behavior than previously observed in air electrodes. The use of two or even more leachable additives to obtain a controlled ratio of small and large pores promises to improve the utilization of electrocatalyst surface. This could lead to even better performance at current densities of practical interest. An interface between tunnel-like macropores and microporous walls that is distributed throughout the volume of the electrode may also be interesting from the point of view of theories of electrode structure.

2.1.4 Electrodes with Other Carbides (W. T. Grubb, L. H. King)

2.1.4.1 Tungsten Carbide Electrodes

During the current period some initial experiments have been performed with Teflon-bonded, tungsten carbide electrodes containing no precious metal.

Pasted, unpressed electrodes were prepared with the finest available tungsten carbide powder (from H. Starck, Goslar, Germany). In two electrodes, the percentage of Teflon binder (based on total weight of electrocatalyst) was 9.5% (electrode No. 1) and 6.7% (electrode No. 2). These electrodes were given the same heat treatment and cure used for boron carbide electrodes.

* Millipore Filter Corp., Bedford, Mass.

Figure 2.1-40 shows performance curves in 14.7 M H_3PO_4 at 145°C for these electrodes in a complete fuel cell with a standard platinum black electrode as the oxygen cathode in the cell. Electrode No. 1 was first operated on propane and then on argon and gave currents which were identical in the two cases and indicated that the electrode was self-oxidizing in the potential region of 0.6 volt anode overvoltage (vs a reversible hydrogen electrode in the same electrolyte). Gas chromatographic analysis showed that CO_2 was produced in these experiments. This is thought to be due to the oxidation of the tungsten carbide and not to propane oxidation, since it was present with argon as the "fuel." This has been discussed in the preceding report (2.1-6). It is assumed that tungsten oxide forms on the surface and may be in a porous, high-area state due to the manner in which it is formed from tungsten carbide with carbon dioxide evolution taking place. Hydrogen was briefly evolved from electrode No. 1 and it was then placed under load with hydrogen as fuel. Its performance was surprisingly good under these conditions. A current density of 150 ma/cm^2 was maintained at steady state with an overvoltage of only about 60 millivolts against reversible hydrogen electrode. The curves in Figure 2.1-40 all show the cell voltages free of ohmic loss. The resistance of the cell with electrode No. 1 was somewhat higher, 0.24 ohm vs. 0.13 ohm, than usually observed with this cell geometry (3/8 inch, 0.95 cm electrolyte gap). This also suggests the formation of an oxide film on the electrode. Electrode No. 2 was run first on hydrogen as shown in Figure 2.1-40. Its performance was lower and the cell resistance was normal (0.13 ohm). This suggests that the anodizing of electrode No. 1 made it more effective for subsequent hydrogen oxidation. Electrode No. 1 was subsequently operated at room temperature and it produced a current density of 100 ma/cm^2 at an overvoltage (vs reversible hydrogen) of 0.28 volt. The performance curve is shown in Figure 2.1-41.

The anodizing of metal carbides seems to present an interesting method for forming metal oxides on an electronically conducting support. It is possible that such materials with or without the addition of noble metals to the surface layer will have more interesting electrocatalytic properties. At present, of course, the long-term stability of such materials is entirely unevaluated and there is no evidence to suggest hydrocarbon activity at present. The high activity of the anodized surface of tungsten carbide for hydrogen at elevated temperature is encouraging. It appears to exceed the activity of anodized titanium carbide (2.1-7), although neither system has been optimized and the titanium carbide was of somewhat lower surface area.

(2.1-7) L.W. Niedrach and H.R. Alford, J. Electrochem. Soc. 112 117 (1965).

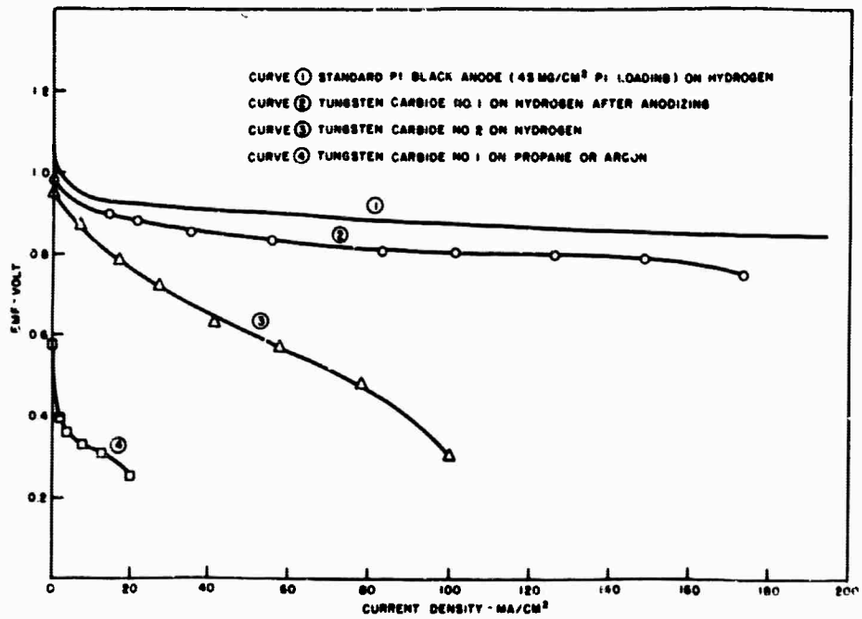

Figure 2.1-40. iR-Free Performance of Cells with Standard Pt Black Cathode, and Various Anodes with 14.7 M H_3PO_4 Electrolyte at 145°C

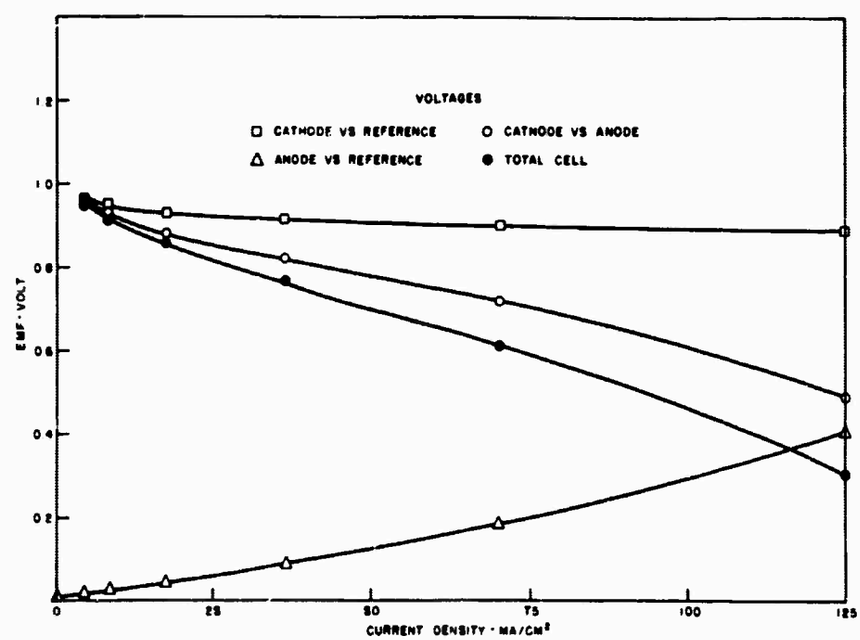

Figure 2.1-41. Performance of the Cell of Figure 2.1-40 Curve 2 on Hydrogen at Room Temperature 6 N H_2SO_4 Electrolyte

2.1.4.2 Conclusions

Further exploratory work with transition metal carbides and mixed carbides is indicated in hope of finding some hydrocarbon activity. Failing this, minimal amounts of platinum activation may be especially effective if the carbide substrate or a surface oxide layer on it can take over some of the functions of the noble metal electrocatalyst. If the surface oxide layer is indeed porous due to CO_2 evolution accompanying its formation, then platinum in the pores would find itself in very intimate contact with both the oxide and the conducting carbide underneath it. Such systems should have an excellent chance of displaying synergistic effects if they exist.

2.1.5 Multipulse Potentiodynamic Studies of the Adsorption of Carbon Monoxide and Hydrogen on Rhodium Electrodes (S. Gilman)

2.1.5.1 Carbon Monoxide Adsorption

A. Introduction

Hydrogen fuel cell anodes of the noble metals show varying sensitivity to the presence of CO in the gas feed (2.1-10). Studies of the mixed adsorption of CO and hydrogen on microelectrodes of these metals may provide insight into the mechanistic details of electrode "poisoning."

While the adsorption of CO on Pt has received some attention in past years (2.1-11 thru 2.1-14), similar studies on Rh electrodes have been lacking. On the other hand, considerable background information has been provided as a result of various voltammetric studies (2.1-15 thru 2.1-20) of the adsorption of oxygen and hydrogen on Rh. The latter work has been reviewed by

---

(2.1-10) D.W. McKee, L.W. Niedrach, I.F. Danzig and H.I. Zeliger, Technical Summary Report No. 9, Hydrocarbon-Air Fuel Cells, 1 January - 30 June 1966, ARPA Order No. 247, Contracts Nos. DA-44-009-ENG-4909, DA-44-009-AMC-479(T), DA-44-ENG-4853, p 2-4.

(2.1-11) S. Gilman, J. Phys. Chem. 66, 2657 (1962); 67, 78 (1963).

(2.1-12) T.B. Warner and S. Schuldiner, J. Electrochem. Soc., 111, 992 (1964).

(2.1-13) R.A. Munson, J. Electroanalyt. Chem. 5, 292 (1963).

(2.1-14) S.B. Brummer and J.I. Ford, J. Phys. Chem. 69, 1355 (1965).

(2.1-15) M. Breiter, C. Knorr and M. Volkl, Z. Elektrochem. 59, 681 (1955).

(2.1-16) M. Breiter, H. Kammermaier and C. Knorr, Z. Elektrochem. 60, 119, 454 (1956)

(2.1-17) K. Franke, C. Knorr, and M. Breiter, Z. Elektrochem. 63, 226 (1959).

(2.1-18) W. Bold, and M. Breiter, Z. Elektrochem. 64, 897 (1960).

(2.1-19) F. Will and C. Knorr, Z. Elektrochem. 64, 258, 270 (1960).

(2.1-20) M. Breiter, K. Hoffmann and C. Knorr, Z. Elektrochem. 61, 1168 (1957).

Frumkin (2.1-21). The voltammetric approach followed in this and the subsequent section is similar to that used in previous studies of Pt electrodes (2.1-11).

B. Experimental

1. Chemicals

The electrolyte (4N H_2SO_4) was prepared using triply-distilled water and Vycor-distilled sulfuric acid. Reagent grade CO and argon were used. Mixtures of these gases were prepared, bottled and analyzed by the Mathieson Co.

2. Electrodes

Platinized Pt counter and reference electrodes were employed. The Rh test electrode was not found to vary gradually in its properties in a manner which might be ascribed to adsorption of Pt ions.

The test electrode was fabricated of 99.98% pure Rh wire, 0.030 inch in diameter. The wire was degreased, etched in aqua regia, washed and dried. It was then resistively heated almost to the melting point in an ultra-high vacuum system. This served to anneal the sample and to cleanse the surface further (actual evaporation of metal was observed). The treated wire was then sealed into a soft ground glass joint (using a hydrogen flame) so as to expose 0.08 cm^2 of surface. The electrode was given a light final etch in aqua regia. Electrodes prepared using a Teflon support instead of glass had similar electrochemical properties, but exhibited a time-variation in properties characteristic of impurity adsorption (see below). This must be ascribed to slow out-diffusion of organic materials from the Teflon.

The charge, ${}_SQ_H$, corresponding to saturation coverage of the electrode with hydrogen atoms, was 0.25 mcoul/cm^2. If it is assumed that all of the low index crystal faces are equally represented on the surface and that one hydrogen atom is adsorbed per Rh atom, then a perfectly smooth surface would correspond to ${}_SQ_H$ = 0.22 mcoul/cm^2. On that basis, the "roughness factor" (ratio of true to geometric area) of the electrode was 1.16.

3. Test Vessel and Electronic Equipment

The electronic equipment was described previously (2.1-11). The test vessel was made of pyrex glass, had separate compartments for counter, test, and reference electrodes and was

---

(2.1-21) A. N. Frumkin, Chapter 5 in "Advances in Electrochemistry and Electrochemical Engineering," Vol. 3, Edited by P. Delahay, Interscience Publishers, Inc., N.Y., 1963.

equipped with a glass paddle-stirrer (water-sealed). All electrodes were attached with ground glass joints and the cell was air-tight.

4. Electrolyte Pretreatment

After "activating" the test electrode, its properties were found to vary in a manner characteristic of contamination by impurities dissolved in the electrolyte (see below). The following procedure was employed in purifying the solution.

A "cleanup" electrode was fabricated of platinized platinum screen. This electrode had a geometric area of 40 cm^2 and a surface area of 4000 cm^2 based on H-deposition measurements. The electrode was degreased, cleaned in hot chromic acid solution and rinsed in distilled water. It was then immersed in 200 cc of 4 N H_2SO_4 contained in a beaker which also contained a large smooth Pt counter electrode. The cleanup electrode was made cathodic under current flow of 1 ampere for 2 minutes to desorb foreign anions. A similar anodic current was passed to desorb cations and organic materials and to generate the "oxygen" film which prevents re-adsorption of materials. After changing the electrolyte, the cycle was repeated. The passivated electrode was then withdrawn from the beaker and transferred to a 200 cc volume of electrolyte in the test vessel. The electrode was then reduced at 0.4 v, and the potential was held at 0.7 v for 4 hours with the solution stirred vigorously with the paddle-stirrer (360 rpm). Under these circumstances, the electrode "getters" ions and organic substances from the solution. The electrode was then withdrawn from the test vessel without previously interrupting the circuit.

5. Experimental Conditions

All measurements were made at 80°C in a thermostatted air bath. All potentials are referred to a reversible hydrogen electrode in 4 N H_2SO_4. All currents and changes are reported on the basis of the geometric area of the electrode.

C. Procedures and Results

1. Steady-State Oxidation of CO and H_2

A slow (0.04 v/sec) linear anodic sweep was applied to obtain the current-voltage curves of Figure 2.1-42. To renew the surface of either the Pt or Rh electrode before each measurement, the electrode was held at 0 v for 10 sec, at 1.8 v for 2 sec, at 1.2 v for 10 sec, and at 0 v for 0.1 sec. The electrolyte, saturated with either CO or H_2, was paddle-stirred (360 rpm) throughout the experiment.

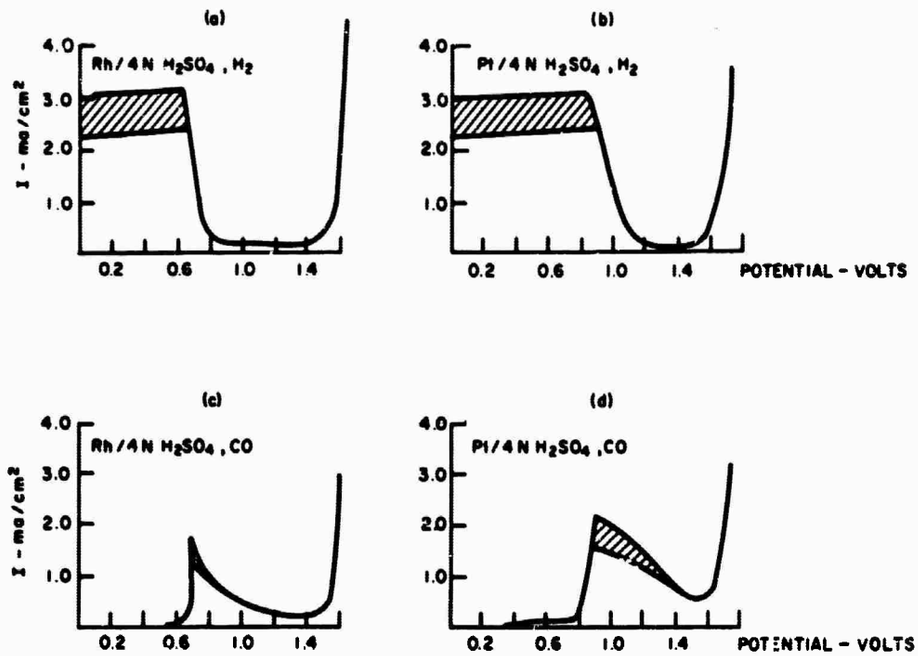

Figure 2.1-42. Current-Voltage Curves Measured for Smooth Pt and Rh Electrodes During Application of a Linear Anodic Sweep of Speed 0.04 v/sec. The electrolyte was saturated with the gas at 80°C and the solution was paddle-stirred (360 rpm) throughout the experiment. The hatched areas correspond to regions of oscillation of the current.

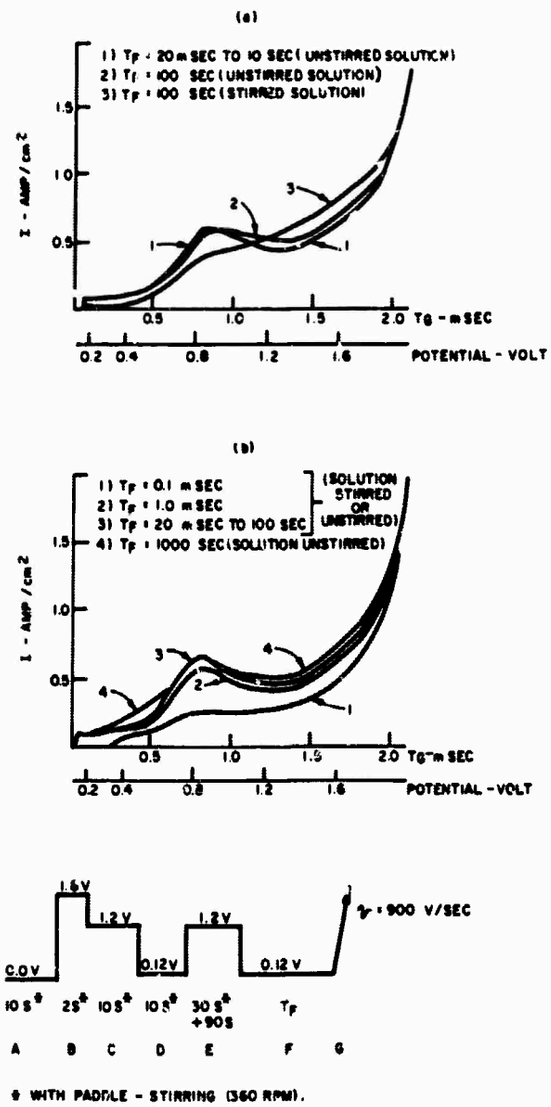

Figure 2.1-43. Linear Anodic Sweep Traces for a Smooth Rh Electrode in Argon-Saturated 4N H_2SO_4 (80°C). The traces were measured during application of sweep G of the indicated potential sequence.
a) Before purification of solution
b) After purification of solution.

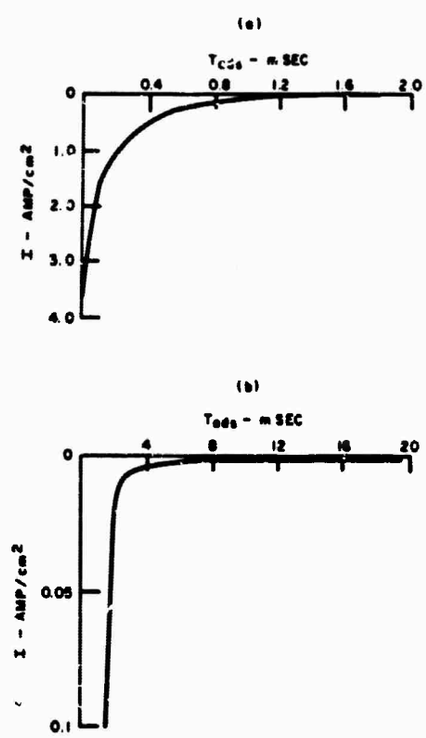

Figure 2.1-44. Current-Time Transients Measured During Reduction of a Rh Electrode. The traces were measured during step F of the potential sequence of Figure 2.1-43.

2. Preparation of a Reproducible Rhodium Surface

A clean Rh surface will become contaminated in the course of an experiment, either due to intentional exposure to an adsorbate (CO) or to unintentional adsorption of solution impurities. It is possible to renew the surface in situ by the application of potential pulses, as in the case of Pt electrodes (2.1-11). The sequence of Figure 2.1-43 was found to serve this purpose. In this sequence, the electrode is normally held at 0 v in a thoroughly reduced state (Step A). At this low potential, the coverage with anions will be small, but the coverage with organic materials may be quite extensive. At the high potential of Step B, even large coverages with organic materials are eliminated. However, the anodic film is so extensive as to require very lengthy (more than 1 sec) reduction for its removal. To cope with this problem, the surface was reduced at 0.12 v (Step D). This results in only moderate coverage with refractory organic materials, readily eliminated during application of the moderately high potential of Step E. The moderate anodic film of Step E suffices to prevent adsorption or reaction of CO and other organic materials while the solution adjacent to the electrode is equilibrated with the bulk. For the experiment of Figure 2.1-43, a 90 sec period was allowed (during Step E) for the solution to become quiescent so as to limit subsequent transport of the adsorbate to ordinary diffusion. This quiescent period was eliminated when solution agitation was required during the subsequent adsorption step. In Step F the electrode was reduced, exposing a clean and reproducible surface to the electrolyte. The state of the surface could be explored by means of the linear anodic sweep, Step G.

Trace 1 of Figure 2.1-43a was obtained for T_F = 20 msec to 10 sec (unstirred solution) and corresponds mainly to oxygen adsorption on the clean Rh surface. Trace 2 was obtained after T_F = 100 sec and is indicative of some change in state of the surface. This change becomes more pronounced with stirring (trace 3) suggesting transport-controlled adsorption of impurities from the solution. After pre-electrolysis of the solution (see section 2.1.5.1.B), the trace characteristic of the clean surface was obtained up to T_F = 100 sec, even in the stirred solution (see trace 3 of Figure 2.1-43b). A slight impurity effect is still noted for T_F = 1000 sec (trace 4 of Figure 2.1-43b). After T_F = 0.1 msec, trace 1 of Figure 2.1-43b was recorded, and is indicative of grossly incomplete reduction of the surface. The reduction is still somewhat incomplete after T_F = 1 msec (trace 2 of Figure 2.1-43b). The reduction process was also followed through measurement of the corresponding current in Figure 2.1-44. In Figure 2.1-44a it is seen that the reduction appears largely complete within 2 msec, but more sensitive measurement (Figure 2.1-44b) reveals that the process is not entirely complete for $T_F > 20$ msec.

After the electrode is reduced at 0.12 v (for more than 0.1 sec) the potential may be raised to some higher value before applying the linear anodic sweep. For potentials up to 0.5 v, applied

for up to 100 sec, the trace recorded was the portion anticipated from trace 1 of Figure 2.1-43a. For potentials of 0.6 v or more, the subsequent sweep currents diminished rapidly with time corresponding to irreversible formation of the anodic film.

3. Measurement of CO Coverage by Anodic Stripping

In the experiment of Figure 2.1-45, traces "1" were measured in argon-saturated electrolyte for T_F = 10 msec to 100 sec, and corresponds mainly to oxidation of the clean Rh surface. Traces "2" were obtained in electrolyte saturated with a CO - argon mixture, and correspond mainly to combined oxidation of adsorbed CO and of the Rh surface. Using Figure 2.1-45d as an example and assuming that the charges corresponding to capacitive charging and to oxidation of the surface are equal for traces 1 and 2, we have the following relationship:

$$\Delta Q = Q_2 - Q_1 \simeq Q_{CO} + Q_{CO}' \qquad (1)$$

where Q_2 is the area under trace 2 from points a to b

Q_1 is the area under trace 1 from points a to b

Q_{CO} is the charge corresponding to anodic stripping of adsorbed CO present before application of sweep G

Q_{CO}' is the charge corresponding to oxidation of CO arriving at the surface by diffusion, after initiation of sweep G.

For the low concentration of CO and the relatively high sweep speeds involved here, $Q_{CO} \gg Q_{CO}'$, and if the other assumptions are correct then:

$$\Delta Q \simeq Q_{CO} \qquad (2)$$

If Q_{CO} corresponds to complete oxidation of CO to CO_2, then ΔQ should be constant over the entire range of sweep speeds. This was tested for v = 4 to 1000 v/sec, and the results appear in Figure 2.1-46. It is apparent from this figure that results exhibit a scatter amounting to only 3% average deviation from the mean value.

4. Measurement of the Rate of Adsorption of CO

The rate of accumulation of CO may be measured by anodic stripping by means of the sequence of Figure 2.1-47. In addition to the pretreatment steps discussed in Section 2 above, steps F and H were introduced to eliminate surface oxygen or hydrogen whenever potential U was considerably removed from 0.12 v. The adsorption of CO occurred from a quiescent solution. Figure 2.1-47a and b correspond to increasing coverage of the surface with CO at 0.12 v. Values of Q_{CO} determined from such traces are plotted against the square root of the adsorption time in Figure 2.1-48. Similar experiments were performed to determine maximum CO coverages from

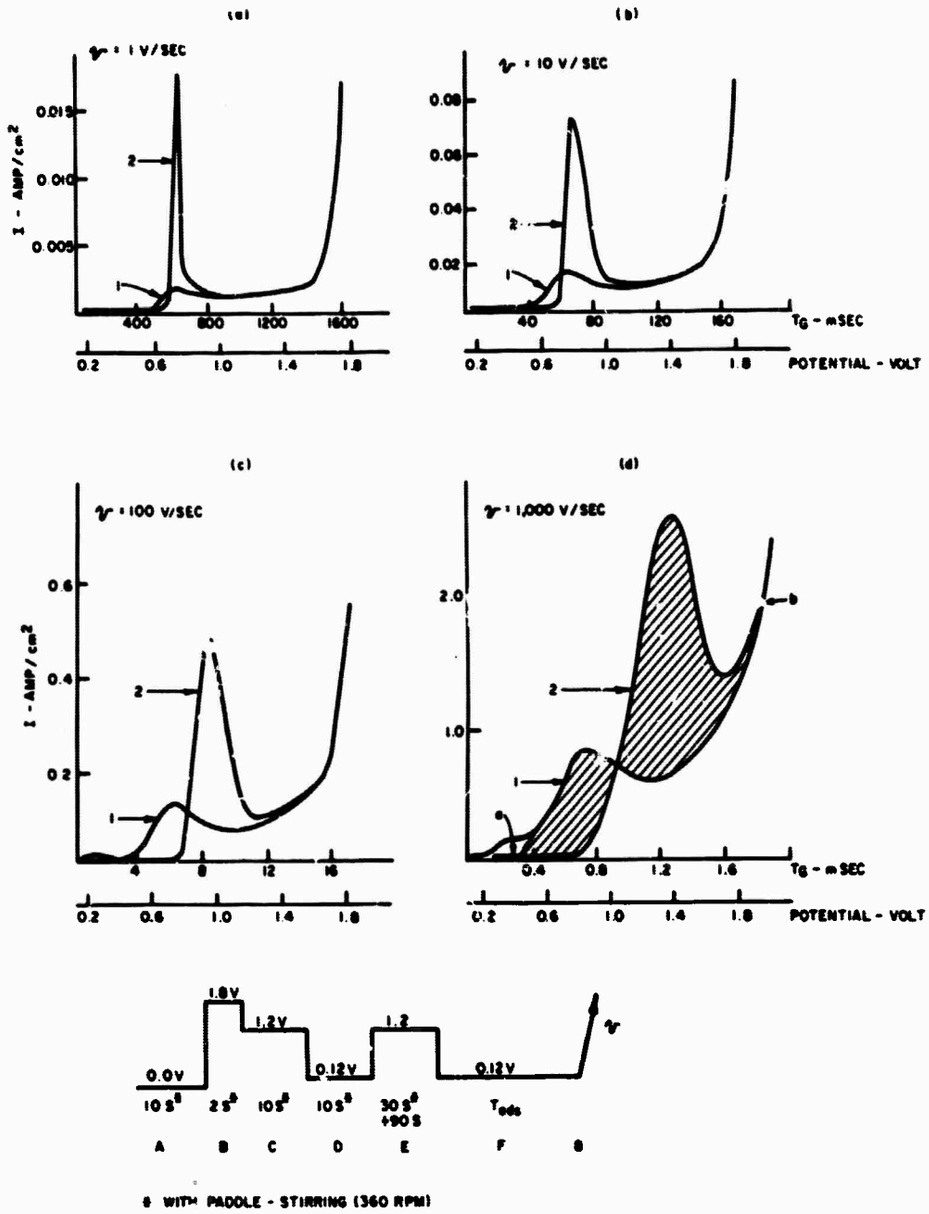

Figure 2.1-45. Determination of CO Adsorbed on Rh by Anodic Stripping. Adsorption occurred during step F and the traces were recorded during the linear anodic sweep (step G) of the sequence. Traces "1" were recorded after T_F = 0.1 sec in argon-saturated 4 N H_2SO_4. Traces "2" were recorded in electrolyte saturated with a gas mixture of 10% CO + 90% argon after adsorption for T_{ads} = 100 sec.

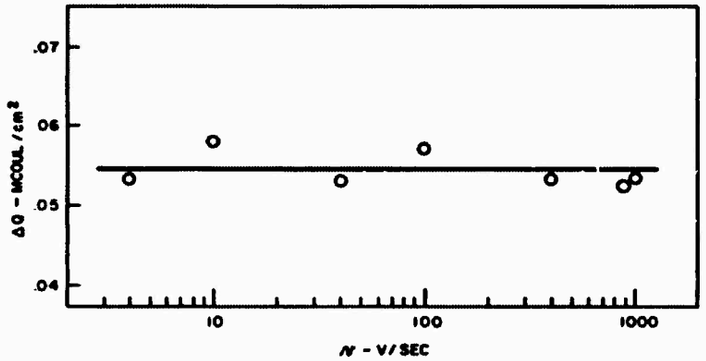

Figure 2.1-46. Frequency-Dependence of the CO Anodic Stripping Charge. The charge was determined from traces such as those of Figure 2.1-45d, where the charge is given by the difference of the two hatched areas.

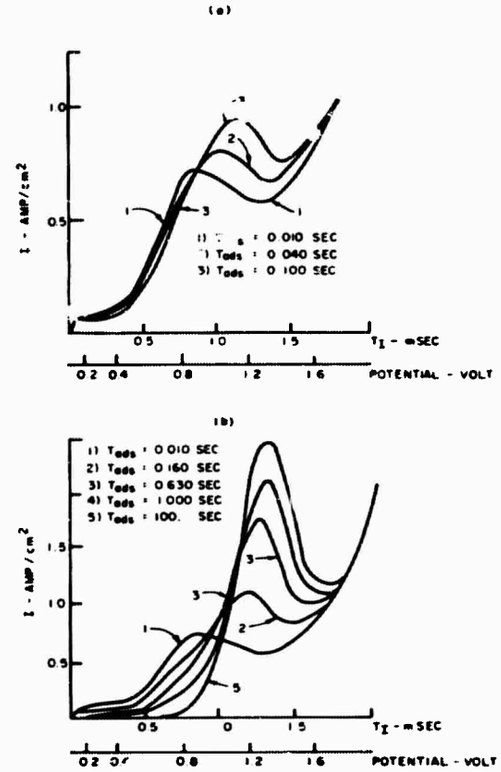

Figure 2.1-47. Determination of the CO Adsorption Rate by Anodic Stripping. Adsorption of CO occurred during step G of the sequence. Steps F and H were introduced to eliminate surface hydrogen and oxygen, and the traces were recorded during sweep I of the optential sequence. The 4 N H_2SO_4 was saturated with pure CO at 80°C.

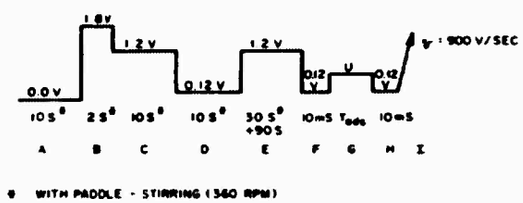

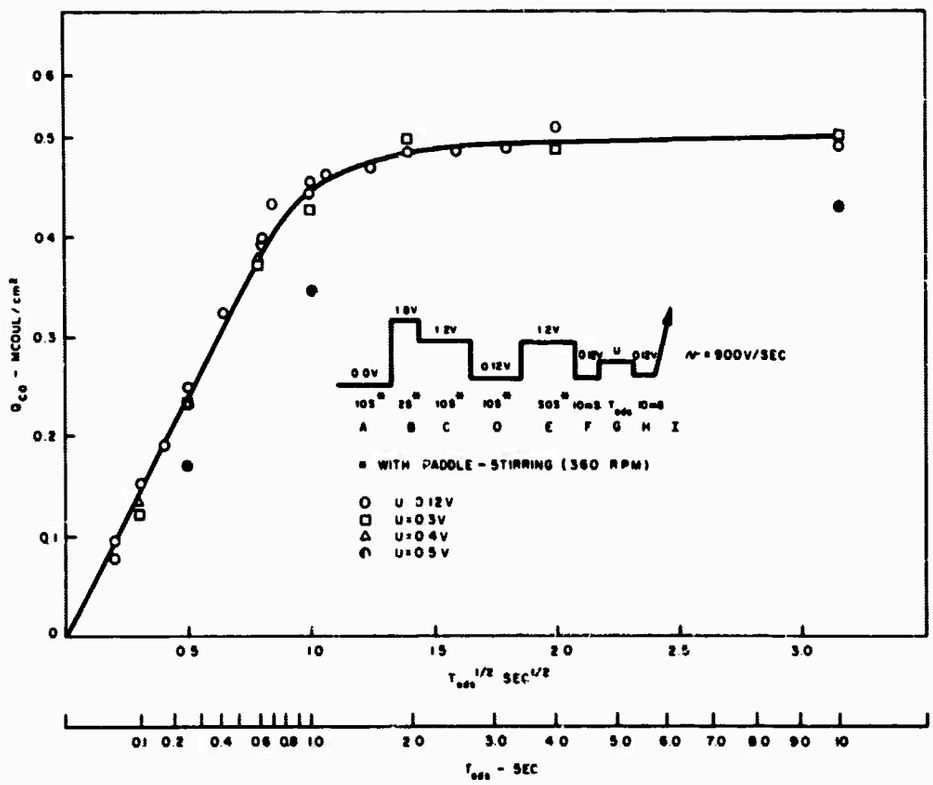

Figure 2.1-48. Adsorption of CO on Rhodium. Values of the anodic stripping charge, Q_{CO}, were determined from traces such as those of Figure 2.1-47 as CO adsorbed from a solution of 4 N H_2SO_4 saturated with pure CO. Fractional and absolute coverages of the electrode are directly proportional to Q_{CO}.

stirred solution (Figure 2.1-49). Traces corresponding to partial CO-coverage at various potentials are compared in Figure 2.1-50.

D. Discussion

A. Steady-State Oxidation of CO and Hydrogen

The polarization curves of Figure 2.1-42 are useful in establishing the approximate range over which the adsorbates of interest will be unstable with respect to oxidation. Results for the more extensively-studied Pt surface are included for comparison.

With hydrogen as depolarizer, a plateau current is observed for both Pt and Rh (Figure 2.1-42a and b), and corresponds to mass transport limitation. For Pt, the current declines above the potential (0.8 v) at which surface oxidation becomes significant. For Rh, the decline comes at a lower potential (0.6 v), corresponding to the tendency for the Rh surface to undergo oxidation at correspondingly lower potential (see trace 1 of Figure 2.1-43a). For both metals, the passivation effect becomes complete within a few tenths of a volt after the initial decline.

The curve obtained for CO on Pt (Figure 2.1-42d) is similar to that previously measured in perchloric acid (2.1-11). It differs markedly from the corresponding curve for H_2 on Pt, in that there is no plateau current, and in that the passivation occurs more gradually after the initial onset. A plateau current is lacking because by the time the overvoltage is sufficiently high for the sluggish oxidation of CO, oxidation of the surface has already begun, leading to passivation. The result is a peak current which is close to the expected mass transport limit. Because the surface is not completely passivated against CO oxidation until high potentials are impressed, a potential of 1.8 v has generally been used (2.1-11) in surface pretreatments when rates of adsorption were studied.

The curve for CO on Rh (Figure 2.1-42c) is similar to that for CO on Pt. One significant difference is that lower overvoltages are required for initial oxidation of CO. The initial passivation of the surface comes at a potential which is somewhat disproportionately lower than for Pt. The balancing effect of these two opposite tendencies is a peak current for CO oxidation which is somewhat smaller for Rh than for Pt. Another significant difference between CO oxidation on Rh and Pt is that the passivation effect on Rh is complete at significantly lower potentials than on Pt. The practical result is that surface pretreatment at only 1.2 v is satisfactory for holding off CO adsorption and oxidation in the studies of CO adsorption rates.

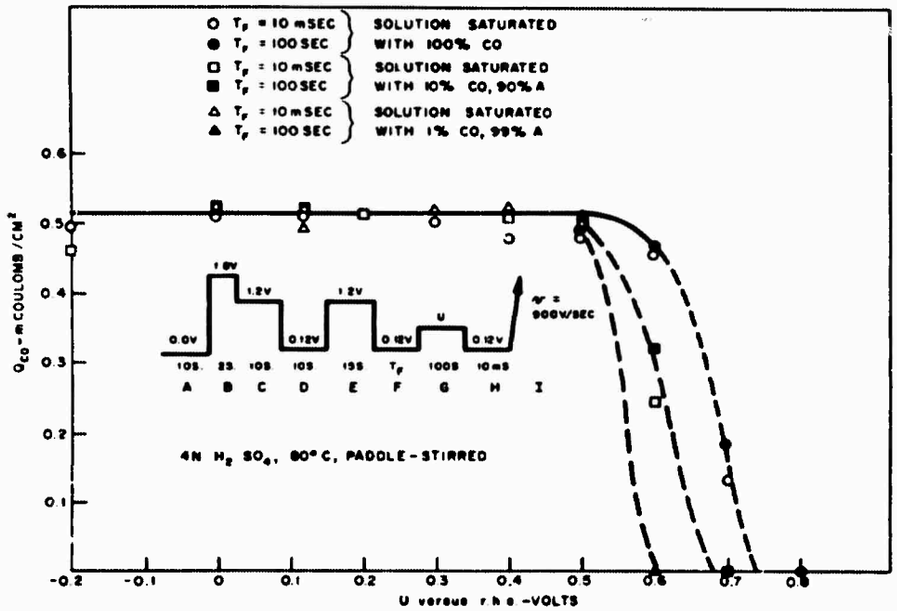

Figure 2.1-49. Steady-State Coverages of the Rh Electrode with CO. The coverage is directly proportional to Q_{CO} which was determined at potential U with or without pre-adsorption at 0.12 v (step F).

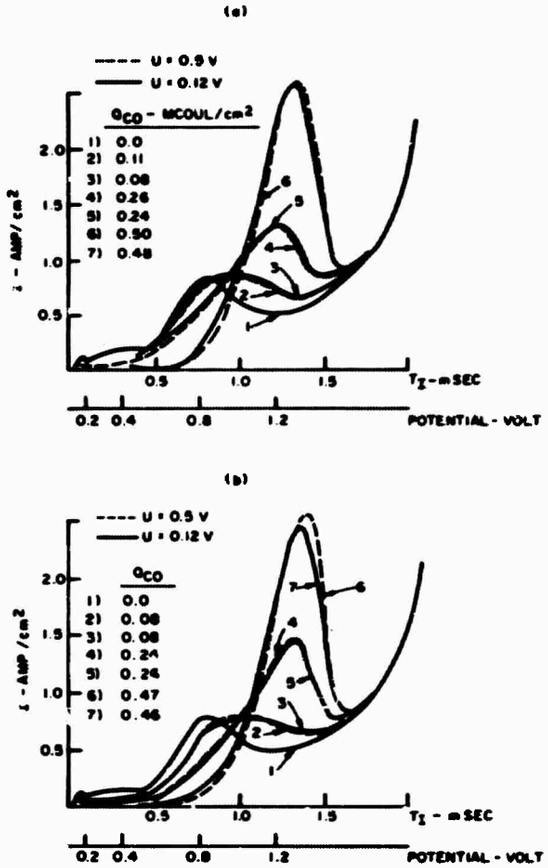

Figure 2.1-50. Comparison of the Linear Anodic Sweep Traces for a Rh Electrode Partially Covered with CO at Different Potentials. Traces were obtained at 0.12 v for increasing CO coverages and compared with traces obtained at the two extremes of potential and at approximately the same coverages.

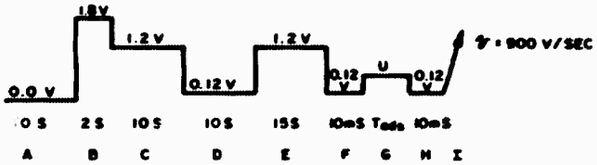

B. Preparation of a Reproducible Rh Surface

eriments similar to those of Figure 2.1-43 reveal that a reproducible surface state may be generated by anodic pulsing and that this state is stable over a period of time (up to 1000 sec) consistent with electrolytc purity. Judging from such traces, the surface state may be reproduced to within a few percent, over many months of experimentation, and many hundred cycles of pretreatment and measurement. An occasional electrode was found to undergo abrupt change in electrode area, and this is believed to have resulted from accidental exposure to a high-speed periodic triangular potential-time signal.

C. Measurement of CO Adsorption Rates

From Figure 2.1-48, it is evident that the plot of Q_{CO} vs. $T_{ads}^{1/2}$ is linear until approximately 80% of full coverage is achieved. Assuming conditions of linear diffusion for the short time involved, and assuming that the adsorption of CO is diffusion-controlled, then the relationship between charge and time must be (2.1-22):

$$\frac{d\,Q_{CO}}{d\,T_{ads}} = I_{ads} = \frac{nF\,D^{1/2}C}{T_{ads}^{1/2}\,\pi^{1/2}} \qquad (3)$$

or the integral expression:

$$Q_{CO} = \left(\frac{2\,n\,FD^{1/2}C}{\pi^{1/2}}\right) T_{ads}^{1/2} \qquad (4)$$

n = number of electrons required to oxidize and desorb one molecule of adsorbed CO.

F = Faraday constant

D = Diffusion coefficient of CO

C = Concentration of dissolved CO

The solubility of CO in water at 80°C is 7.62 cc/1 (S.T.P.). (See 2.1-23.) Making appropriate correction for the vapor pressure of 4 N sulfuric acid, and assuming the solubility of CO in the acid is the same as in pure water, $C = 2.02 \times 10^{-7}$ moles/cm^3. Assuming that n = 2 and that the slope of the linear portion of Figure 2.1-48 (0.48 mcoul/sec$^{1/2}$) is equal to the term in brackets of Equation 4, we deduce a value of D of 1.08×10^{-4} cm/sec. This is larger than the value deduced

(2.1-22) H.A. Laitinen and I.M. Kolthoff, J. Am. Chem. Soc. 61, 3344 (1939).

(2.1-23) "Solubility of Inorganic and Organic Compounds," Vol. 1, part 1, edited by H. Stephen and T. Stephen, Macmillen Co., N.Y., 1963, p. 364.

(2.1-11) at 30°C by a factor of 3.5. A factor of 2 (2%/°C) is reasonable (2.1-22) for the increased temperature. The additional factor of 1.7 could derive from an error of only 30% in estimating the solubility of CO. The evidence therefore strongly suggests that the adsorption of CO is initially diffusion-controlled at potentials lower than 0.5 v and that the method for determining the surface coverage is quantitative. At 0.5 v, according to Figure 2.1-48, the adsorption rate is smaller than that at lower potentials. This is probably due to the onset of significant CO oxidation at that potential.

D. Structure of the Adsorbed Layer

For an organic substance it is always possible that the parent molecule will undergo a major change in composition (bond-splitting, oxidation, or reduction) in the course of adsorption. Such a process might be expected to depend on the potential. To obtain an indication of structural variation of the adlayer, the sweeps for anodic stripping were compared at approximately equal values of the charge, Q_{CO}. From Figure 2.1-50, we see that the traces are almost identical for potentials extending from - 0.2 to 0.5 v, suggesting constant structure of the adlayer over this wide potential range. For CO on Pt, the results were similar, except that some variation was suggested at very low (-0.2v) potential (2.1-24).

E. Steady-State Surface Coverage of Rhodium with CO

The absolute coverage, Γ_{CO} (moles/cm^2), of the surface is related to the charge Q_{CO} by:

$$Q_{CO} = 2F\,\Gamma_{CO} \tag{5}$$

Values of Q_{CO} were determined over a wide range of potentials and of CO concentrations (Figure 2.1-49). Up to 0.5 v the coverage is essentially constant over the entire range of CO concentrations, and independent of whether or not CO was pre-adsorbed on the electrode at 0.12 v. Above 0.5 v, the results do depend on the concentration of CO and steady-state is somewhat sluggishly established (the mean of the value achieved with and without pre-adsorption at 0.12 v). It seems reasonable to conclude that for this highly irreversible chemisorption, there is the tendency for full monolayer coverage over the entire range of concentrations and potentials, and that only the opposing rate of oxidation of CO to CO_2 tends to drive the coverage down at high potentials.

(2.1-24) S. Gilman, J. Phys. Chem. 70, 2880 (1966).

2.1.5.2 Mixed Adsorption of CO and Hydrogen

A. Introduction

In Section 2.1.5.1, it was shown that CO adsorption on rhodium may be studied in a quantitative manner (by anodic stripping) if a "multipulse potentiodynamic" sequence is used to establish reproducible initial conditions. In this section, comparisons will be made between the amount of CO and of hydrogen atoms co-adsorbed under dynamic conditions.

B. Experimental

Chemicals and equipment were as previously described. The rhodium test electrode was similar to the one used previously. It had a geometric area of 0.08 cm^2, and the charge, ${}_SQ_H$, corresponding to "saturation coverage" with hydrogen atoms had the value 0.23 $mcoul/cm^2$. The "roughness factor" for this electrode was 1.06 if ${}_SQ_H$ = 0.22 $mcoul/cm^2$ is taken to correspond to R.F. = 1.0. As previously all values of current and of charge will be reported on the basis of the geometric area. All measurements were made at 80°C in a 4 N H_2SO_4 electrolyte.

C. Procedures and Results

1. Determination of CO Coverage Through Anodic Stripping

In a solution saturated with CO, the adsorption occurs within 1 second. Under those conditions, the adsorption is diffusion-controlled until approximately 80% complete and exhibits a linear dependence on the square root of time. A linear dependence on the first power of time may be obtained by using a more dilute solution of CO and by agitating the solution, as in the experiments of Figure 2.1-51. The results of Figure 2.1-51 show the desired dependence of surface coverage (proportional to Q_{CO}) upon adsorption time for potentials less than 0.5 v, and for coverages less than approximately 0.8.

2. Determination of "Saturation Coverage" with Hydrogen Atoms

The sequence of Figure 2.1-52 was used in determining the charge, ${}_SQ_H$, corresponding to saturation coverage of the surface with hydrogen atoms. As previously discussed, steps A-E of the potential sequence serve to cleanse the surface and to protect it against adsorption of or reaction with a dissolved adsorbate. During step F, the protective "oxygen" film is reduced and dissolved materials may adsorb. Step G quickly eliminates adsorbed hydrogen. In step H, hydrogen atoms are deposited on the surface and the corresponding cathodic current is recorded. Trace 1 of Figure 2.1-52 was obtained in argon-saturated electrolyte. The current which flows up to point b corresponds mainly to deposition of atomic hydrogen, but also contains contributions to

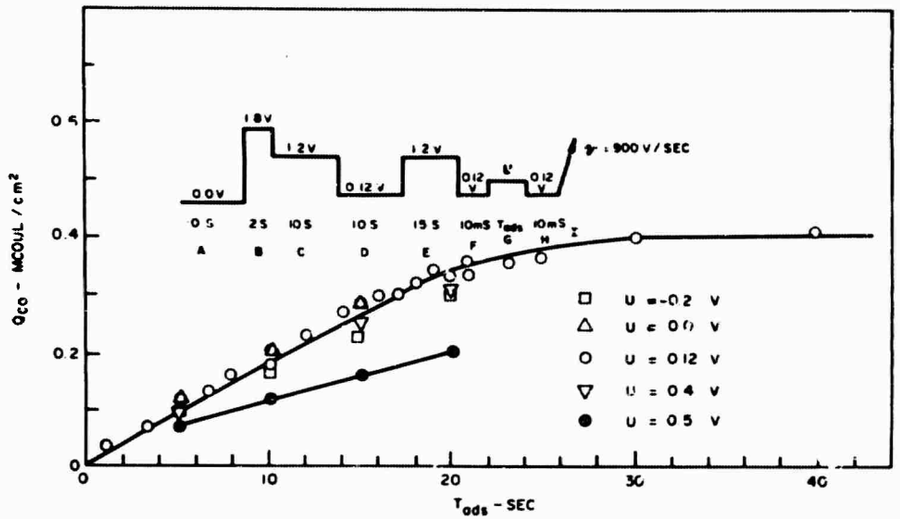

Figure 2.1-51. Adsorption of CO on Rh from a Stirred Solution. The adsorption occurred during step G of the potential sequence. Values of Q_{CO} were determined by application of sweep I. Relative and absolute coverages are directly proportional to Q_{CO}. The 4 N H_2SO_4 solution was saturated with a gas mixture of 1% CO, 99% argon at 80°C. The paddle-stirrer was rotated at 360 rpm.

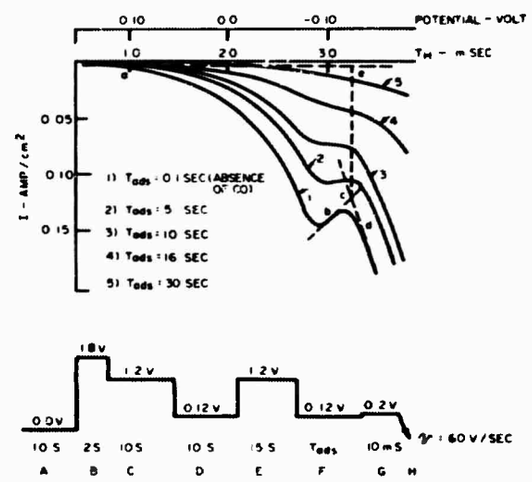

Figure 2.1-52. Determination of Saturation Coverage with Hydrogen Atoms on a Surface Partially Covered with CO. The adsorption of CO occurred during step F, from 4 N H_2SO_4 saturated with a gas mixture of 1% CO, 99% argon (except 100% argon for trace 1). Traces of hydrogen were removed during step G, and hydrogen was redeposited to saturation during sweep H. The construction lines of trace 1 serve to define a closed area corresponding to the hydrogen charge.

charging of the ionic double layer and to evolution of molecular hydrogen gas. Past point b the current becomes steeply cathodic corresponding to a sharply increasing rate of H_2 evolution. For Rh, the rates of hydrogen atom deposition and H_2 evolution are significantly sluggish so that the potentials of the cathodic trace have no simple thermodynamic significance at this sweep speed.

Assuming that the hydrogen atom monolayer is approximately complete before gas evolution becomes very rapid, we may attempt to derive the corresponding charge by means of the construction lines on trace 1 of Figure 2.1-52. The vertical line ae was drawn from the point of intersection of tangents bc and dc. The line ae was drawn as an extrapolation of the capacitive current measured above 0.1 v. The area aecba is taken as ${}_SQ_H$. Keeping v constant at 60 v/sec, ${}_SQ_H$ was measured for values of T_{ads} from 0.01 to 100 sec in the argon-saturated solution. This charge was found to maintain the average value of 0.23 mcoul/cm^2 with an average deviation of 3%. At much longer values of T_{ads} or when the solution was agitated, ${}_SQ_H$ was found to decrease. This corresponded to the adsorption of impurities, as already detected through anodic stripping. Keeping T_{ads} constant at 1 sec, and varying v from 10 to 1000 v/sec, ${}_SQ_H$ was again found to remain constant with an average deviation of 5%.

The effect of CO adsorption upon ${}_SQ_H$ was examined in traces 2 - 6 of Figure 2.1-52. As in previous studies (2.1-25), it was ascertained that the cathodic sweep caused no desorption of adsorbed CO. For the CO - containing solution, values of ${}_SQ_H$ are plotted against the adsorption time in Figure 2.1-53.

3. Determination of Hydrogen Atom Coverage by Anodic Stripping

At any potential, the charge corresponding to transient hydrogen-coverage may be determined by application of a linear anodic sweep. In the sequence of Figure 2.1-54, steps A-E serve as electrode pre-treatment. The surface is quickly reduced at potential U (step F) and hydrogen atoms are quickly adsorbed on the clean surface. There is subsequent slow desorption of hydrogen as CO adsorbs from solution. The amount of hydrogen present at any moment may be determined by applying sweep H and recording the resulting current-time transient. Trace 1a was obtained for T_{ads} = 0.1 sec and corresponds to the essentially clean surface. The initial current maximum corresponds mainly to the stripping of adsorbed hydrogen. After the minimum, the current rises again as both the surface and adsorbed CO are oxidized. To correct for the non-hydrogen currents, trace 1b was measured after applying step G which quickly eliminates adsorbed hydrogen. Trace 1b was back-extrapolated (c-a) to correct for capacitive charging and the resulting closed area

(2.1-25) S. Gilman, J. Phys. Chem. 67, 78 (1963).

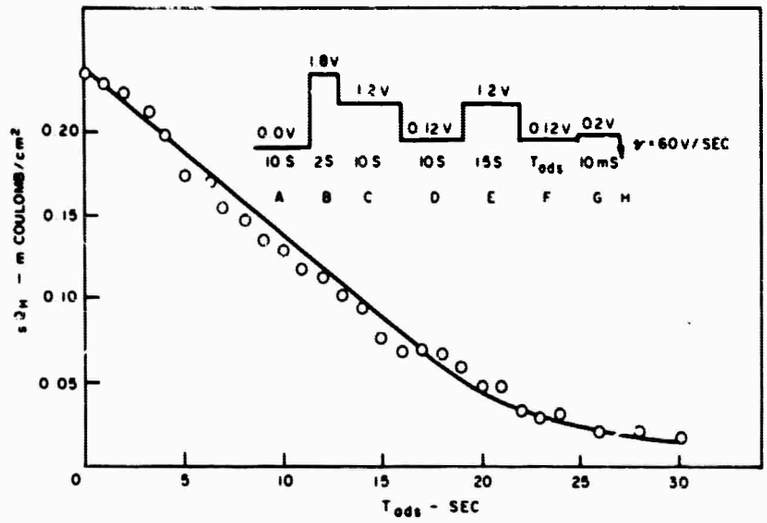

Figure 2.1-53. Variation of Saturation Coverage with Hydrogen as CO is Adsorbed on Rh. The saturation coverage with hydrogen is proportional to the charge, $_SQ_H$, and was determined from traces such as those of Figure 2.1-52. The accumulation of CO is given by Figure 2.1-51. The 4 N H_2SO_4 solution was saturated with a gas mixture of 1% CO, 99% argon at 80°C, and paddle-stirred (360 rpm) throughout the experiment.

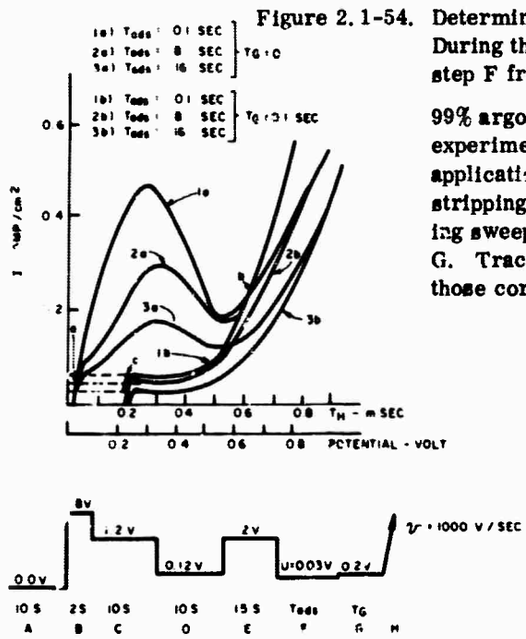

Figure 2.1-54. Determination of the Hydrogen Atom Coverage at Potential U, During the Adsorption of CO. The adsorption occurred during step F from 4 N H_2SO_4 saturated with a gas mixture of 1% CO, 99% argon which was paddle-stirred (360 rpm) throughout the experiment. Traces "a" were measured during step H without application of step G, and include a current corresponding to stripping of adsorbed hydrogen. Traces "b" were obtained during sweep H, after previously removing hydrogen during step G. Traces "b" serve as a correction for currents other than those corresponding to stripping of hydrogen.

abca defines Q_H. Traces 2 and 3 show how Q_H may also be determined when the surface is largely covered with CO. Values of Q_H were obtained both in the CO - free (Figure 2.1-55) and CO - containing solution (Figure 2.1-56).

D. Discussion

1. Structure of the CO Adlayer

From Figure 2.1-51, the absolute coverage, Γ_{CO}, under transient conditions may be obtained:

$$Q_{CO} = 2F\,\Gamma_{CO} \tag{6}$$

It is seen that the rate of adsorption (which is mass transport controlled up to large coverages) is independent of potential over the entire range of hydrogen adsorption (below 0.15 v). Decreased rates of adsorption above 0.5 v are probably entirely due to the competitive oxidation of CO to CO_2. Under the same conditions, Figure 2.1-53 reveals how ${}_SQ_H$ varies with CO adsorption. For ${}_SQ_H$, the following relationship may hold:

$${}_SQ_H = F\,{}_S\Gamma_H = F\left(\left({}_S\Gamma_H\right)_o - m\,\Gamma_{CO}\right) \tag{7}$$

where ${}_S\Gamma_H$ = "saturation coverage" (moles/cm^2) of the surface with H atoms in the presence of some adsorbed CO

$\left({}_S\Gamma_H\right)_o$ = "saturation coverage" of the surface with H atoms in the absence of adsorbed CO.

m = number of hydrogen sites obscured per molecule of CO adsorbed.

Dividing the slope of the plots of Figures 2.1-53 and 2.1-51 gives the value of m at any instantaneous value of the coverage with CO. With some scatter, m was found to have a constant value of 0.9 until the coverage is almost complete. This implies that one adsorbed CO molecule occupies one hydrogen adsorption site. This situation contrasts with that found for Pt at lower temperature (2.1-25). In the latter case, the results suggested that each adsorbed CO molecule occupies two hydrogen adsorption sites ("bridged" structure) in the earlier stage of adsorption, and only one site ("linear" structure) in the later stage of adsorption. These analyses assume, of course, that CO and hydrogen adsorption sites are similar, and that hydrogen adsorption is blocked in only a direct manner by the formation of the surface-organic bond.

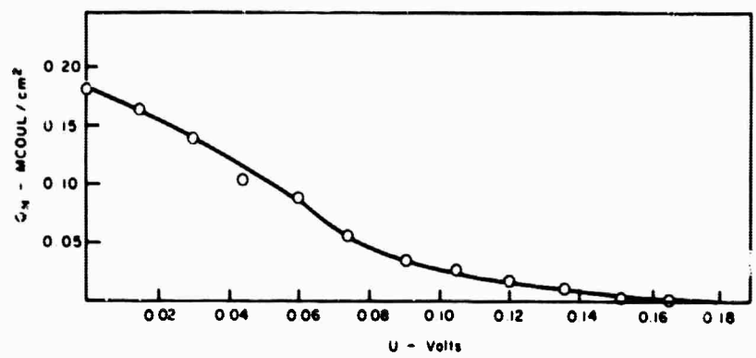

Figure 2. 1-55. Hydrogen Coverage on a Clean Rh Electrode. The hydrogen coverage is proportional to the charge Q_H, measured in the argon-saturated electrolyte by the method of Figure 2. 1-54.

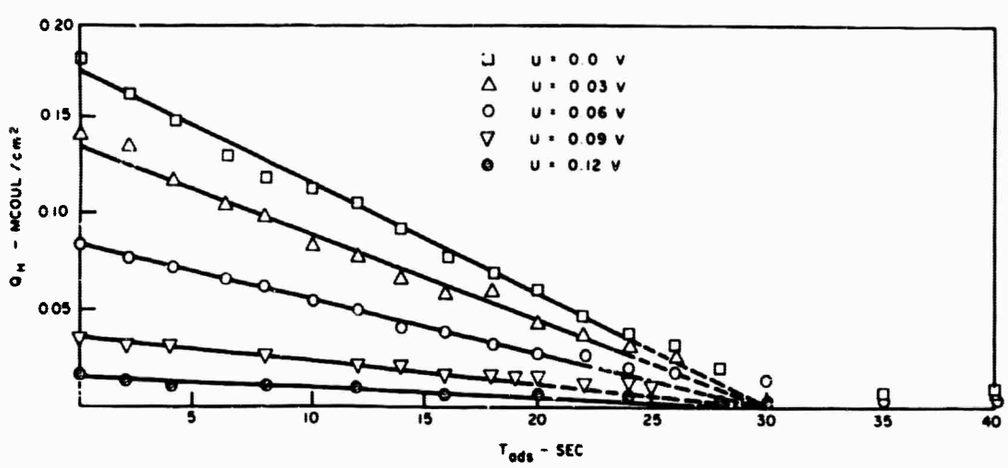

Figure 2. 1-56. Hydrogen Coverage on an Rh Electrode Partially Covered with CO. The charge Q_H was measured by means of the procedures of Figure 2. 1-54 while CO was adsorbing from 4N H_2SO_4 saturated with a gas mixture of 1% CO, 99% argon (80°C), paddle-stirred at 360 rpm. The accumulation of CO under the same circumstances is given by Figure 2. 1-51.

2. The Hydrogen Adsorption Isotherm and CO Adsorption

The plot of Figure 2.1-55, obtained in argon-saturated electrolyte, is similar to that obtained by Will and Knorr (2.1-26) and by Bold and Breiter (2.1-27) by integration of slow periodic triangular potential-time sweeps. The abscissa of Figure 2.1-55 might alternatively be represented in units of the logarithm of hydrogen partial pressure (through the Nernst equation) and hence the plot is an experimental adsorption isotherm. Such isotherms have been studied in detail by Bold and Breiter (2.1-27), who found that the apparent heat of adsorption of hydrogen decreases irregularly with increasing hydrogen coverage. Such an observation suggests heterogeneity of the surface. Such heterogeneity may generally be "original" (corresponding to such structural variations as imperfections, crystal orientations, etc.) or "induced" (caused by the very act of adsorption).

Figure 2.1-56 shows that the hydrogen coverage at any fixed potential drops off linearly with increasing time (and hence increasing coverage with CO, according to Figure 2.1-51) until high coverages are achieved. The empirical relationship followed for coverages less than approximately 80% of maximum is:

$$\theta_H = \left(\theta_H\right)_o \left(1 - \frac{\theta_{CO}}{1.4}\right) \tag{8}$$

where: θ_H = fractional coverage with hydrogen atoms = $Q_H/{}_SQ_H$

$\left(\theta_H\right)_o$ = θ_H in absence of adsorbed CO

θ_{CO} = fractional coverage with CO = $Q_{CO}/\left(Q_{CO}\right)_{maximum}$

The significance of the factor 1.4 in Equation 8 is that (according to the extrapolations of Figure 2.1-56) θ_H would drop to zero only if the surface coverage with CO exceeded by 40% the maximum amount observed in Figure 2.1-51. From Equation 8 it must be concluded that the adsorption isotherm retains its original form when CO adsorbs, i.e., that there does not appear to be preferential CO adsorption on sites with the highest heats for hydrogen adsorption. This may be interpreted in two different ways. One possibility is that "original" heterogeneity leads to no significant differences in the heats of adsorption of CO on various sites. A surface partially covered with CO simply acts as if the effective area had been decreased and retains the same adsorption isotherm. The alternative is that heats of adsorption do vary over the surface due to original heterogeneity, but

(2.1-26) F. Will and C. Knorr, Z. Elektrochem. 64, 258, 270 (1960).

(2.1-27) W. Bold and M. Breiter, Z. Elektrochem. 64, 897 (1960).

under conditions of mass transport controlled adsorption there is a completely random distribution of CO molecules over the various sites. Due to immobile adsorption, there is no subsequent re-distribution of adsorbed CO according to the heats of adsorption of the surface sites. Hence, a random distribution of CO molecules is retained as is the form of the original hydrogen adsorption isotherm.

E. Conclusions

Polarization curves for oxidation of hydrogen and CO on Rh are similar to those for Pt. One major difference is that the passivation of CO and H_2 oxidation occurs at lower potentials for Rh than for Pt, corresponding to earlier oxidation of the Rh surface. A second major difference is that the oxidation of CO occurs at lower potentials on Rh than on Pt. The difference in reactivities for CO on the two metals might be understood through careful study of the adsorption of CO and of the oxidation of adsorbed CO. The adsorption process for Rh was examined in this work.

The adsorption of CO on Rh was found to be diffusion controlled from -0.12 to 0.5 volt. Over the same range of potentials, the steady-state coverage with CO (based on hydrogen-codeposition measurements) was found to correspond approximately to a monolayer of singly-bound CO molecules. At higher potentials the coverage decreases (presumably due to competitive oxidation of CO to CO_2) and the coverage depends on the partial pressure of CO. Over the entire range of potentials, the evidence suggests that the structure of the CO adlayer remains constant.

At any potential in the hydrogen region, the (reversible) fractional hydrogen coverage decreased linearly with increase of CO coverage. This dependence does not vary with potential. This implies that CO does not adsorb preferentially on "active sites" under the (diffusion-controlled) conditions of these experiments.

2.2 MULTI-COMPONENT FUELS

2.2.1 Extended Life Tests With Multi-Component Fuels (Unsupported Platinum Anodes)

(J. Lennon, E. Luksha, E. Weissman)

In the previous report (2.2-1) certain long-term aspects of the electrochemical oxidation of multi-component fuels were presented. It was found that several additives, up to 5 mole % naphthenes, 5 mole % olefins, and 1 mole % aromatics do not affect anode performance on a cumulative detrimental basis for extended periods of operation. It was also shown that the overall decrease in anode performance can be intolerably severe if the abovementioned concentrations are exceeded.

This report represents a completion of the work on multi-component fuels started during the previous report period (2.2-1). The concentrations of the "unreactive" components studied was extended up to 50 mole % in an effort to determine whether the tolerance to certain species changes in the presence of high concentrations of others. These tests were conducted directly on a long-term basis since no further short-term screening was needed. In addition, some uncertainties in the previous data, especially those involving methylcyclopentane, were studied in further detail.

2.2.1.1 Experimental

The experimental apparatus used in this investigation was described in an earlier report (2.2-2). The electrodes, both anode and cathode, contained 35 mg Pt/cm^2 (85 wt % Pt-15 wt % TFE) on gold-coated tantalum screens for anodes and platinum screens for cathodes.

The following procedure was used for the collection of the experimental data. After establishing the desired gas flow rates, usually 20 μ l fuel/min. corresponding to 10 times the stoichiometric octane requirement at 1.0 amp and 10 times the stoichiometric requirements of oxygen (from air), and isothermal conditions (350°F), an open-circuit potential was recorded and data for an initial polarization curve were obtained. Thereafter, the cell was maintained at 1.5 amps (30 ASF) and the cell potential and current were continuously recorded on dual-channel strip chart Varian recorders. IR-free potential data were obtained by means of a Kordesch-Marko bridge.

The circulating electrolyte was maintained at 95-98% H_3PO_4 by means of controlled addition of water to the electrolyte sump.

(2.2-1) Technical Summary Report No. 9, Hydrocarbon-Air Fuel Cells, 1 Jan-30 June 1966, ARPA Order No. 247, Contract DA44-009-AMC-479(T), p. 2-121 ff.

(2.2-2) Technical Summary Report No. 5, Hydrocarbon-Air Fuel Cells, Jan-June 1964, ARPA Order No. 247, Contract DA44-009-ENG-479(T).

Polarization curve data points, usually obtained at the end of each experiment and at prescribed intervals, were taken by first activating the anodes to greater than 0.90 volt vs. H_2/H^+ and waiting for the cell output to stabilize (usually 3 to 4 minutes). In this way, cycling disturbances were avoided. A more thorough description of the life testing procedure was given earlier (2.2-1).

During this report period, 27 life tests of different fuel cells with "unreactive" components were performed. The fuels tested are listed in Table 2.2-1.

2.2.1.2 Interpretation of Test Data

Generally, in all tests with octane-based fuels, four distinctly different periods of operation were observed:

1. Induction period
2. Ripple period
3. Onset-of-cycling period
4. Cycling period

A detailed description of these various modes of operation was described previously (2.2-1). Two exceptions from this generalized four-step sequence were noted, when there was no cycling at all. First, when anode performance penalties produced anode potentials in excess of 680 mv (H_2/H^+). This result was to be expected in view of previous results on anode performance at high potentials (2.2-1).

The second, and more important exception, was noted when anodes were operated on fuels containing high concentrations of methylcyclopentane. The absence of cycling and the unusually good performance for these types of fuel will be described in the following section.

The life test data was interpreted using the same rationale established in the previous report (2.2-1, pg. 2-123). The anode performance effects of the various additives were compared after an initial 25-hour period. Measurements after longer periods of time would have included the bias contributed by electrode structure deterioration.

2.2.1.3 Results and Discussion

The long-term tests of the fuels listed in Table 2.2-1 were made in order to corroborate existing data and obtain additional information regarding the performance of multi-component fuels. For comparison with n-octane, see Ref. 2.2-1, pg. 2-124ff. Detailed tabulations and graphical representation of all the life tests are given in Appendix 4.3. The following are summaries of each category of t[illegible].

Table 2.2.1

Summary of Life Test Data

	Cell No.	Fuel	Time, hr	C.D., A/ft²	P.D., w/ft²	Anode vs. H_2 H^+ D.C. Potential, volt	Resistance, ohm
A	183	1% toluene 5% octene-2 5% MCH* 15% MCP** 74% iso + n-octane	2 18	30 60 15	10.5 17.4 0.0	0.420 0.515 >1.0	0.006
	205	1% toluene 5% octene-2 5% MCH 15% MCP 74% iso + n-octane	1 168 	30 60 30 20	12.0 16.4 0.0 7.2	0.440 0.540 >1.0 0.410	0.010
B.	204	1% toluene 5% octene-2 15% MCH 30% MCP 49% n-octane	1 168 	30 60 30 20	11.8 14.7 6.0 5.0	0.465 0.580 0.500 0.815	0.008
C.	182	5% toluene 10% octene-2 10% MCH 30% MCP 45% iso + n-octane	1 	30 60	4.5 4.5	0.700 0.730	0.010
	184	-ibid-	1 144	30 60 30 10	9.9 16.8 0.0 1.0	0.500 0.310 >1.0 0.800	0.006
	107	5% toluene 5% octene-2 5% MCH 15% MCP 70% n + iso-octane	1 30 	30 60 30 15	8.1 12.0 0.0 3.5	0.580 0.590 >1.0 0.920	0.010
D.	160	7% toluene 93% n-octane	1 144	30 60 30 60	9.2 9.9 6.9 0.0	0.510 0.610 0.440 >1.0	0.010
	195	10% toluene 90% n-octane	1 130	30 60 30 20	6.8 7.8 0.0 2.4	0.625 0.715 >1.0 0.766	0.010
	206	10% toluene 90% n-octane	1	30	7.4	0.570	0.010
	201	5% octene-2 95% n-octane	1 	30 60	14.0 23.8	0.360 0.440	0.007
E.	207	5% octene-2 95% n-octane	30	30	9.0	0.500	0.011
	211	5% octene-2 95% n-octane	1 72	30 30 60	11.7 11.5 18.5	0.520 0.530 0.500	0.010
F.	199	10% MCH 90% n-octane	1 179	30 60 30 30	9.0 14.4 1.1 3.0	0.520 0.550 0.590 0.700	0.010
	192	10% MCH 90% n-octane	1 350	30 60 30	7.9 0.0 7.2	0.565 1.0+ 0.600	0.010
	198	15% MCH 85% n-octane "	1 165	30 60 30 60	10.8 14.4 9.5 6.0	0.500 0.600 0.560 0.050	0.010
	193	20% MCH 80% n-octane	1 	30 60	9.4 13.8	0.520 0.550	0.008
	197	20% MCH 80% n-octane	1 142	30 60 30 60	10.2 12.0 6.9 0	0.505 0.910 0.020 >1.0	0.010
	196	30% MCH 70% n-octane	1 143	30 60 30 60	8.3 11.4 3.4 3.0	0.840 0.590 	0.008
	202	50% MCH 50% n-octane	1 	30 60	9.0 0	0.570 >1.0	0.007
	203	70% MCH 30% n-octane	1 95	30 60 30 60	8.7 7.2 3.0 0.0	0.370 0.075 0.750 >1.0	0.010
G.	191	30% MCP 70% n-octane	1 284	30 60 30 60	14.1 21.6 11.9 19.8	0.365 0.450 0.440 0.500	0.010
	194	50% MCP 50% n-octane	1 040	30 60 30	14.7 22.5 4.0	0.360 0.423 0.600	0.009
H.	212	10% MCH 20% MCP 70% n-octane	1 45	30 60 30 60	9.4 10.2 8.1 2.8	0.545 0.450 0.580 0.770	0.010
	210	20% MCH 40% MCP 40% n-octane	1 98	30 60 30 60	0.4 10.8 0.0 0.0	0.550 0.010 0.050 >1.0	0.012

* MCH - Methylcyclohexane
** MCP - Methylcyclopentane

A. 74% Iso + n-octane + 15% methylcyclopentane + 5% octene - 2 + 5% methylcyclohexane + 1% toluene

It has been shown (2.2-1) that additions not exceeding 1 mole % aromatics, 5 mole % olefins, and 5 mole % naphthenes did not affect anode performance by more than a 50 mv penalty to the polarization obtained when oxidizing pure n-octane. This conclusion had been demonstrated on the basis of four separate tests, of an average duration of 124 hours. Specifically, the additives tested were: 1 mole % toluene, 5 mole % octene-2, and 5 mole % methylcyclohexane. It will be recalled that addition of 15% methylcyclopentane to this fuel resulted in an unexpected additional anode performance penalty of 40 mv. On the basis of no performance penalty for 15 mole % methylcyclopentane, when present as a single additive, or good performance when run pure (slightly better than n-octane), this extra 40 mv polarization was rather unexpected.

To further check this point, two additional cells were operated on this particular fuel combination. At the end of the initial 25 hour period, the DC anode vs. H_2/H^+ potential was greater than 625 mv at 30 ASF in both cases. The previous two tests showed DC anode voltages of 640 mv under similar circumstances. It is noted that the 1 mole % toluene, 5 mole % octene-2, 5 mole % methylcyclohexane combination produced anode potentials ranging from 580-600 mv vs. H_2/H^+. The added performance penalty discussed above has therefore been confirmed by the latest results.

B. 49% n-octane + 30% methylcyclopentane + 15% methylcyclohexane + 5% octene-2 + 1% toluene

A fuel consisting of 1 mole % toluene, 5 mole % octene-2, 15 mole % methylcyclohexane, 30 mole % methylcyclopentane, with n-octane brought the DC anode potential, at 30 ASF, to 660 mv vs. H_2/H^+ after an initial 25 hour period. Initial power density was greater than 10 WSF. However, as with other high-percent additives (except methylcyclopentane when taken as a single additive) performance decayed to less than 6.[illegible] after the initial 25 hours of operation. The cycling pattern followed the sequence described in Section 2.2.1.2.

C. 70% n + iso-octane, + 5% toluene + 5% methylcyclohexane + 15% methylcyclopentane + 5% octene-2

This cell was run with the relatively high concentration of aromatics, 5 mole %. As was to be expected, initial performance was low (~8.0 WSF at 30 ASF) and it decreased abruptly after 1 hour (< 6.0 WSF at 30 ASF); after 25 hours the cell would not support 30 ASF. During its operation the cell cycled as described in Section 2.2.1.2. DC anode potential vs. H_2/H^+ after 15 hours was 700 mv.

D. 93% n-octane + 7% toluene

This cell was operated in order to investigate long relative reactivity effects at higher concentrations of aromatic additives to a base octane fuel. The initial performance was low (9.2 WSF at 30 ASF) and decreased with time. After one hour the power output decreased to approximately 7.0 WSF and after 25 hours to approximately 6.0 WSF. After 150 hours the DC anode potential vs. H_2/H^+ was 650 mv. "Typical" cycling was apparent throughout the test.

90% n-octane + 10% toluene

Two more cells were operated with 10% toluene as a single additive. Initial performance in both cases was approximately 7.0 WSF. Performance decreased abruptly within one hour to $<$ 5.0 WSF and after five hours to approximately 3.0 WSF. In both cases, DC anode potential vs. H_2/H^+ was greater than 730 mv. At these potentials, no cycling was present, as expected from previous findings on the subject (2.2-1, pg. 2-171).

E. 95% n-octane + 5% octene-2

Three tests were conducted using 5 mole % octene-2 as a single additive. In two of the tests, the DC anode potential did not exceed 600 mv vs. H_2/H^+ at 30 ASF after the initial 25 hours had elapsed. The other did exceed 650 mv vs. H_2/H^+ reference during the initial 25 hours (as great as 650 mv after 20 hours). There was no immediate explanation of this variation from expected performance. All of the cells exhibited good initial performance (12.3 WSF at 30 ASF average). One decayed to approximately 7.5 ASF after the initial 25 hours of operation. Cycling occurred in the previously described sequence in all cases.

F. n-octane with 10-70% methylcyclohexane

In this series of tests, varying additions of methylcyclohexane were evaluated. A plot of the IR-included anode potential vs. H_2/H^+ indicates a linear trend of performance degradation with an increase in the concentration of methylcyclohexane in the fuel (Figure 2.2-2). Initial performance varied from 8.0 - 10.0 WSF at 30 ASF and the rate of performance decay appeared to increase with an increase in the naphthene concentration. Interestingly enough, cycling was absent only for the case of 70 mole % methylcyclohexane, although the DC anode potentials for the naphthene concentration range 30-70% were all higher than 650 mv within several hours after the start of a given run.

G. n-octane with 30-50% methylcyclopentane

One of the interesting results obtained in the two tests, was the performance of fuels containing relatively large amounts of methylcyclopentane. In both instances, the DC anode potentials

did not rise above 580 mv vs. H_2/H^+ at 30 ASF after the initial 25 hours of operation. Furthermore, no cycling was evident in either test.

The cell fed with 50 mole % methylcyclopentane was operated in excess of 500 hours with no cycling and with a maximum DC anode potential of 630 mv vs. H_2/H^+ at 30 ASF.

H. n-octane with 20-40% methylcyclopentane in the presence of 10-20% methylcyclohexane

As indicated in Table 2.2-1, two tests were conducted in this category. The initial performance of both cells was similar (approximately 9 WSF at 30 ASF) and after 25 hours both cells reached a DC anode potential of 680 mv vs. H_2/H^+ at 30 ASF. As expected, there was no cycling under these conditions.

I. General

The overall results of these tests appear to confirm the fact that while anode operation is possible with a great variety of additives over a relatively wide range of concentrations, the performance penalty will be severe at higher concentrations of additive. The only desirable byproduct of this situation is the absence of performance cycling. This is represented in Figure 2.2-1 where DC anode potential measured after the initial 25 hours of testing is plotted vs. mole % addition to the base octane fuel. For more than 1 mole % toluene, 5 mole % octene-2, and 5 mole % methylcyclohexane, it is seen that there is an increase in performance penalty with any additive including methylcyclopentane.

A plot of anode potential after 25 hours is presented in Figure 2.2-2 for various concentrations of single additives (naphthenes). A similar performance degradation trend is observed for increasing additive concentrations.

2.2.1.4 Conclusions

It has been shown that a platinum-catalyzed fuel cell anode, operating at steady-state on octane at temperatures of the order of 350°F with concentrated phosphoric acid as an electrolyte, can tolerate a much greater variety of types and concentrations of organic fuel additives than previously thought possible.

A remarkable feature of the results of the test program described here is the high reactivity of methylcyclopentane, when taken as a single additive to n-octane. Not only can this paraffin-naphthene mixture be oxidized with naphthene concentration of up to 50 mole % and conceivably higher, but the resulting anode potential is of the same order of magnitude or better than that for pure octane. Furthermore, the oxidation process is not accompanied by any performance cycling.

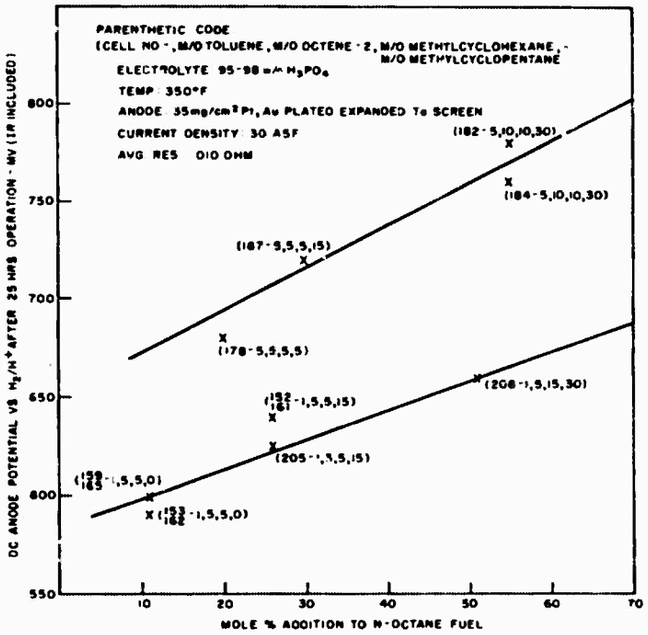

Figure 2.2-1. Dependence of Anode Potential on Concentration of Several Additives to n-Octane

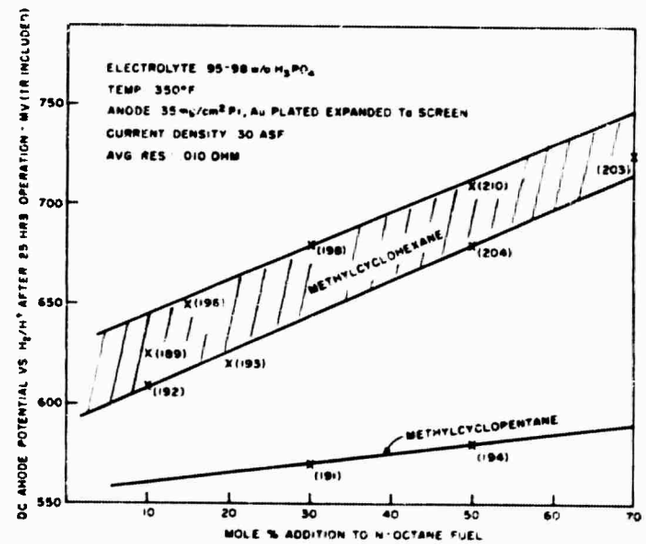

Figure 2.2-2. Dependence of Anode Potential on Concentration of Napthene Additives to n-Octane

In general though, very high steady-state DC anode potentials of the order of 600-700 mv vs. H_2/H^+ for 10-60 mole % of various additives are encountered. The only advantageous byproduct of this situation is the absence of performance cycling.

2.2.2 Relative Reactivities of Hydrocarbon Fuel Components (E. Luksha, E.Y. Weissman)

In the previous report (2.2-3) the tolerance of a fuel cell anode to n-octane containing various types of hydrocarbon additives, aromatic, olefinic, and naphthenic was determined. It was found that the octane-based fuel of the composition shown in Table 2.2-2 behaved very similarly (50 mv or less difference), at least on a short term basis, to n-octane alone.

Table 2.2-2

Model Hydrocarbon Fuel Cell Fuel

Compound Type	Concentration Mole %
Olefins	0-5
Aromatics	1
Naphthenes (cyclohexane type)	5
(cyclopentane type)	15
n + i octane	balance

If the reactivities of each one of the fuel components in Table 2.2-2 are different it can be inferred that anodic oxidation will proceed, at steady-state, according to the extent of electrode coverage by the most reactive species. This implies, of course, that probably a major portion of the anode will be covered by more refractory species; these may be present in the original fuel and may also consist of reaction intermediates.

The question of relative reactivities in a binary mixture consisting of n-octane plus one hydrocarbon additive was briefly treated in the preceding report (2.2-3) with respect to benzene. This work was completed during the present report period and expanded to include the mixtures: 5 mole % pentene-1 + 95 mole % n-octane; 5 mole % cyclohexane + 95 mole % n-octane; 0.1 mole % diethylsulfide + 99.9 mole % n-octane; and a much more complex fuel consisting of 74 mole % n-octane + 5 mole % pentene-1 + 5 mole % methylcyclohexane + 15 mole % methylcyclopentane + 1 mole % m-xylene. The concentrations of these various additives were chosen consistent with the findings summarized in Table 2.2-2.

(2.2-3) Technical Summary Report No. 9 Hydrocarbon-Air Fuel Cells, January 1966-June 1966, ARPA Order No. 247, Contract Nos. DA44-009-ENG-4909, DA44-009-AMC-479(T), and DA44-009-ENG-4853, p. 2-107 et. seq.

2.2.2.1 Experimental

The experimental details of this investigation have been previously described (2.2-3). Essentially, a fuel mixture after making a single pass through a fuel cell anode (anode compartment volume 7.5 cm^3) was passed together with its oxidation products into a Perkin-Elmer 801 gas chromatograph equipped with a heated gas sampling valve and a differential flame ionization detector.

The anodes were platinum-Teflon-screen composites of a type described in the literature (2.2-4). They were of 3 x 3 inch (0.05 ft^2) active geometric area. The electrolyte was phosphoric acid, maintained at 95 wt. % by controlled addition of water. All measurements were made at 350°F.

The measurement of the exhaust composition with the gas chromatograph, together with the cell current and the inlet fuel composition and flow rate, supplied enough data to calculate the current contributions from each component in each fuel. The calculations were performed on a General Electric 625 computer using programs written in Fortran IV. The complete programs are given in Appendix 4.4.

The anodes were operated, for the most part, at potentials in the range of 0.5 volt vs. H_2/H^+; this is a practical potential at which hydrocarbon anodes can be operated for extended periods with reasonable power outputs (2.2-3).

2.2.2.2 Results

A. Binary Fuels

1. Aromatic Additive (benzene/n-octane)

To study the relative reactivity of aromatics and n-paraffins, a binary fuel consisting of benzene + n-octane was examined. A large part of this work was completed in the last report period (2.2-3) but will be summarized here, together with new data so as to present a complete picture of the problem.

For this particular fuel the benzene concentration was varied from 1 to 5 mole %, and the liquid fuel flow rate was varied from 5 to 40 μ l/min. For n-octane, this corresponds to at least two times the stoichiometric amount for all cases. The experimental results for all the benzene/n-octane mixtures studied are summarized in Table 2.2-3 Columns 4 and 7, respectively, give the exhaust composition of the cell* and the current contribution from benzene. A comparison

(2.2-4) L.W. Niedrach and H.R. Alford, J. Electrochem. Soc., 112, 117 (1965).

*This composition is referred to the total mix of hydrocarbons only, since the flame ionization method used for the analyses cannot detect CO_2 or H_2O.

Table 2.2-3

Current Contribution and Exhaust Composition for Benzene

Inlet Fuel Composition, mole %	Liquid Fuel Flow Rate, μ l/min.	Benzene Flow Rate, mole/min. x 10^6	Benzene Concentration in Exhaust, mole % x 10^2	Total Current, I_T - amp	Anode Potential vs. H_2/H^+, volt	Current from Benzene, I_A - amp
99% n-octane + 1% benzene	5	0.313	13.0	1.46	0.510	0.014
	11	0.688	5.0	1.55	0.447	0.032
	20	1.25	5.3	1.53	0.525	0.047
	30	1.88	4.6	1.52	0.456	0.087
	38	2.38	4.39	1.52	0.550	0.110
	40	2.48	26.8	0.49	0.505	0.089
	40	2.48	29.2	0.49	-----	0.086
	40	2.48	16.5	1.01	0.530	0.101
	40	2.48	15.6	1.01	0.525	0.102
	40	2.48	10.9	1.46	0.514	0.108
	40	2.48	11.7	1.44	0.540	0.107
	40	2.48	16.9	1.50	0.525	0.101
	40	2.48	14.7	1.51	0.500	0.104
	40	2.48	7.95	2.03	0.490	0.111
	40	2.48	6.55	2.00	0.510	0.113
	40	2.48	5.35	2.00	0.480	0.114
	40	2.48	7.62	2.52	0.520	0.112
	40	2.48	6.35	2.49	0.497	0.113
	40	2.48	5.55	2.97	0.500	0.114
	40	2.48	4.97	3.01	0.500	0.114
97% n-octane + 3% benzene	10	1.87	17.8	0.78	0.485	0.085
	20	3.73	9.72	2.54	0.535	0.176
	30	5.62	26.8	1.26	0.540	0.25
	38	7.03	23.5	1.39	0.535	0.315
95% n-octane + 5% benzene	10	3.15	24.5	0.75	0.502	0.146

of columns 1 and 4 indicates that benzene is preferentially oxidized. In Figure 2.2-3 the quantity I_A/I_T the current fraction from benzene, is plotted against the fuel flow rate for a fuel consisting of 95 mole % n-octane + 1 mole % benzene. These data points were obtained at an essentially constant current (~1.5 amps) and anode potential (~0.5 volt vs. N.H.E.). The current fraction from benzene is directly proportional to the fuel flow rate. This indicates that the aromatic is consumed as rapidly as it is supplied, at least for the range of flow rates studied, and provided that $I_T > I_A$.

Further generalization is provided by Figure 2.2-4 which is a plot of I_A, the current from benzene, vs. the benzene flow rate, for fuels consisting of n-octane + 1, 3, and 5 mole % benzene. The current from benzene is proportional to the benzene flow rates, again indicating that the aromatic is consumed as rapidly as it is supplied, independent of whether it is supplied at high concentrations and low total fuel flow rates or low concentrations and high total fuel flow rates.

The current contribution from benzene, I_A, under these conditions can be represented by the relation:

$$I_A = 4.51 \times 10^4 V_A \tag{1}$$

where V_A is the benzene flow rate in units of gm. mole/min.

If this result can be generalized to all aromatics, at these conditions of operation, the following relationship can be obtained:

$$I_A = 0.934\, nF\, \mu N_A \tag{2}$$

where:

μ = mole feed rate, moles per minute

N_A = mole fraction of aromatic in feed stream

and the other terms have their usual significance.

2. <u>Olefin Additive (pentene-1/n-octane)</u>

The reactivity of olefins in a fuel was determined by studying a binary fuel consisting of 95 mole % n-octane + 5 mole % pentene-1. The experimental data is summarized in Table 2.2-4. Columns 4 and 7 give the exhaust composition of the cell and the current contribution for pentene-1, respectively. A comparison of columns 1 and 4, the pentene-1 inlet and exhaust concentrations, respectively, shows that the olefin is preferentially oxidized irrespective of the fuel flow rate. As for the case with benzene, this indicates that the olefin is consumed as rapidly as it is supplied for the range of flow rates studied, and provided that $I_T > I_{ol}$.

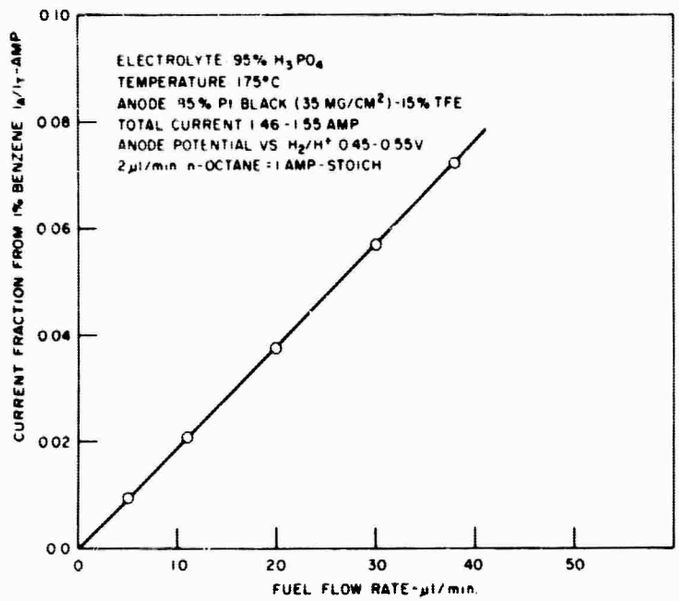

Figure 2.2-3. Current Fraction from Benzene vs. Fuel Flow Rate

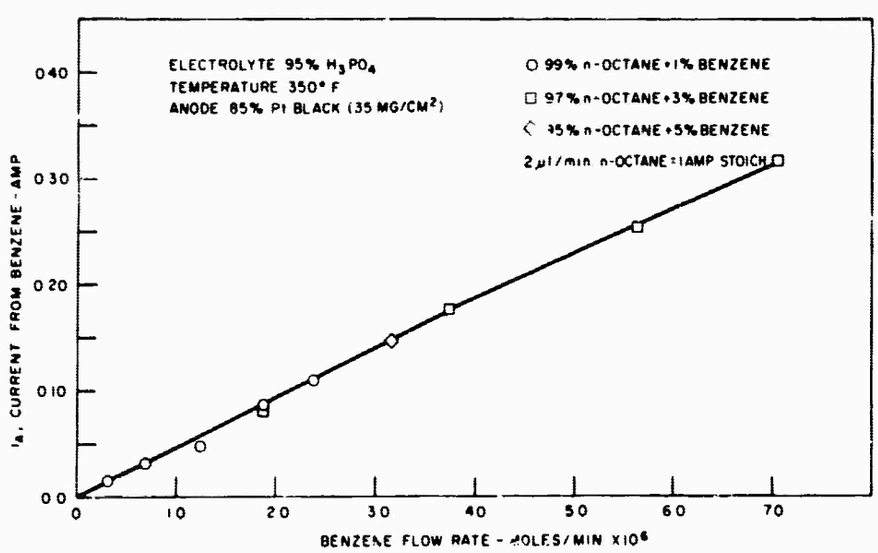

Figure 2.2-4. Current from Benzene vs. Benzene Flow Rate for Fuels Containing 1-5 mole % Benzene

Table 2.2-4

Current Contribution and Exhaust Composition for Pentene-1

Inlet Fuel Composition, mole %	Liquid Fuel Flow Rate, μ l/min.	Pentene-1 Flow Rate, moles/min. x 10^6	Pentene-1 Concentration in Exhaust, mole % x 10^1	Total Current, I_T, amp	Anode Potential vs. H_2/H^+, volt	Current from Pentene-1 I_{o1}, amp	
95% n-octane + 5% Pentene-1	5	1.58	2.82	1.00	0.445	0.074	
	10	3.16	0.054	1.00	0.483	0.152	
	10	3.16	0.067	1.00	0.485	0.152	
	10	3.16	0.058	1.00	0.520	0.152	
	10	3.16	0.060	1.00	0.496	0.152	Ave.
	20	6.31	0.043	2.00	0.535	0.304	
	20	6.31	0.037	2.00	0.510	0.304	
	20	6.31	0.033	1.50	0.505	0.304	
	20	6.31	0.030	1.50	0.525	0.304	
	20	6.31	0.075	1.50	0.475	0.304	
	20	6.31	0.077	1.50	0.475	0.304	
	20	6.31	0.109	1.00	0.480	0.304	
	20	6.31	0.114	1.00	0.475	0.304	
	20	6.31	0.174	0.50	0.475	0.304	
	20	6.31	0.153	0.50	0.515	0.304	
	20	6.31	0.105	0.50	0.510	0.304	
	20	6.31	0.124	0.50	0.525	0.304	
	20	6.31	0.090	----	0.500	0.304	Ave.
	30	9.47	0.100	0.99	0.525	0.456	
	30	9.47	0.112	0.99	0.525	0.456	
	30	9.47	0.106	0.99	0.525	0.456	Ave.
	40	12.6	3.06	1.00	0.550	0.575	

The average values of the current contribution from pentene-1, I_{o1}, are plotted against the pentene-1 flow rate in Figure 2.2-5. It can be seen that there is a linear relationship between the current, I_{o1}, and flow rate, and since there is virtually no pentene-1 in the exhaust, the current produced is the stoichiometric amount calculated from its flow rate. It is noted that at the higher flow rates there is a curvature towards the abscissa. This suggests that at high flow rates or high concentrations of the olefin the current from this compound will probably reach a limiting value.

The current contribution from pentene-1 for these reaction conditions and at low flows, as determined from Figure 2.2-5, can be expressed as:

$$I_{o1} = 4.83 \times 10^{4} V_{o1} \tag{3}$$

where V_{o1} is the pentene-1 flow rate in gm mole/min. If the results are generalized to apply to all olefins the following result is obtained:

$$I_{o1} = nF \mu N_{o1} \tag{4}$$

where the symbols have the same meaning as described above for benzene.

3. Naphthene Additive (cyclohexane/n-octane)

Experiments to determine the relative reactivity of cyclohexane-type naphthenes and n-octane were conducted on a binary fuel consisting of 95 mole % n-octane and 5 mole % cyclohexane. The experimental results are summarized in Table 2.2-5.

The cyclohexane-type naphthenes are considerably different from the aromatic and the olefin compounds previously discussed. By comparing columns 1 and 4 which show the cyclohexane concentration in the inlet and exhaust streams, respectively, it is seen that only 27 to 44% of the naphthene is removed. This is in marked contrast to the aromatics and olefins which were virtually entirely removed (93 to 100%). However, it is of importance to note that the cyclohexane concentration in the exhaust is always substantially lower than the inlet concentration. This is shown in Figure 2.2-6 in which the cyclohexane concentration in the exhaust is plotted against the liquid fuel flow rate. It is seem that the cyclohexane concentration levels out at about 44% of the inlet concentration.

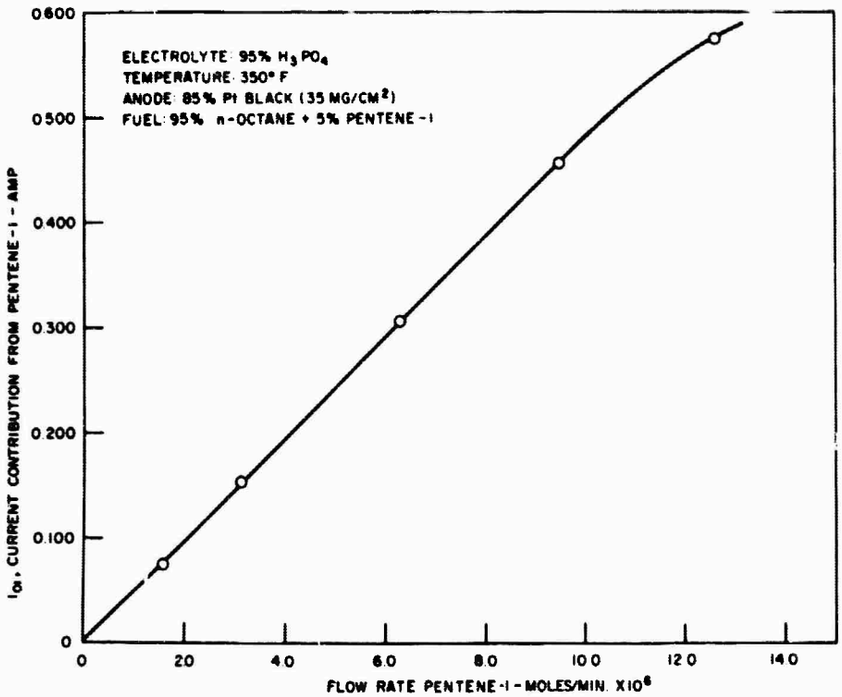

Figure 2.2-5. Current Contribution from Pentene-1 vs. Pentene-1 Flow Rate from a Fuel Containing 5 mole % Pentene-1

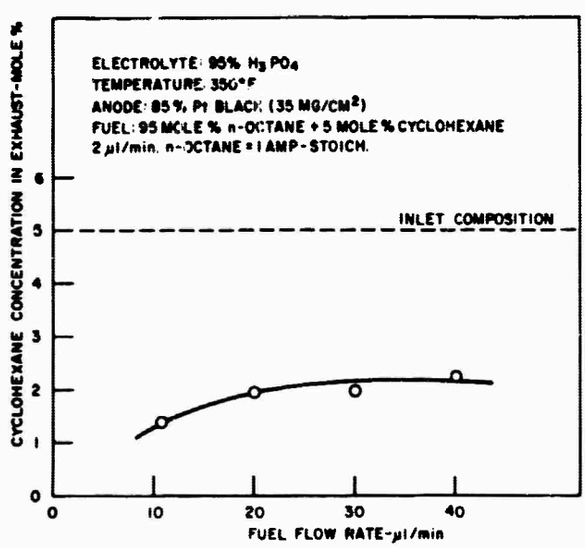

Figure 2.2-6. Effect of Liquid Fuel Flow Rate on Cyclohexane Concentration in Exhaust for a Fuel Containing 5 mole % Cyclohexane at Inlet

Table 2.2-5

Current Contribution and Exhaust Composition for Cyclohexane

Inlet Fuel Composition Mole %	Liquid Fuel Flow Rate, μl/min.	Cyclohexane Flow Rate, mole/min. x 10^6	Cyclohexane Concentration in Exhaust, mole %	Total Current, I_T, amp	Anode Potential vs. H_2/H^+, volt	Current from Cyclohexane I_N, amp	
95% n-octane + 5% cyclohexane	10.7	3.34	1.39	0.800	0.475	0.148	
	10.7	3.34	1.37	0.800	0.485	0.149	
	10.7	3.34	1.35	0.800	0.485	0.149	
	10.7	3.34	1.37	0.800	----	0.149	Ave.
	20	6.25	1.94	0.990	0.525	0.236	
	20	6.25	1.98	0.990	0.525	0.233	
	20	6.25	1.99	0.980	0.525	0.233	
	20	6.25	1.97	0.987	----	0.234	Ave.
	30	9.37	1.89	0.980	0.510	0.352	
	30	9.37	2.01	0.960	0.540	0.339	
	30	9.37	1.93	0.960	0.510	0.347	
	30	9.37	1.94	0.967	-----	0.346	Ave.
	40	12.5	2.23	0.980	0.540	0.419	
	40	12.5	2.19	0.970	0.500	0.426	
	40	12.5	2.20	0.960	0.510	0.423	
	40	12.5	2.21	0.970	-----	0.423	Ave.

From a consideration of thermodynamic equilibrium data (2.2-5) for the gas phase dehydrogenation reaction:

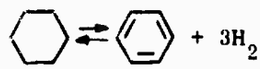

$$+ 3H_2 \qquad (5)$$

it follows that, for the conditions prevailing at the anode, the product of Reaction (5) will contain 2.3 mole % benzene and 2.7 mole % cyclohexane. The benzene (and hydrogen) will be rapidly and almost completely consumed (see Section 2.2.2.2 on binary fuels and aromatic additives).

From these equilibrium considerations, 46% of the benzene would be consumed with some consumption of the accompanying cyclohexane. This compares favorably with the experimental values ranging from 56 to 72% (Table 2.2-5). The agreement with the low value (56%) obtained at the higher flow rates is in better agreement since under high flow conditions the electrochemical utilization of cyclohexane is lower than under low flow conditions.

The average values of the current contributing from the naphthene, I_N, is plotted vs. the naphthene flow rate in Figure 2.2-7. A linear relationship is again obtained as with benzene and pentene-1, but here it is noted that the line does not pass through the origin.

The experimental results in Figure 2.2-7 can be fitted to the following empirical equation:

$$I_N = 0.05 + 3.55 \times 10^4 V_N \qquad (6)$$

where V_N is the flow rate of cyclohexane in mole/min.

Once again, if the results are generalized to all cyclohexane-type naphthenes the following relationship is obtained:

$$I_N = nF\,(8.65 \times 10^{-7} + 0.613\ \mu N_N) \qquad (7)$$

when N_N is the mole fraction of the naphthene at the inlet and the other terms have the significance described above.

4. Sulfur Additive (diethylsulfide/n-octane)

A brief study was made to determine the reactivity of sulfur-bearing compounds at the fuel cell anode. A fuel consisting of 0.1 mole % diethylsulfide (~300 ppm sulfur) in n-octane was studied. Diethylsulfide was chosen because it was believed that a basic (Lewis base) sulfur compound would be very harmful to anode performance. The experimental data is given in Table 2.2-6. It can be seen

(2.2-5) F. D. Rossini et. al., "Selected Values of Properties of Hydrocarbon," Circular C461 N. B. S. 1947.

Table 2.2-6

Current Contribution and Exhaust Composition for Diethylsulfide

Inlet Fuel Composition, mole %	Liquid Fuel Flow Rate, μl/min.	DES Flow Rate, moles/min. x 10^6	DES Concentration in Exhaust, mole %	Total Current, I_T, amp	Anode Potential vs. H_2/H^+, volt	Current from DES, amps x 10^3	
99.9% n-octane + 0.1% diethylsulfide	5	0.03	0.136	0.800	0.510	0.11	
	5	0.03	0.135	0.780	0.490	0.11	
	5	0.03	0.136	0.790	-----	0.11	Ave.
	10	0.06	0.102	0.97	0.480	0.53	
	10	0.06	0.103	0.97	0.480	0.50	
	10	0.06	0.103	0.97	-----	0.52	Ave.
	20	0.12	0.106	0.88	0.510	0.18	
	30	0.19	0.0887	1.0	0.530	1.5	
	30	0.19	0.0827	1.0	0.500	2.1	
	30	0.19	0.0857	1.0	0.515	1.8	Ave.
	40	0.25	0.0814	1.5	0.520	3.0	
	40	0.25	0.0817	1.5	0.530	3.0	
	40	0.25	0.0816	1.5	0.525	3.0	Ave.

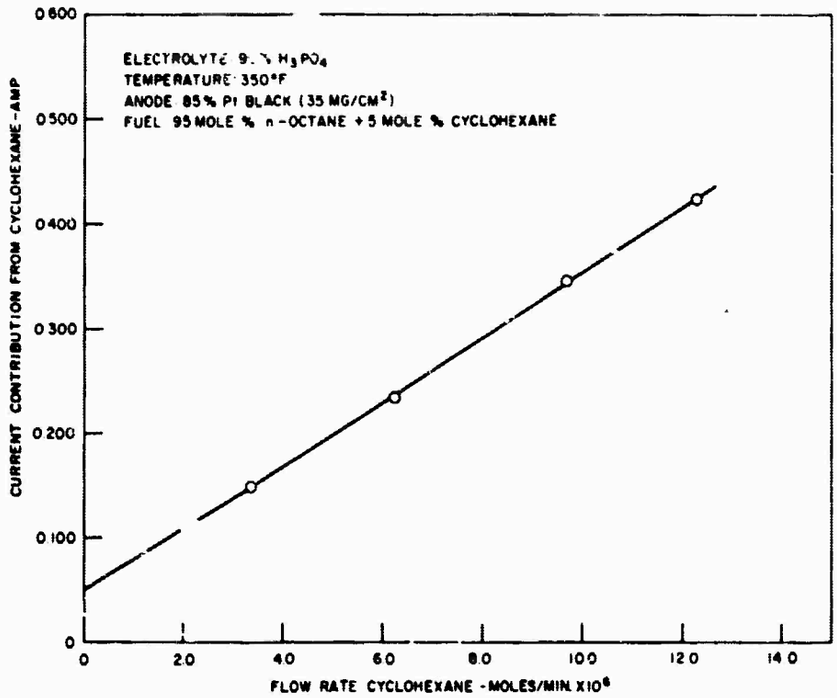

Figure 2.2-7. Current Contribution from Cyclohexane vs. Cyclohexane Flow Rate for a Fuel Containing 5 mole % Cyclohexane

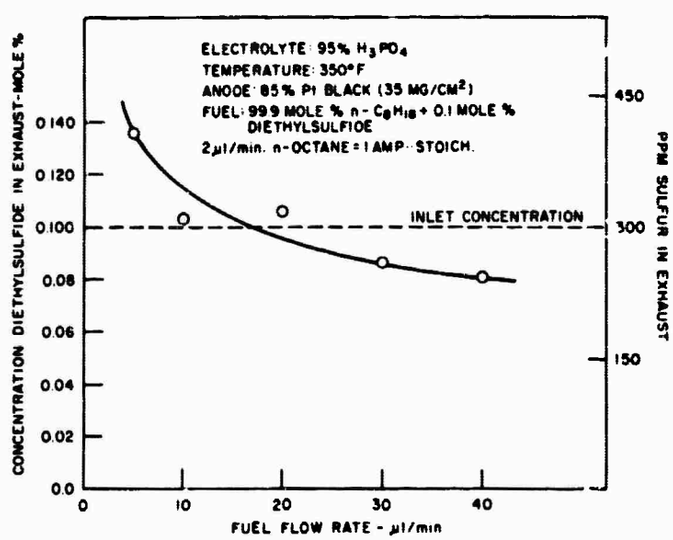

Figure 2.2-8. Effect of Liquid Fuel Flow Rate on Diethylsulfide Concentration in Exhaust for n-Octane Containing 0.1 mole % Diethylsulfide (~ 300 ppm Sulfur)

in column 7 that the current contribution from this compound is in the milliamp range and is therefore of no consequence. It is also noted that the anode potential is normal (see column 6).

Most noteworthy is column 4 which shows that the exhaust becomes enriched in the sulfur-bearing compound as the fuel flow rate is decreased. In Figure 2.2-8 the diethylsulfide concentration in the exhaust is plotted against liquid fuel flow rate. It is seen that the diethylsulfide concentration in the exhaust can be increased by some 50%. This is the only case encountered in which an "unreactive" compound actually becomes enriched in the anode exhaust. This result is indicative of weak electro-sorption so that the sulfides under these conditions are probably not strong poisons and are real examples of unreactive compounds. Studies of other classes of sulfur compounds should prove to be interesting.

B. Five Component Fuel

A fuel consisting of 74 mole % n-octane + 15 mole % methylcyclopentane + 5 mole % methylcyclohexane + 5 mole % pentene-1 + 1 mole % m-xylene was studied to determine whether the results reported above using binary fuels are applicable to more complex fuels. It is possible that one or more of the components are selectively oxidized at the expense of the others. A fuel of this particular composition was chosen since it was previously shown (2.2-3) to behave very similarly to pure n-octane. Furthermore, this study comes closer to simulating operations with a real commercial fuel. The experimental results are given in Table 2.2-7.

For the sake of better resolution in the chromatographic analysis, benzene and cyclohexane, which had been used as model additives in studies with binary fuels, were replaced by m-xylene and methylcyclohexane, respectively. The results should not be greatly affected. The exhaust compositions of the five fuel components are shown as a function of liquid fuel flow rate in Figures 2.2-9 thru 2.2-13. It is important to note that the n-octane concentration in the fuel actually increases from 74 to 96 mole % after a single pass through the cell as is shown in Figure 2.2-9. The naphthene concentrations for both the five and six-membered ring types are substantially reduced in the exhaust stream, especially at low fuel flow rates; this is shown in Figures 2.2-10 and 2.2-11.

Figures 2.2-12 and 2.2-13 show the pentene-1 and m-xylene concentrations in the exhaust, respectively, plotted as a function of liquid fuel flow rate. As for the case of binary fuels, the unsaturated compounds are virtually entirely depleted from the fuel stream at low fuel flow rates (approximately 10 μl/min.). The breakthrough of these compounds above these flow rates must be a result of competition for surface sites between the various fuel component molecules. However, the concentrations of these compounds are greatly reduced; thus, better than 70% removal of the aromatic compound and better than 80% of the olefin is observed. This fact is extremely significant, since it

Table 2.2-7

Current Contributions and Exhaust Composition of Components of a Synthetic Fuel

Inlet Fuel Composition, mole %: 74% n-octane + 15% methylcyclopentane + 5% methylcyclohexane + 5% pentene-1 + 1% m-xylene

Liquid Fuel Flow Rate, μl/min.	10	20	30	40
Octane Flow Rate, moles/min. x 10^6	49.16	98.32	147.5	196.6
MCP Flow Rate, moles/min. x 10^6	9.92	19.8	29.8	39.7
MCH Flow Rate, moles/min. x 10^6	3.32	6.64	9.96	13.28
Pentene-1 Flow Rate, mole/min. x 10^6	3.32	6.64	9.96	13.28
Xylene Flow Rate, mole/min. x 10^5	0.664	1.33	1.99	2.66
n-Octane Concentration, mole %	95.6	85.0	83.0	80.7
MCP Concentration, mole %	3.49	11.7	13.1	14.1
MCH Concentration, mole %	0.822	2.84	3.19	4.17
Pentene-1 Concentration, mole %	0.0581	0.267	0.534	0.774
M-Xylene Concentration, mole %	0.000	0.177	0.226	0.273
Total Current, amp	1.20	1.45	1.50	1.50
Anode Potential, volt	0.550	0.550	0.590	0.580
I_p, Octane-amp	0.320	0.422	0.268	0.267
I_N, MCP-amp	0.479	0.405	0.396	0.326
I_{N2}, MCH-amp	0.198	0.239	0.292	0.217
I_{ol} Pentene-1, amp	0.159	0.306	0.436	0.551
I_A, m-Xylene, amp	0.0449	0.0768	0.108	0.135

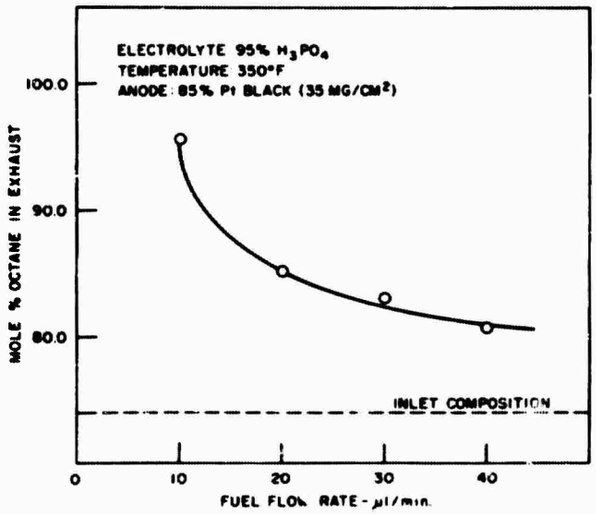

Figure 2.2-9. Effect of Liquid Fuel Flow Rate on Octane Concentration in Exhaust for a Fuel Containing 74% n-Octane + 15% Methylcyclopentane + 5% Methylcyclohexane + 5% Pentene-1 + 1% m-Xylene

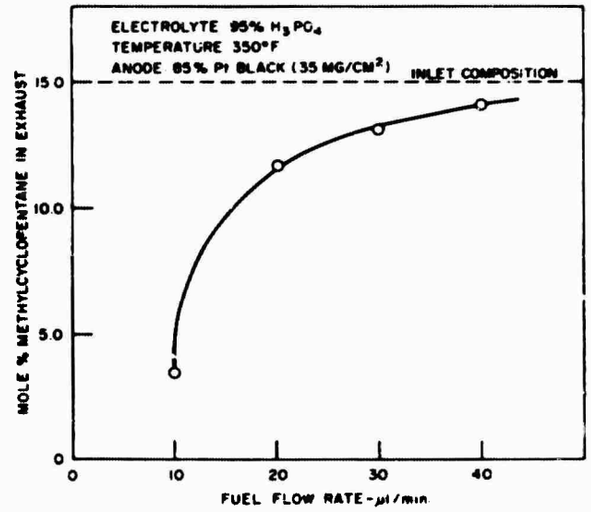

Figure 2.2-10. Effect of Liquid Fuel Flow Rate on Methylcyclopentane Concentration in Exhaust for a Fuel Containing 74% n-Octane + 15% Methylcyclopentane + 5% Methylcyclohexane + 5% Pentene-1 + 1% m-Xylene

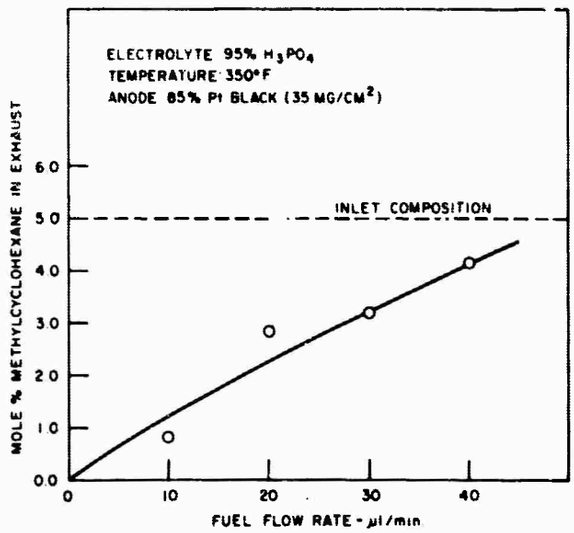

Figure 2.2-11. Effect of Liquid Fuel Flow Rate on Methylcyclohexane Concentration in Exhaust for a Fuel Containing 74% n-Octane + 15% Methylcyclopentane + 5% Methylcyclohexane + 5% Pentene-1 + 1% m-Xylene

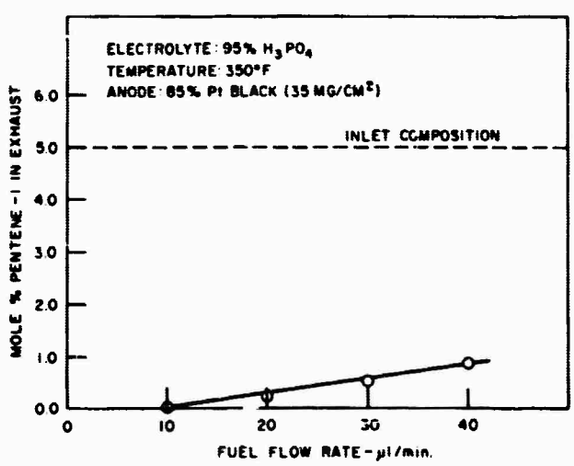

Figure 2.2-12. Effect of Liquid Fuel Flow Rate on Pentene-1 Concentration in Exhaust for a Fuel Containing 74% n-Octane + 15% Methylcyclopentane + 5% Methylcyclohexane + 5% Pentene-1 + 1% m-Xylene

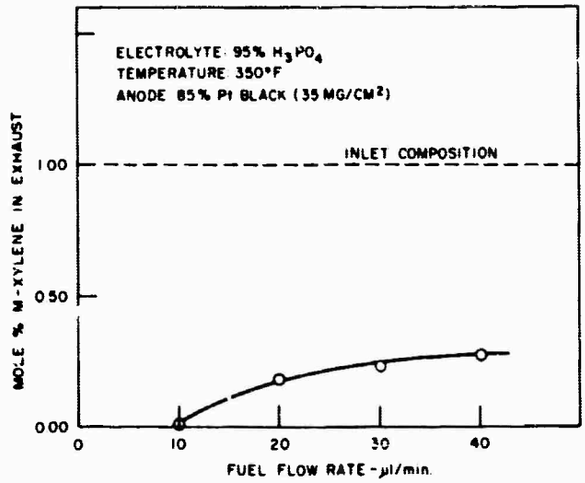

Figure 2.2-13. Effect of Liquid Fuel Flow Rate on m-Xylene Concentration in Exhaust for a Fuel Containing 74% n-Octane + 15% Methylcyclopentane + 5% Methylcyclohexane + 5% Pentene-1 + 1% m-Xylene

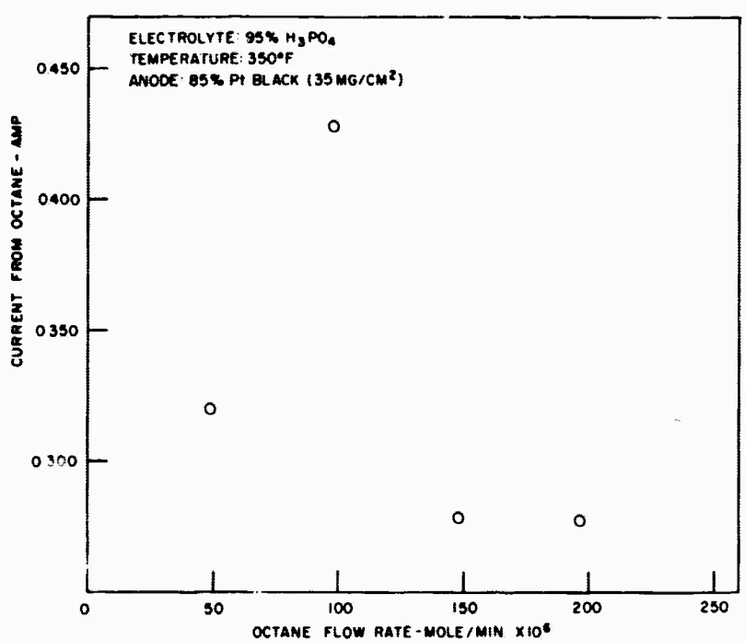

Figure 2.2-14. Effect of Octane Flow Rate on Current Contribution from Octane for Fuel Containing 74% n-Octane + 15% Methylcyclopentane + 5% Methylcyclohexane + 5% Pentene-1 + 1% m-Xylene

indicates that the more harmful components are preferentially oxidized resulting in an "exhaust fuel" that is richer in the more desirable components.

The current contributions of the five components unde consideration are shown in Figures 2.2-14 thru 2.2-18. They were obtained by means of the simultaneous solution of five linear equations (see Appendix 4.4). Unfortunately, the solutions are quite sensitive to relatively small variations in each of the variables. Thus, an experimental error of about 1 to 3% in the chromatographic analysis can cause rather severe distortions in the calculated current contributions of the components for which the errors were made. Furthermore, the assumptions made for the parameter n (number of gm-equivalents/gm-mole) of each species and for the Faradiae efficiency, which was assumed to be 100%, will also influence the results.

These comments are pertinent, in view of the curve discontinuities observed in Figures 2.2-14 thru 2.2-16. These discontinuities were unexpected, considering the smooth variation of the exhaust composition data with flow rate (Figures 2.2-9 thru 2.2-11).

On the other hand, the relative reactivity of olefins and aromatics yield results as exhibited in Figures 2.2-17 and 2.2-18. These results are reminiscent of the binary fuel results and reflect the situation where it was shown that there is not necessarily an additive effect on performance when two or more "refractory" additives are present in a given fuel (2.2-3).

It is clear from the above discussion that the current contributions from n-octane, methylcyclopentane, and methylcyclohexane are difficult to calculate. This is not the case, however, for m-xylene and pentene-1. The current contributions for each of these components, at low flow rates, are given by the equations:

$$I_{ol} = 0.963\, n F \mu N_{ol} \tag{8}$$

$$I_A = 0.93\, n F \mu N_A \tag{9}$$

Equations (8) and (9) are in very good agreement with Equations (2) and (4) which apply to binary fuels. It should be noted that a different aromatic additive was used in the binary mixture. This is an alternate way of expressing the fact that the electrochemical oxidation of olefins and aromatics at low fuel flow rates appears to proceed independent of the other species present in the fuel.

C. General Considerations

Figure 2.2-19 shows that aromatics, olefins, and naphthenes in pure form exhibit considerably poorer polarization characteristics than n-octane when oxidized electrochemically.

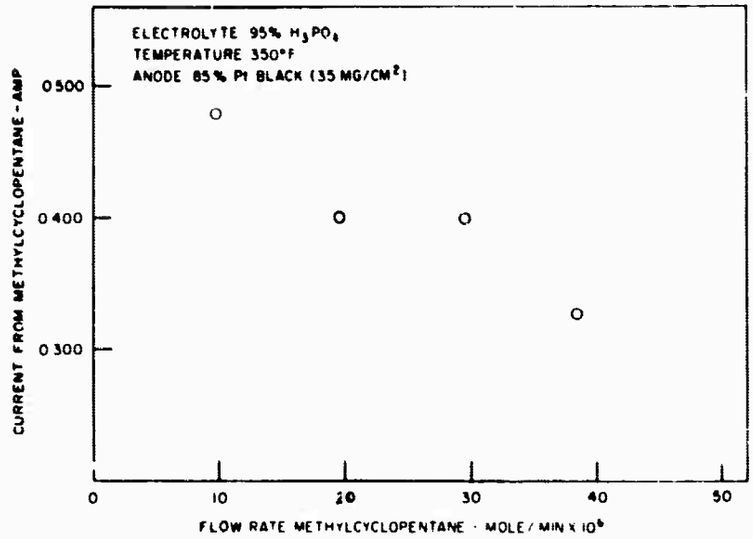

Figure 2.2-15. Effect of Methylcyclopentane Flow Rate on Current Contribution from Methylcyclopentane for Fuel Containing 74% n-Octane + 15% Methylcyclopentane + 5% Methylcyclohexane + 5% Pentene-1 + 1% m-Xylene

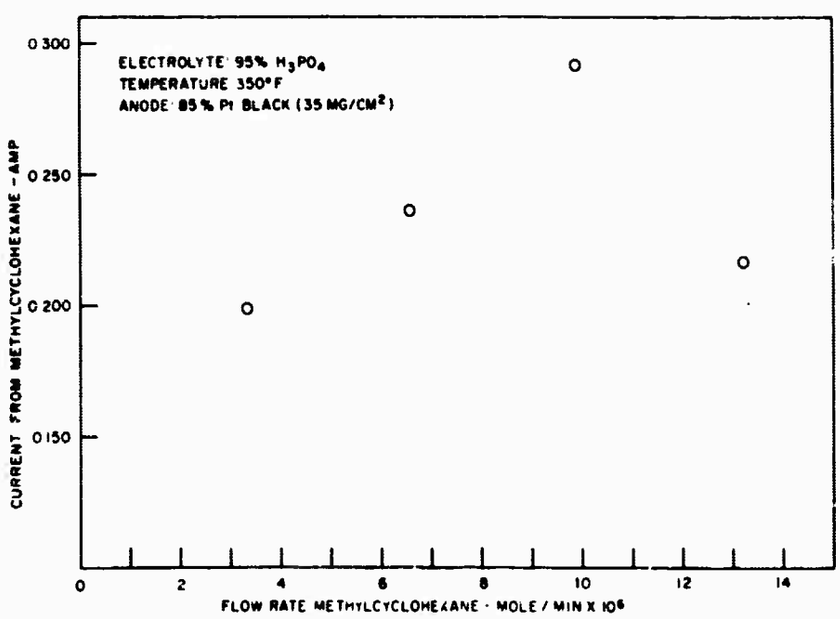

Figure 2.2-16. Effect of Methylcyclohexane Flow Rate on Current Contribution from Methylcyclohexane for Fuel Containing 74% n-Octane + 15% Methylcyclopentane + 5% Methylcyclohexane + 5% Pentene-1 + 1% m-Xylene

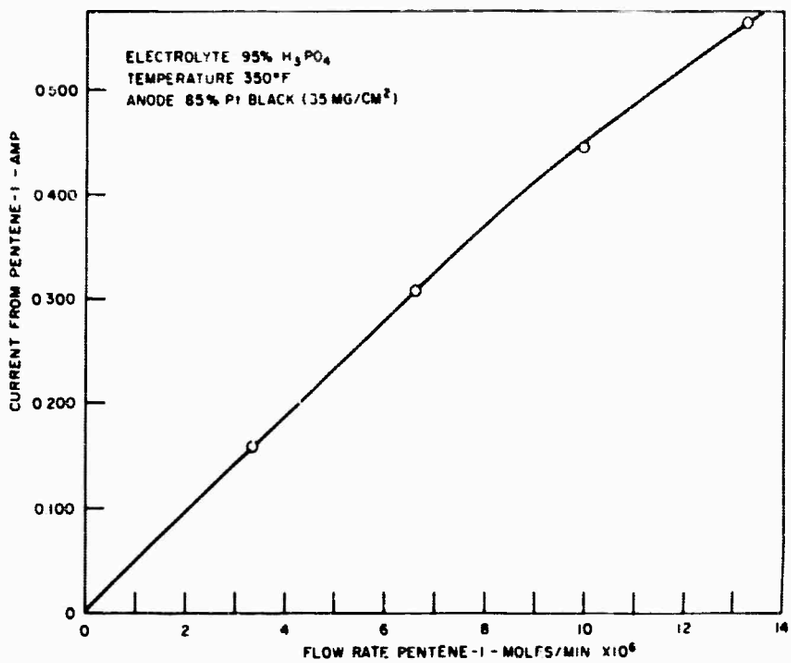

Figure 2.2-17. Effect of Pentene-1 Flow Rate on Current Contribution from Pentene-1 for Fuel Containing 74% n-Octane + 15% Methylcyclopentane + 5% Methylcyclohexane + 5% Pentene-1 + 1% m-Xylene

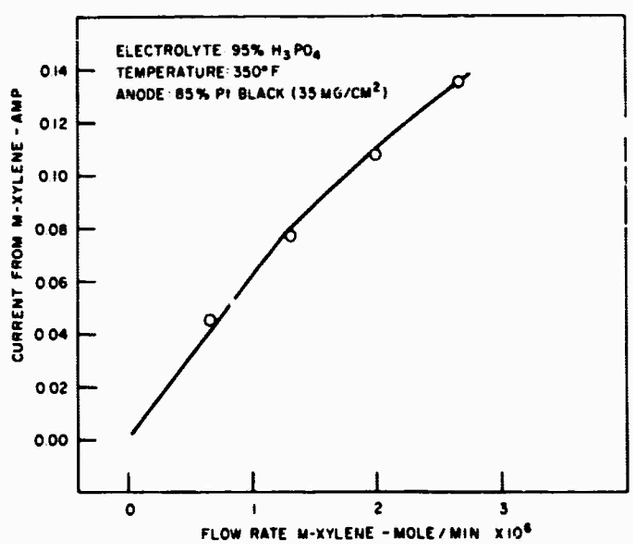

Figure 2.2-18. Effect of m-Xylene Flow Rate on Current Contribution from m-Xylene for Fuel Containing 74% n-Octane + 15% Methylcyclopentane + 5% Methylcyclohexane + 5% Pentene-1 + 1% m-Xylene

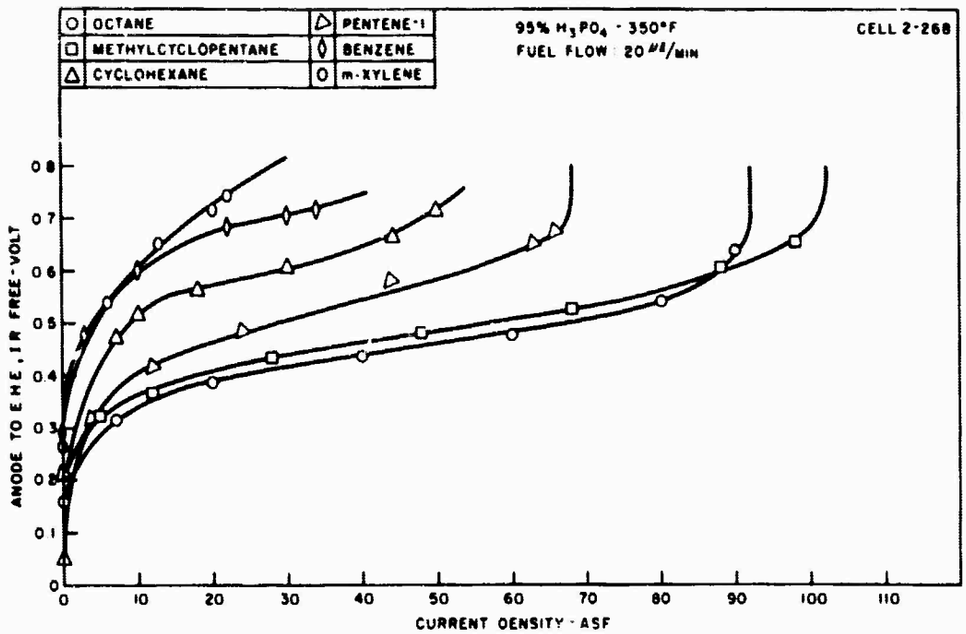

Figure 2.2-19. Polarization Curves for n-Octane, Methylcyclopentane, Cyclohexane, Pentene-1, Benzene, and m-Xylene

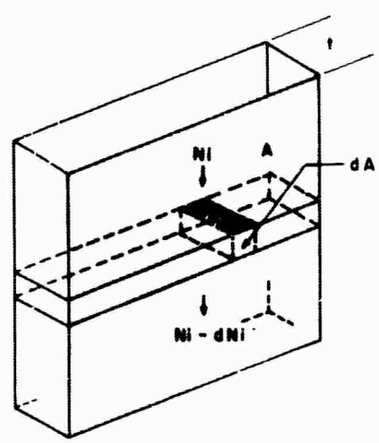

Figure 2.2-20. Fuel Cell Anode Compartment

The rather unexpected relative reactivities observed in the present work for fuel mixtures is, therefore, probably due to competitive adsorption effects, with the more refractory species achieving high coverages of the active sites and being selectively oxidized. Unfortunately, no electrosorption data are available for the classes of compounds studied to put this discussion on a more quantitative basis.

2.2.2.3 Discussion

A clearer understanding of the preceding results can be obtained from some fundamental relationships. Consider an anode compartment of thickness t, containing an electrode of area A, as is shown in Figure 2.2-20. There is a steady flow, μ, of reactant mixture expressed as moles per unit time. A volume element, dA, is selected so that the concentration of component i is N_i expressed as mole fraction and the concentration leaving is $N_i - dN_i$. The rate of change in the number of moles of component i at a given point in the anode compartment, m_i, can be expressed by the equation:

$$\frac{dm_i}{dt} = \mu dN_i + r_i \, dA \tag{10}$$

where r_i is the rate of oxidation of component i in the anode compartment expressed as moles of reactant converted per unit area of electrode per unit time, and the remaining symbols have their customary significance.

Considering the anode compartment as a flow reactor at steady-state, Equation (10) simplifies to:

$$r_i \, dA = - \mu dN_i \tag{11}$$

Considering mainly activation effects and expressing the current density of a component i in terms of the reaction rate, we obtain:

$$i_i = n_i F r_i \tag{12}$$

Combining Equations (11) and (12) and integrating yields:

$$\int_0^A dA = -nF\mu \int_{N_o}^{N} \frac{dN}{i} \tag{13}$$

here the subscript i has been eliminated for sake of simplicity and N_o is the mole fraction of the component under consideration at the inlet.

Expressing the current density in terms of the electrochemical kinetics of an activation limited, anodic, forward reaction

$$\left| \eta_a \right| >> \frac{RT}{nF} ,$$

where η_a is the anodic activation polarization, we can write:

$$i = nFN^{\gamma} k \exp\left(\frac{-\Delta G^*}{RT}\right) \exp\left(\frac{-\alpha nFE^{\circ}}{RT}\right) \exp\left(\frac{(1-\alpha)nF\eta_a}{RT}\right) \tag{14}$$

where γ is the reaction order, k is a rate constant, ΔG^* is the standard free energy of activation, E° is the reversible potential, and α is the transfer coefficient. It is recognized that Equation (14) is the correct kinetic expression for the hydrocarbons studies, but for our purposes the following simplified equation can be

$$i = k' N^{\gamma} e^{\beta E} \tag{15}$$

more easily fitted to the experimental data, where k' and β are now constants to be fit to the experimental data. Substituting Equation (15) into Equation (13) yields:

$$\int_0^A dA = \frac{-nF\mu e^{-\beta E}}{k'} \int_{N_o}^{N} \frac{dN}{N^{\gamma}} \tag{16}$$

which upon integration and rearrangement gives:

$$\frac{k' A(1-\gamma)}{nF\mu} e^{-\beta E} = N_o^{(1-\gamma)} - N^{(1-\gamma)} \tag{17}$$

for the case where $\gamma \neq 1$. Since none of the additives studied have a reaction order of unity this case was not considered. The constants in Equation (17) are listed in Table 2.2-8 for the additives studied.

Table 2.2-8

Constants for Equation (17)

Compound	k', ASF	β	γ
Benzene	0.039	9.3	-0.11
m-xylene	0.17	6.7	-0.11 *
Methylcyclohexane	0.029	11.4	
Pentene-1	0.26	9.3	-0.16 *
N-octane	0.12	13.1	~0.5

*estimated

The empirical constants k' and β were determined from the linear portion of curves in Figure 2.2-21. The reaction order for benzene was given in a recent study by Bockris et. al.(2.2-6) and the values of the orders for m-xylene and pentene-1 were estimated from Bockris's data. The other values for γ were obtained by fitting the binary fuel data to Equation (17). Equation (17) permits the calculation of the exhaust composition of any compound for which the constants are known. It is hoped that the constants for various compounds in a particular class will be sufficiently similar to make Equation (17) general enough to calculate the exhaust composition (and therefore current contribution) of a fuel cell anode at any given set of anode operating conditions.

The fit of the experimental data for the five component fuel to Equation (17) is only fair if the condition:

$$e^{\beta E} \leq \frac{nF\mu \quad N^{(1-\gamma)}}{k' A (1-\gamma)} \tag{19}$$

is obeyed. The utilization of the components that were believed to be unreactive prior to this investigation can be explained by Equation (18), indicating that the results obtained can be explained from simple fundamental considerations.

2.2.2.4 Conclusions

1. Under anode operating conditions that present-day direct hydrocarbon fuel cell technology permits, the components of a practical fuel (aromatics, olefins, and to a certain extent naphthenes) can be preferentially oxidized. This is apparently a result of the magnitude of the relative coverage of the active sites with the components in question. The anode effluent becomes enriched in the more desirable paraffin component.

Sulfur compounds that are basic in nature are not preferentially adsorbed and oxidized in the manner described above.

2. The preferential oxidation of the "unreactive" components can be explained by simple kinetic considerations.

The engineering significance of these findings is extremely important since it is now evident that no fuel pretreatment beyond established limits is necessary and that the fuel can be recycled without any harmful side effects.

(2.2-6) J. O. M. Bockris, et. al., Trans. Faraday Soc., 61, 515, 1965.

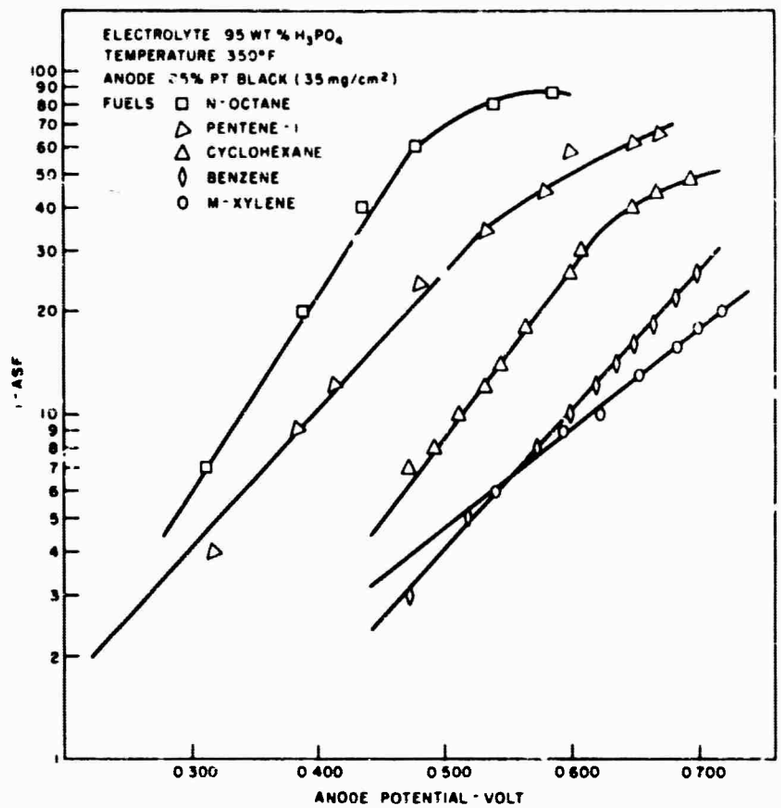

Figure 2.2-21. Current Density vs. Anode Potential for n-Octane, Pentene-1, Cyclohexane, Benzene, and m-Xylene

2.3 INVESTIGATIONS WITH ALTERNATE ELECTROLYTES (J. Paynter, J. R. Morgan)

The previous work with carbon-supported electrocatalysts using liquid octane fuel and hydrofluoric acid electrolyte has been extended to include higher area graphitic and non-graphitic substrates.

2.3.1 Experimental

2.3.1.1 Electrocatalyst Preparation

Properties of the substrate materials chosen for evaluation, together with the corresponding catalyst identification numbers are given in Table 2.3-1. Except for that corresponding to Prep. No. 51, all of the substrates are non-graphitic carbons. The Prep. No. 51 substrate was obtained by heat treatment of Prep. No. 60 substrate to 2700°C for approximately two hours in an inert atmosphere.

Table 2.3-1

Properties of Carbon Substrates

Source: Cabot Corp.

Name	Type	Surface Area (a), m^2/gm	Average Particle Diameter (b), Millimicron	Volatile Content, %	pH	Catalyst Prep. No.
Sterling 10	Oil furnace non-graph.	42	41	1.0	8.0	70
Spheron 6	Regular color channel non-graph.	110	25	5.0	4.5	80
Black Pearls 71	Medium color channel non-graph.	380	16	5.0	5.0	90
Black Pearls 2	High color channel non-graph.	850	12	13.0	3.0	60
Black Pearls 2	Graphitic	212	--	0.0	10.0	51

(a) N_2 S. A.
(b) From electron micrographs.

(2.3-1) E. J. Cairns, E. J. McInerney, and J. Paynter, Technical Summary Report No. 9, Hydrocarbon - Air Fuel Cells, Jan. 1 - June 30, 1966, ARPA Order No. 247, Contract No. DA44-009-AMC-479 (T).

The substrates were activated by making a slurry with a nitric acid solution of Pt $(NH_3)_2(NO_2)_2$ and heating in air to decompose and oxidize the Pt salt, following procedures similar to those outlined in Appendix 3.4 of Technical Summary Report No. 8. Recently, results of thermogravimetric analysis have indicated that the optimum decomposition temperature is around 250°C (2.3-1). However, with the higher area non-graphitic carbons used in the present work, final decomposition temperatures over 200°C generally resulted in vigorous burning of the catalysts. It was found that a final oxidation temperature of 200°C, together with prolonged heating at 100°C, did not result in any visible reaction with the highest area material studied (850 m^2/g). The time - temperature profile used for all laminations in the preparation of the electrocatalysts is shown in Figure 2.3-1. Three laminations were made on each substrate corresponding to 10 w/o Pt increments. Large agglomerates were broken up before transfer to the air thermostat. The catalysts were ground and sieved through 200 mesh screen after the third lamination.

2.3.1.2 Electrode Preparation

All anodes were of the dry - blended variety (2.3-1) fabricated with 45 v/o T-7, a 0.27 - 0.31 mg/cm^2 porous TFE film, and a press force of 5000 lb. The Al foil backing material was removed by electrochemical oxidation in dilute KOH solution at a potential above O_2 evolution to prevent premature reduction and sintering of the platinum by the H_2 evolved in the chemical stripping process.

Two types of dry - blended electrodes were used, differing only in the method of mixing catalyst and Teflon powders. One set was made following the grinding and sieving procedures described previously (2.3-1). The agglomeration and leathering of the Teflon encountered with this procedure was avoided in the second set by using boiling liquid nitrogen to simultaneously wet, disperse, and sieve (100 mesh screen) the powders. This technique is much less time-consuming than the standard one and should result in a dry blend of better homogeneity and smaller agglomerate size.

2.3.1.3 Fuel Cell Studies

The electrolyte used in this study was the 36 m/o HF - H_2O azeotrope at 105°C. Normal - octane (Phillips research grade) was fed to the anode compartment in the liquid state by means of a constant - speed syringe drive. The anodes were reduced electrochemically in situ under octane at about 7 ma/cm^2.

The performance measurements were made using the usual interrupter technique. All results are reported on a resistance - free basis unless otherwise indicated. The reference electrode was a reversible hydrogen electrode in the same electrolyte at the same temperature.

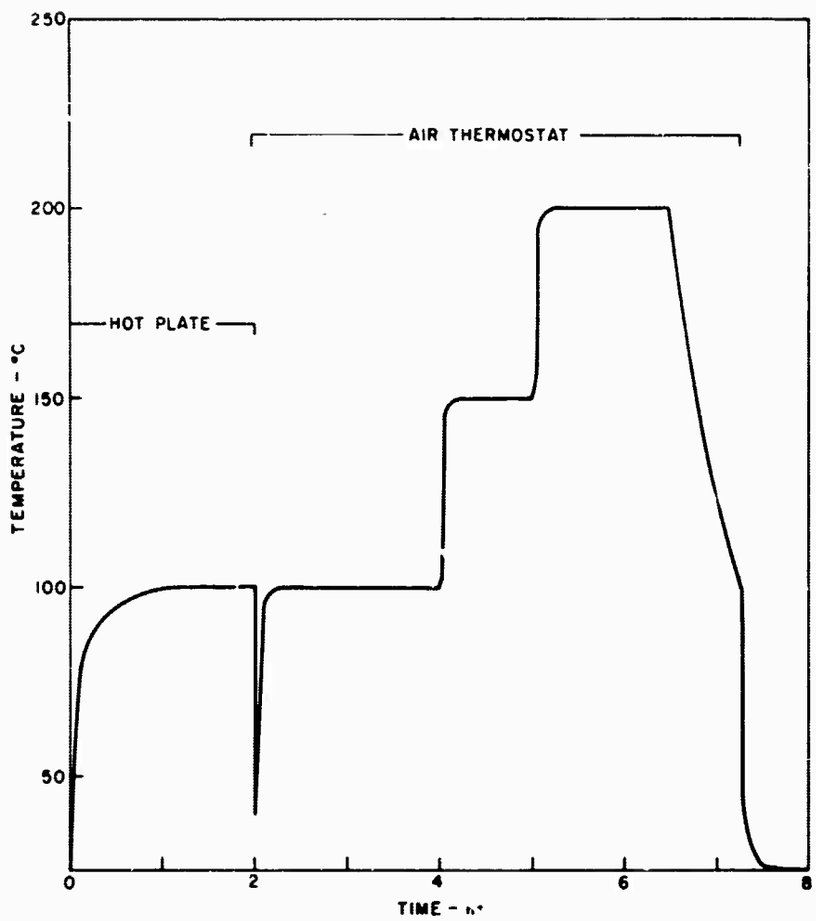

Figure 2.3-1. Time - Temperature Profile Used for Preparation of Carbon-Supported Platinum Electrocatalysts

2.3.2 Results and Discussion

Performance data expressed as current density and specific current (ma/mg Pt) at anode-reference voltages of 0.4 and 0.5 V are given in Table 2.3-2. Suffix A in the "Catalyst" column refers to electrodes made using the modified dry - blending technique. It is apparent that both types of electrodes gave similar results.

The effect of the specific surface area of the substrate on the average specific current of the two types of electrodes at E_{a-r} = 0.4 and 0.5 V is shown in Figure 2.3-2. At the lower areas performance improved with increasing surface area, but above approximately 350 m^2/g performance fell off sharply. The areas used in this plot are those given by the supplier for the untreated substrates.

The effect of Pt activation on the original surface areas was investigated by estimating average particle diameters from electron micrographs of the electrocatalysts. It is seen from the results summarized in Table 2.3-3 (c.f. Table 2.3-1) that the 850 m^2/g carbon lost much of its original surface area during the activation procedure. Figures 2.3-3 and 2.3-4 show electron micrographs of the electrocatalysts made using the 850 (Prep. No. 60) and the 380 (Prep. No. 90) m^2/g carbons, respectively. Note that the Pt crystallite size of Prep. No. 60 is the same order of magnitude as the carbon particle size of Prep. No. 90. As shown in Figure 2.3-5, there is a good correlation between performance and actual electrocatalyst surface area, expressed as the reciprocal of the diameter of the average electrocatalyst particle.

The following are some of the experimental observations which suggest the cause of the loss in surface area occurring during activation of the substrates. The weight gain of the carbons as a result of Pt activation decreased with increasing volatile content of the untreated substrate. The apparent weight loss is accounted for fairly well by assuming removal of the substrate volatile content. These data are summarized in Table 2.3-3. A sample of the 850 m^2/g carbon which was subjected to the activation procedure without the addition of Pt salt showed no significant weight change. These facts suggest that Pt catalyzes the oxidation of the carbon volatile content during activation of all the carbons studied. Under the conditions used for activation, the heat of this reaction is sufficiently high to cause sintering of the 850 m^2/g carbon, which has a relatively large volatile content and small particle size. The reaction is sufficiently vigorous above 200°C to ignite the non-graphitic carbons.

(2.3-2) E. J. Cairns and E. J. McInerney, Technical Summary Report No. 7, Hydrocarbon - Air Fuel Cells, Jan. 1 - June 30, 1965, ARPA Order No. 247, Contract Nos. DA-44-009-ENG-4909 and DA-44-009-AMC-479 (T).

Table 2.3-2

Electrocatalyst Comparisons

$C_8H_{18(l)}$ (30 w/o Pt/C)/36 m/o HF/(Pt)O_2 T = 105°C

Press force 5000 lb; Binder 45 v/o T-7; Film 0.27-0.31 mg TFE/cm^2; Dry blend

Catalyst	Pt Loading, mg Pt/cm^2	i (E_{a-r} = 0.4 V), ma/cm^2	i (E_{a-r} = 0.5 V), ma/cm^2	ma/mg Pt, (E_{a-r} = 0.4 V)	ma/mg Pt, (E_{a-r} = 0.5 V)	Cell
Prep. No.						
51	10.29	5.31	16.6	0.516	1.61	8620-4
54	10.29	4.05	12.0	0.394	1.17	-16
51A	15.19	7.20	15.5	0.474	1.02	-5
60	13.80	2.63	4.92	0.191	0.357	8656-1
60A	13.12	2.76	5.53	0.210	0.421	8620-12
70	11.40	1.96	4.08	0.172	0.358	-6
70A	12.52	2.01	4.57	0.161	0.365	-7
80	13.55	5.92	11.6	0.437	0.856	-8
80A	16.41	4.90	10.6	0.299	0.646	-9
90	12.96	5.55	[illegible].1	0.428	1.04	-10
90A	15.88	8.05	17.1	0.507	1.08	-13

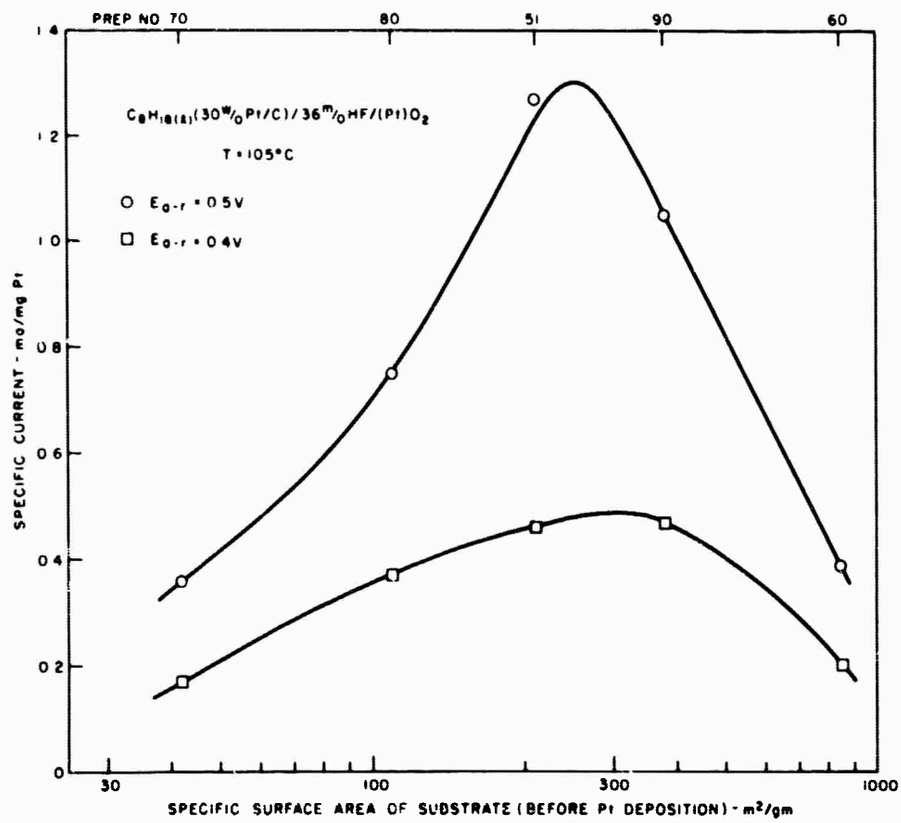

Figure 2.3-2. Effect of Specific Surface Area of Carbon Substrate on Specific n-Octane Performance at E_{a-r} = 0.4 and 0.5V

Table 2.3-3

Properties of Carbon-Supported Catalysts

Nominally 30 w/o Pt/C in Three 10 w/o Laminations

Pt Salt: $Pt(NH_3)_2(NO_2)_2$

Amount of Substrate: 3.00 gm

Theoretical Weight Gain as PtO_2: 1.50 g

Catalyst Pre. No.	Average Particle Diameter (a), Millimicron	Total Weight Gain of Substrate, gm	Total Weight Gain + Substrate Volatile Content, gm
70	59.1	1.51	1.54
80	28.7	1.42	1.57
90	16.3	1.28	1.43
60	50.6	0.99	1.38
51	15.2	1.58	1.58

(a) Estimated from electron photomicrographs.

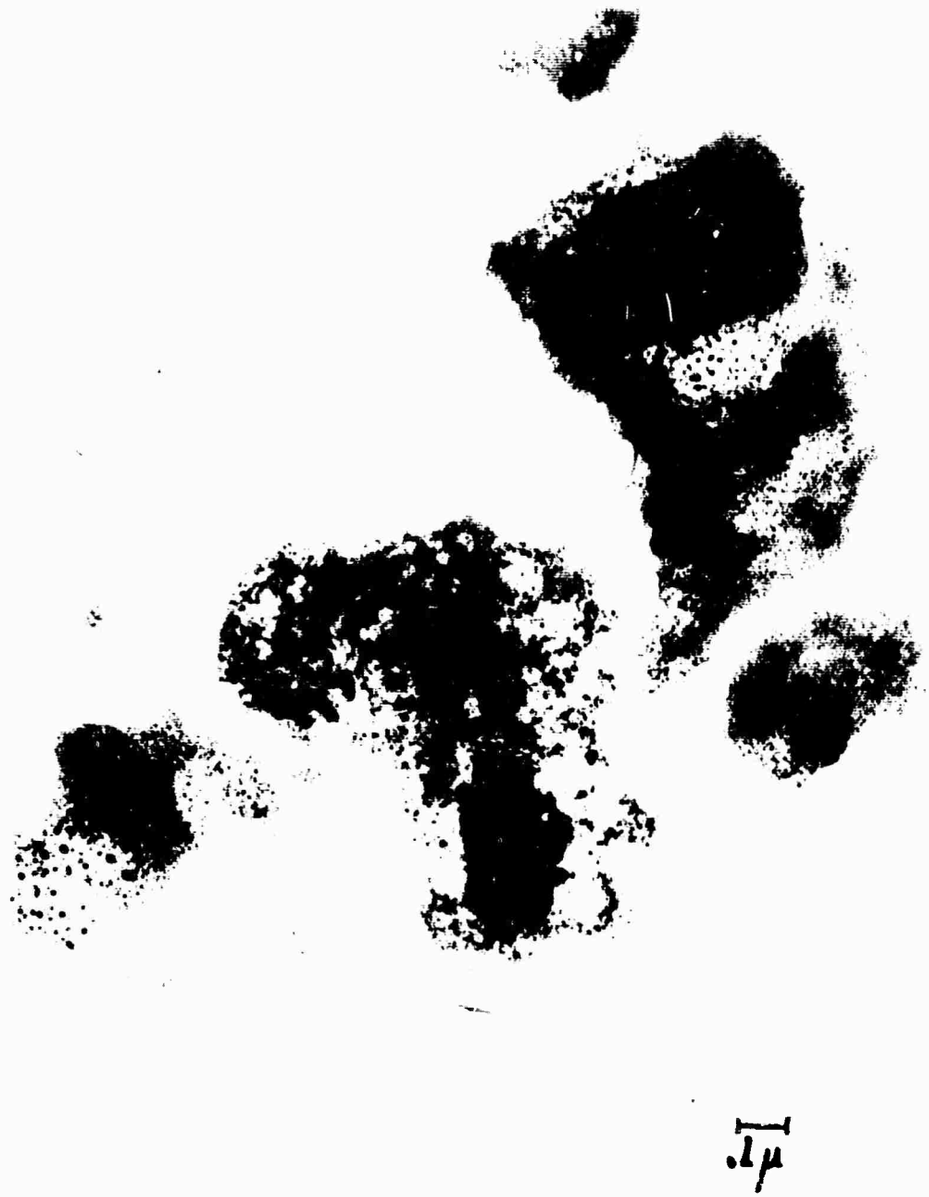

Figure 2.3-3. Electron Micrograph of Non-Graphitic Carbon Powder (850 m^2/g Carbon, Prep. No. 60) Activated with 30 w/o Pt. 100,000 x (before reduction for printing)

Figure 2.3-4. Electron Micrograph of Non-Graphitic Carbon Powder (380 m^2/g Carbon, Prep. No. 90) Activated with 30 w/o Pt. 100,000 x (before reduction for printing)

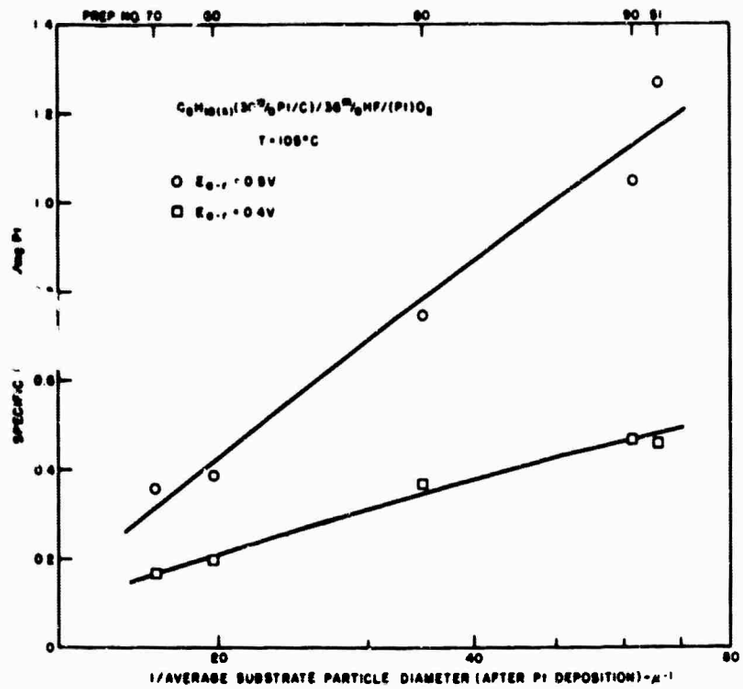

Figure 2.3-5. Effect of Average Particle Size of Pt/C Electrocatalyst on Specific n-Octane Performance at E_{a-r} = 0.4 and 0.5V

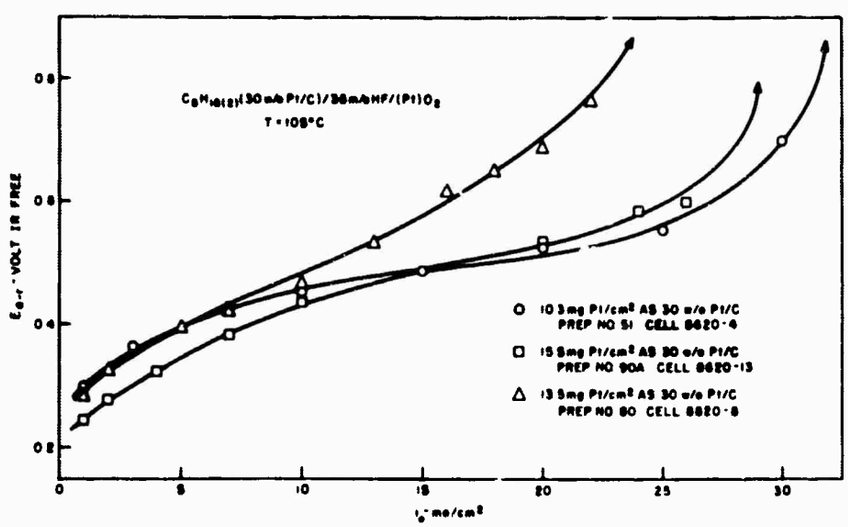

Figure 2.3-6. Anode Performance on n-Octane with 30 w/o Pt on C, Preparations 51, 80 and 90A

It should be possible to avoid sintering by preheating the untreated carbons at 800 - 1000°C in an inert atmosphere. This will result in a significant loss of volatiles without appreciable loss in surface area. Alternatively, milder conditions of activation may be used.

Performance curves for the three best electrocatalysts are shown in Figure 2.3-6. Assuming an average standard cathode performance (2.3-2), Prep. No. 51 gave 0.83 watt/g Pt at the anode at an I-R free cell voltage of 0.4 V, or 0.69 watt/g Pt at 0.4 V I-R included with an 1/8 inch electrolyte spacer. The results are encouraging, especially in view of the fact that no attempt was made to optimize electrode structure for any substrates tested. The electrode structure used was designed for an 11.4 m^2/g graphitic substrate (2.3-1) and is not necessarily optimum for any of the carbons used here. Further improvements are likely through the use of higher area substrates in an optimized electrode structure.

2.3.3 Conclusions

1. Of the catalysts tested for the anodic oxidation of octane in HF at 105°C a 212 m^2/g graphite - supported material is the most active, yielding 0.83 watt/g Pt at the anode based on an average standard cathode performance at an I-R free cell voltage of 0.4 V.

2. Increasing the surface area of the non-graphitic carbon substrate (up to at least 380 m^2/g) improves octane performance, using given electrocatalyst and electrode preparation procedures.

3. Non-graphitic carbons having surface areas greater than about 500 m^2/g and high volatile contents undergo sintering under the conditions of the Pt activation procedure presently used.

BLANK PAGE

3.0 ANALYSIS OF DIRECT HYDROCARBON/AIR FUEL CELL SYSTEM FOR LIQUID FUELS

(P. J. Chludzinski, D. C. Shah)

3.1 Background

3.1.1 Summary

Much research and development has been conducted on the direct hydrocarbon/air fuel cell during recent years. A variety of fuels, electrolytes, and electrode structures have been investigated in order to develop a high performance fuel cell system. At this point it was decided to review all these studies, and analyze the direct hydrocarbon cell as an integral component in a total fuel cell system. The intention was to point up the capabilities of such a system, as well as the limitations which must be further explored for future improvement.

Based on the data assembled under these government contracts, certain choices of components which seemed logical from the standpoint of high performance were chosen. Phosphoric acid seemed to be the best electrolyte in spite of the anodic cycling which has been observed in single cells. Teflon-bonded platinum electrodes supported on tantalum screens were chosen in spite of their limited life and high cost. Normal octane was chosen as the fuel, even though it also is expensive. The result of the system study was, therefore, a view of the upper limit in performance attainable today, even though the system is expensive.

The fuel cell stack was optimized on the basis of weight and efficiency, taking into account the electrode physical properties, current density, electrode size and shape, and the electrolyte gap. By an examination of trends in weight and efficiency optimization, coupled with practical considerations of mechanical integrity, one "design point" at each of two operating temperatures was chosen for detailed system analysis. The cell stack was integrated into a total system containing the necessary vaporizers, preheaters, condensers and pumps. Operating conditions were found at which the system was water conservative. The weight, volume, parasitic power, heat losses, and overall thermal efficiency were calculated. A conceptual layout of 0.5 KW fuel cell system was drawn, which showed the relative sizes and functions of the components.

The "optimum" system was composed of 15 by 10 inch electrodes separated by 1/16 inch of phosphoric acid at 150°C. The fuel was normal octane, the oxidant was air at three times stoichiometric flow rate. The system produced a net power of 540 watts with an overall thermal efficiency of 20% based on the higher heating value of the fuel. Parasitic power was 60 watts if condensers were cooled by free convection air. The system weight was 220 lb and occupied about 8 ft^3. If forced convection cooling were used, a weight and volume decrease of 10 and 20%, respectively, could be attained, at the expense of additional parasitic power and a second air pump. The additional parasitic power was

tolerable only if cooling air could be supplied and distributed properly at very low pressures (less than 1 inch H_2O). Since this may not be practical, it is probably better to suffer the volume and weight penalty for the convenience of free convection at a higher overall efficiency.

It was found that the weight of the stack was strongly reduced by thinner electrolyte gaps. The system weight was affected less strongly because large amounts of electrolyte were needed in the fuel vaporization equipment. System weight was affected very strongly by designing for a higher temperature of operation, but the high acid concentration needed for self-sustained operation poses the problem of electrolyte solidification when the system is shut down and cooled.

This study did not include the effects of anodic cycling, i.e., the power pulsations observed when single cells operate in phosphoric acid, since not much is known about the cycling behavior of multi-cell stacks. If the anodic cycling of individual cells in a stack are self-cancelling, then phosphoric acid is a practical electrolyte. If not, the only alternative at this time is hydrofluoric acid, which is the only electrolyte which prevents cycling. However, it is doubtful that hydrofluoric acid can be engineered to be a practical electrolyte. This points up the great need to study anodic cycling behavior in multi-cell stacks before consideration is given to build a system.

Additional study areas suggest themselves. There is need for scale-up to the large sizes already mentioned. Noble metal cost reduction has always been a goal in fuel cell development. It has been found that it is desirable to decrease electrolyte gaps. It seems that all of these goals could be greatly augmented by the use of the matrix electrolyte currently under development. The matrix affords a low weight, non-leaking substrate upon which it is possible to apply thin layers of electrocatalyst. Of course, a secondary coolant system would be needed, the weight and complexity of which has not been assessed in this study.

3.1.2 Introduction

The purpose of this task is to evaluate the data accumulated under the previous ERDL contracts and using it as a basis, investigate a direct hydrocarbon/air fuel cell system, including cell stack and auxiliaries. In the course of the investigation some optimization would be done, and some problem areas would be uncovered which would give direction for future development work. The objective of the task can best be amplified by the contractual wording as follows:

"The experimental information obtained under parts I - III (of this contract) will be reviewed and the optimum direct hydrocarbon-air fuel cell system for use with liquid hydrocarbon fuel will be selected. This will include the:

a. Choice of electrolyte.

b. Choice of cell operating temperature.

c. Choice of fuel vaporization or injection procedure.

d. Choice of electrolyte containment method.

e. Choice of electrode composition.

"Based on these prime choices of approach and operating conditions a system analysis of the total system will be made which will include detailed heat, water and mass balance calculations. Major components will be described in terms of the functions they perform and the approximate sizings, and a preliminary conceptual layout of a 0.5 KW direct hydrocarbon fuel cell system will be prepared."

3.2 CHOICES OF COMPONENTS AND OPERATING CONDITIONS

Upon reviewing the data assembled under previous contracts, certain choices of components and operating conditions were made, keeping as many as possible of the conditions general enough so that they would be chosen by the results of the detailed heat and mass balances.

3.2.1 Choice of Electrolyte

From the many electrolytes which have been experimentally studied only one was chosen for analytical study, namely, phosphoric acid, the temperature and concentration of which would be determined by the results of the analysis. Other electrolytes studied experimentally and reasons for their rejection are:

Potassium Hydroxide. Hydrocarbons used directly with this electrolyte exhibit very low performance. Conservation of electrolyte is impossible, since the electrolyte is chemically neutralized by carbon dioxide generated by the hydrocarbon reaction, as well as that carried in the ambient air.

Cation Exchange Membranes. Sulfonic acid ion exchange membranes show low performance for the direct electrochemical oxidation of hydrocarbons, primarily because of their low operating temperature limit, which limits fuel reactivity.

Aqueous Sulfuric Acid. Here again, operation is limited to relatively low temperatures, with consequent low performance. Higher operating temperature would require higher electrolyte concentration which causes sulfur compounds to be formed from chemical reduction of the sulfuric acid. The sulfur compounds produced are usually detrimental to the performance of fuel cell electrodes.

Aqueous Hydrofluoric Acid. Water conservation is possible with this electrolyte, but conservation of hydrogen fluoride is not. There is a sufficiently high vapor pressure of HF above the liquid, so that excessive quantities of acid are exhausted to the surroundings from the cathode and anode exhausts. For example, a 500 watt battery operating continuously, using three times stoichiometric air, with the air being cooled to 70°F before being exhausted, would lose almost 4 oz per day of anhydrous HF, which would have to be replaced to maintain electrolyte invariance. If the air were exhausted at 90°F, the loss of HF would almost double.

Cesium Fluoride + Aqueous Hydrofluoric Acid. The same general remarks apply to this electrolyte as to hydrofluoric acid, although the loss of HF is less severe.

Cesium Carbonate. Although unaffected by carbon dioxide, this electrolyte has shown poor performance with hydrocarbons.

One problem which is experienced with phosphoric acid, and not with hydrofluoric acid, is anodic cycling. Single cells have shown considerable power fluctuations as a function of time. If a stack were constructed with many cells in series, the power pulsations from the individual cells might tend to cancel one another, resulting in a smoothing of the overall output, or the surges may occur simultaneously, causing massive periodic pulsations. Before a direct hydrocarbon system is built to operate on phosphoric acid, the cycling behavior of multi-cell stacks must first be determined.

For purposes of this study, it was assumed that the ability of the system to maintain conservation of mass was in principle more important than the cycling behavior of multi-cell arrangements which is as yet undetermined. Conservation of mass, as implied here, not only refers to water conservation, but more vitally, that the system needs no makeup of non-logistical and possibly hazardous constituents. Phosphoric acid meets these requirements, since no phosphorous-bearing compounds leave the system, but in the case of hydrofluoric acid, fluorine-bearing compounds (HF) are present in the exhaust air and fuel streams. The recapture of HF would involve unconventional separation techniques, unknown at this time, or refrigeration techniques complicated by the corrosive nature of aerated, moist hydrogen fluoride. For military applications of low power (500 watts) systems, the parasitic power (perhaps 200 watts) for refrigeration techniques would be excessive.

3.2.2 Choice of Fuel Vaporization or Injection Procedure

The fuel chosen for the system study was n-octane. The performance of fuels ranging from pentane to octane are closely comparable at practical current densities. On the other hand, the fuel efficiency is quite dependent on the boiling point of the fuel. For instance, if the fuel exhaust leaves the system at 85°F, the product carbon dioxide will carry away enough raw fuel to lower the fuel efficiency to 85% in the case of octane, and 60% for heptane (or a common raffinate).

Fuel will be pumped mechanically, since relatively high pressure will be required to overcome manifold and condenser flow resistances. Preliminary calculations showed that ten times stoichiometric fuel could reasonably be vaporized by exchanging heat with the electrolyte. This would allow fuels with boiling points as high as octane to be vaporized at efficient thermal gradients (say, 50°F). Some of the raffinates could be completely vaporized, and fuels such as JP-4 could be partially distilled by adjusting electrolyte temperature.

3.2.3 Choice of Electrolyte Containment Method

Only free phosphoric acid has been experimentally studied under contract, therefore only a free electrolyte was considered for the system analysis. The bulk of the electrolyte, used for circulation and cooling was held in a "pan" located beneath the cell stack. The pan thus served as an air

exhaust manifold, electrolyte reservoir, leakage sump, a cooler for heat dissipation during operation, and a heater for starting the unit with burner flue gas.

3.2.4 Choice of Electrode Composition

Electrodes made of Teflon-bonded platinum on tantalum screen were chosen. These are expensive, but have good performance. Platinum on a boron carbide substrate could have been chosen, which would give longer life and lower cost, at the expense of much poorer performance. Suffice it to say that the "optimum" electrode choice would be a boron carbide electrode exhibiting the performance shown by pure platinum electrodes. Platinum screens were used in some of experimental work, but they are out of the question because of cost (about $7.00 per square inch).

3.3 PROCESS STREAM ARRANGEMENTS

Preliminary investigations indicated that particular arrangements of process streams were more feasible than others. For example, fuel could be adequately vaporized by exchanging heat from the electrolyte. Reaction air was best preheated by the hot moist exhaust air. Start-up of the unit could be accomplished by heating the electrolyte. The flow sheet based on these concepts is shown in Figure 3.3-1. The system is composed of five main components: fuel cell stack, electrolyte cooler, exhaust air condenser, fuel condenser, and fuel tank. Three pumps are also shown for air, fuel, and electrolyte. In the practical layout, the fuel cell stack and electrolyte cooler are combined into one unit. Fuel is preheated by the electrolyte and fed to the anodes. The electrolyte cooler also serves to catch the acid leakage from the cells. It contains heat transfer surfaces for removing some reaction heat during steady-state operation, and to be used for start-up by heating with flue gas derived from burning raw fuel.

The fuel tank and pump were sized for ten times stoichiometric fuel flow, (with fuel condensate return) for ten hours continuous operation.

The exhaust air condenser is used to preheat the reaction air, and to cool the exhaust air sufficiently to condense enough water to be returned to the electrolyte for system water conservation. Similarly, the fuel condenser cools and condenses excess fuel and water to be returned to fuel tank and electrolyte, respectively. In the arrangement shown here the cooling air is under forced convection, being supplied from a common pump.

As detailed calculations were being made, it became apparent that the parasitic power required to pump cooling air was excessive because of the arrangement of the exhaust air condenser. The temperature of the exhaust air after it preheats the reactant air is low enough, so that large quantities of cooling air are required to further cool and condense. To avoid the parasitic power requirements, free convection was used for cooling the exhaust air condenser as well as the fuel condenser. Figure 3.3-2 shows a process flow sheet in which free convection cooling is used. The exhaust air flow is split to the reactant air preheater and the exhaust air condenser. The fuel condenser is also free convection cooled. Otherwise the functions of the components are the same as in Figure 3.3-1. Free convection cooling not only eliminated much of the parasitic power requirements, but also eliminated the necessary ductwork and control valves needed with forced convection streams split from a common air pump. The volume of heat exchangers was not prohibitive, since the free convection heat transfer coefficients were reasonably high. On the other hand, forced convection cooling air might have to be pumped to reasonably high pressures (4 inches H_2O or more), not because of pressure drops through heat exchanger cores, but because of built-in restrictions necessary for proper air distribution. Free convection heat exchangers have intrinsically good air distribution because of the nature of the free convective buoyant driving forces.

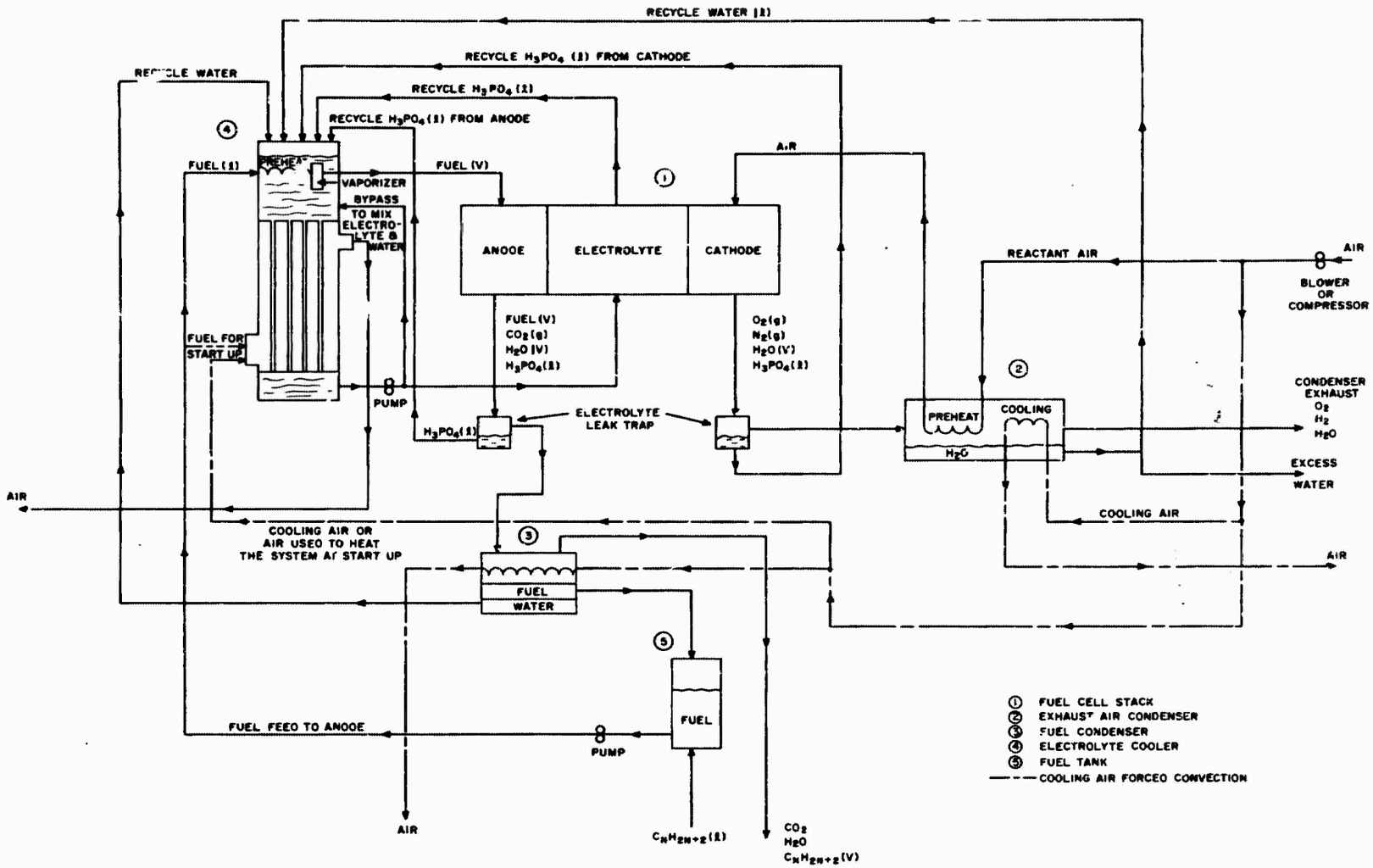

Figure 3.3-1. Process Flow Sheet - Hydrocarbon/Air Fuel Cell System, Forced Convection Cooling

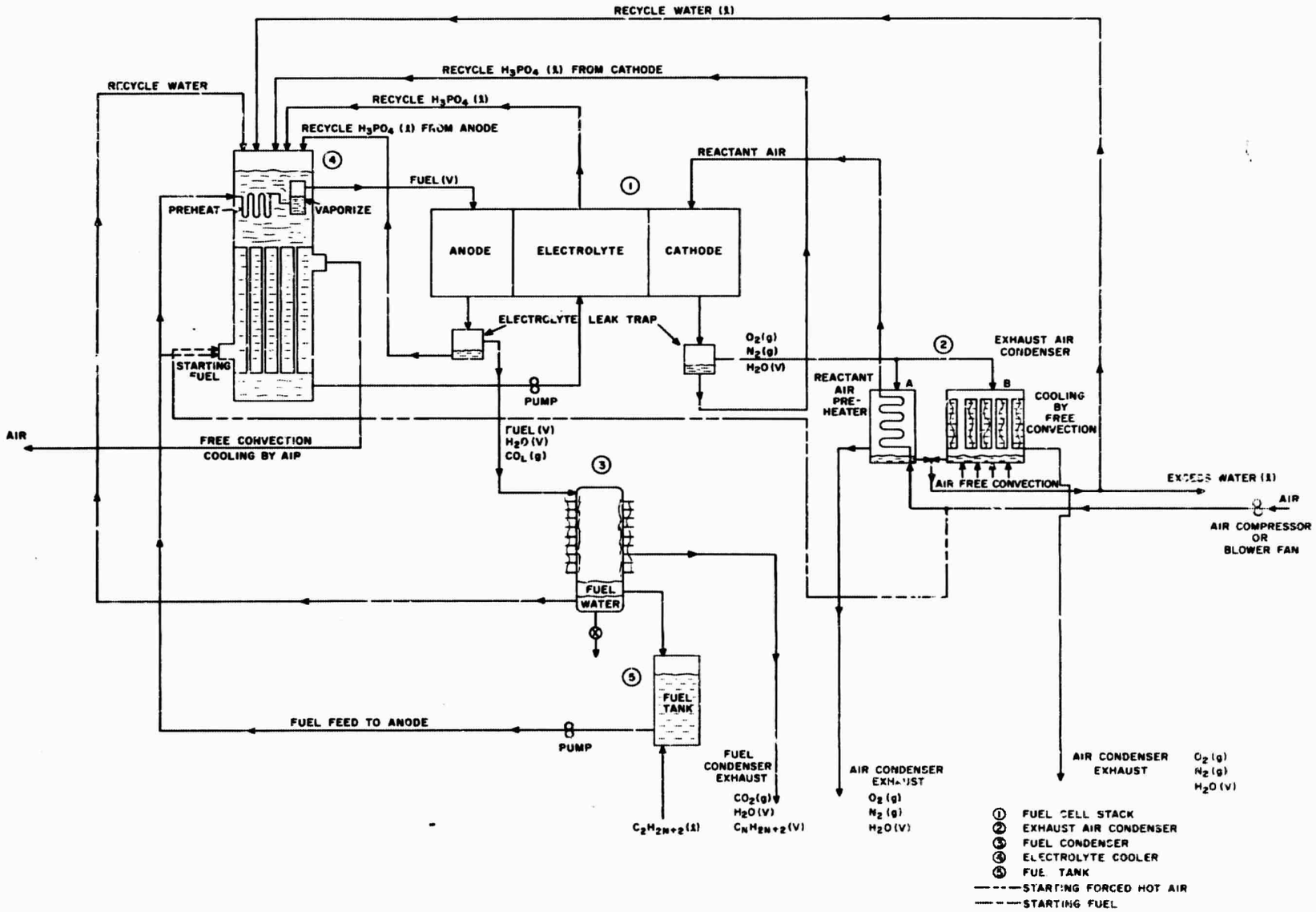

Figure 3.3-2. Process Flow Sheet -- Hydrocarbon/Air Fuel Cell System, Free Convection Cooling

3.4 SYSTEM OPTIMIZATION

In a complete system optimization the question first arises as to what basis to use for an optimization. It has already been inferred that cost was not an overriding factor in the optimization study, since platinum electrodes were chosen. It was felt that at this time, the major factors to consider were weight, volume, and overall efficiency. These factors depend on numerous interrelated parameters, such as current density, polarization characteristics, air and fuel flow, ambient temperature, heat losses, and the geometry of the stack. To include all these factors simultaneously in a complete system study would involve an intractable hand calculation, or a complicated computer program for which time and money were lacking. It was more advisable to initially separate the cell stack core from the auxiliaries and see if an optimum weight vs. efficiency could be obtained. The optimum found from the core analysis would then be integrated to the appropriate auxiliaries for a detailed heat and mass balance calculation, assuming that the optimum core would produce a correspondingly optimum system. Appendix 4.5 pursues the core optimization in more detail. A small computer program was run for the following cell arrangement.

A. Niedrach-Alford type electrodes on expanded tantalum screen, the active area measuring 2 (H) inches high and (L) inches wide. The current was collected from the two opposite edges of the screen in the direction of the height. The type of screen and physical properties were varied to find an optimum.

B. Frames for forming anode and cathode compartments were assumed to be made from a material such as polyphenylene oxide or polysulfone. These were chosen for their low density and good strength as compared to Teflon, for example. Gas frames were assumed to be 0.5 inch wide and 0.125 inch thick, with one anode chamber feeding two anodes, and likewise for the cathode chamber. The electrolyte frame was assumed to be made of PPO or polysulfone, 0.5 inch wide. The thickness was varied in the optimization study.

The computer plotted curves of the specific weight of the battery core, SWB (lb/KW), vs. the height 2 (H) of the electrode active area for various electrode widths (L). A sample of the computer output is shown in Figure 3.4-1. It can be seen that a minimum specific weight (SWB) is obtained at various values of (H) depending on the screen geometry, electrolyte gap, electrode resistivity, current density, and temperature. It can be seen that as (L) is varied from 5 to 25 inches, the specific weight of the battery decreases continuously, and there probably is no maximum value of the electrode width which gives a minimum weight, nor is there any reason for believing such a maximum value should exist. However, above electrode widths of 15 inches, it seems as though little weight reduction of the stack is obtained. Fifteen inches was thus chosen as a somewhat

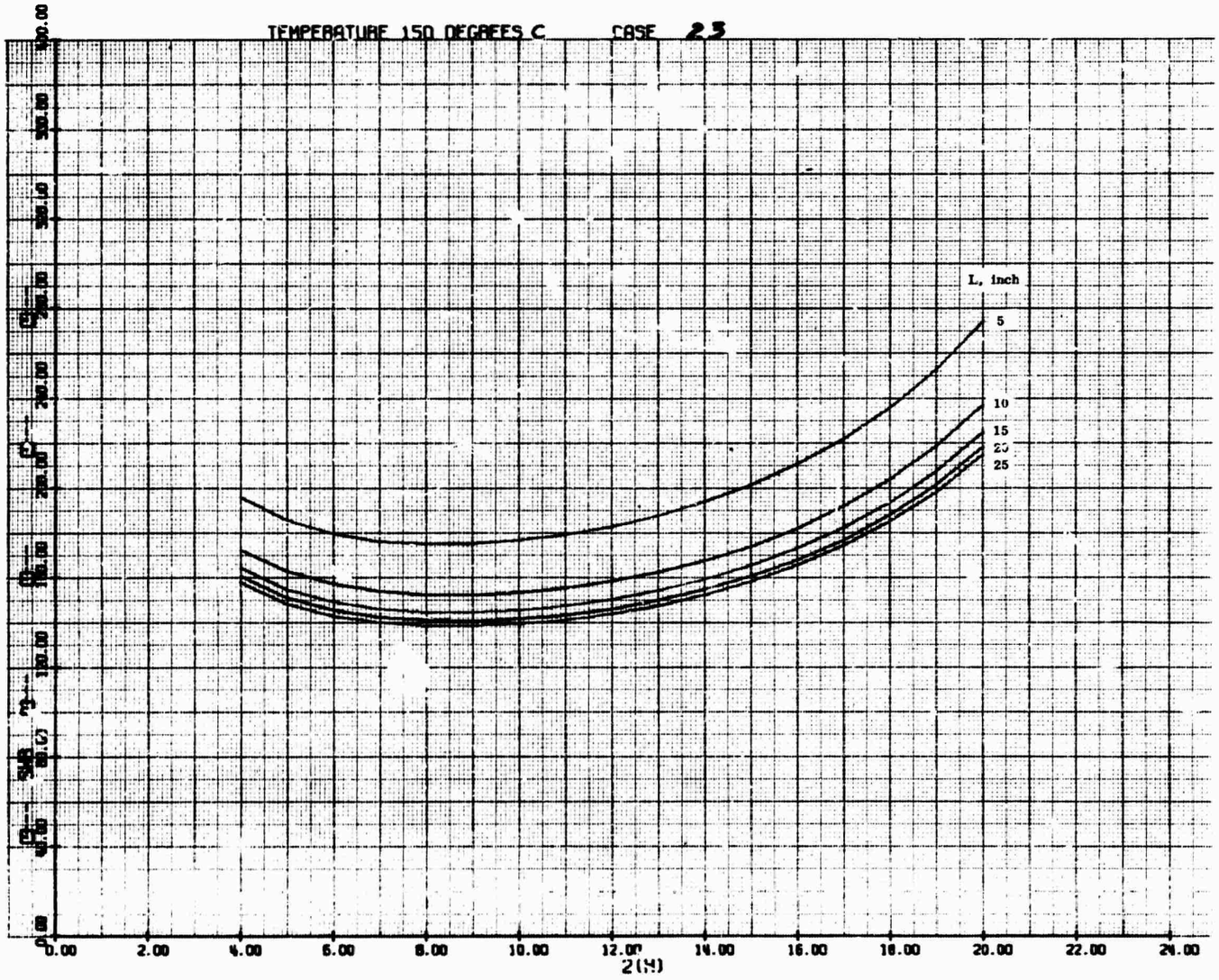

Figure 3.4-1. Sample Computer Output for Stack Core Optimization

arbitrary although seemingly practical value of the width of the electrode active area. Of course, the choice of electrode widths higher than this value is entirely valid, limited only by manufacturing considerations, such as availability of screen, hydraulic press dimensions, and catalyst spreading techniques.

The specific weight of the stack minimizes at values of the electrode height in the vicinity of 10 inches. Below 10 inches, more cells are needed to produce the same power, since the cell area is smaller. At these conditions, the weight increased because the plastic frames contribute proportionately more weight to the system. Above 10 inches, more cells are needed because a power loss is suffered by the cell current running along large distances (in the direction of the electrode height). Because of this loss, more cells are needed to obtain the same power.

The values of the electrode active area were chosen at 10 inches for the height, which produced minimum weight, and 15 inches for the width, which seemed a practical value, producing a "minimal" weight.

When the data for 2 (H) = 10, (L) = 15 was analyzed, a parameter called η_{LHV}/SWB was chosen as a rating factor for a core. The efficiency η_{LHV} is defined as the cell net potential divided by the theoretical voltage obtained from the heats of formation of the (octane) reaction:

$$C_8H_{18}(v) + \frac{25}{2} O_2 \rightarrow 8\ CO_2 + 9\ H_2O(v) \quad .$$

The heats of formation are evaluated at the cell operating temperature for all reactants and products, all in the gas phase. This is different from the actual lower heating value of a fuel, where reactants and products are evaluated at 25°C with the product water as a gas. In the ensuing detailed heat and mass balance, the overall efficiency was calculated by dividing the net power out of the system by the higher heating value of the fuel used, where the product water is considered at 25°C in the liquid phase. SWB is the specific weight of the cell stack core, lb/KW, exclusive of end plates, insulation, and auxiliaries. The core (and perhaps the whole system) will be rated more favorably as η_{LHV} is higher, and as SWB is lower. As SWB decreases, probably the volume of the system also decreases.

For the cases studied, the results are plotted in Figure 3.4-2 and 3.4-3. If one examines the trend in the "efficiency weight" parameter with electrode screen resistivity, it is apparent that there is a value of screen resistivity producing a maximum value of the parameter. Electrodes having higher resistivity and correspondingly lower weight, produce higher power losses because of the method of collecting current from the edges of the screen. More cells and more weight are needed to make up the power loss. Screens of low resistance cause less power loss, but because they weigh more per square foot, they also cause the stack weight to increase. For the conditions

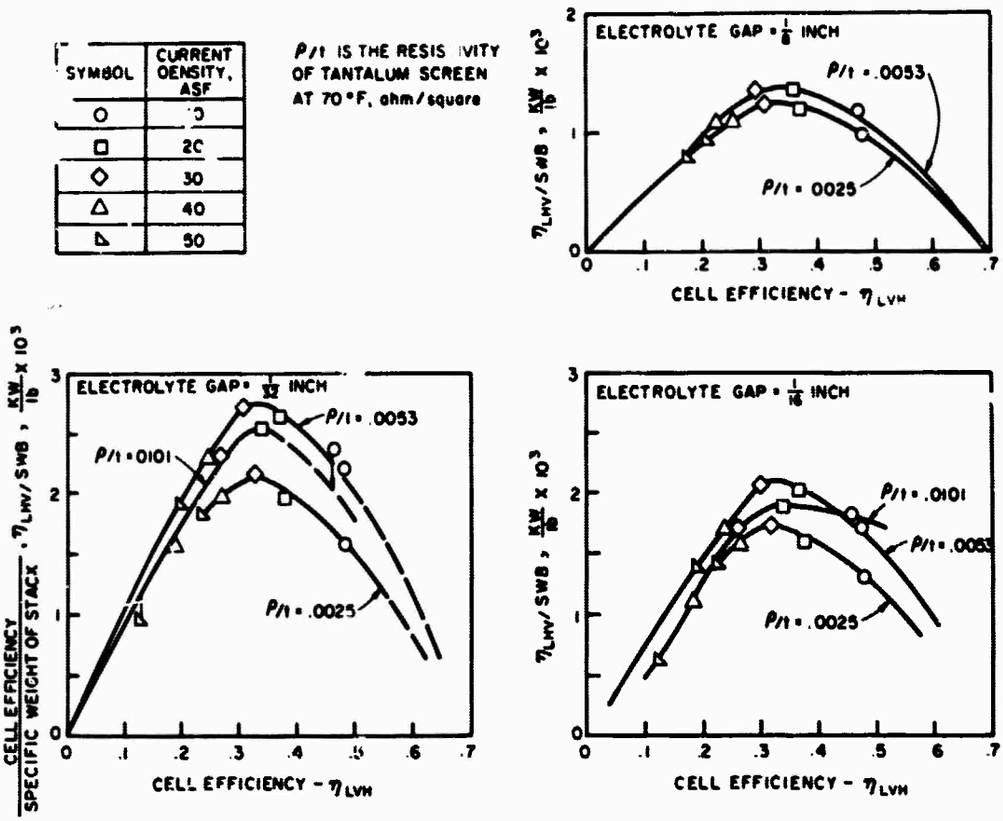

Figure 3.4-2. Efficiency, Weight Parameter for n-Octane/96% wt % H_3PO_4/Air, 600 Watts Gross Output, Operating Temperature = 150°C, Electrode Geometry: 10 inch High x 15 inch Wide

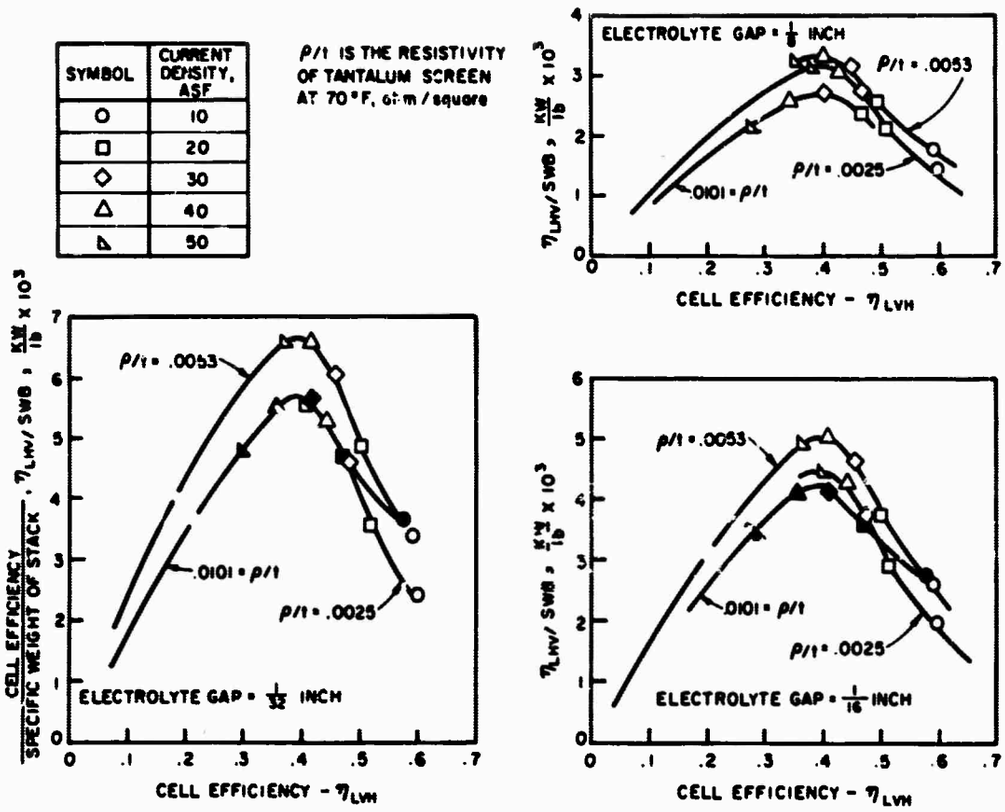

Figure 3.4-3. Efficiency, Weight Parameter for n-Octane/100 wt. % H_3PO_4/Air, 600 Watts Gross Output, Operating Temperature = 180°C, Electrode Geometry: 10 inch High x 15 inch Wide

studied here, a tantalum screen having a resistivity of 0.0053 ohm per square proved to be the best choice for maximizing the "efficiency, weight" parameter. This particular screen happens also to be one which had been used in the manufacture of most of the electrodes life tested under the ERDL contracts. Appendix 4.6 explains the term "ohm per square" in detail.

Examination of the trend in the weight, efficiency parameter with electroylte gap (Figure 3.4-4) shows that the rate of increase of the parameter increases with decreasing electrolyte gap. This means that it is advantageous from a weight standpoint to decrease the gap as much as possible. The pumping power is not great even at very small gaps as is evident from Table 3.4-1.

Table 3.4-1

Pumping Power and Pressure Drop to Pump Electrolyte Through Stack, Exclusive of Manifolds. Flow Rate of Electrolyte = 274 lb/hr.

Electrolyte gap, inch	Pressure Drop, inch H_2O	Pumping Power, watt
0.01	38.48	0.1952
0.02	4.81	0.0244
0.04	0.60	0.0031
0.06	0.18	0.0009

The electrolyte gap, therefore, can be reduced to very small values without much penalty in parasitic power, although below 0.02 inch the pressure drop is very high and this may be the real limitation in reducing the electrolyte gap.

For the detailed analysis the electrolyte gap was chosen at 1/16 inch, mainly for reasons of mechanical integrity. The weight was then estimated for the same type of system using 1/32 inch gap. Actually, the total system weight for the 1/32 inch electrolyte gap was only about 7% lower than for the 1/16 inch gap, since the weight of electrolyte in the pan and the auxiliary weights was a large fraction of the total system weight. After laying out the total system, it was apparent that the pan had to contain a relatively large mass of bulk electrolyte in order to heat the fuel vaporizer contained in the pan. While considerable decrease in weight could be obtained in the stack itself by lowering the gap, the same amount of electrolyte had to be maintained in the pan, which buffered the overall weight decrease to only 7%.

Two cases were taken for detailed calculation at heat and mass balance and conservation for the system. They were:

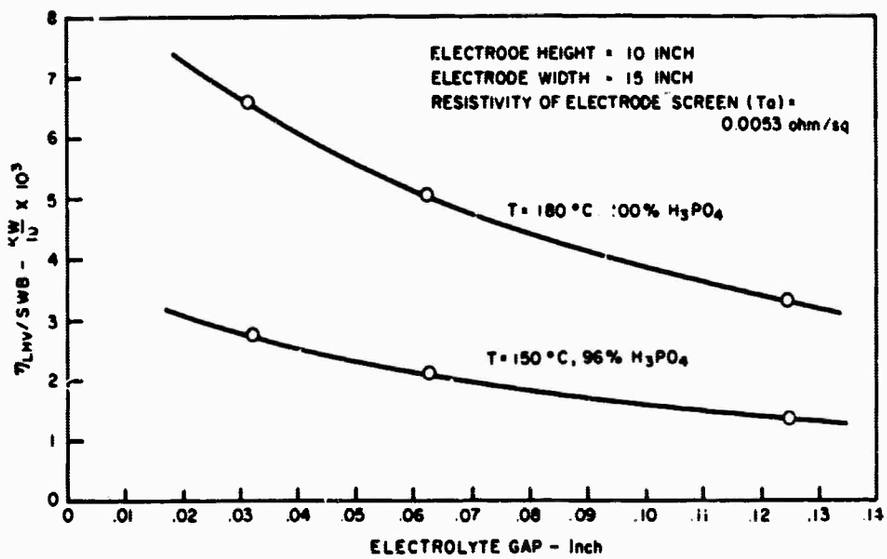

Figure 3.4-4. Peak Values of Efficiency, Weight Parameter for n-Octane/H_3PO_4/Air

Case I

T = 150°C operating temperature

J = 30 ASF, 600 watts gross power

(ρ/t) = 0.0053 ohm per square

Electrolyte gap = 1/16 inch

Electrolyte concentration ≈ 95% by weight

Case II

T = 180°C operating temperature

J = 40 ASF, 600 watts gross power

(ρ/t) = 0.0053 ohm per square

Electrolyte gap = 1/16 inch

Electrolyte concentration ≈ 100% by weight

The two cases previously mentioned were calculated by hand according to equations in Appendix 4.7. In essence, the system components were analyzed separately for heat and mass transport to assure self-sustained operation of the fuel cells and then analyzed as a total system for the conservation of water and an overall heat balance. The heat exchangers were sized, parasitic power and heat losses were determined, and overall thermal efficiencies were determined. The detailed results of these calculations are presented in Appendix 4.8.

Table 3.4-2 summarizes the pertinent results as taken from Appendix 4.8, and Table 3.4-3 lists the weight breakdown.

The parasitic power requirements if forced convection cooling were used would be 220 watts, if cooling air were supplied at 4 inches H_2O. This would drop the efficiency of the system by 6 percentage points. If cooling air could be properly distributed by 0.5 inch H_2O pressure, the total parasitic power would be 80 watts, lowering the system efficiency by only 2 percentage points. Since reaction air must be supplied at about 14 inches H_2O, a separate blower would be needed for the cooling air. The weight of the forced air-cooled system would be 10% less, and the volume 20% less than the free convection system. The heat exchangers would be about one fourth the size of the free convection case. The weight of the free convection cooled system using 1/32 inch electrolyte gap at 180°C is about 67% of that of the system using 1/16 inch gap at 150°C. In order to obtain this more attractive condition, an electrode with considerably better life would have to be developed, with a minimum of performance penalty. Also, experimental work using very small electrolyte gaps and internal manifolding would have to be done.

Table 3.4-2

Summary of Results for Direct Hydrocarbon/Air/H_3PO_4 Fuel Cell System, Free Convection Cooling

Cell Active Area = 15 x 10 inch = 150 in.^{2}

	Case I		Case II	
Cell operating temperature, °C	150	150	180	180
Electrolyte gap, inch	1/16	1/32	1/16	1/32
Gross power, watts	600	600	600	600
Net power, watts	543	543	548	548
Overall HHV thermal efficiency, %	20	20	28	28
Total system weight, lb	219	202	151	147
Total system envelope volume, ft^3	8.2	≈8	≈6.5	≈6.5
Number of cells in stack	61	61	34	34
Current density, ASF	30	30	40	40
Cell voltage, net, volts	0.32	0.32	0.43	0.43
Weight of cell stack core, lb	87	70	49	43
Volume of auxiliaries, % of total	40	40	50	50
Ambient temp. at which water conservation is maintained, °F	85	85	85	85

It is interesting to note that the optimum current density for the 180°C operating temperature is only 40ASF (vs. 30 ASF for the 150°C case), even though the performance on a resistance free basis is much higher at 180°C. This is a result of "edge" current collection, whereby the current must traverse a large portion of the electrode before it is collected at the outer edge of the screen. Even though the higher temperature system is capable of much higher current density, it is wasted by voltage drop in the tantalum screen, and the real advantage to the higher temperature is the lower anodic overpotential.

Table 3.4-3

Component Weights for the 0.5 KW System, Free Convection Cooling

Electrolyte gap, inch		1/16	1/32	1/16	1/32
Cell operating temp, °C		150	150	180	180
Cell core + electrolyte		87.2	70.0	48.4	43.0
0.04 inch thick Ta electrolyte pan		13.6	13.0	6.0	6.0
Electrolyte in pan		31.0	31.0	12.1	12.0
End plates, 0.5 inch thick PPO		6.4	6.4	6.4	6.4
Fuel preheater (Teflon)		1.0	1.0	1.0	1.0
Starter-heater (Ta)		1.0	2.0	1.0	2.0
Insulation		6.6	6.6	4.0	4.0
Pumps		15.0	15.0	15.0	15.0
**Reaction air preheater + headers (Al)	*(2.1)	8.4	8.4	8.4	8.4
**Air exhaust condenser + headers (Al)	*(4.1)	16.4	16.4	16.4	16.4
**Fuel condenser + headers (Al)	*(1.5)	6.0	6.0	6.0	6.0
Catalytic burner		1.4	1.4	1.4	1.4
Auxiliary battery		2.0	2.0	2.0	2.0
Manifolds and piping		18.0	18.0	18.0	18.0
Fuel tank (0.04 inch thick Al)		0.8	0.8	1.0	1.0
Fuel charge for 10 hours		3.8	3.8	4.0	4.0
Total system weight, lb		218.6	201.8	151.1	146.6
		*(195.5)	(178.7)	(128.0)	(123.5)
Specific weight of system, lb/KW		404	384	276	268
Percent decrease in specific weight compared to 404 lb/KW		0	5	32	34

* Numbers in parentheses are values for forced convection case.

** Assuming 8% of exchanger core is solid metal and header weight=core weight.

3.5 CONCEPTUAL LAYOUT OF A 0.5 KW DIRECT HYDROCARBON FUEL CELL SYSTEM

The simplified layout of a 0.5 KW system for the fuel cell operating temperature of 150°C is shown in Figure 3.5-1. Components are drawn to scale and located in their final positions except where noted below. Piping and valves have been shown only schematically to simplify the drawing. The system is shown for the free convection cooling case.

The sizing was done on the basis of the detailed heat, mass, and energy balance, based on the use of an optimum cell stack core as derived from the core optimization program. Each component has sizes and functions as described below.

3.5.1 Fuel Cell Stack

The stack consists of 54 fuel cells, each having electrode areas measuring 10 x 15 inches. The electrodes are held together by 0.5 inch wide frames made of polypropylene oxide or polysulfone. Plenum chambers above and below the stack serve as air inlet and exhaust manifolds, respectively. The air exhaust manifold also serves to catch electrolyte leakage from the cathodes and direct it to the electrolyte sump. A standpipe on the air exhaust manifold dips into the electrolyte bulk so that a slight exhaust manifold pressure can be maintained to force exhaust air to the downstream condensers.

Beneath the fuel cell stack and air exhaust manifold is an electrolyte sump, or pan, which holds about the same amount of electrolyte as do the cells. The tantalum pan holds the fuel vaporizer and preheater in the bath of circulating hot electrolyte. Fuel is preheated and vaporized by the electrolyte heat, distributed to the cells through an end plate, and ported through the plastic frames to the individual anode chambers. The fuel exhaust is gathered by the end-plate and exits at position B in Figure 3.5-1, on its way to the fuel exhaust condenser. At position J, the electrolyte leakage from the anodes is drained off and returned to the bottom of the electrolyte pan.

Electrolyte enters the cell stack at position D and flows upward through the electrolyte chamber. Electrolyte exits through the frames and downward in channels in the other end plate, returning to the pan via the air exhaust manifold. Gas bubbles carried by the electrolyte are easily purged back to the manifold if the return channels in the end plate are large enough. The fuel cell stack and electrolyte pan are covered with 2 inches of "fiberfrax" insulation to avoid excess heat loss. The weight of the cell stack, pan with electrolyte and the fuel vaporizer is about 130 lb and occupies about 4.6 ft^3.

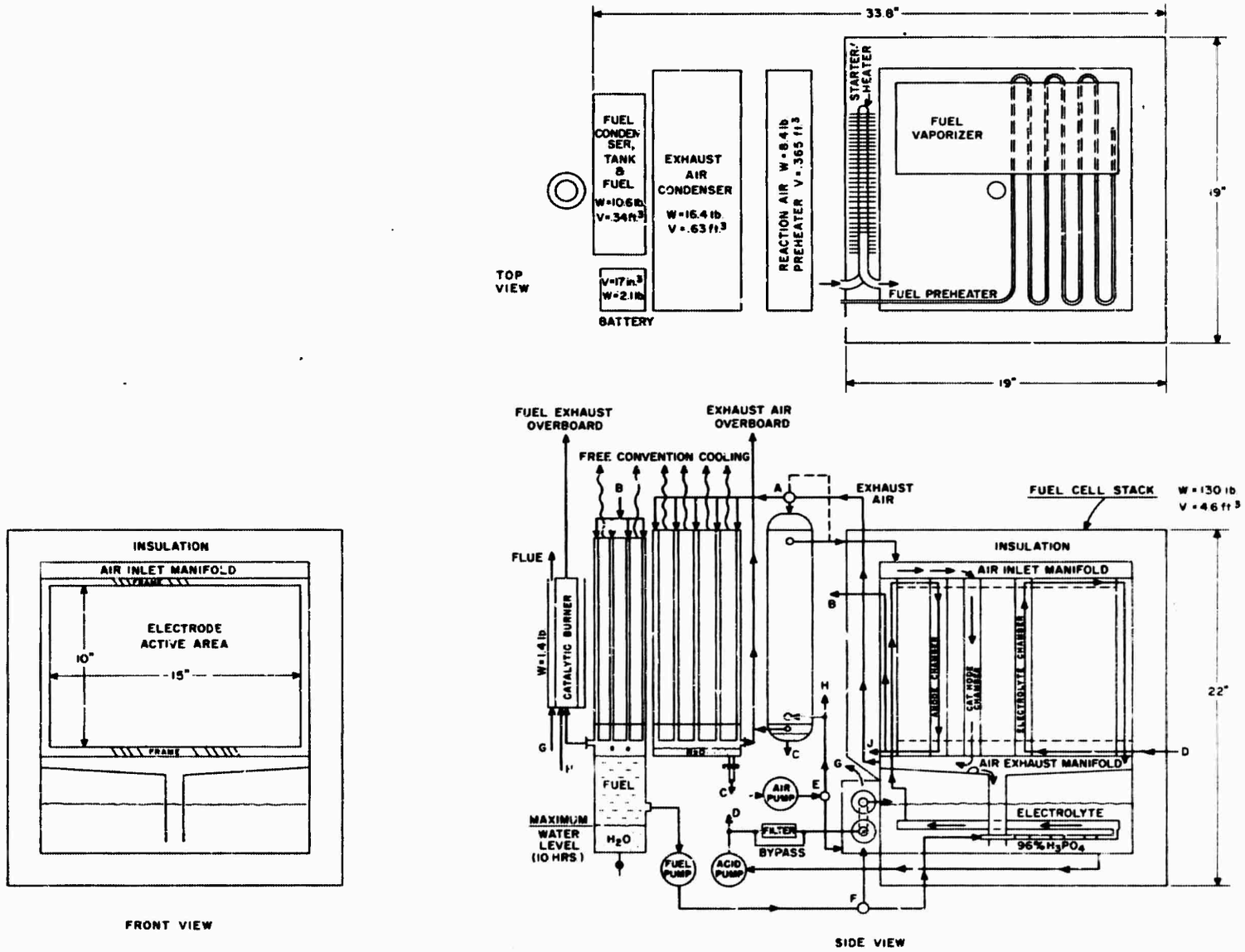

Figure 3.5-1. Conceptual Layout of 0.5 KW Direct Hydrocarbon/Air/H_3PO_4 Fuel Cell System, 150°C Operating Temperature

3.5.2 Reaction Air Preheater

The reaction air preheater is an aluminum plate-fin heat exchanger which accepts part of the hot, moist cathode exhaust and preheats the ambient reaction air by forced convection. The exhaust air flow is split by a valve at position A which is thermostatically controlled by sensing the preheated reaction air temperature. The water condensate at position C is fed under gravity back to the electrolyte pan.

The exhaust air is split into parallel streams through the preheater and the exhaust air condenser so that reaction air can be preheated efficiently by taking advantage of the high exhaust air temperature and at the same time minimize the size of the exhaust air condenser. If the exhaust air cooling were done in two series arranged heat exchangers, the exhaust air condenser would be larger, because the temperature rise available for subcooling the air exhaust would be lower.

The reaction air preheater weighs 8.4 lb and occupies about 0.365 ft^3.

3.5.3 Exhaust Air Condenser

This unit accepts the remainder of the exhaust air, cools it, and condenses water by use of free convection air on the fin side of an aluminum plate-fin heat exchanger. Water condensate is returned to the electrolyte pan. Free convection heat exchanger characteristics were sized on the basis of experimental work done on another General Electric-sponsored fuel cell program. The weight of the exhaust air condenser is 16.4 lb and occupies 0.63 ft^3.

3.5.4 Fuel Condenser and Tank

Fuel exhaust is ducted to this aluminum plate-fin heat exchanger and is cooled by free convection air, condensing water and excess fuel. The water is not needed for water conservation in the system and may either be drained off every 10 hours and discarded, or returned manually to the electrolyte pan just prior to shutdown. This extra water will dilute the electrolyte to help avoid solidification upon cooling down the unit. The weight of the condenser and aluminum fuel tank filled with 10 hours worth of fuel is 10.6 lb and occupies 0.34 ft^3.

3.5.5 Electrolyte Cooler and Starter-Heater

This unit consists of a burner box with a finned tube through which electrolyte is circulated. The finned tube is 1/2 inch OD tantalum tubing, 20 inches long, with ten 1.5 inch diameter fins to the linear inch. At steady-state operation, free convection air takes residual heat from the electrolyte. For start-up, raw fuel and air is burned and heats up the flowing electrolyte and the cell stack in 15 minutes. The weight of this component is about 1 lb and its volume is contained within the envelope of the fuel cell stack.

3.5.6 Air Pump

Reaction air is fed at about 14 inches H_2O pressure. Some air is split off at position H to be fed to the catalytic burner to burn residual hydrocarbons in the fuel exhaust. Air is diverted by a selector valve at position E to the starter-heater for system start-up. The power required for a drag compressor type pump is about 50 watts for the needed capacity. Such a pump would weigh about 1 lb.

3.5.7 Acid and Fuel Pumps

The pumping power is low (10 watts) to pump fuel and acid, but the pumps will probably have to be of special design. The two pumps will probably be run from a common motor. The acid pump recirculates electrolyte in the sump, providing uniform temperature and mixing. It also pumps part of the electrolyte flow through the cell stack at location D. The fuel pump has a selector valve, F, which allows raw fuel to be diverted to the starter-heater for warm-up of the unit. If exceptionally low ambients are encountered, the fuel may be needed continuously to keep the unit running in a self-sustained mode.

3.5.8 Auxiliary Battery for Start-Up

A nickel cadmium battery sized for 25 watthours will provide start-up power to run pumps and blowers and a spark plug system for 15 minutes. The battery will be recharged over an 8-hour period, for which the fuel cell is penalized. The characteristics of 12 watthour/lb and 1.5 watthour/cubic inch give a battery which weighs about 2 lb and occupies about 17 in.^{3}.

3.5.9 Catalytic Burner

In order to lower the amount of raw hydrocarbons thrown overboard from the anode exhaust, a catalytic burner is used. This unit contains a platinoid catalyst on a ceramic substrate which chemically burns hydrocarbons in the vapor phase if about 200% excess air is present. The unit must operate at 800°F. With the amount of exhaust octane in Case I (150°C cell operating temperature), the flame temperature would be about 1300°F. With heat losses and adjustment in excess air if desired, the 800°F operating temperature could easily be maintained. The burner can operate up to 1100°F with the only penalty being a sacrifice in longevity.

The reactor was designed as a cylindrical bed of 1-1/4 inch OD tubing, 8 inches long. This will hold the required 8 in.^{3} of catalyst operating at a total gas space velocity of 10,000 ft^3 per hour of total gas per ft^3 of catalyst. To start the reactor, exhaust flue gases will be diverted from the starter-heater at location G to heat the catalytic burner, while the rest of the unit is heating up.

Combustion air will be taken from the air fan at location H. The catalytic burner would more likely be located just above the starter-heater, so that full advantage could be taken of the burner flue gas for fast start-up. The weight of the catalytic burner is about 1.4 lb.

Exhaust gas treatment by adsorption was also investigated. If a bituminous activated carbon, such as Pittsburg Activated Carbon Company's BPL carbon, is used, which has a capacity of about 0.3 gram of octane per gram of carbon, a volume of 152 in.^{3} would be required. This would last about 20 operating hours if used to full capacity, and then would either have to be regenerated or discarded. In view of the bulky size of the unit and the inconvenient logistics, the adsorption concept was dropped.

3.6 CONCLUSIONS AND RECOMMENDATIONS

1. The most practical electrolyte to use for the direct hydrocarbon fuel cell is phosphoric acid, because it shows good performance, does not form poisonous chemical byproducts, is invariant and tolerant to carbon dioxide, and is mass conservative in phosphorous compounds. Anodic cycling with this electrolyte may prove to be a difficulty, but as yet, no other practical electrolyte has solved the problem. Hydrofluoric acid, although it prevents anodic cycling, is not considered a practical electrolyte from the standpoint of conservation of hydrogen fluoride as well as corrosion and hazard to personnel.

Anodic cycling of multi-cell stacks using phosphoric acid has not been evaluated. This must be investigated before any attempt is made to build a total system, because the possibilities exist that cycling in a multi-cell arrangement might be self-damping or self-amplifying.

2. The optimum electrode structure is a Teflon-bonded platinum electrode which shows potentially the best performance. The very high cost of this structure, compounded with its short life, could possibly be solved in the future with substrates such as boron carbide, although today they give relatively poorer performance.

Substrates should continue to be emphasized, and a step beyond may also be taken, namely, the study of matrix electrolytes, which would allow both cost and weight reduction.

3. The fuel for a direct hydrocarbon system should have good performance commensurate with a low enough vapor pressure to minimize fuel losses. The fuel most favorable in these respects is normal octane, although its cost is high.

4. Calculations indicate that the electrode size should be large for minimum system weight. Additional work should be done to scale up to sizes in the vicinity of 10 by 15 inches active area. Since such electrodes for use with liquid electrolytes are extremely difficult to manufacture, the matrix cell may prove beneficial to solve these problems.

5. Calculations have shown that for a 500 to 600 watt system, free convection cooling of the fuel and water condensers is necessary to minimize parasitic power and to eliminate a second air pump for supplying cooling air. If forced convection cooling air can be supplied and properly distributed at very low pressures, say 0.5 inch H_2O, then parasitic power is not excessive and the system weight and volume can be reduced by 10 and 20%, respectively.

6. The system should operate at 150°C with about 96% phosphoric acid. Conservation of mass is possible at reasonable ambients, the system efficiency is reasonable, and electrode life is superior to that at higher temperature. Electrolyte gap affects the stack weight strongly, but the system weight slightly, unless the bulk electrolyte used for preheating the fuel can be reduced appreciably. Designing for higher operating temperature lowers the system weight very strongly, but life is shorter and more elaborate arrangements to prevent acid solidification from hampering start-up and operation may have to be devised.

4.0 APPENDIX

4.1 METAL OXIDE - NOBLE METAL CATALYSTS

4.1.1 Oxide Catalysts (L. W. Niedrach, J. Haworth)

Table 4.1-1 lists the characteristics and properties of oxide catalysts. Table 4.1-2A thru 4.1-2C gives electrode composition and cell performance data with oxide catalysts of the PB series, PW and Ti series, and the Cr and Nb series, respectively. Table 4.1-3 lists corrosion test results on oxides.

4.1.2 Preparation of a Supported Pt/Ru Electrode (D. W. McKee)

The preparation of a typical electrode of composition 10% (Pt - 20%Ru) - B_4C, as used for fuel cell tests with hydrogen-carbon monoxide fuels, is described below.

Stock solutions containing 12.34 gm Pt "P" salt, $Pt(NH_3)(NO_2)_2$, and 5.019 gm ruthenium nitrosohydroxide, $RuNO(OH)_3 \cdot H_2O$, in 100 ml of 50% nitric acid were prepared. These solutions contained 0.0753 gm Pt/ml and 0.0273 gm Ru/ml, respectively.

To 15 gm of boron carbide, which had been previously ground and sieved to 400 mesh, were added 15.9 ml of the Pt salt solution and 10.8 ml of the Ru salt solution and the mixture diluted to 50 ml. The suspension was mixed thoroughly and then evaporated to dryness under a heat lamp. The dry catalyst was then ground and sieved through a 400 mesh nylon screen. Finally, the catalyst was reduced in flowing hydrogen at 125°C in a tube furnace for three hours and then cooled in nitrogen.

To 0.468 gm of the dry catalyst were added 24 drops of water, 15 drops of Triton X-100 wetting agent and 0.07 ml Teflon T-30 suspension (containing 59% solids). The paste was then spread on a weighed 1 7/8 inch disc of platinum gauze (45 mesh, 0.0078 inch diameter wire). After drying on a hot plate in air and then in a vacuum desiccator overnight, the electrode was weighed again to determine the total weight of catalyst. The electrode was then sprayed on one side with a Teflon suspension, using 2.25 ml of a 1:7 T-30:water suspension on a 5 x 5 inch area. The electrode was finally cured on a hot plate at 350°C to give a final composition of 10% (Pt - 20%Ru) - B_4C and a catalyst loading of 2.6 mg/cm^2 of electrode area.

The exact details of preparation vary according to the composition of the catalyst.

Table 4.1-1

Characteristics and Properties of Oxide Catalysts

Sample No.	Actual	Nominal Composition	Prepared from Sample No.	Treatment H_2 Red'n. Conditions	Phases Ident. from X-ray	Resistivity, ohm	Surface Area, m^2/gm
8528-53A		.10 $Cr_2O_3 \cdot WO_3$	$CrCl_3 + H_2WO_4$	Ppt. air dried at 150°C	—	—	
8528-55B		.16 $Cr_2O_3 \cdot WO_x$	8528-53A	Reduced at 600°C, 4 hr; cooled Ar	WO_2 + W(tr)	.10	
8028-55A		"	8528-53A	Reduced at 600°C, 4 hr; cooled Ar	WO_2 + W(tr)	.12	3.8
8028-55H		"	8528-55A	9% Pt'zd[a] air dried, reduced at 150°C, 2 hr	Pt + WO_2 + tetr.[a]	1,300	
8528-56A		"	8528-55H	Re-reduced at 150°C, 2 hr	Pt + WO_2 + tetr.[a]	250	
8528-57G		"	8328-55A		Pt + WO_2 + ? (tr)	2.5	
8528-57A		"	8028-55A	2% Pt'zd[a] vac dried, reduced at 150°C, 2 hr	Pt + WO_2 + ? (tr)	0.2	
8528-53B		.15 $Cr_2O_3 \cdot WO_3$	$CrCl_2 + H_2WO_4$	Ppt. air dried at 150°C			
8528-55[illegible]		.13 $Cr_2O_3 \cdot WO_x$	8528-53B	Reduced at 600°C, 4 hr; cooled Ar	WO_2 + W(tr)	0.20	
8328-54D		"	852[illegible]-53B	Reduced at 600°C, 4 hr; cooled Ar	WO_2 + W(tr)	0.31	0.2
8528-60A		"	8328-54D	9% Pt'zd[a] vac dried, reduced at 150°C, 2 hr	Pt + WO_2 + tetr.[a]	2.0	
8528-29-2		.33 $Cr_2O_3 \cdot WO_2$	$CrCl_2 + H_2WO_4$	Ppt. air dried at 150°C	—	—	
8028-35A		.32 $Cr_2O_3 \cdot WO_x$	8528-29-2	Reduced at 600°C, 4 hr; cooled Ar	WO_2 + tetr + W(tr)	0.2	
8528-49A		.23 $Cr_2O_3 \cdot WO_3$	$CrCl_2 + H_2WO_4$	Ppt. air dried at 150°C			
8928-49B		.33 $Cr_2O_2 \cdot WO$	8528-49A	Reduced at 600°C, 4 hr; cooled Ar	WO_2 + tetr.[a]	6.7	
8528-50A		"	8328-49A	Reduced at 600°C, 4 hr; cooled Ar	WO_2 + tetr.[e]	1.2	9.2
8928-60B		"	8528-50A	Pt'zd[a] vac dried, reduced at 150°, 2 hr	Pt + tetr.[e]	5.8	
8528-85A		"	8528-49A	Air at 600°C, 4 hr → H_2 at 600°C, 4 hr; cooled Ar	WO_2 + tetr.[e] (< 49B)	-	9.4
8028-85B		"	8328-49A	H_2 at 600°C, 4 hr → air at 800°C, 4 hr → H_2 at 600°C, 4 hr	WO_2 + tetr.[e] + W(tr)	-	9.1
0028-162B		.80 $Cr_2O_2 \cdot WO_2$	$Cr(NO_3)_3 + H_2WO_4$	Ppt. air dried at 150°C	—	—	
8528-104B		.80 $Cr_2O_3 \cdot WO_x$	8528-107P	Reduced at 600°C, 4 hr; cooled Ar	WO_2 > W + Cr_2O_2(tr) + tetr[c](tr)	1,870	
8618-50-2Pt		"	8028-104B	9% Pt'zd[a] vac dried		2,050	
8528-162A	.79	.80 $Cr_2O_3 \cdot WO_2$	$CrCl_3 + H_2WO_4$	Ppt. air dried at 150°C			
8520-103A		.90 $Cr_2O_3 \cdot WO_x$	8528-162A	Reduced at 600°C, 4 hr; cooled Ar	tetr[a] + Cr_2O_3(tr) + W(tr)	734	
8641-36A + B		"	8528-103A	9% Pt'zd[b] air dried 150°C		280,000	
8641-71B		"	8641-36A + B	Reduced at 150°C, 2 hr			
8641-58		"	8028-103A	28% Pt'zd[b] air dried 150°C			
8641-59		"	8641-58	Reduced at 150°C, 2 hr		285	
8618-50-1Pt		"	8028-103A	9% Pt'zd[a] vac dried, reduced at 150°C, 2 hr		200	
8670-19A		"	0528-162A	Reduced at 600°C, 4 hr; cooled Ar	W + tetr[e] + Cr_2O_2		
8641-93		"	8528-162A	Reduced at 700°C, 4 hr; cooled Ar	Cr_2O_3>WO_2 + W + WO_3 (tr)	17,000	
8670-21A		.80 $Cr_2O_2 \cdot WO_2$	$CrCl_3 + B_2WO_4$	Ppt. air dried at 150°C			
8641-107B		.50 $Cr_2O_2 \cdot WO_x$	8670-21A	Reduced at 800°C, 4 hr; cooled H_2[d]	W > Cr_2O_2 + β W	2×10^9	
8641-108B		"	8670-21A	Reduced at 200°C, 4 hr; cooled H_2[d]	W + tetr[e] > Cr_2O_3	25,700	
8641-112A		"	8670-21A	Reduced at 900°C, 4 hr, cooled H_2[d]	W + tetr[e] > Cr_2O_3	39,000	
8641-109B		.80 $Cr_2O_3 \cdot WO_x$	8676-21A	9% Pt'zd[b] air dried at 150°C		2.5×10^9	
8641-114B		"	8641-109B	Reduced at 900°C, 4 hr; cooled H_2[d]	Pt + Cr_2O_3 + tetr[e]	3,100	
8641-110B		"	0976-21A	9% Pt'zd[c] air dried at 150°C		—	
8641-113B		"	8670-21A	9% Pt'zd[c] air dried at 150°C		$.9 \times 10^9$	
8641-116D		"	8641-110B + 113B	Reduced at 600°C, 4 hr; cooled H_2[d]	Pt + WO_2 + tetr[e] + Cr_2O_2(tr)	209	
8641-112D		"	8970-21A	9% Pt'zd[a] air dried at 150°C, reduced at 150°C, 2 hr		340,000	
8641-114D		"	8641-112D	Reduced at 600°C, 4 hr; cooled H_2[d]	Pt + WO_2 + tetr[a] + Cr_2O_2(tr)	3,400	
8328-29-1	.92	$Cr_2O_2 \cdot WO_3$	$CrCl_3 + H_2WO_4$	Ppt. air dried at 150°C		—	
8528-32A		$Cr_2O_3 \cdot WO_x$	8528-29-1	Reduced at 800°C, 4 hr; cooled Ar	tetr.[a] + Cr_2O_2	400	
8528-93A		$Cr_2O_2 \cdot WO_3$	$CrCl_3 + H_2WO_4$	Ppt. air dried at 150°C		—	
8929-95B		$Cr_2O_2 \cdot WO_x$	8528-93A	Reduced at 600°C, 4 hr; cooled Ar	var. tetr.[e] + Cr_2O_2	2,000	7.0
8528-96N		"	8528-93A	Air 800°C, 4 hr → red. H_2 600°C, 4 hr; Ar	var. tetr.[e] + Cr_2WO_9	8,800	11.4
8528-96P		"	8528-93A	H_2, 800°C, 4 hr → air, 900°C, 4 hr → H_2, 900°C, 4 hr	var. tetr.[e] + Cr_2O_3	6,500	0.0
8328-94A		"	8528-93A	Air, 600°C, 4 hr	var. tetr.[e] + Cr_2WO_9	4,000	
8528-96M		"	8328-93A	H_2 600°C, 4 hr → air, 900°C, 4 hr	var. tetr.[a] + Cr_2O_3	24,000	
8528-96L		"	8528-92A	9% Pt'zd[a] vac dried, reduced at 150°C, 2 hr	var. tetr.[e] + Cr_2O_3 + Pt	8,300	

(a) H_2PtCl_6 platinization.

(b) "P" salt ($Pt(NH_3)_2(NO_2)_2$) platinization.

(c) $(NH_3)_4PtCl_2$ platinization.

(d) Cooled to with H_2, then Ar to room temperature.

(e) Unidentifi[illegible] tragonal phase believed to be Cr_2WO_9.

Table 4.1-1 (Cont.)

Sample No.	Actual	Nominal Composition	Prepared from Sample No.	Treatment H_2 Red'n. Conditions	Phases Ident. from X-ray	Resistivity, ohm	Surface Area, m^2/gm.
8641-11		$Cr_2O_3 \cdot WO_x$	8528-93H	9% Pt'zd[b] air dried at 150°C	var. tetr.[e] + Cr_2O_3	31,000	
8641-13A		"	8528-93B	9% Pt'zd[b] vac dried	var. tetr.[e] + Cr_2O_3	17,000	
8641-12		"	8641-13A	Dried at 150°C	var. tetr.[e] + Cr_2O_3	50,000	
8641-71A		"	8641-12	Reduced at 150°C, 2 hr			
8641-81		"	8528-93A	Reduced at 700°C, 4 hr; Ar cooled	tetr.[e] + Cr_2O_3 + ?	43,000	
8641-86		"	8528-93A	Reduced at 800°C, 4 hr; Ar cooled	$Cr_2O_3 + WO_3$	230,000	
8641-87A		"	8641-86	Reduced at 800°C, 4 hr, Ar cooled	$Cr_2O_3 + WO_3$ + W(am)	190,000	
8641-87B		"	8641-87A	Reduced at 800°C, 4 hr; Ar cooled	$Cr_2O_3 + WO_3$ + W(m)	79,000	
8641-94		"	8528-93A	Reduced at 750°C, 4 hr; Ar cooled	$Cr_2O_3 + WO_3$ + W(m)	54,000	
8641-107A		"	8528-93A	Reduced at 800°C, 4 hr; cooled H_2[d]	W + Cr_2O_3(m) + W_3O	10^6	
8641-108A		"	8528-93A	Reduced at 700°C, 4 hr; cooled H_3[d]	tetr.[e] > W > Cr_2O_3	33,000	
8641-111		"	8528-93A	Reduced at 800°C, 4 hrs; cooled H_2[d]	tetr.[e] + Cr_2O_3(tr) + W(tr)	24,000	
8641-109A		"	8536-93A	9% Pt'zd.[b] air dried at 150°C		10^6	
8641-114A		"	8641-109A	Reduced at 800°C, 4 hr; cooled H_2[d]	Pt + W + (Cr_2O_3 + WO_2) ?	380	
8641-110A		"	8528-93A	9% Pt'zd.[c] air dried at 150°C		—	
8641-113A		"	8528-93A	9% Pt'zd.[c] air dried at 150°C		6,600	
8641-116C		"	8641-110A + 113A	Reduced at 800°C, 4 hr; cooled H_3[d]	Pt + tetr.[e] + WO_2 + Cr_2O_3(tr)	517	
8641-113C		"	8528-93A	9% Pt'zd.[a] air dried at 150°C		200,000	
8641-114C		"	8641-113C	Reduced at 800°C, 4 hr; cooled H_2[d]	Pt + tetr.[e] + WO_2 + Cr_2O_3(tr)	53	
8711-17		"	8528-93A	17% Pt'zd.[a] air dried at 150°C			
8711-19		"	8711-17	Reduced at 800°C, 4 hr; cooled H_3[d]			
8528-96K		WO_3	8418-14-4	8% Pt'zd.[a] vac dried, reduced at 150°C, 2 hr		2,800	
8528-36-1	.783	1 $TiO_2 \cdot WO_3$	$TiCl_4 + H_2WO_4$	Ppt. air dried at 150°C			
8528-42G		1 $TiO_2 \cdot WO_x$	8528-36-1	Reduced 650°C, 4 hr	W > "βW" > WO_2	8.2	
8528-38A		"	8528-36-1	Vacuum 900°C, 2 hr	$WO_3 + WO_2 + TiO_2$	1.3	
8528-41A		"	8528-36-1	Vacuum 900°C, 2 hr → H_2 650°C, 4 hr	W + W_3O + TiO_3 + WO_3	.15	
8528-46A		"	8528-36-1	Reduced 650°, 20 hr	W + TiO_2	.2	
8528-47J		"	9528-36-1	Reduced 650°, 4 hr	WO_2 + W_3O + W(am)	.54	
8670-20A		"	8528-36-1	Reduced 850°, 4 hr			
8641-182A		"	8670-70A	Pt'zd.[a] vac dried, reduced 150°C, 2 hr			
8528-36-2	.26	.33 $TiO_2 \cdot WO_3$	$TiCl_4 + H_2WO_4$	Ppt. air dried at 150°C			
8528-42H		.33 $TiO_2 \cdot WO_x$	8528-36-3	Reduced 650°C, 4 hr	W > "βW" > WO_2	0.1	
8528-41B		"	8528-36-2	Vacuum 900°C 2 hr → H_2, 650°C, 4 hr	"βW" + WO_2 + TiO_2	0.08	
8528-46B		"	8528-36-2	Reduced 650°C, 20 hr	W + "βW"	.12	
8528-47K		"	8528-36-2	Reduced 800°C, 4 hr	WO + W(tr)	.16	
8528-36-3	.071	.18 $TiO_2 \cdot WO_3$	$TiCl_4 + H_2WO_4$	Ppt. air dried at 150°C	WO_2 >> W + "βW"		
8528-42I		.10 $TiO_2 \cdot WO_x$	8528-36-3	Reduced 650°C, 4 hr	W > "βW" >> WO_2	0.2	
8528-102C		3 $TiO_2 \cdot WO_3$	$TiCl_4 + H_2WO_4$	Ppt. air dried at 150°C			
8528-104G		3 $TiO_2 \cdot WO_x$	8528-102C	Reduced 650°C, 4 hr	$TiO_2 + WO_2$ (?)		
8528-100A		TiO_2	$TiCl_4$	Ppt. air dried at 150°C			
8528-104F		TiO_x	8528-100A	Reduced 650°C, 4 hr	TiO_3		
8528-102F		$TiO_2 + B_4C$	$TiCl_4 + B_4C$	Ppt. air dried at 150°C			
8528-103B			8528-102F	Reduced 650°C, 4 hr	$TiO_2 + B_4C$ (?)		
8528-102G		TiO_2 + graphite	$TiCl_4$ + graphite	Ppt. air dried at 150°C			
8528-104A			8528-102G	Reduced 650°C, 4 hr	TiO_2		
8528-102E		$Nb_2O_5 \cdot WO_3$	$Nb_3Cl_8 + H_2WO_4$	Ppt. air dried at 150°C			
8528-104E		$Nb_2O_5 \cdot W_x$	8528-102E	Reduced 650°C, 4 hr	W + 5 Nb_3O_8 + NbO_2 (?)		
8528-102D		3 $Nb_2O_5 \cdot WO_3$	$Nb_3Cl_8 + H_2WO_4$	Ppt. air dried at 150°C			
8528-104D		3 $Nb_2O_5 \cdot WO_x$	8528-102D	Reduced 650°C, 4 hr	5 Nb_2O_8 > W + NbO_2		
8528-100C		Nb_2O_3	Nb_2Cl_5	Ppt. air dried at 150°C			
8528-104C		Nb_3O_x	8528-100C	Reduced 650°C, 4 hr	Nb_2O_5 + NbO_2 + ?		
8641-13BC		B_4C	Norbide	25% pt'zd.[b], air dried 150°C			
8711-41B		B_4C	Lot No. 1000 FW	9% pt'zd.[b], air dried 150°C			
8711-42B		B_4C		17% pt'zd.[b], air dried 150°C			

Table 4.1-2A

Electrode Composition and Cell Performance Data[a] with Oxide Catalysts

The PB- Series

Electrode No.	Pt, mg/cm²	Comments	gm	Pt'ad Material	gm	Material	T-30, cc	Electrode Preparation Painted Pressed	Cell No.	% CO	Anode vs Ref. Volts @ ____ ma/cm² 20	50	100	200	300
958	5	0.1 Cr_3O_3 WO_x	0.31	8641-13B + C	0.31	8528-55A	0.10	X	PB-1	2	.020	.059	.093	.112	.126
962	3	0.9 $Cr_2O_3 \cdot WO_x$	0.3	"	0.3	8528-103A	0.20	X	PB-3	3	.028	.062	.140	.440	----
962*	5	"	0.3	"	0.3	"	0.20	Above 200 psi	PB-3	2	.055	.127	.207	.306	----
968	5	"	0.3	"	0.3	"	0.10	X	PB-4	2	.035	.073	.084	.129	.140
969	3	"	0.3	"	0.5	"	0.133	X	PB-5	2	.033	.137	.203	256	.294
963	3	"	0.3	"	0.3	"	0.10	X 200 psi	PB-6	2	.050	.105	159	.305	.333
973	5	"	0.3	"	0.3	"	0.10	X	PB-7	2	.055	.110	.162	.283	.290
974	3	"	0.3	"	0.3	"	0.06	X	PB-8	2	.028	.059	.095	.118	.122
979	5	0.33 $Cr_2O_3 \cdot WO_x$	0.3	"	0.3	8528-50A	0.10	X	PB-9	2	.015	.036	.065	.082	.089
984	3	$Cr_2O_3 \cdot WO_x$	0.3	"	0.3	8528-95B	0.06	X	PB-10	2	.020	.040	.060	.077	.084
										5	.025	.056	.098	.133	----
										10	.052	.098	.185	.390	----
985	5	0.8 $Cr_2O_3 \cdot WO_x$	0.3	"	0.3	8528-103A	0.04	X	PB-11	2	.012	.032	.071	.114	----
										5	.032	.071	.104	.146	----
										10	.067	.125	.183	----	----
992	5	$Cr_2O_3 \cdot WO_x$ red. 700°C	0.3	"	0.3	8641-61	0.06	X	PB-12	2	.019	.033	.051	.057	----
										5	.030	.065	.097	.188	----
										10	.088	.150	.210	.328	----
993	3	.8 $Cr_2O_3 \cdot WO_x$ red. 700°C	0.3	"	0.3	8641-63	0.06	X	PB-13	2	.017	.036	.065	.090	.110
										5	.032	.065	.094	.179	.166
										10	.050	.099	.135	.197	.272
1009	5		0.3	"	0.3	Cr_2O	0.10	X	PB-14	2	.233	.288	.305	.304	----
										5	.305	.356	.388	.397	----
1013	3	$Cr_2O_3 \cdot WO_x$ red. 800°C	0.3	8641-13B + C	0.3	8641-107A	0.10	X	PB-15	2	.017	.042	.082	.108	.122
										5	.039	.083	.115	.159	.205
										10	.064	.113	.171	----	----
1014	3	$Cr_2O_3 \cdot WO_x$ red. 700°C	0.3	"	0.3	8641-108A	0.10	X	PB-16	2	.018	.045	.081	.108	.117
										5	.036	.078	.111	.137	.206
										10	.058	.103	.149	.295	----
1015	5	$Cr_3O_3 \cdot WO_x$ red. 600°C	0.3	"	0.3	8641-111	0.10	X	PB-17	2	.014	.036	.068	.089	.099
										5	.027	.066	.095	.127	.149
										10	.038	.093	.140	.218	----
1016	5	.8 $Cr_3O_3 \cdot WO_x$ red. 600°C	0.3	"	0.3	8641-112A	0.10	X	PB-18	2	.020	.047	.083	.110	.124
										5	.024	.060	.091	.120	.140
										10	.034	.092	.112	.145	.176
									after Ar purge	3	.017	.048	.084	.106	.119
1017	3	.8 $Cr_3O_3 \cdot WO_x$ red. 700°C	0.3	"	0.3	8641-108B	0.10	X	PB-19	2	.014	.040	.073	.099	.112
										5	.028	.071	.103	.148	.195
										10	.042	.094	.131	.221	----
1018	8	.9 $Cr_3O_3 \cdot WO_x$ red. 800°C	0.3	"	0.3	8641-107B	0.10	X	PB-20	2	.020	.057	.094	.120	.146
										5	.026	.066	.094	.123	.155
										10	.042	.083	.112	.161	.296
									after Ar purge	3	.018	.050	.081	.104	.122
1007	3	$Cr_2O_3 \cdot WO_x$	0.3	"	0.3	8528-93B	0.10	X	PB-21	2	.028	.060	.092	.116	.128
										3	.042	.096	.128	.177	----
										10	.080	.150	[illegible]	----	----
1024	1.6	$Cr_2O_3 \cdot WO_x$	0.3	8711-41B 9% Pt B_4C	0.3	8641-111	0.10	X	PB-22	2	.096	.226	.303	----	----
1025	1.6	.8 $Cr_3O_3 \cdot WO_x$	0.3	"	0.3	8641-112A	0.10	X	PB-23	H_2	Polarized at 30 ma/cm³				
1026	3	$Cr_2O_3 \cdot WO_x$	0.3	8711-42B 17% Pt B_4C	0.3	8641-111	0.10	X	PB-24	2	.047	.103	.147	.239	.263
										3	.091	.173	.333	----	----
1027	3	.8 $Cr_3O_3 \cdot WO_x$	0.3	"	0.3	8641-112A	0.10	X	PB-25	2	.040	.093	.144	.254	.262
										5	.054	.106	.175	----	----

[a] Cell performance data is for an 65°C 5 N H_2SO_4 acid cell using synthetic reformer gas as a fuel.

Table 4.1-2B

Electrode Composition and Cell Performance Data[a] with Oxide Catalysts

The PW- and Ti- Series

Electrode No.	Pt, mg/cm^2	Comments	gm	Pt'zd Material	gm	Material	T-30, cc	Electrode Preparation Painted	Pressed	Cell No.	% CO	Anode vs. Ref. Volts @ ____ ma/cm^2 20	50	100	200	300
900	3	9% Pt'zd $Cr_2O_2 \cdot WO_x$	0.6	8641-12			0.10	X		PW-1	2			H. R.[b]		
959	3	"	0.0	"			0.06		2100 psi	PW-2	2			H. R.		
961	2	9% Pt'zd .6 $Cr_2O_3 \cdot WO_x$	0.6	8641-36AB			0.20	X		PW-3	2			H. R.		
962	1.0	"	0.3	"	0.3	B_4C	0.20	X		PW-4	2	.060	.131	.183	.393	----
863*	1.8	"	0.3	"	0.3	"	0.20	Above 200 psi		PW-5	2			H. R.		
879	5	28% Pt'zd .8 $Cr_2O_3 \cdot WO_x$	0.2	8041-59	0.3	"	0.1	X		PW-6	2	.037	.070	.158	.301	----
863	3	" + .6 $Cr_2O_2 \cdot WO_x$	0.3	"	0.3	8528-102A	0.06	X		PW-7	2			H. R.		
802	6	28% Pt'zd .8 $Cr_2O_3 \cdot WO_x$	0.3	"	0.3	B_4C	0.00	X		PW-8	2 5 10	.015 .021 .058	.064 .081 .241	.098 .145 .463	.152 .370 ----	
980	0	"p" salt pt'zd ".8" after red.	0.4	8641-36AB	0.2	8641-13BC	0.10	X		PBW-1	2 3 10		.033 .071 .093	.060 .107 .143	.112 .147 .202	
1010	5	"p" salt pt'zd "1" before red.	0.44	8641-114A	0.16	"	0.10	X		PW-9	2 5 10	.014 .025 .034	.039 .067 .088	.074 .107 .133	.106 .172 .245	.131 .244 ----
1011	5	H_2PtCl_6 pt'zd "1" before red.	0.44	8641-114C	0.10	"	0.10	X		PW-10	2 5 0	.037 .045 .074	.066 .109 .146	.117 .189 .471	.171 .418 ----	.231 .395 ----
1012	5	$(NH_3)_4PtCl_2$ pt'zd "1" before red.	0.44	8641-110C	0.10	"	0.10	X		PW-11	2 5 10	.028 .038 .068	.072 .031 .129	.106 .131 .234	.144 .229 .016	.190 .258 ----
1022	3	"p" pt'zd "1" alone	0.6	8641-114A			0.10	X		PW-12	2 5 10	.018 .038 .129	.045 .098 .379	.093 .125 ----	.127 ---- ----	.174 ---- ----
1019	0	"p" salt pt'zd ".8" before red.	0.44	8641-114B	0.18	8641-128C	0.1	X		PW-13	2 6 10	.022 .038 .069	.055 .097 .122	.099 .142 .209	.133 .278 ----	.181 ---- ----
1020	5	H_2PtCl_6 pt'zd ".8" before red.	0.44	8641-114D	0.10	"	0.1	X		PW-14	2 5 10	.020 .038 .078	.050 .085 .132	.085 .117 .241	.105 .174 ----	.122 ---- ----
1021	8	$(NH_3)_4PtCl_2$ pt'zd ".8" before red.	0.44	8641-116D	0.16	"	0.1	X		PW-15	2 0	.033 .062	.077 .102	.103 .161	.171 ----	---- ----
856	24	$TiO_2 \cdot WO_3$ 800°C vac	0.0	Pt black	0.12	0528-38A	0.06		X	Ti-1	2		.123	.236	.456	----
666	24	" + red.	0.6	"	0.12	8020-41A	0.06		X	Ti-2	2		.012	.122	.178	----
859	24	.32 $TiO_2 \cdot WO_3$ 800°C vac and red.	0.6	"	0.12	8528-41B	0.06		X	Ti-3	2		.018	.036	.067	.110
882	34	$TiO_2 \cdot WO_3$ red. 050°C	0.6	"	0.12	8529-42G	0.06		X	Ti-4	2		.010	.022	.032	.064
863	34	.32 $TiO_2 \cdot WO_3$ red. 050°C	0.0	"	0.12	8228-42H	0.06		X	Ti-5	2		.029	.058	.068	.106
664	24	.10 $TiO_2 \cdot WO_3$ red. 850°C	0.6	"	0.12	0028-42I	0.06		X	Ti-6	2		.038	.064	.146	----
871	34	$TiO_2 \cdot WO_3$ red. 050°C, 20 hr	0.6	"	0.12	0228-46A	0.06		X	Ti-7	2		.021	.056	.084	.122
672	24	$TiO_2 \cdot WO_3$ red. 000°C	0.6	"	0.12	8528-47J	0.06		X	Ti-8	2		.028	.070	.144	.183
856	24	$TiO_2 + B_4C$ red.	0.8	"	0.12	8528-104A	0.06		X	Ti-10	2		.200	.222	.244	.270
860	34	$TiO_2 + C$ red	0.0	"	0.12	8528-104A	0.06		X	Ti-11	2		.103	.205	.206	.249
987	24	TiO_2 red.	0.1	"	0.12	0528-104F	0.06		X	Ti-12	2		.098	.188	.212	.215
888	34	2 $TiO_2 \cdot WO_x$ red.	0.0	"	0.12	8528-104G	0.06		X	Ti-12	2		.077	.111	.132	.146
994	0	"	0.3	8041-13BC	0.3	8828-104G	0.06	X		Ti-14	2		.066	.096	.131	.157
996	0	"	0.3	"	0.3	8528-104G	0.06		X	Ti-10	2		.101	.149	.261	.304

[a] Cell performance data is for an 85°C 0 N H_2SO_4 acid cell using synthetic reformer gas as a fuel.

[b] H. R. = the cell resistance was high and the polarization data is not reliable.

Table 4.1-3C

Electrode Composition and Cell Performance Data[a] with Oxide Catalysts

The Cr- and Nb- Series

Electrode No.	Pt, mg/cm²	Comments	gm	Pt'sd Material	gm	Material	T-30, cc	Electrode Preparation Painted	Pressed	Cell No.	% CO	Anode* vs Ref. Volts @ ____ ma/cm² 20	50	100	200	300
921	2	0.1 $Cr_2O_3 \cdot WO_3$	0.354	25% Pt'sd C	.354	8528-55A	0.10	X		CR-24	2	.050	.108	.150	.217	.260
922	5	"	0.310	28% Pt'sd B_4C	.310	8528-55A	0.10	X		CR-25	2	.010	.024	.044	.068	.100
928	5		0.310	"	0.10	B_4C	0.10	X		CR-28	2	.045	.242	.319	.383	----
929	5		0.354	25% Pt'sd C	0.10	graphite	0.10	X		CR-27	2	.300	.330	----	----	----
925	5	"	0.150	28% Pt'sd B_4C	1.0	8528-55A	0.10	X		CR-29	2	.030	.079	.126	----	----
											5	.180	.419	----	----	----
											10	.375	.584	----	----	----
926	5	"	0.310	"	.620	"	0.10	X		CR-30	2	.030	.057	.082	.110	.130
											5	070	.137	----	----	----
											10	.100	.240	----	----	----
930	5	"	0.310	"	.150	"	0.10	X		CR-31	2	.031	.068	098	.152	----
											5	.048	.113	.210	----	----
											10	.056	.182	----	----	----
934	1.6	"	0.310	8% Pt'sd B_4C	.310	"	0.10	X		CR-32	2	.388	500	----	----	----
935	3	"	0.310	17% Pt'sd B_4C	.310	"	0.10	X		Cr-33	2	.070	.165	----	----	----
937	34	"	0.6	Pt-R 1-39	0.12	"	0.06		X	CR-34	2	.011	.006	.016	.53	.158
											5	.009	.015	.031	.068	.210
											10	.018	.033	.042	.087	.260
											30	.020	.034	.067	.150	----
938	34	"	0.9	Pt-Ir N-7	0.12	"	0.06		X	CR-35	2	.011	011	.030	.70	.135
											5	.013	.022	.040	.98	----
											10	.029	.050	066	.129	.187
											30	.034	.067	.139	----	----
940	34	"	0.6	Pt-Rh L-16	0.12	"	0.06		X	CR-41	2	.017	.024	.35	.074	.154
941	5	0.1 $Cr_2O_3 \cdot WO_3$	0.354	25% Pt'sd C	0.354	8528-55A	0.10	X		CR-36	2	.127	.242	.352	.413	----
944	5	"	0.354	"	0.354	"	0.20	X		CR-37	2	.097	.100	.129	.150	----
943	5	"	0.354	"	0.354	"	0.02	X		CR-38	2	.115	.372	.435	.465	.500
51A	5	"	0.354	"	0.354	"	0.40	X		CR-42	2	.114	.164	.282	.230	.382
997	5	"	0.354	"	0.354	"	0.30	X		PC-3	2	.043	.103	.135	.176	.19[illegible]
945	34	".33" ox. -red.	0.9	Pt black	0.12	8528-85A	0.06		X	CR-39	2	.030	.058	.104	----	----
949	34	".22" red. -ox. -red.	0.6	"	0.12	8529-85B	0.06		X	CR-40	2	.014	.022	.035	----	----
953	34	"1" red. ox. red.	0.9	"	0.12	8528-94P	0.06		X	CR-43	2	.105	.18[illegible]	.287	.490	----
221B	34	"1" red.	0.6	"	0.12	8528-93B	0.06		X	CR-44	2	.080	.229	.290	.320	----
952	34	"1" ox. red.	0.6	"	0.12	2522-54N	0.06		X	CR-45	2	----	----	----	----	----
946	34	.9 $Cr_2O_2 \cdot WO_x$	0.6	"	0.12	9529-103A	0.06		X	CR-46	2	.018	.038	.060	.105	.235
989	5	Nb_2O_5 red.	0.3	"	0.3	9528-104C	0.06	X		NB-1	2		.124	.164	.243	.282
990	9	3 $Nb_2O_2 \cdot WO_x$	0.3	"	0.3	9528-104D	0.06	X		NB-2	2		.138	.266	.354	.411
991	5	$Nb_2O_5 \cdot WO_x$	0.2	"	0.3	9529-104E	0.06	X		NB-3	2		.066	.106	.147	.184
995	5	"	0.3	"	0.3	"			X	NB-4	2		.089	.118	.141	.172

[a] Cell performance data is for an 65°C 5 N H_2SO_4 acid cell using synthetic reformer gas as a fuel.

Table 4.1-3

Corrosion Test Results On Oxides

5 N H_2SO_4 ; 65°C. ; 8 days exposure;

50 ml soln. /500 mg solids

Sample No.	Oxide	Amt. and Source of Pt	Atmosphere	Powder Resistivity, ohm-m Orig.	After Pt.	After Corr.	Appearance of Product Powder	X-ray Analysis of Product Powder	Amount in Solution, mg W	Cr(Ti)	Per Cent Attacked
96K	WO_2	9% - H_2PtCl_6 vac dried	$N_2(H_2)$	0.20	2600	3.0×10^4	blue-gray	WO_2 ; $WO_2 \cdot H_2O$		----	---
96K	"	"	Air	.33	3000	9.8×10^4	yellow-green	WO_3 H_2O			
55H	0.1 $Cr_2O_3 \cdot WO_x$	9% - H_2PtCl_6 air dried	$N_2(H_2)$	.12	1300	3×10^6	blue-gray	H_2WO_4 ; tetra. ; WO_3	0.1	0.22	1.0
57A	"	" vac dried	"	.13	0.2	1.3×10^6	blue-gray	$H_2WO_4 \cdot H_2O$; tetra ; WO_2 (?)	0.4	.21	1.0
55H	"	" air dried	Air	.12	1300	0.6×10^6	yellow-gray	Cr_2O_3 ; H_2WO_4	0.1	8.3	91
57A	"	" vac dried	Air	.12	0.3	0.8×10^8	green-gray	Cr_2O_3 ; $H_2WO_4 \cdot WO_3$	<0.1	10.8	45
60A	0.15 $Cr_2O_3 \cdot WO_x$	0% - H_2PtCl_6 vac dried	$N_2(H_2)$	0.36	2.0	0.5×10^0	black	$H_2WO_4 \cdot H_2O$; tetra. ; WO_2 (?)	<0.1	0.55	1.7
60A	"	" vac dried	Air	0.20	2.0	0.4×10^6	yellow-gray	H_2WO_4 ; WO_2 ; [illegible]	<0.1	22	74
54D	"	No Pt	Air	0.26	---	0.7×10^6	green-gray	H_2WO_4 ; WO_2	0.1	17	
60B	0.33 $Cr_2O_3 \cdot WO_x$	9% - H_2PtCl_6 vac dried	$N_2(H_2)$	1.3	5.8	860	black	tetra. ; WO_2(trace)	0.6	0.50	0.85
60B	"	" vac dried	Air	1.2	5.8	0.2×10^0	gray	$WO_3 \cdot H_2O$; Cr_2WO_6 ; Cr_2O_3	<0.1	30	91
50A	"	No Pt	Air	1.3	---	1.4×10^4	gray	$WO_3 \cdot H_2O$; Cr_2WO_6 ; Cr_2O_3	0.1	16	27
65B	" (a)	No Pt	Air	---	---	8.0×10^4	gray	$WO_3 \cdot H_2O$; Cr_2WO_6 ; Cr_2O_3	<0.1	11	18
65A	" (b)	No Pt	Air	---	---	1.4×10^5	gray	$WO_3 \cdot H_2O$; Cr_2WO_6 ; Cr_2O_3	<0.1	8.4	14
50-1Pt	0.8 $Cr_2O_3 \cdot WO_x$	9% - H_2PtCl_6 vac dried	$N_2(H_2)$	734	200	7200	black	tetra. ; Cr_2O_3 ; $WO_3 \cdot H_2O$(tr)	0.1	0.91	0.73
50-1Pt	"	" vac dried	Air	734	200	2.4×10^4	gray	$WO_3 \cdot H_2O$; tetra. ; Cr_2O_3	0.[illegible]	.12	0.11
50-2Pt	" (c)	" vac dried	$N_2(H_2)$	.670	2650	9.6×10^4	gray-blue	$WO_3 \cdot H_2O$; Cr_2O_3	<0.1	.16	.14
50-2Pt	" (c)	" vac dried	Air	1670	2650	5.7×10^4	blue	$WO_3 \cdot H_2O$; Cr_2O_3	0.1	.88	.91
96L	1.0 $Cr_2O_3 \cdot WO_x$	0% - H_2PtCl_6 vac dried	$N_2(H_2)$	3600	6300	7000	black	tetra. ; Cr_2O_3(tr)	0.2	.54	0.42
96L	"	"	Air	3600	6300	1.3×10^4	black	tetra. ; Cr_2O_3(tr)	<0.1	.60	0.45
03B	"	No Pt	Air	3600	----	1.5×10^4	black	tetra. ; Cr_2O_3(tr)	0.3	.48	0.35
47J	1.0 $TiO_2 \cdot WO_x$	0% - H_2PtCl_6 vac dried	$N_2(H_2)$	0.54	---	3.3×10^4	blue black	WO_3 ; TiO_2	[illegible].0	2.0	20

(a) Hydroxide ppt oxidized at 600°C before final reduction in H_2 at 600°C.

(b) Hydroxide ppt reduced, oxidized and rereduced at 600°C.

(c) Prepared from $Cr(NO_3)_3$, rather than $CrCl_3$.

4.2 ACTIVATED BORON CARBIDE ELECTRODES

4.2.1 Platinum Analysis in Nitric Acid Solutions (W. T. Grubb, L.H. King)

During the preparation of boron carbide electrodes activated with platinum from the thermal decomposition of platinum diammine dinitrate, the finished electrode has been leached to 50 v/o nitric acid for 1 hour at 100°C. This was found in the past to improve performance of electrodes which had been made from pre-reduced electrocatalyst (platinum on boron carbide). The improvement was thought to be due to the removal of traces of iron and other metal oxides, in line with the observation that the high iron content boron carbide gave poor results when employed as a support for platinum in electrocatalysts (4.2-1).

The method of analyzing for platinum in the nitric acid leachant described in Section 2.1.3.1 could not be employed due to the strong absorption of nitric acid in the ultraviolet region of interest. Consequently, the following method for determining the platinum content of the nitric acid leachant was developed and used. The nitric acid leachant solution was diluted to a known volume, an aliquot was mixed with an equal volume of concentrated sulfuric acid and heated to fuming. The fuming residue was diluted with water to about 100 ml and 2 grams of hydrazine sulfate added. After boiling, the solution was filtered, the platinum-containing residue was ignited for 1 hour at 550°C, and the platinum was weighed as platinum metal.

4.2.2 Preparation and Activation of Leached Nickel Foam Electrodes (W. T. Grubb, L.H. King)

The general method of preparation of these electrodes was the same as previously described (4.2-2). When a second leachable additive was used, conditions of leaching were adjusted to promote its removal. In the case of Cab-O-Sil (electrodes No. 436 and 461 of Table 4.2-1), the nickel was leached out with 10% nitric acid and then the silica was removed with 50% NaOH solution. In the case of the Cab-O-Lite electrodes, the nickel and the calcium metasilicate were removed in a single leaching with 10% nitric acid, 1% HF in water.

The leached nickel foam structure presents a myriad of preparation variables. A few of these variables have been selected as most important: the percentage of Teflon; the heat treatment

---

(4.2-1) W. T. Grubb, Technical Summary Report No. 6, Hydrocarbon-Air Fuel Cells, ARPA Order Order No. 247, Contract No. 44-009-ENG-4909 and DA 44-009-AMC-479(T), p. 5-6.

(4.2-2) W. T. Grubb and L. H. King, Technical Summary Report No. 9 Hydrocarbon-Air Fuel Cells, ARPA Order No. 247, Contract No. DA 44-009-AMC-479(T), p. 3.1 (1966).

of the electrode during its preparation; and, the activity of the platinum-activated boron carbide which is a complex effect of its preparation variables. The present optimal procedure for activation of boron carbide with platinum is reported in Appendix 4. 2. 3.

The general trend of improvement in performance by selecting and optimizing the important variables is evident from the trend of specific performance in ma/mg of Pt (column 4 in Table 4. 2-1) in which a general improvement is noted when comparing early electrodes at the top of the table with later electrodes at the bottom of the table. The first 27 electrodes of the leached nickel foam structure averaged 30. 3 ma/mg at 0. 7 volt. The second 27 electrodes averaged 44. 5 ma/mg. The last electrode tested gave $72._6$ ma/mg, representing partly the effect of using Cab-O-Lite as a second leachable additive.

Further reduction of the Teflon binder content to 10% has been explored (electrodes No. 515 and 436), and this shows little or no improvement. A different technique of preparation involving the use of a paint brush to spread the activated boron carbide-Teflon suspension mixture onto the screen current collector appears to be somewhat inferior (electrodes No. 440 and 459). An unpressed electrode (No. 454) was both leaky and not outstanding in performance. An electrode (No. 455) prepared from a platinum-activated boron carbon composition with atomic B/C ratio of 0. 76 instead of the usual value for Norbide boron carbide of 1. 86, gave poorer results.

The weight of the nickel foam, indicative of the diameter of the nickel strands (and therefore the pores) was varied by a factor of 2 with little effect (electrodes No. 447, 448 and 449). Two iron-containing additives, Fe_3O_4 (electrode No. 463) and crocidolite asbestos (electrode No. 469), did not produce any great improvement in performance.

Two preparations of platinum-activated boron carbide, one in which solvent was driven off at a higher temperature from the slurry of platinum diammine dinitrite solution with boron carbide, were evaluated in electrodes No. 434 and 435. The variation in catalyst preparation was found to be detrimental. Nevertheless, it (Catalyst 84X) was used in carrying out comparison experiments. Electrode No. 420 shows another variation in catalyst preparation which was inferior to the standard procedure.

In the preparation of an electrode, standard practice has been to heat the electrode to 260°C to decompose the wetting agent in the Teflon suspension and stabilize the platinum-diammine dinitrite on the boron carbide surface. Where Table 4. 2-1 indicates "extra preheat", this step was carried out at 280°C. Where "post heated" is indicated the electrode was heated for 30 minutes at 280°C after the final curing step. Both these procedures may be beneficial to performance (electrode No. 442, 460, 462, 470 and 473).

The improvement in performance produced by using a second leachable additive to produce smaller pores intersecting the larger pores produced by removal of nickel foam strands is discussed in Section 2.1.3.2. The Preparation Sheet for electrode No. 473 gives further details on the method of preparation.

4.2.3 Preparation of Platinum-Activated Boron Carbide (W. T. Grubb, L. H. King)

The current best procedure for preparing the platinum-activated boron carbide is typified by the procedure employed in the preparation of Catalyst No. 84 (see Table 4.2-1). Five grams of Norbide* boron carbide relatively free of metal oxide impurities and containing about 60 w/o boron (less than the stoichiometric value of 78.3%) (4.2-3) was mixed with 6.25 ml of a solution of platinum diammine dinitrite prepared by dissolving 13.16 g of this salt in a mixture of 70 ml of concentrated nitric acid with 30 ml of water. After thoroughly mixing to form a uniform slurry, the mixture was heated from room temperature to about 100°C in an open dish on a hot plate in a fume hood and held with occasional stirring for about 1 hour until fuming stopped. It was then further heated in an oven for 1 hour at 150°C. This mixture was then rough ground in a boron carbide mortar and the above treatment repeated a number of times depending upon the platinum content desired. After the last repetition of the treatment, the mixture was ground thoroughly in a boron carbide mortar and sieved through a 400 mesh Nylon sieve. The first treatment with platinum salt yields 9.1 w/o Pt, the second 16.7 w/o Pt, the third 23.1 w/o Pt, and the fourth 28.6 w/o Pt. Catalyst 84 was prepared with four activations to achieve a platinum content of 28.6 w/o Pt. A yield of 5.045 grams of finished catalyst was obtained in this preparation.

Catalyst 84X of Table 4.2-1 was inadvertently heated to 220°C in one of the nitric acid evaporation steps. The results obtained with this material in fuel cell electrodes indicate that the activity was lower due to this anomaly in the preparation, even though the material was heated to much higher temperatures in the preparation and curing of the electrode.

The above preparation has been evolved empirically over a considerable period of time. It holds no guarantee of being the ultimate optimization. However, the behavior of Catalyst 84X suggests that large deviations from the procedure are likely to lead to poorer results.

(4.2-3) W. T. Grubb, Technical Summary Report No. 8, Hydrocarbon-Air Fuel Cells, ARPA Order No. 247 Contract No. DA 44-009-ENG-4909, DA 44-009-AMC-479(T), DA 44-009-ENG-4853, p 3-1 ff, (1965).

*Norton Co., Worcester, Mass.

BLANK PAGE

Electrode Number	Major Variable Change	Platinum Loading mg/cm^2	ma/mg of Pt at 0.7 V	ma/cm^2 at E_{ca} = 0.6 V	ma/cm^2 at E_{ca} = 0.7 V	E_{ca} at 75.5 ma/cm^2 at 80°C	E_{ca} at 75.5 ma/cm^2 at Room Temp.	E_{ca} at 200 ma/cm^2	E_{ca} at 300 ma/cm^2	E_{ca} at 400 ma/cm^2	E_{ca} at 790
	CONVENTIONAL ELECTRODES										
255	Unpressed Plain Electrode	5.71	36.6	46	209	----	.78	.71	.64	.49	
286	Pressed Plain Electrode	4.88	30.4	38	148	.610	.76	.66	.57	.12	
311	Pressed "Baymal" Electrode	4.58	17.9	14	82	.766	.71	.64	.60	.56	
404	Platinum Black (Control)	45.00	8.1	105	365	.866	.82	.76	.73	.69	
	POROUS ELECTRODES										
324	36.4% TFE Electrode	2.25	13.3	6	30	----	.63	.48	.26	.17	
325	20% TFE Electrode	2.18	38.1	15	83	.779	.71	.65	.62	.59	
326	23.5% TFE Electrode	2.36	35.2	14	83	.798	.71	.65	.63	.62	
328	20% TFE Electrode	1.55	43.6	6	68	----	.89	.64	.62	.61	
329	Film on Screen Side	1.25	48.9	19	63	.742	.69	.66	.64	.84	
330	Double Foam Electrode	1.45	55.1	15	80	----	.76	.66	.64	.63	
331	23% TFE Electrode	1.43	44.7	8	64	.750	.69	.63	.61	.69	
334	Pressed Foam at Reduced Press	3.00	28.8	13	86	.792	.71	.63	.64	.63	
335	Double Foam at Reduced Press.	4.40	18.8	18	63	.773	.71	.61	.50	.23	
336	Reduced Foam Electrode	1.79	18.4	6	33	.720	.65	.60	.56	.33	
337	Activated After Fabrication	2.42	11.1	5	27	----	.62	.52	.48	.24	
340	Platinum Deposited on Foam	1.05	9.5	Nil	19	----	.54	.59	Nil	Nil	
342	Additional Post Activation	2.62	28.2	15	80	.775	.70	.64	.61	.39	
345	Heavy Foam	1.53	32.8	7	50	----	.66	.61	.57	.53	
348	Heavy Foam with Reduced Press	3.34	18.3	11	61	.740	.69	.62	.39	.56	
349	Non-porous Back	2.78	32.6	15	96	.769	.71	.63	.56	.46	
353	Unpressed Foam Electrode	1.65	45.5	10	75	.725	.70	.64	.62	.60	
356	High Platinum Catalyst	2.95	25.4	10	73	.770	.79	.65	.62	.61	
357	High Pt Catalyst-High Loading	4.69	35.2	27	183	.607	.75	.66	.66	.65	
366	Double Screen-Heavy Foam	4.64	14.4	17	67	----	.68	.51	.39	.27	
376	Dual Porosity-Elyte Side More Porous	2.37	24.0	6	37	.755	.68	.64	.62	.62	
377	Dual Porosity-Gas Side More Porous	2.26	35.6	12	83	.773	.71	.65	.63	.62	
390	Film on Foam Side-High Pt Catalyst	3.40	23.8	15	86	.780	.71	.64	.48	.35	
397	Film on Foam Side-Heavy Foam	3.78	31.2	20	118	.785	.73	.64	.57	.51	
(404)	Platinum Black (Control)	45.00	8.1	105	365	.860	.82	.76	.73	.69	
405	Film on Foam Side-High Loading	4.92	16.0	18	79	.760	.71	.61	.53	.43	
409	20% TFE - High Pt	5.00	42.0	39	219	.806	.75	.79	.68	.64	
413	15% TFE - High Pt	3.76	45.3	26	179	.806	.75	.86	.67	.66	
414	Post Heated (15% TFE)	4.30	59.4	40	255	.621	.77	.72	.69	.67	
415	10% TFE - High Pt	4.07	52.9	35	213	.612	.76	.71	.66	.66	
420	Extra Stabilized Cat. 61A	2.60	14.5	7	43	.710	.65	.37	.41	.23	
426	New Stabilized Catalyst 83	1.62	28.2	9	62	.754	.69	.64	.61	.38	
(427)	Pasted Electrode	3.72	21.4	22	122	.803	.74	.66	.50	.31	Cu
434	New Catalyst 84	4.31	54.6	23	235	.812	.76	.71	.69	.66	
435	New Catalyst 64X	4.17	42.5	23	177	.802	.73	.66	.67	.64	
436	5% "Cab-O-Sil" (19% TFE)	2.15	33.4	12	105	.780	.71	.67	.66	.63	
(440)	Painted Electrode-WithTitron-X	4.67	18.1	31	50	.740	.72	----------Cut Off----------			
442	Extra Stabilized-Extra Preheat	3.73	56.4	27	210	.796	.75	.70	.68	.67	
444	5% "Cab-O-Lite" (15% TFE)	3.29	88.8	32	225	.612	.76	.71	.68	.65	
445	Etched Foam	3.58	41.0	24	163	.802	.74	.66	.67	.63	
446	20% "Cab-O-Lite"	3.26	50.4	20	165	.765	.75	.66	.67	.66	
447	Light Wt. Foam (Unetched)	3.76	40.7	21	152	.784	.74	.66	.66	.54	
448	Standard Wt. Foam (Etched)	3.58	39.2	20	140	.764	.74	.66	.64	.63	
449	Heavy Wt. Foam (Unetched)	4.52	36.6	22	165	.796	.74	.69	.66	.63	
454	Unpressed Cat. 64X	3.61	48.6	35	166	.806	.76	.79	.66	.62	
455	New Low Boron Cat. 85	2.54	6.7	8	25	.686	.63	.55	.44	.36	
(459)	Painted Electrode Without Titron-X	4.62	29.2	52	143	.617	.76	.61	----------Cut Off----------		
460	Extra Preheat I	3.38	53.4	23	160	.619	.73	.66	.67	.66	
461	3.6% "Cab-O-Sil"	1.97	56.5	13	113	.766	.72	.66	.67	.66	
462	Extra Preheat II	3.31	54.5	26	160	.808	.75	.65	.67	.64	
462	Added 1% Fe_3O_4 I	3.16	52.6	25	163	.804	.75	.66	.66	.64	
464	Unpressed Catalyst 84	4.12	42.6	36	180	.812	.76	.69	.64	.58	
468	Added 1% Fe_3O_4 II	3.66	43.7	25	160	.807	.76	.66	.66	.64	
469	Added 5% Crocidolite	3.38	22.6	16	110	.767	.72	.66	.62	.56	
470	Post Heated	4.25	45.6	30	165	.812	.75	.76	.67	.62	
473	5% "Cab-O-Lite" (Optimized)	3.65	72.6	29	263	.817	.76	.71	.69	.67	

A

Table 4.2-1

E_{ca} at 400 ma/cm^2	E_{ca} at 790 ma/cm^2	Percent Teflon Binder	Porosity as Volume Percent Void	Catalyst Weight, gram	Electrode Thickness, inch	Foam + Screen Thickness, inch	1000 Cycle Bridge Res., ohm	K-M Bridge Curve Res., ohm	Electrolyte-Side Foam Weight, gram	Press Force on Electrolyte-Side Foam, lb	Gas-Side Foam Weight, gram	Press Force on Gas-Side Foam, lb	Electrode Side With TFE Film	Percent Platinum in Catalyst	Catalyst Number
.49	----	20.0	66.3	.607	.0296	-----	----	.130	-----	----	----	----	Gas	16.7	77A
.43	----	20.0	42.6	.520	.0158	.0092	.110	.112	-----	----	----	----	Gas	16.7	77A
.56	----	20.0	46.6	.466	.0165	.0093	.115	.128	-----	----	----	----	Gas	16.7	77B
.66	.38	----	63.1	.700	.0116	.0084	.100	.113	-----	----	----	----	Gas	100.0	---
.17	----	36.4	72.6	.250	.0237	-----	.138	.170	-----	----	.776	20K	Foam	16.7	80
.59	----	20.0	76.4	.832	.0264	.0153	.123	.185	-----	----	.850	20K	Foam	16.7	80
.63	----	22.3	----	.253	-----	.0106	.117	.120	-----	----	.740	20K	Foam	16.7	80
.61	.45	20.0	61.7	.163	0143	-----	.135	.130	-----	---	.820	20K	Foam	16.7	80
.64	----	22.0	61.6	.138	.0139	-----	.123	.166	.828	20K	----	----	Scr'n	16.7	80
.63	----	23.0	67.7	.150	.0171	-----	.123	.140	.800	20K	900	20K	Gas	16.7	80
.60	----	23.0	61.0	.163	.0141	-----	.120	.130	-----	----	.788	20K	Foam	16.7	80
.63	46	23.0	56.6	.231	.0167	-----	.149	.170	.720	2K	----	----	Scr'n	16.7	80
.23	---	33.0	67.6	.464	0271	.0316	----	.160	.761	2K	.701	2K	Gas	16.7	80
.53	.41	23.0	66.5	.161	.0142	.0160	.136	.193	.459	2K	----	----	Scr'n	16.7	80
24	----	----	----	----	.0175	-----	.149	.160	.820	20K	----	----	Scr'n	-----	--
Nil	----	----	----	----	.0139	.0140	.147	.200	.835	20K	----	----	Scr'n	-----	---
.66	.50	----	----	----	.0162	-----	.137	.130	.816	20K	----	----	Scr'n	16 7	80
.53	----	23.0	61.8	.163	.0147	.0161	.147	.835	1.350	20K	----	----	Scr'n	16.	80
.56	----	23.0	64.4	.356	.031	.0358	.247	.260	1.332	2K	----	----	Scr'n	16.7	80
.48	----	33.0	55.6	.284	.0158	.0132	.120	.130	.631	20K	----	----	Scr'n	16.7	61
.60	----	33.0	58.3	.175	.0141	.0138	.116	.173	.904	20K	----	----	Scr'n	16.7	61
.61	----	63.0	66.1	.164	.0167	.0140	.113	.150	.648	20K	----	----	Scr'n	66.6	62
.65	.51	25.8	61.4	.282	.0176	.0132	.103	.125	.941	20K	----	----	Scr'n	28.8	62
.57	----	23.0	----	.495	.0466	.0667	.103	.113	4.381	2K	----	----	Gas	16.7	61
.62	.31	23.0	70.1	.262	.0316	.0260	.152	123	.948	20K	1.001	3K	Gas	16.7	61
.62	.50	23.0	65.3	.253	.0113	.0234	.131	.150	.983	3K	1.000	20K	Gas	16.7	61
.55	.40	23.3	61.6	.318	.0157	.0147	.123	.130	-----	----	1.003	20K	Foam	86.6	88
.31	.06	25.2	33.3	.233	.0133	.0167	.343	.130	-----	----	1.473	20K	Foam	28.6	68
.66	.38	----	63.1	.700	.0116	.0084	.100	.113	-----	----	----	----	Gas	100.0	---
.43	----	25.3	67.6	.306	.0163	.0140	.123	.140	-----	----	1.103	20K	Foam	28.6	62
.84	.43	20.0	60.8	.312	.0172	.0133	.115	.125	-----	----	.799	20K	Foam	86.6	62
.66	.67	18.0	63.4	.234	.0160	.0149	.130	.110	-----	----	.955	20K	Foam	86.6	82
.67	.36	18.0	60.6	.266	.0156	.0138	.117	.116	-----	----	.969	20K	Foam	28.6	88
.66	.56	10.0	63.4	.254	.0100	.0137	.186	.100	-----	----	.963	20K	Foam	28.6	62
.23	----	22.8	64.4	.276	.0150	.0131	.147	.130	-----	----	.830	20K	Foam	10.7	61A
.58	.35	32.3	56.6	.173	.0139	.0133	.117	.128	-----	----	.792	20K	Foam	16.7	63
.51	Cut Off	20.0	56.3	.409	.0228	-----	----	.122	-----	----	----	----	Gas	16.7	62
.68	.59	10.0	61.0	.286	.0152	.0140	.109	.196	-----	----	1.140	20K	Foam	86.6	64
.64	.48	1. 0	64.4	.260	.0166	-----	.126	.116	-----	----	1.140	20K	Foam	28.6	84X
.35	.57	10.0	62.6	.196	.0145	.0103	.118	.134	-----	----	1.140	20K	Foam	28.6	84
----------	----------	6.3	30.4	.530	.0169	.0080	.107	.108	-----	----	-----	----	Gas	16.7	83
.67	.60	15.0	61.3	.238	.0181	.0129	.108	.116	-----	----	.909	20K	Foam	28.6	84
.65	.53	13.0	64.0	.204	.0156	.0150	.120	.122	-----	----	.711	20K	Foam	28.6	84
.65	.51	16.0	58.1	.248	.0146	.0149	.105	.122	-----	----	.809	20K	Foam	28.6	84
.66	.59	15.0	60.4	.204	.0162	-----	.134	.128	-----	----	1.086	20K	Foam	28.6	84
.64	.31	16.0	81.2	.224	.0101	.0156	.108	.122	-----	----	.664	20K	Foam	28.6	84X
.63	.41	16.0	67.0	.223	.0134	.0139	.156	.126	-----	----	.713	20K	Foam	28.6	84X
.63	.45	15.0	64.2	.282	.0175	.0168	.107	.124	-----	----	1.434	20K	Foam	28.6	84X
.63	.42	18.0	61.8	.246	.0154	-----	.099	116	-----	----	1.180	20K	Foam	28.6	84X
.36	.08	20.0	00.6	.271	.0148	.0167	.111	.150	-----	----	1.181	20K	Foam	16.7	85
Cut Off	----------	0.3	61.6	.525	.0172	.0086	.273	.110	-----	----	-----	----	Gas	16.1	62
.65	.63	15.0	58.7	.810	.0137	.0131	.099	.114	-----	----	.843	20K	Foam	28.6	64
.66	.55	16.0	59.6	.183	.0122	.0133	.102	.136	-----	----	.900	20K	Foam	25.6	64
.64	.54	15.0	58.0	.206	.0137	.0133	.081	.110	-----	----	.836	20K	Foam	28.6	64
.64	.46	16.0	60.6	.184	.0141	.0130	.103	.120	-----	----	.828	20K	Foam	28.6	64X
.56	.04	16.0	08.8	.257	.0137	.0138	.098	.110	-----	----	.818	20K	Foam	28.6	64
.64	.46	16 0	60.2	.228	.0146	.0136	.109	.184	-----	----	.800	10K	Foam	28.6	64X
.56	.09	13.0	58.7	.210	.0137	.0126	.106	.126	-----	----	.794	20K	Foam	28.6	84X
.62	.10	18.0	61.1	.284	.0107	.0140	.099	.118	-----	----	.758	20K	Foam	28.6	84X
.67	.58	18.0	58.6	.228	.0141	.0133	.097	.116	-----	----	.81[illegible]	20K	Foam	28.6	84

POROUS ELECTRODE PREPARATION RECORD

ELECTRODE NUMBER 473

Optimized Electrode
5% Cab-O-Lite and Post Heated

Preparation

Screen: Material Pt. Weight 5.207 gm. Thickness 0.0083 inch.

Foam Weight 0.814 gm (etched from 1.330 gm foam w/1.33 cc HNO_3 + 100 cc H_2O in 7 hours).

Press foam into screen in 350°C press at 20,000 lb. Thickness 0.0133 inch.

Weigh out catalyst: 0.363 gm No. 84 at 28.6 wt % Pt.

Add 0.018 gm Cab-O-Lite (5%).

Add 0.44 cc T-30 mixture 2/11 H_2O = 0.0611 gm TFE = 15%.

Stir mixture and paste electrode.

Air dry overnight.

Cure on hot plate at 250°C for 30 minutes including heating time; then cool 30 minutes on hot plate.

Press in 350°C press for 10 minutes at 7000 to 8000 lb with foam side down. Weight 6.321 gm.

Leach 6 hours on hot plate in 10 vol. HNO_3 + 90 H_2O + 1 HF, dry. Weight 5.474 gm.

Check for pinholes. Patch, if necessary.

Spray _____ film on foam side using 4.4 cc of H_2O + T-30 mixture diluted 7:1 in a 5 inch square area.

Oven cure 2 minutes at 350°C.

Number tab on the film side.

Check wetting-brush dry boron carbide on with soft brush.

Post heat on hot plate set at 280°C for 30 minutes; cool 30 minutes.

Cell test vs. Electrode No. 247 Electrolyte H_2SO_4 Resistance 0.097 ohm.

Specifications

				Electrode Thickness
				0.0141 inch (average)
Wt. of Cat, Teflon	0.267	gm,	15.0 mg/cm^2	.0145
Weight of Dry Catalyst	0.228	gm,	12.8 mg/cm^2	.0148
Weight of Platinum	0.065	gm,	3.65 mg/cm^2	.0136
Additive Leached Out	0.847	gm	= 104.0 %	.0137
Calculated Porosity 59%				

4.3 SUMMARY OF CELL LIFE TESTS WITH MULTI-COMPONENT FUELS

A summary of cell life testing with various multi-component fuels is given in Table 4.3-1. Plots of anode polarization data vs. time for these cells are shown in Figures 4.3-1 thru 4.3-24.

Table 4.3-1

Summary of Electrochemical Cell Life Testing

Note: All anodes were composed of 00% Pt, 10% T-30 on gold vapor-deposited (3 mg/in.^{2}) expanded tantalum screen. All cathodes were 85% Pt, 15% T-30 on platinum wire-woven screen. Electrolyte was 95-91% H_3PO_4 at 350°F.

Cell No.	Electrodes	Reactants	Performance: θ, hr	Current Density, ASF	Power Density, WSF	Anode Potential vs. H_2/H^+ Ref., volt	R, ohm	Life, hr	Anode Surface Area*, m^2
162	A - 3620 C - 3504	22.5% n-octane 22.0% iso-octane 5% toluene 10% octene-2 10% MCH** 30% MCP***	1	30	4.0	.700	.010	90	9.38
				00	4.5	.730			
103	A - 3639 C - 3. "	37% n-octane 37% iso-octane 5% octene-2 1% toluene 5% MCH 15% MCP	2	30	10.0	.480	.007	18	Not Taken
				00	17.4	.515			
			.18	15	0.0	>1.0			
104	A - 3636 C - 3504	22.5% n-octane 22.5% iso-octane 5% toluene 10% octene-2 10% MCH 30% MCP	1	30	9.9	.000	.008	144	10.90
				00	16.0	.510			
			144	30	0.0	>1.0			
				10	1.0	.800			
186	A - 3637 C - 3504	35% n-octane 35% iso-octane 0% toluene 5% octen. 0% MCH 15% MCP	1	30	1.0	.600		22	Not Taken Leaky Cathode. Replaced in LT-187.
187	A - 3677 C - 3507	Same as Cell '46.	1	30	9.1	.070		20	Not Taken
				00	12.0	.090			
			20	30	0.0	>1.0			
				15	3.8	.920			
189	A - 3640 C - 3504	90% n-octane 10% MCH	1	30	9.9	.520	.019	358	10.02
				90	14.4	.550			
			179	30	0.1	.090			
				50	3.0	.700			
190	A - 3652 C - 3589	93% n-octane 7% toluene	1	30	8.2	.510	.010	402	Not Taken
				00	9.0	.910			
			144	30	6.9	.640			
				60	0.0	>1.00			
191	A - 3655 C - 3604	70% n-octane 30% MCP	1	30	14.1	.385	.010	286	Not Taken
				00	21.6	.450			
			264	30	11.9	.440			
				60	19.0	.500			
192	A - 3654 C - 3507	90% n-octane 10% MCH	1	30	7.9	.565	.010	375	Not Taken
				60	9.0	>1.00			
			360	30	7.2	.900			
193	A - 3642 C - 3589	00% n-octane 20% MCH	1	30	9.1	.020	.006	01	10.52
				60	13.9	.550			
194	A - 3656 C - 3604	50% n-octane 50% MCP	1	30	14.7	.360	.008	645	10.57
				80	22.6	.420			
			640	30	6.0	.600			
195	A - 3663 C - 3671	80% n-octane 10% toluene	1	30	0.8	.620	.010	115	9.21
				60	7.6	.715			
			120	30	0.0	>1.00			
				20	2.4	.765			

*As measured by B. E. T. method prior to test.
**MCH = Methylcyclohexane
***MCP = Methylcyclopentane

Table 4.3-1 (Cont'd.)

Cell No.	Electrodes	Reactants	θ, hr	Performance Current Density, ASF	Power Density, WSF	Anode Potential vs H_2/H^+ Ref., volt	Ohm	Life, hr	Anode Surface Area, m^2
196	A - 3680 C - 3372	88% octane 18% MCH	1	30	10.8	.800	.010	188	Not Taken
				80	14.4	.600			
			160	30	8.6	.590			
				60	6.0	.650			
197	A - 3661 C - 3569	80% n-octane 20% MCH	1	30	10.2	.506	.010	189	Not Taken
				60	12.0	.810			
			143	20	5.9	.620			
				60	0.0	>1.00			
198	A - 3666 C - 3507	70% n-octane 20% MCH	1	20	8.2	.880	.008	144	
				60	11.4	.860			
			143	20	8.4	.650			
				60	2.0	.700			
201	A - 3666 C - 2589	98% n-octane 2% octene-2	1	20	14.6	.260	.007	220	
				60	22.6	.440			
202	A - 3673 C - 3668	50% n-octane 50% MCH	1	30	9.0	.590	.00[illegible]	144	
				90	0.0	>1.00			
202	A - 3662 C - 3507	30% n-octane 70% MCH	[illegible]	20	6.7	.270	.010	92	
				90	7.2	.675			
				20	2.0	.750			
				80	0.0	>1.00			
204	A - 3664 C - 3673	80% n-octane 20% MCH						92	
206	A - 3659 C - 3673	37% n-octane 37% iso-octane 1% toluene 8% octene-2 8% MCH 15% MCP	1	20	12.0	.480	.010	160	
				80	16.8	.840			
			158	20	0.0	>1.00			
				20	2.2	.910			
206	A - 3604 C - 3670	90% n-octane 10% toluene	1	20	9.0	.870	.010	120	
207	A - 3679 C - 2507	95% n-octane 6% octene-2	1	30	9.0	.500		140	
208	A - 3669 C - 3672	24.5% n-octane 24.2% iso-octane 1.0% toluene 8% octene-2 15% MCH 30% MCP	1	20	11.6	.485	.008	188	
				60	14.7	.880			
			186	30	0.0	.600			
				20	5.10	.616			
209	A - 2667 C - 3704	95% n-octane 5% octene-2	3	20	12.8	.450	.010	24	
				60	24.0	.470			
210	A - 3660 C - 3604	40% n-octane 20% MCH 40% MCP	1	20	8.4	.550	.012	100	
				60	10.8	.610			
			98	30	9.0	.650			
				90	0.0	>1.00			
211	A - 2676 C - 3704	95% n-octane 5% octene-2	1	20	11.7	.520	.010	100	
				60	19.0	.540			
			72	20	11.5	.830			
				80	18.8	.550			
212	A - 3661 C - 3507	70% n-octane 10% MCH 20% MCP	1	30	9.4	.245	.010	48	
				80	10.2	.850			
			45	20	6.1	.580			
				80	2.0	.770			

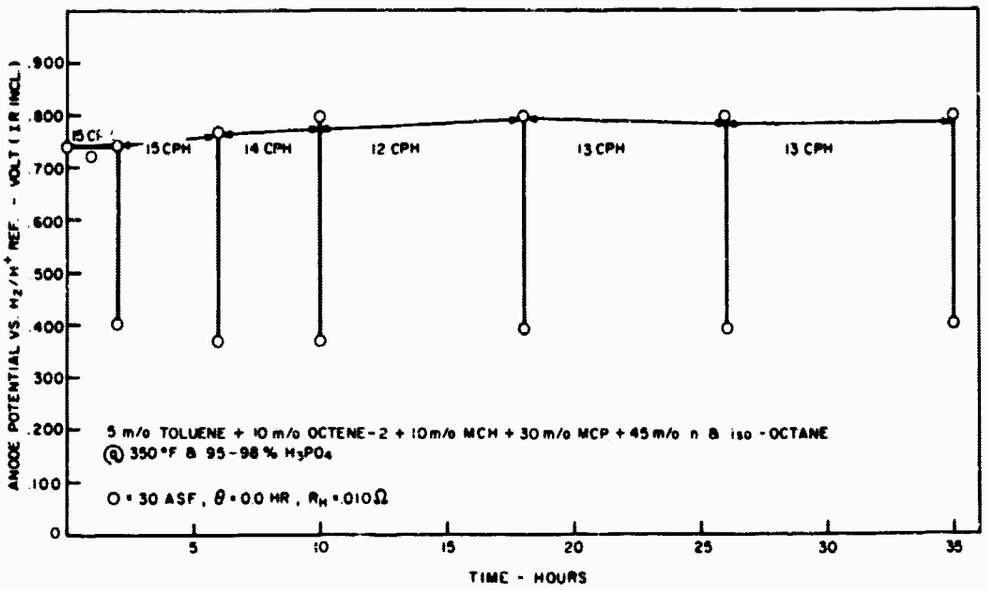

Figure 4.3-1. Cell LT-182

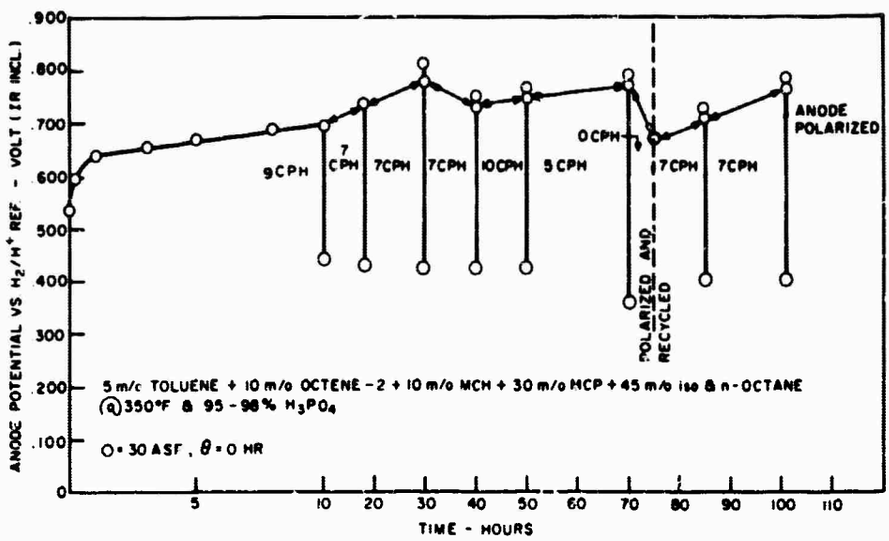

Figure 4.3-2. Cell LT-184

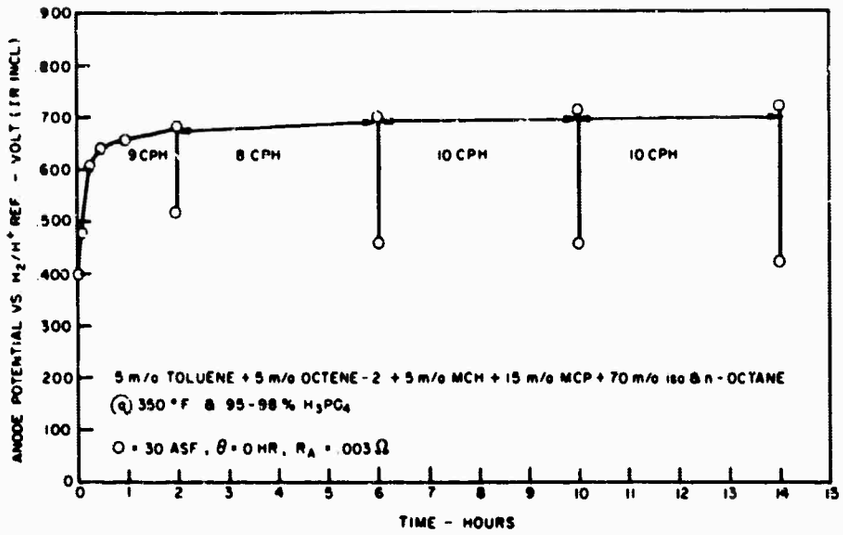

Figure 4.3-3. Cell LT-187

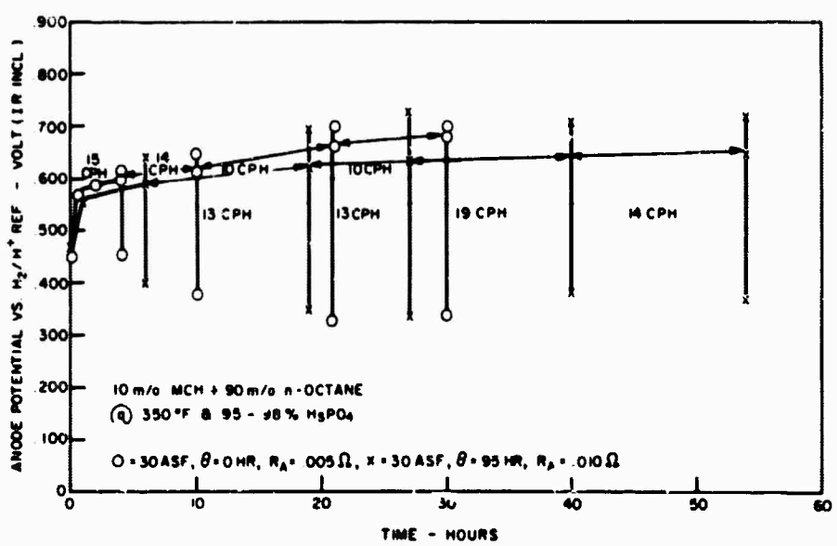

Figure 4.3-4. Cell LT-189

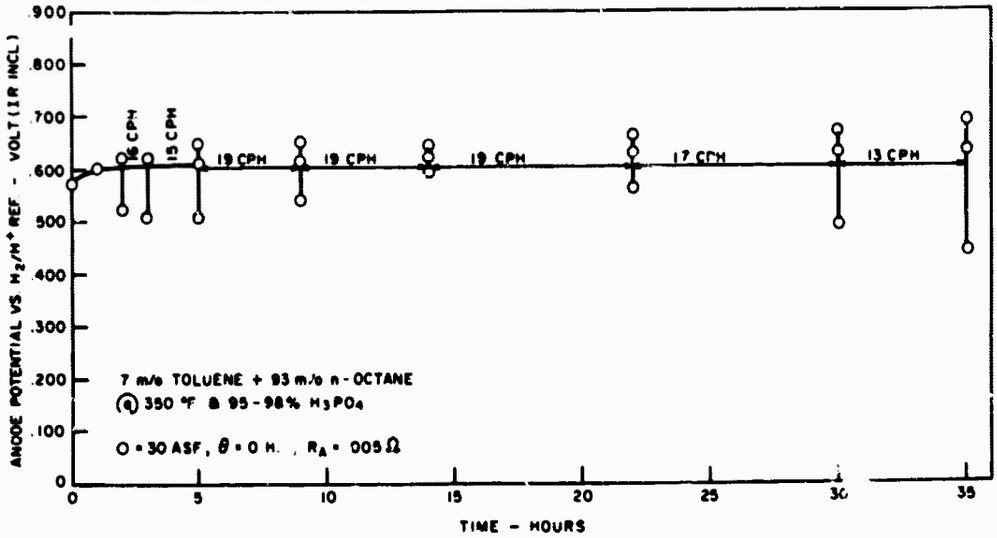

Figure 4.3-5. Cell LT-190

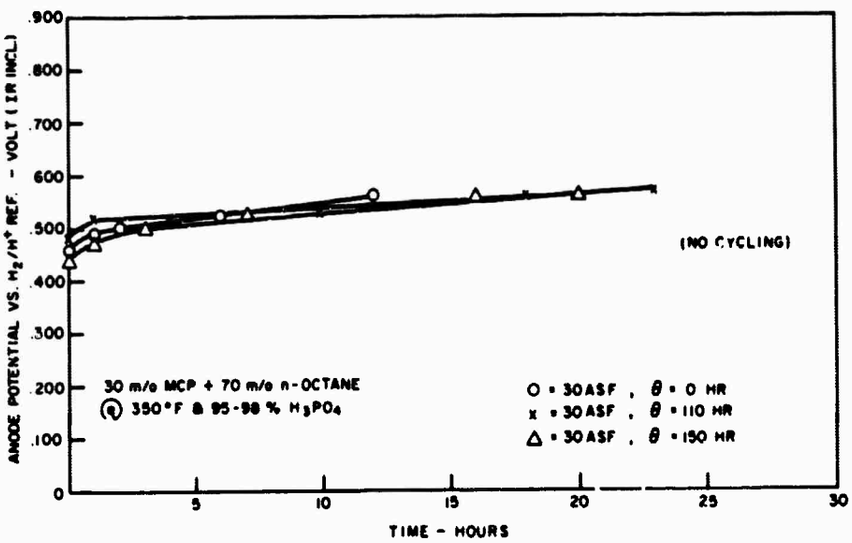

Figure 4.3-6. Cell LT-191

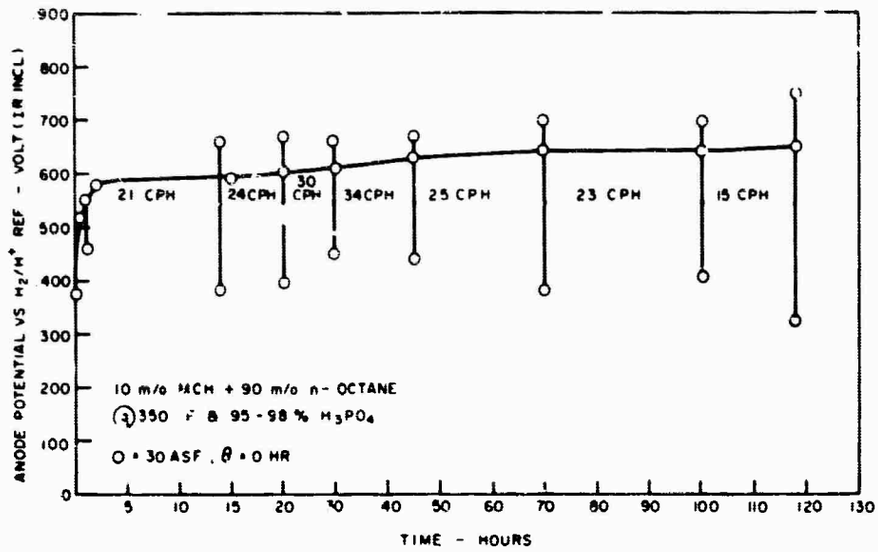

Figure 4.3-7. Cell LT-192

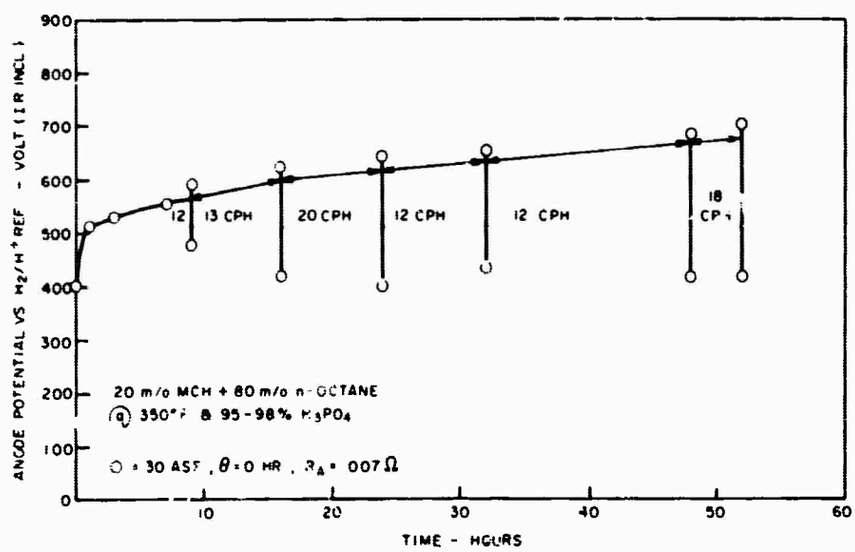

Figure 4.3-8. Cell LT-193

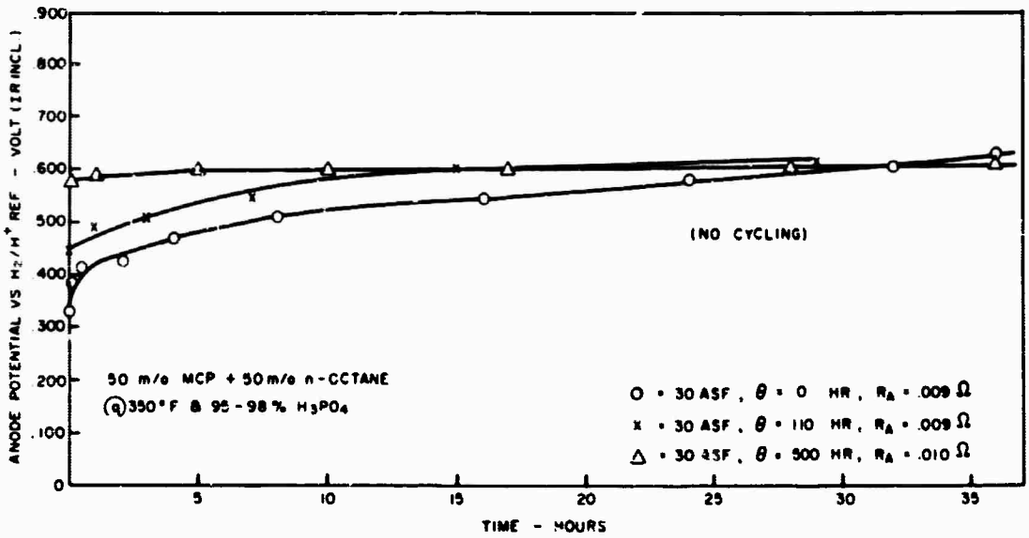

Figure 4.3-9. Cell LT-194

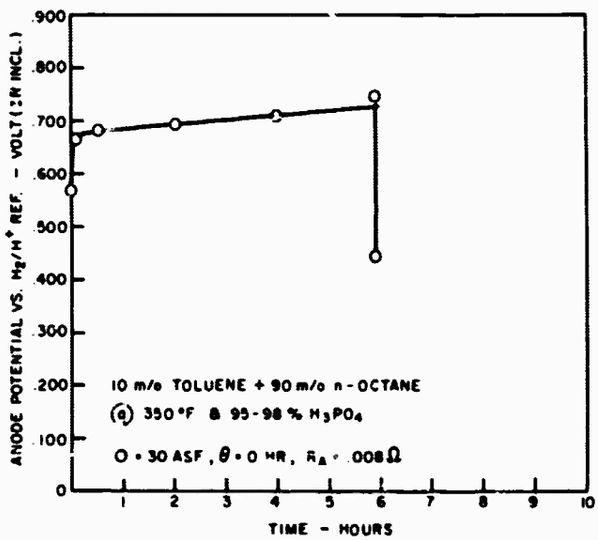

Figure 4.3-10. Cell LT-195

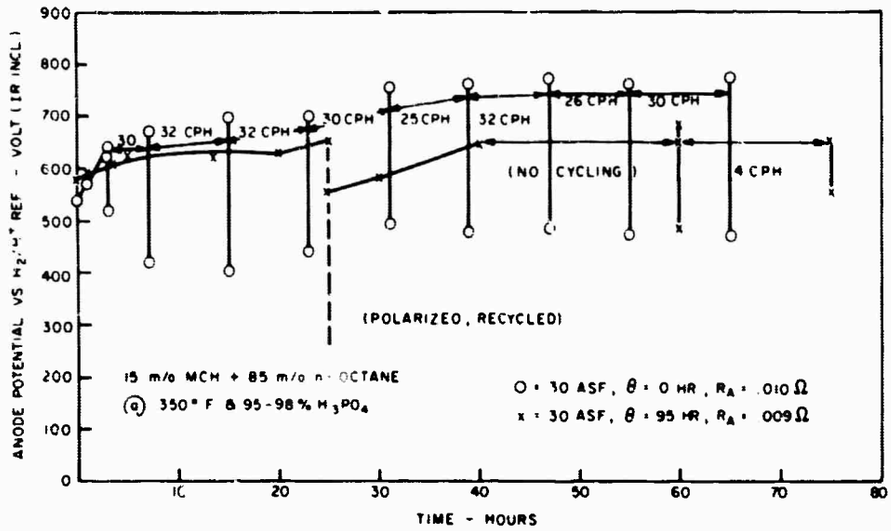

Figure 4.3 11. Cell LT-196

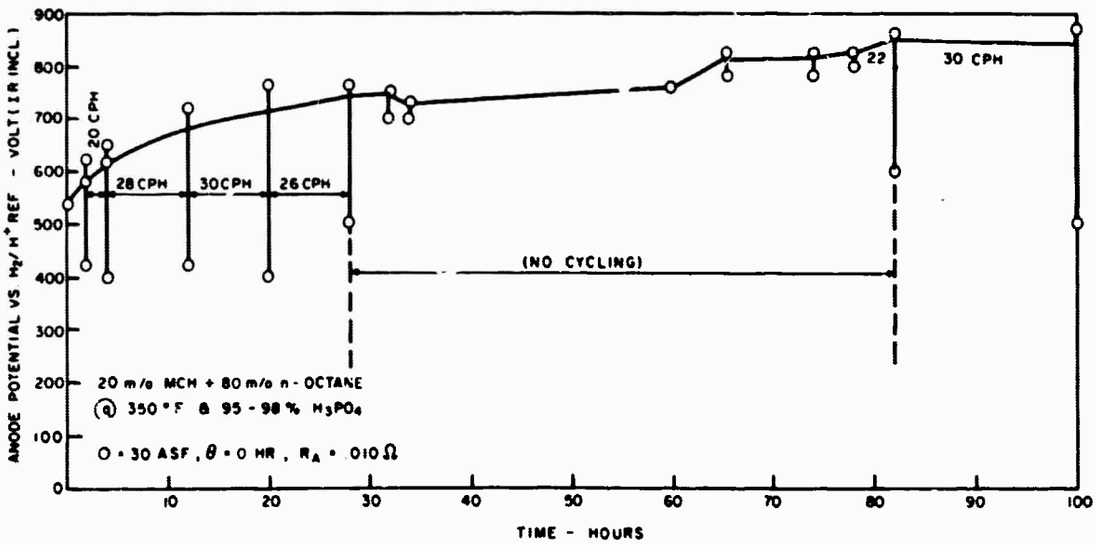

Figure 4.3-12. Cell LT-197

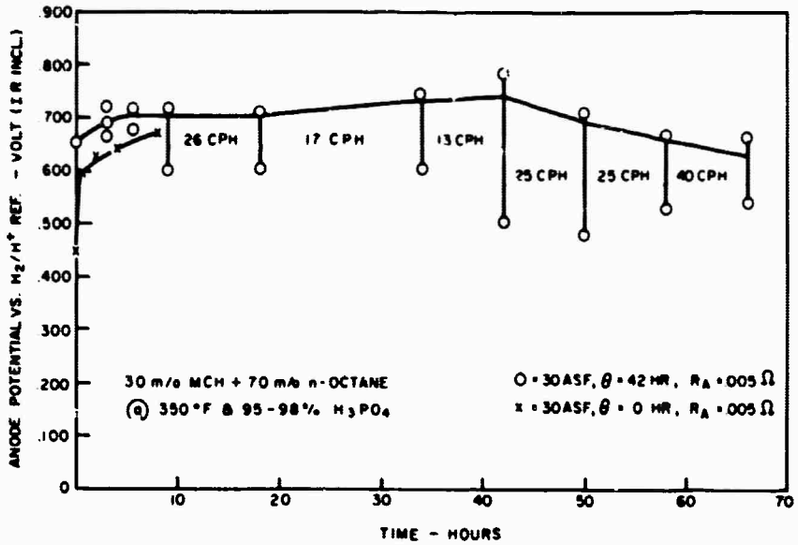

Figure 4.3-13. Cell LT-198

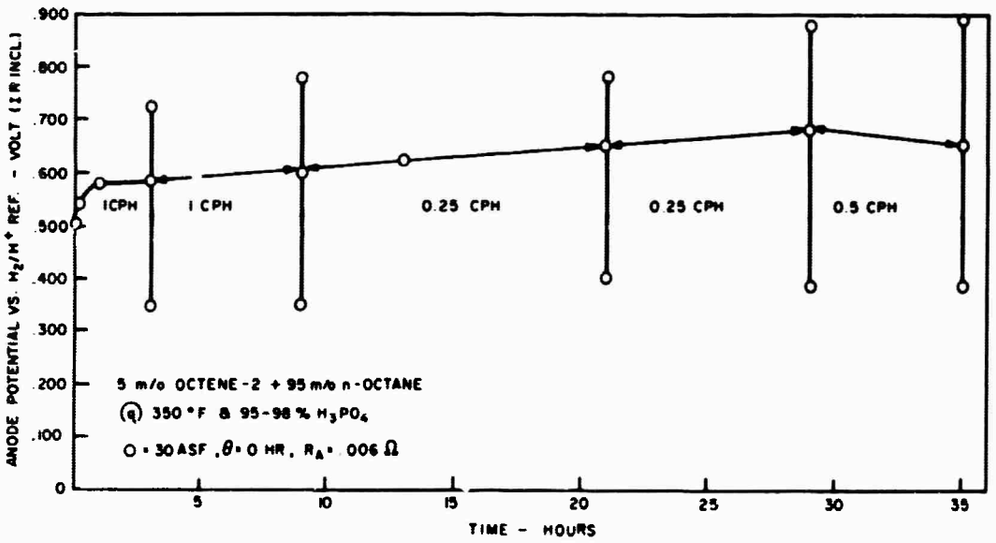

Figure 4.3-14. Cell LT-201

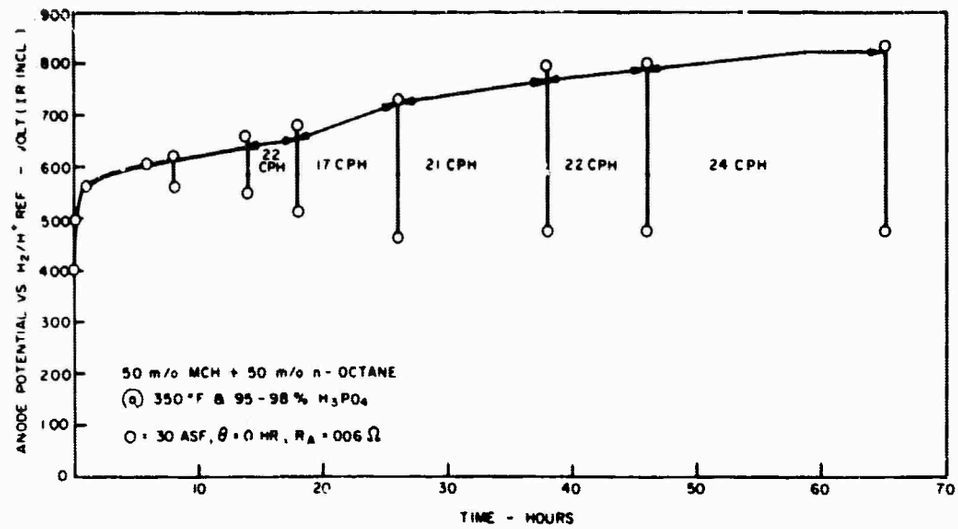

Figure 4.3-15. Cell LT-202

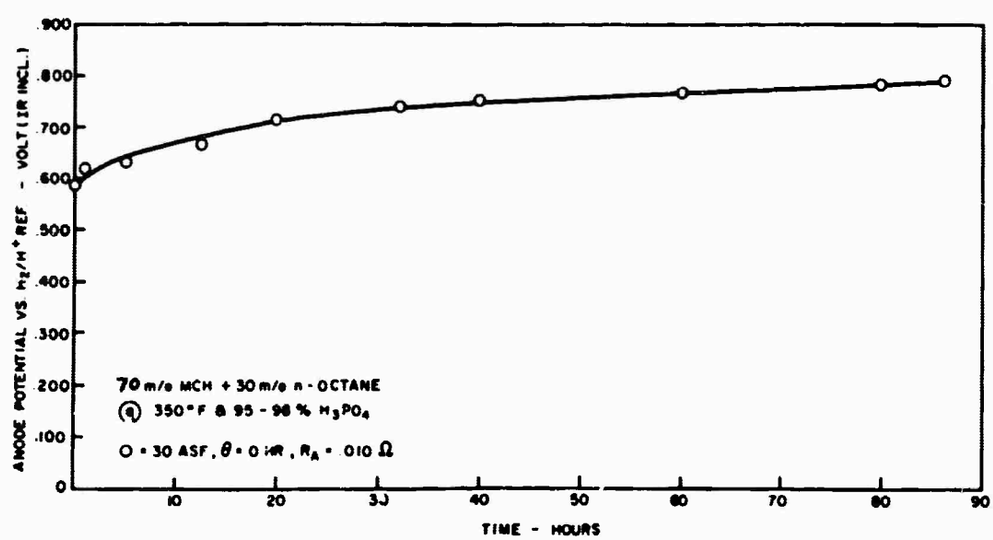

Figure 4.3-16. Cell LT-203

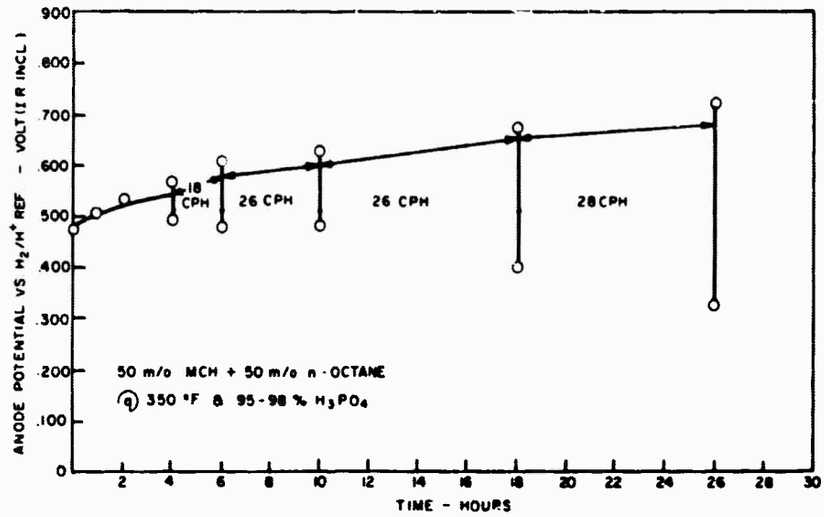

Figure 4.3-17. Cell LT-204

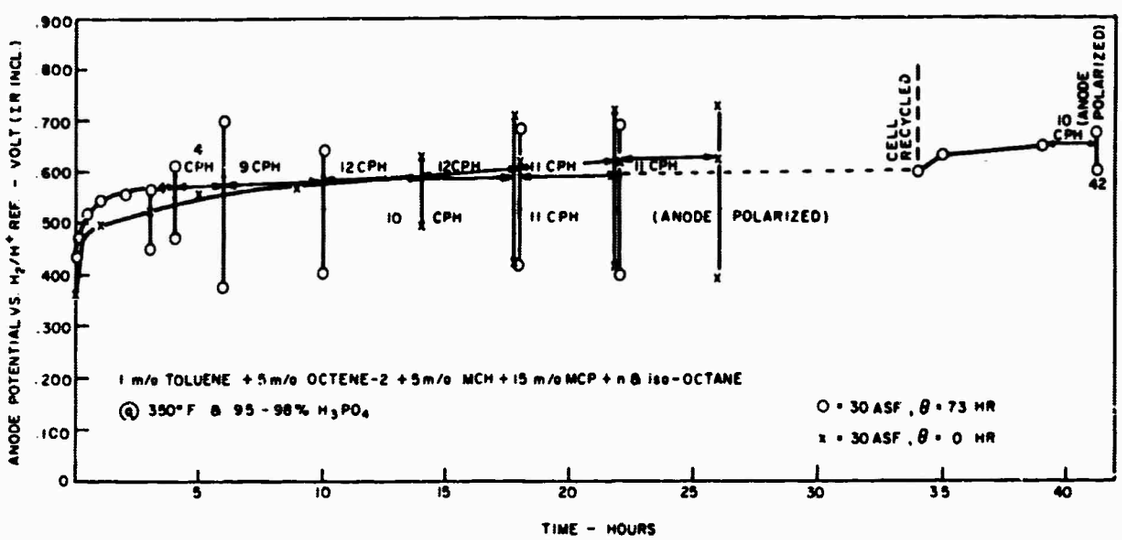

Figure 4.3-18. Cell LT-205

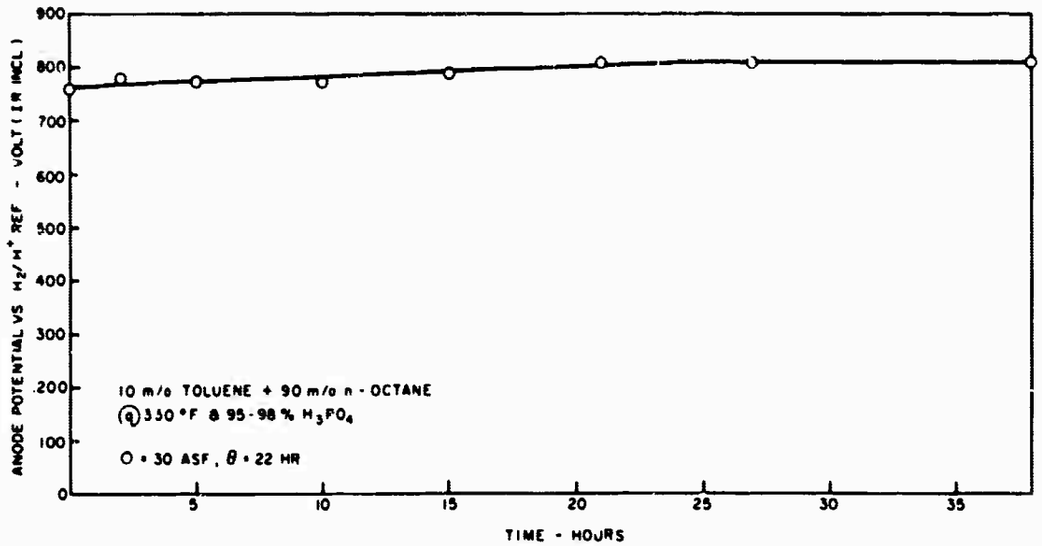

Figure 4.3-19. Cell LT-206

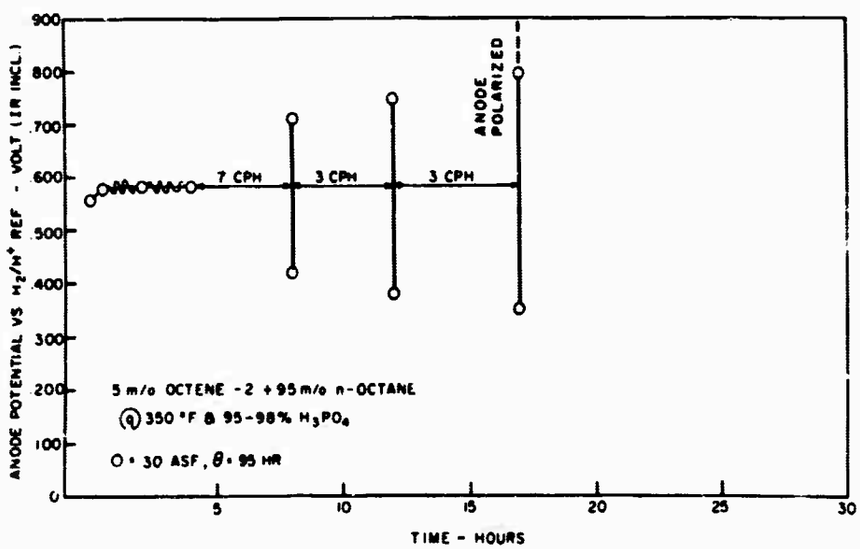

Figure 4.3-20. Cell LT-207

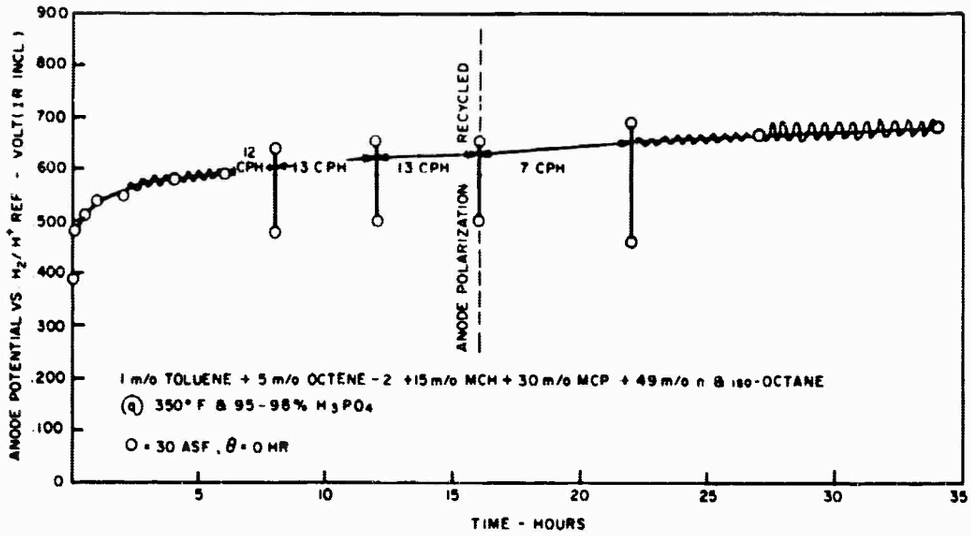

Figure 4.3-21. Cell LT-208

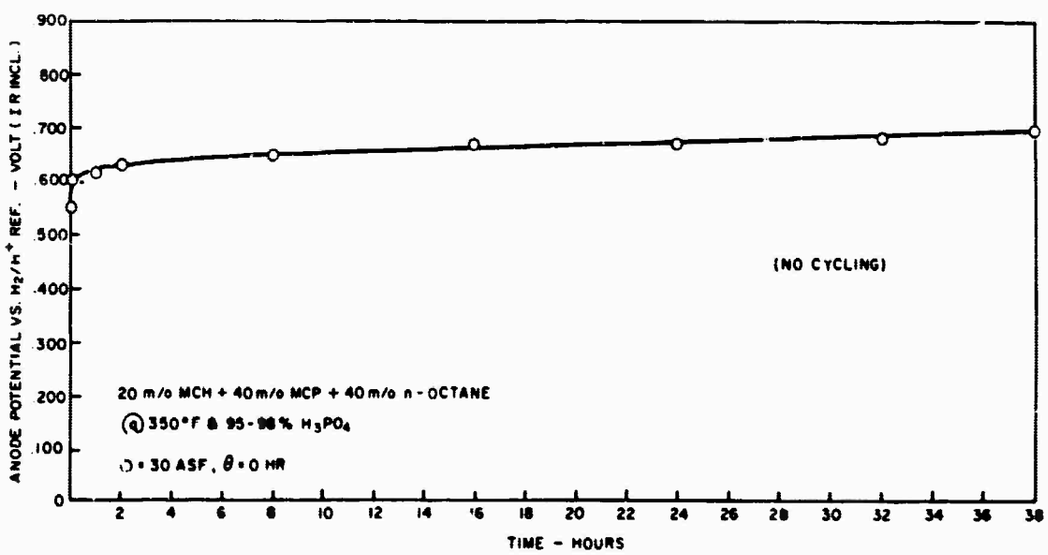

Figure 4.3-22. Cell LT-210

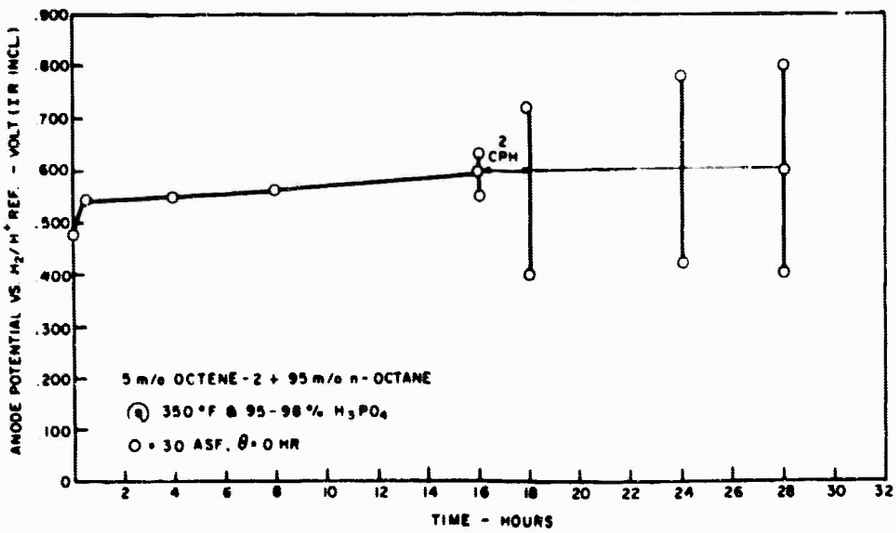

Figure 4.3-23. Cell LT-211

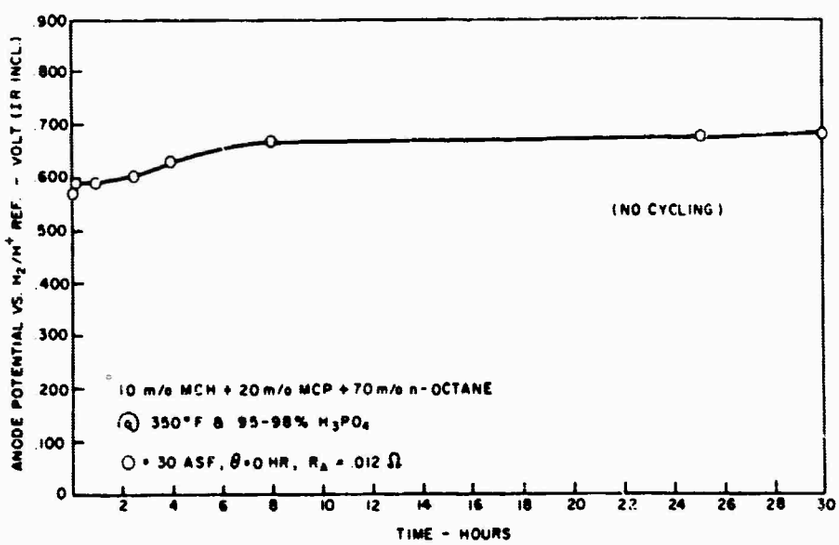

Figure 4.3-24. Cell LT-212

4.4 CALCULATIONS FOR BINARY AND MULTI-COMPONENT FUELS

4.4.1 Calculations for Binary Fuels

The details of the calculation of the exhaust compositions and current contributions of the components of a binary fuel were given in an earlier report (4.4-1). For this report period these calculations were automated using a program, an example of which is shown below.

INPUT

A'_a	=	APA	=	265.00	A'A*	=	APA*	=	2000.00
A'_b	=	ABP	=	2569.00	A'_b*	=	APB*	=	50000.00
A_a	=	AA	=	478.00	AA*	=	AA*	=	50.00
A_b	=	AB	=	1077.00	A_b*	=	AB*	=	50000.00
m_a'	=	MAP	=	1.00	m_b'	=	MBP	=	99.00
V	=	V	=	0.04	d_o	=	DO	=	0.71
m_b	=	MB	=	114.22	m_a	=	MA	=	78.11
I	=	I	=	1.46	F	=	F	=	1608.30
N_a	=	N	=	30.00	N_b	=	NB	=	50.00

OUTPUT

NA = 0.0010853 WB = 0.9931398

WA = 0.0068602

BX	=	0.00024589	MOLES/MINUTE OF COMPONENT B AT THE INLET
BY	=	0.00000248	MOLES/MINUTE OF COMPONENT A AT THE INLET
SX	=	0.00001681	MOLES/MINUTE OF COMPONENT B CONSUMED
SY	=	0.00000223	MOLES/MINUTE OF COMPONENT A CONSUMED
IA	=	0.10783066	CURRENT CONTRIBUTION OF COMPONENT A
IB	=	1.35216935	CURRENT CONTRIBUTION OF COMPONENT B
I	=	1.46000000	TOTAL CURRENT

(4.4-1) Technical Summary Report No. 9 Hydrocarbon-Air Fuel Cells, January 1966-June 1966, ARPA Order No. 247, Contract Nos. DA44-009-ENG-4900-AMC-479(T), and DA44-009-ENG-4853, Pg. 3-9, 3-10.

4.4.2 Calculations for Five Component Fuels (M. W. Gloor)

DECO 24

OXIDATION OF MULTICOMPONENT FUELS: RELATIVE REACTION RATES

i = 1, ... Number of equations

i + 1 = Number of components

Feed Rate:

$$A(i) = r \cdot 10^3 \cdot \rho \times \frac{X(i)}{\sum (X(i) \times M(i)) + (X(i+1) \times M(i+1))}$$

$$A(i+1) = r \cdot 10^3 \cdot \rho \times \frac{X(i+1)}{\sum (X(i) \times M(i)) + (X(i+1) \times M(i+1))}$$

Coefficients for matrix used in solution of i (Cramer's Rule) simultaneous linear equations i = row j = column

Coefficients:

$$M(i, j) = N(i) \times \left(1 - \frac{N(j)}{N(i+1)}\right), \quad i \neq j$$

$$M(i, j) = N(i) \times \left(1 - \frac{N(j)}{N(i+1)}\right) - 1, \quad i = j$$

Constants:

$$\alpha(i) = N(i) \sum A(i) - 621.761658 \frac{N(i)}{n(i+1)} \frac{1}{} - A(i)$$

Moles used up in electrochemical reaction are the solutions to the i simultaneous equations = $\alpha(i)$

Current Contribution $I(i) = 1.60833333 \cdot 10^{-3} \cdot \alpha(i) n(i)$

Mole used up of component i + 1

$$\alpha(i+1) = 621.761658 \frac{I(t)}{n(i+1)} - \frac{I}{n(i+1)} \times \sum \alpha(i) \times n(i)$$

Mole fraction of component (i+1) in exhaust:

$$N(i+1) = \frac{A(i+1) - a(i+1)}{\sum A(i) - \sum (\alpha(i)) + A(i+1) - \alpha(i+1)}$$

i = 1, ... Number of equations.

i+1 = Number of fuel components.

X (i) is mole fraction in feed of component i.

M (i) is molecular weight of component i.

n (i) is electrons/mole in electrochemical reaction for component i.

N (i) is measured molfraction in exhaust of component (i).

r is Feed rate (μliters/min).

I (t) is total cell current (amps).

ρ is density of feed (gr/cm^3).

```
      COMMON C(50,50),A(50)
      DIMENSION SN(51),X(51),BM(51),CON(10),BN(50),AI(50),AA(20),
     1VAR(25),HEAD1(10),HEAD2(10),HEAD3(10)
    2 CALL FLGERR(5,ERR)
      EOF=0.0
      NAMELIST/DEC024/CON,SN,X,BM,EOF,HEAD1,HEAD2,HEAD3/INPUT/BN,VAR,EOF
    5 READ(5,DEC024)
      IF(ERR.NE.0.0)GO TO 200
      IF(EOF.NE.0.0)GO TO 999
      P=CON(1)
      NEQ=CON(2)
      NOC=0
    7 CALL FLGERR(5,ERR)
      EOF=0
      READ(5,INPUT)
      IF(ERR.NE.0.0)GO TO 250
      IF(EOF.NE.0.0)GO TO 2
      BI=VAR(1)
      R=VAR(2)
      SUMA=0.0
      SUMAA=0.0
      SUMXM=0.0
      SUMAN=0.0
      DO 8 I=1,NEQ
      A(I)=0.0
    8 CONTINUE
      NOC=NOC+1
      K=NEQ+1
      WRITE(6,1300)HEAD1,HEAD2,HEAD3,NOC
      WRITE(6,1350)NEQ
      WRITE(6,1400)(SN(I),I=1,NEQ)
      WRITE(6,1450)K,SN(K),NEQ
      WRITE(6,1400)(X(I),I=1,NEQ)
      WRITE(6,1500)K,X(K),NEQ
      WRITE(6,1400)(BM(I),I=1,NEQ)
      WRITE(6,1550)K,BM(K),NEQ
      WRITE(6,1400)(BN(I),I=1,NEQ)
      WRITE(6,1600)BI,R,P
      DO 10 I=1,K
      SUMXM=SUMXM+(X(I)*BM(I))
   10 CONTINUE
      WRITE(6,1650)SUMXM,NEQ
      DO 15 I=1,K
      AA(I)=R*1.E 3*P*(X(I)/(SUMXM))
      SUMAA=SUMAA+AA(I)
   15 CONTINUE
      WRITE(6,1400)(AA(I),I=1,NEQ)
      WRITE(6,1700)K,AA(K),K,SUMAA,NEQ
      DO 30 I=1,NEQ
      DO 20 J=1,NEQ
      IF(I.EQ.J)GO TO 18
```

```
      C(I,J)=BN(I)*(1.0-(SN(J)/SN(K)))
      GO TO 20
   10 C(I,J)=BN(I)*(1.0-(SN(J)/SN(K)))-1.0
   20 CONTINUE
   30 CONTINUE
      DO 40 I=1,NEQ
      C(I,K)=BN(I)*SUMAA-(621.761658*(-N(I)*BI/SN(K)))-AA(I)
   40 CONTINUE
      MNT=0
      M=K
      CALL TRIANG(M,MNT)
      IF(MAT.EQ.1)GO TO 300
      K=NEQ+1
      WRITE(6,1400)(A(I),I=1,NEQ)
      DO 50 I=1,NEQ
      SUMA=SUMA+A(I)
      SUMAN=SUMAN+(A(I)*SN(I))
   50 CONTINUE
      DO 70 I=1,NEQ
      AI(I)=1.60R3*33*1.E-3*A(I)*SN(I)
   70 CONTINUE
      A(K)=621.761658*(BI/SN(K))-(1.0/SN(K))*SUMAN
      HNN=(AA(K)-A(K))/(SUMAA-SUMA-A(K))
      WRITE(6,1750)K,A(K),NEQ
      WRITE(6,1400)(AI(I),I=1,NEQ)
      WRITE(6,1800)K,HNN
      GO TO 7
  200 WRITE(6,1000)
      GO TO 2
  250 WRITE(6,1050)
      GO TO 7
  300 WRITE(6,1200)
      GO TO 2
  999 CALL EXIT
 1000 FORMAT(1H1///12X,47HINPUT ERROR IN DECO24 - SKIPPING TO NEXT DECO2
     14)
 1050 FORMAT(1H1///15X,45HINPUT ERROR IN INPUT - SKIPPING TO NEXT INPUT)
 1200 FORMAT(1H1///5X,70HERROR IN TRIANGULARIZED MATRIX OF SUBROUTINE -
     :SKIPPING TO NEXT DECO24)
 1300 FORMAT(1H1/2*X,34HOXIDATION OF MULTI-COMPONENT FUELS//13X,10A6/
     110X,10A6/10X,10A6//35X,5HCASE  ,I3)
 1350 FORMAT(/30X,19H***    INPUT    ***//10X,40HELECTRONS/MOLE IN ELECT
     1ROCHEMICAL REACTION FOR COMPONENTS 1-,I3)
 1400 FORMAT(6X,4(E14.7,3X))
 1450 FORMAT(/2X,57HELECTRONS/MOLE IN ELECTROCHEMICAL REACTION FOR COMPO
     1NENT ,I3,3H = ,E14,///20X,28HMOLEFRACTION OF COMPONENTS 1-,I3,08H I
     2N FEED)
 1500 FORMAT(/14X,25HMOLEFRACTION OF COMPONENT ,I3,11H IN FEED = ,E14,///
     122X,33HMOLECULAR WEIGHT OF COMPONENTS 1-,I3)
 1550 FORMAT(/16X,30HMOLECULAR WEIGHT OF COMPONENT ,I3,3H = ,E14,///14X,
     149HMEASURED MOLEFRACTION IN EXHAUST FOR COMPONENTS  -,I3)
 1600 FORMAT(/000021A,21HTOTAL CELL CURRENT = ,E14.7,5  AMPS//37A,
```

```
104          112HFEED RATE = ,E14,7,16H MICROLITERS/MIN//24X,18HDENSITY OF FEED
105          2= ,E14,7,7H GR/CM3)
106      1650 FORMAT(//30X,20H***     OUTPUT     ***//16X,35HAVERAGE MOLECULAR WEI          153
107          1GHT OF FEED = ,E14,7//16X,45HFEED RATE IN MICROMOLES/MIN FOR COMPO
108          2NENTS 1=,I3)
109      1700 FORMAT(/09X,42HFEED RATE IN MICROMOLES/MIN FOR COMPONENT ,I3,          153
110          13H = ,F14.7//13X,33HSUM OF FEED RATE OF COMPONENTS 1-,I3,3H = ,
111          2F14,7//23X,31HMOLES USED UP FOR COMPONENTS 1=,I3)
112      1750 FORMAT(/16X,28HMOLES USED UP FOR COMPONENT ,I3,3H = ,E14,7//20X,       153
113          137HCURRENT CONTRIBUTION OF COMPONENTS 1-,I3)
114      1800 FORMAT(/12X,36HMOLFRACTION IN EXHAUST OF COMPONENT ,I3,3H = ,          153
115          1E14,7)
116      5000 END                                                                    153
```

```
      SUBROUTINE TRIANG(M,MNT)
      COMMON C(50,50),A(50)
C     THIS SUBROUTINE SOLVES SIMULTANEOUS LINEAR EQUATIONS BY THE
C     METHOD OF TRIANGULARIZATION, THE ONE ARGUMENT M IS THE NUMBER
C     OF EQUATIONS PLUS ONE, THE COEFFICIENTS SHOULD BE PLACED IN
C     THE C ARRAY IN COMMON, THE SOLUTIONS RETURN THRU COMMON IN
C     THE A ARRAY.
C     TRIANGULARIZES MATRIX
      IF(M.LE.2)GO TO 520
      MM=M-2
      DO 510 J=1,MM
      NN=M-1
      KK=J+1
      DO 500 K=KK,NN
      XXX=C(K,J)/C(J,J)
      JJ=J
      DO 490 L=JJ,M
      C(K,L)=C(K,L)-(XXX*C(J,L))
  490 CONTINUE
  500 CONTINUE
  510 CONTINUE
C     TO MAKE DIAGONAL EQUAL ONES
  520 K=M-1
      DO 540 I=1,K
      ZZ=C(I,I)
      DO 530 J=I,M
      C(I,J)=C(I,J)/ZZ
  530 CONTINUE
  540 CONTINUE
C     CHECKS IF MATRIX IS TRIANGULARIZED
      IK=M-1
      DO 550 I=1,IK
      IF(C(I,I).NE.1.0)GO TO 770
  550 CONTINUE
C     FINDS A(1) THRU A(M-1)
  695 I=M-1
  700 K=M
      A(I)=A(I)+C(I,K)
      IF(I.EQ.M-1)GO TO 750
  725 K=K-1
      A(I)=A(I)-C(I,K)*A(K)
      IF(I.NE.K-1)GO TO 725
  750 IF(I.EQ.1)GO TO 800
      I=I-1
      GO TO 700
  770 MNT=1
  800 RETURN
      END
```

4.5 COMPUTER PROGRAM FOR CORE WEIGHT OPTIMIZATION (P.J. Chludzinski, D.C. Shah)

The optimization of the total fuel cell system depends on the geometry of the battery stack, the functions and operating conditions of the accessories and their interrelations as affected by the heat and mass transport.

Since the fuel cell battery itself has an optimum weight depending on the geometry of electrodes, the framing material, and electrode screens, it was decided to optimize the core of the battery on these bases. Assuming that the optimum battery core will also produce the optimum system, selected configurations from the sub-program would be further investigated in a detailed calculation of heat and mass balance.

To determine the minimum weight system for the battery core, exclusive of end plates, insulation, and accessories, general layout of the fuel cell shown in Figure 4.5-1 was chosen. The active area of the electrode is 2(H) inches high and L inches wide. The frames which hold the electrodes are (Y1) inches wide, the thickness of the electrolyte frame being (Y6), and the gas frames (Y5). The current from the electrode will be carried by the electrode screen and collected externally. To minimize resistance losses, the current is carried out of two ends of the electrode.

It was intended to find a relationship between geometric factors such as L, H, Y's, the polarization curve and the electrical resistivity of the electrodes, at various temperatures to minimize the battery weight for a certain power level. The weight minimizes for a certain value of H (other factors being constant) because of the relationship of the screen resistivity and screen weight. For highly conductive screens, fewer cells are needed to obtain a certain power level, but the weight of the screen is high, producing a high overall battery weight. For highly resistive screens, the weight per screen is low, but more cells are needed because of higher voltage drop per screen. In between the two extremes, the weight will minimize. A computer program was devised to calculate the specific weight of a battery under various choices of parameters. A polarization curve was chosen for octane/air at various temperatures, and Table 4.5-1 shows the polarization curve.

Table 4.5-1

Performance of Octane/Air Fuel Cell

	J (Current density) ASF						
	5	10	15	20	30	40	50
V' (IR free voltage), volts T = 150°C	.60	.52	.47	.42	.37	.32	.29
V' (IR free voltage), volts T = 180°C	.70	.64	.60	.56	.53	.50	.47
V' (IR free voltage), volts T = 204°C	.80	.73	.68	.65	.61	.57	.54

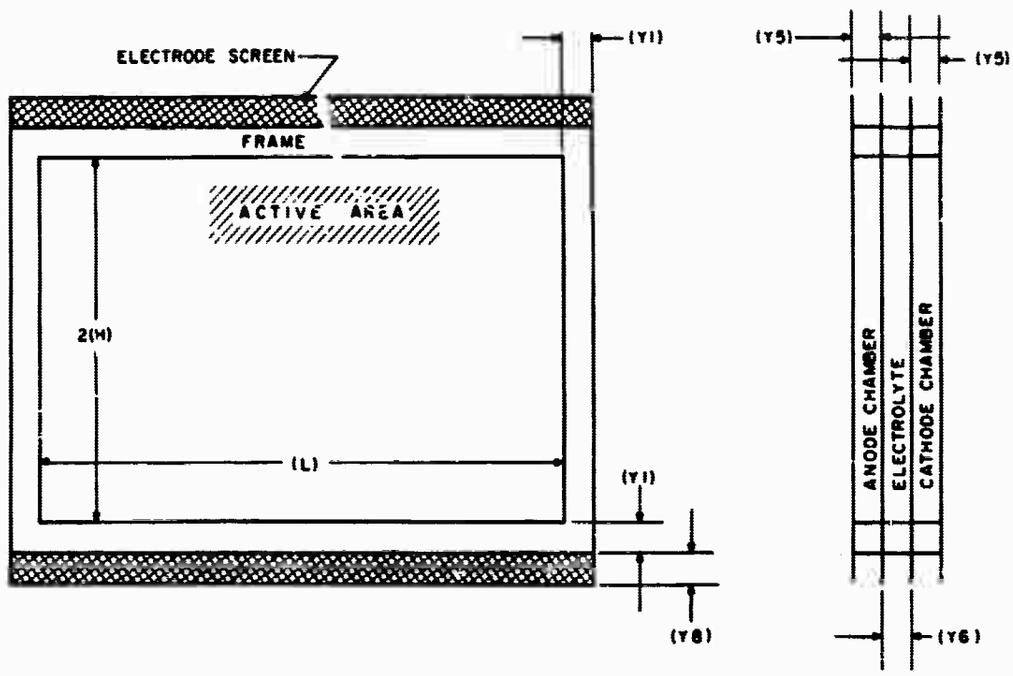

Figure 4.5-1. Layout of Cells for Core Optimization

If the geometry shown in Figure 4.5-1 is used, and the current density is assumed constant over the face of the electrode, then the voltage drop encountered by the current traversing two screens is:

$$.001738\ (2H)^2\ (\rho/t)\ (J)\quad \text{volts}$$

where: H is longest path length traversed by an electron (half the active area height in this case), inches.

ρ/t is the electrode resistivity in the direction of current flow, ohm per square

J is the current density, ASF

The voltage drop due to electrolyte resistance is:

$$.00273\ (\rho e)\ (Y6)\ (J)\quad \text{volts}$$

where: ρe is the electrolyte resistivity, ohm-cm

(Y6) is the electrolyte thickness, inch

J is current density, ASF

The cell net potential can be obtained from the iR free potential by combining the expressions in the form:

$$V = V' - .001738(2H)^2\ (\rho/t)\ (J) - .00273\ (\rho e)\ (Y6)\ (J) \qquad (1)$$

The total current, I is obtained from:

$$I = \frac{W}{V}\quad \text{amps} \qquad (2)$$

where: W is the gross battery power, watts

The current per cell is:

$$i = \frac{2(H)(L)(J)}{144}\quad \text{amps} \qquad (3)$$

where: L is the width of the electrode.

The number of cells in the stack is:

$$N = \frac{I}{i} \qquad (4)$$

The weight of the battery is the combined weight of:

a. The frames for gas and electrolyte spaces, (LB11)

b. The weight of the screens, (LB12)

c. The weight of the catalyst, (LB13)

d. The weight of the electrolyte (LB14)

$$(LB1) = (BL11) + (LB12) + (LB13) + (LB14) \tag{5}$$

The frame weight, (LB11) is:

$$(LB11) = \frac{2N(\rho 1)(Y1)}{1728} \Big((L) + 2(H) + 2(Y1)\Big) \Big(2(Y5) + (Y6)\Big) \tag{6}$$

where: N is the number of cells

$(\rho 1)$ is the density of the frame material, lb/ft^3

(Y1) is the width of the frames, inch

(Y5) is the thickness of the gas frames, inch

(Y6) is the thickness of the electrolyte frame, inch

The screen weight, (LB12) is:

$$(LB12) = \frac{4(N)}{144} \Big((L) + 2(Y1)\Big) \Big((H) + (Y1) + (Y8)\Big) (\rho 2) \tag{7}$$

where: (Y8) is the distance which the screen projects beyond the stack for bus bar connections, inch.

$(\rho 2)$ is the specific weight of the screen, lb/ft^2

The catalyst weight, (LB13), is:

$$(LB13) = \frac{4(H)(L)(\rho 3)(N)}{144} \tag{8}$$

where: $(\rho 3)$ is the average catalyst loading for anode and cathode, lb/ft^2

The electrolyte weight, (LB14), is:

$$(LB14) = \frac{2(H)(L)(Y6)(\rho 4)(N)}{1728} \tag{9}$$

where: $(\rho 4)$ is the density of the electrolyte at 70°F, lb/ft^3

The specific weight of the battery, (SWB), is:

$$(SWB) = \frac{(LB1)\ (1000)}{(W)} \quad lb/KW \tag{10}$$

For the system chosen, Figure 4.5-2 shows the relationship between tantalum expanded screen resistivity and specific weight of screen at 70°F. The change in resistivity with temperature is shown for tantalum in Figure 4.5-3, and was taken into account when the cell operating temperature was varied.

The computer input that was kept constant was:

W, gross power = 600 watts

(Y1), width of frames = 0.5 inch

(Y5), thickness of gas frames = 0.125 inch for a "back-to-back" design where one anode chamber feeds two anodes.

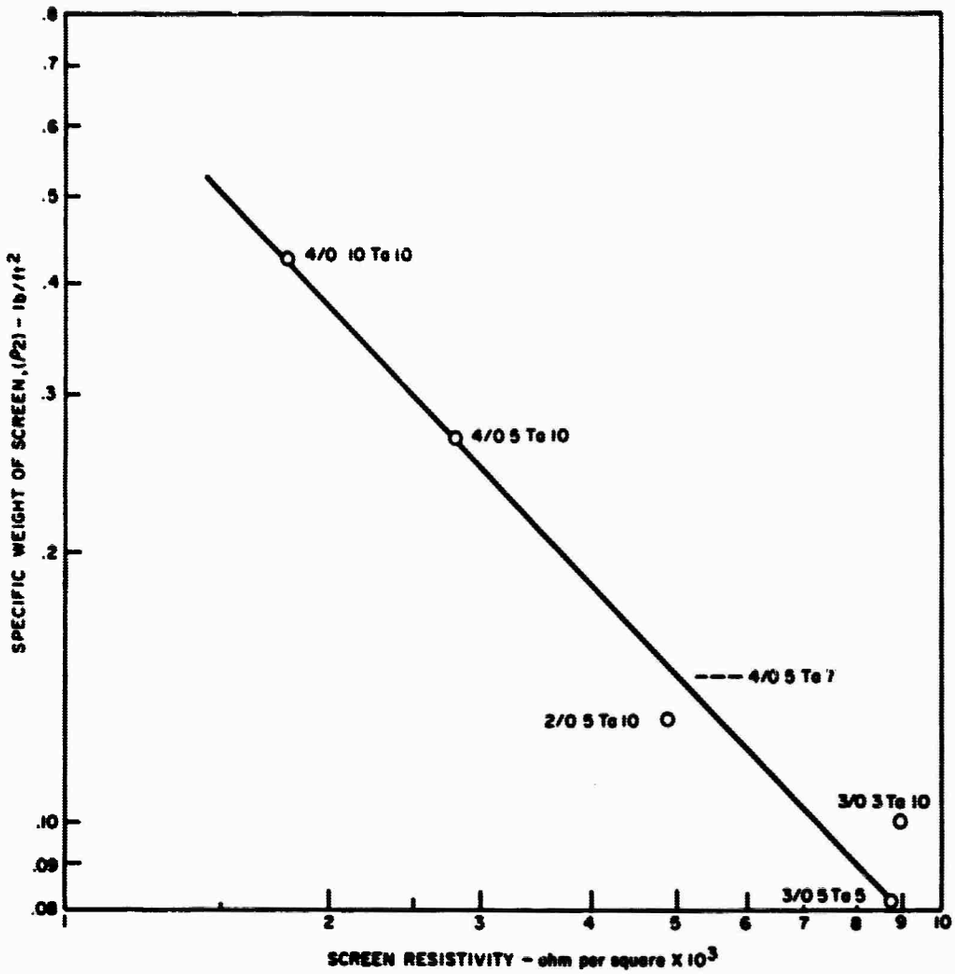

Figure 4.5-2. Measured Resistance of Tantalum Expanded Screens

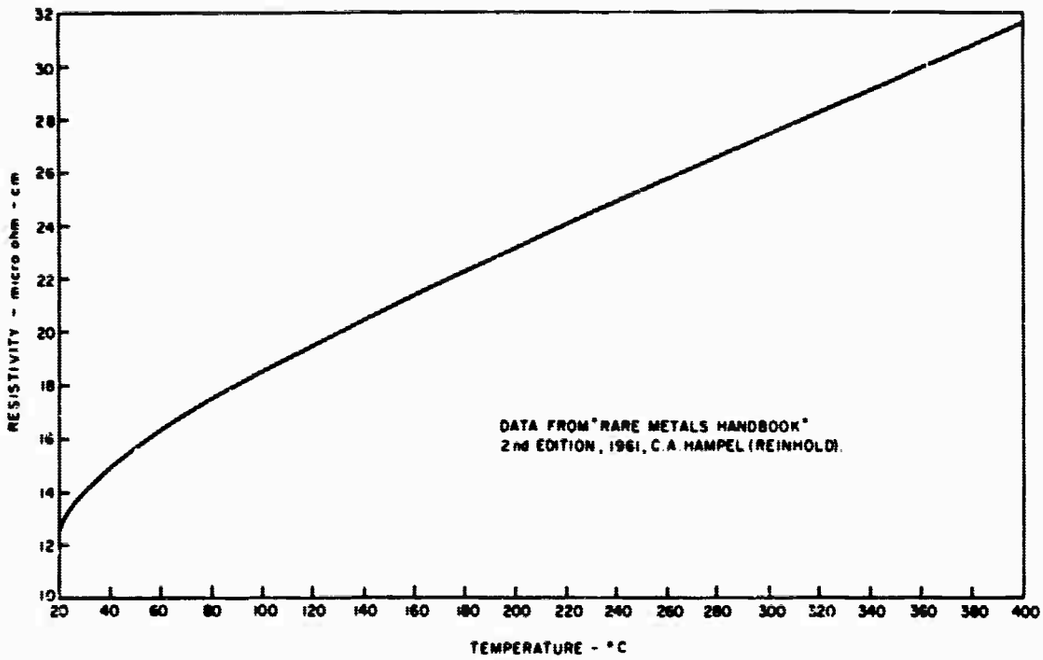

Figure 4.5-3. Resistivity of Tantalum

(ρ_1), density of frame material = 66.1 lb/ft^3. This is the density for polyphenylene oxide or polysulfone.

(ρ_3), catalyst loading = 0.1 lb/ft^2

(ρ_4), density of electrolyte at 70°F = 106 lb/ft^3

(Y8), projection of screen beyond the frames = 0.5 inch.

The computer input that was varied was:

Cell temperature, two values 150°C and 180°C.

Screen resistivity and corresponding screen specific weight, three values.

Electrolyte gap, 3 values: 1/32, 1/16 and 1/8 inch.

Current density, and corresponding .R free potential, 5 values.

Electrode height, 5 values.

Electrode width, 5 values.

The following tabulations are equations, input sheets, and the program as used on the G-E 625 computer. Sample computer output sheets are included for the actual case chosen for detailed heat and mass balances.

DECØ 30

OPTIMIZATION OF SPECIFIC WEIGHT OF DIRECT HYDROCARBON/AIR/H3PO4 FUEL CELL BATTERY

$$V = Vprime - .006952(H)^2 (RHO/T)(J) - .00273(RHO\ E)(Y6)(J)$$

$$I\ (Total) = \frac{W}{V}$$

$$I\ \ Cell) = \frac{2(J)(H)(L)}{144}$$

$$N = \frac{I\ (Total)}{I\ (Per\ Cell)}$$

$$LB1 = LB11 + LB12 + LB13 + LB14$$

$$LB11 = \frac{2N(RHO\ 1)(Y1)}{1728} \quad L + 2(H) + 2(Y1) \quad 2(Y5) + Y6$$

$$LB12 = \frac{4N}{144} \quad L + 2(Y1) \quad H + Y1 + Y8 \quad RHO\ 2$$

$$LB13 = \frac{4(H)(L)(RHO\ 3)(N)}{144}$$

$$LB14 = \frac{2(H)(L)(Y6)(RHO\ 4)(N)}{1728}$$

$$SWB = \frac{(LB1)(1000)}{W}$$

Input Values:

2(H), RHO/T, J, RHO E, Y6, L, RHO 1, Y1, Y5, Y8, RHO 3, RHO 4, W, T, RHO 2

Built in the program:

V prime - dependent on T and J

67A200279A

OPTIMIZATION OF SPECIFIC WEIGHT OF DIRECT HYDROCARBON/AIR/H_3PO_4 FUEL CELL BATTERY

If a plot is desired:

(1) Set NG=1 and fill the rest of the PLOT array appropriately where:

NC = number of curves to be plotted (maximum 5)
DELX= value of 1 inch on X-axis
XMX = maximum value of X-axis
XMN = minimum value of X-axis
INX = number of values in X-array (maximum 50)
IIX = memory increment for X-array:
1.plot every point
2.plot every second point, etc.

IND { -1 plot only symbols
0 plot a line without symbols
1 plot a line with symbols

Fill a value in for each curve. If there aren't 5 curves, put a value in all 5 places anyway.

(2) Fill the plot title in the IDENT line.

(3) Fill the axis titles in the HOLI line - 6 characters are allowed for each title - if all 6 characters are not needed, fill in spaces.

(4) All curves are plotted on the same Y-axis - the Y-axis scale is set up by the computer.

(5) On $ TAPE card (after $ LIMITS card), make sure there's a D in Column 21.

If no plot is desired:

(1) Set NG=0 and fill the rest of the PLOT array with zeros.

(2) The HOLI and IDENT cards may be completely excluded.

(3) On $ TAPE card (after $ LIMITS card), make sure there's an R in Column 21.

67A200279B

DECØ 30

OPTIMIZATION OF SPECIFIC WEIGHT OF DIRECT HYDROCARBON/AIR/H3PO4 FUEL CELL BATTERY

625 INPUT SHEET

```
Col. 2                                                                  Col. 70
  $DECØ30,
  IDENT=60H
                        graph title

Col. 2   Col. 10   Col. 16                          Col. 52
  HØLI 42H
                X-axis        Y-axis
Col. 2
  VAL=                                        Col. 2
                                                PLØT=
        ,  W                                          |
        ,  Y1                                   ,     | NG
        ,  Y5                                   ,     | NC
        ,  RHO1                                 ,     | DELX
        ,  Y8                                   ,     | XMX
        ,  RHO3                                 ,     | XMN
        ,  RHO4                                 ,     | INX
        ,  T                                    ,     | IIX
        ,  RHOE                                 ,     | IND (1)
        ,  MIN. L                               ,     | IND (2)
        ,  MAX. L                               ,     | IND (3)
        ,  DELTA L                              ,     | IND (4)
        ,  MIN. Y6                              ,     | IND (5)
        ,  MAX. Y6                          0   ,     | MMI
        ,  DELTA Y6                        60   ,     | NIDENT
        ,  MIN. J                           0   ,     | YMAX (1)
        ,  MAX. J                           0   ,     | YMIN (1)
        ,  DELTA J
        ,  MIN. 2(H)
        ,  MAX. 2(H)
        ,  DELTA 2(H)
        ,  Number of RHØ/T, P2 combinations given
        ,  RHØ/T  } Repeat as many
        ,  P2     } times as needed
        ,
        ,                 At end of each case:   Col. 2
        ,                                          $
        ,                 At end of all cases:   Col. 2
                                                   $DECØ30,EØF=1$
```

6.A200279C

#1254 1 11-14-66

```
      DIMENSION HOLI(7),JCHARI(6),YMAX(6),YMIN(6),IND(6),IDENT(10),
     1PLOT(20),VAL(50),YY1(50),YY2(50),YY3(50),YY4(50),YY5(50),X(50),
     2POT(5),P2(5),BUF(692),YY6(50)
      ISIZ=692
      ICDE=7
      CALL PLOTS(BUF,ISIZ,ICDE)
    9 CALL FLGERR(5,ERR)
      EOF=0.0
      NAMELIST/DECO30/PLOT,VAL,EOF,HOLI,IDENT
      READ(5,DECO30)
      IF(ERR.NE.0.0)GO TO 888
      IF(EOF.NE.0.0)GO TO 999
      NG=PLOT(1)
      NC=PLOT(2)
      DELX=PLOT(3)
      XMX=PLOT(4)
      XMN=PLOT(5)
      INX=PLOT(6)
      IIX=PLOT(7)
      IND(1)=PLOT(8)
      IND(2)=PLOT(9)
      IND(3)=PLOT(10)
      IND(4)=PLOT(11)
      IND(5)=PLOT(12)
      MMI=PLOT(13)
      NIDENT=PLOT(14)
      YMAX(1)=PLOT(15)
      YMIN(1)=PLOT(16)
      CALL MAH(BITS)
      IF(YMAX(1).EQ.0.0)YMAX(1)=BITS
      IF(YMIN(1).EQ.0.0)YMIN(1)=BITS
      X=VAL(1)
      Y1=VAL(2)
      Y5=VAL(3)
      P1=VAL(4)
      Y8=VAL(5)
      P3=VAL(6)
      P4=VAL(7)
      TT=VAL(8)
      FFE=VAL(9)
      ALMIN=VAL(10)
      ALMAX=VAL(11)
      DELAL=VAL(12)
      Y6MIN=VAL(13)
      Y6MAX=VAL(14)
      Y6MULT=VAL(15)
      AJMIN=VAL(16)
      AJMAX=VAL(17)
      DELAJ=VAL(18)
      P2MIN=VAL(19)
      P2MAX=VAL(20)
```

#1254 1 11-14-66

```
      DELH2=VAL(21)
      NL1=VAL(22)
      III=23
      DO 10 II=1,NL1
      PDT(II)=VAL(III)
      III=III+1
      P2(II)=VAL(III)
      III=III+1
   10 CONTINUE
      I=1
      INC=0
   70 PDTT=PDT(I)
      P22=P2(I)
      Y6=Y6MIN
   80 AJ=AJMIN
   85 IF(II.EQ.180.0)GO TO 84
      IF(II.EQ.205.0)GO TO 86
      IF(AJ.EQ.5.0)VP=.60
      IF(AJ.EQ.10.0)VP=.52
      IF(AJ.EQ.15.0)VP=.47
      IF(AJ.EQ.20.0)VP=.42
      IF(AJ.EQ.30.0)VP=.37
      IF(AJ.EQ.40.0)VP=.32
      IF(AJ.EQ.50.0)VP=.29
      GO TO 89
   84 IF(AJ.EQ.5.0)VP=.70
      IF(AJ.EQ.10.0)VP=.64
      IF(AJ.EQ.15.0)VP=.60
      IF(AJ.EQ.20.0)VP=.56
      IF(AJ.EQ.30.0)VP=.53
      IF(AJ.EQ.40.0)VP=.50
      IF(AJ.EQ.50.0)VP=.47
      IF(AJ.EQ.60.0)VP=.445
      IF(AJ.EQ.70.0)VP=.422
      IF(AJ.EQ.80.0)VP=.401
      GO TO 89
   86 IF(AJ.EQ.5.0)VP=.80
      IF(AJ.EQ.10.0)VP=.73
      IF(AJ.EQ.15.0)VP=.68
      IF(AJ.EQ.20.0)VP=.65
      IF(AJ.EQ.30.0)VP=.61
      IF(AJ.EQ.40.0)VP=.57
      IF(AJ.EQ.50.0)VP=.54
   89 INC=INC+1
      WRITE(6,800)INC
      WRITE(6,810)W,Y1,P1,DEF,AJ,Y5,P22,PDTT,II,Y6,P3,VP,Y8,P4
   90 H2=H2MIN
      L=1
   95 H=H2/2.0
      X(L)=H2
      AL=ALMIN
      M=1
```

#1254 1 11-14-86

```
  100 V=VP-.000869*H**2*PUTI*AJ-.00273*PFE*YA*AJ
      AI=W/V
      BI=(2.0*AJ*H*AL)/144.0
      ANUM=AI/BI
      ALB11=((2.0*ANUM*P1*Y1)/1728.0)*(AL+H2+2.0*Y1)*(2.0*Y5+Y6)
      ALB12=((4.0*ANUM)/144.0)*(AL+2.0*Y1)*(H+Y1+Y8)*P22
      ALB13=(4.0*H*AL*P3*ANUM)/144.0
      ALB14=(H2*AL*YA*P4*ANUM)/1728.0
      ALB1=ALB11+ALB12+ALB13+ALB14
      SWB=(ALB1*100.0)/W
      RAT1=ALB11/ALB1
      RAT2=ALB12/ALB1
      RAT3=ALB13/ALB1
      RAT4=ALB14/ALB1
      WRITE(6,820)AL,H2,V,AI,BI,ANUM,ALB1,ALB11,ALB12,ALB13,ALB14,
     1SWB,RAT1,RAT2,RAT3,RAT4
      IF(M.EQ.1)GO TO 1101
      IF(M.EQ.2)GO TO 1102
      IF(M.EQ.3)GO TO 1103
      IF(M.EQ.4)GO TO 1104
      IF(M.EQ.5)GO TO 1105
      IF(M.EQ.6)GO TO 1106
 1101 YY1(L)=SWB
      GO TO 102
 1102 YY2(L)=SWB
      GO TO 102
 1103 YY3(L)=SWB
      GO TO 102
 1104 YY4(L)=SWB
      GO TO 102
 1105 YY5(L)=SWB
      GO TO 102
 1106 YY6(L)=SWB
  102 IF(AL.EQ.ALMAX)GO TO 105
      AL=AL+DELAL
      M=M+1
      GO TO 100
  105 IF(H2.EQ.H2MAX)GO TO 107
      H2=H2+DELH2
      L=L+1
      GO TO 95
  107 IF(NG.EQ.0)GO TO 109
      CALL CPLOT(NG,NC,HOLT,JCHARI,DELX,YLENGT,XMX,XMN,YMAX,YMIN,
     1INX,IIX,X,YY1,YY2,YY3,YY4,YY5,YY6,IND,MMI,IERR,IDENT,NIDENT)
      IF(IERR.EQ.1)WRITE(6,910)NG
      IF(IERR.EQ.2)WRITE(6,920)IIX
      IF(IERR.EQ.3)WRITE(6,930)INX
  109 IF(AJ.EQ.AJMAX)GO TO 110
      AJ=AJ+DELAJ
      GO TO 82
  110 IF(Y6.EQ.Y6MAX)GO TO 115
      Y6=Y6+Y6MULT
```

```
156          GO TO 80
157      115 I=I+1
158          IF(I-1.EQ.N)GO TO 2
159          GO TO 70
160      500 WRITE(6,1000)
161          GO TO 2
162      900 CALL PLOTP
163          CALL EXIT
164      800 FORMAT(1H1///20X,64HSPECIFIED AFCSHI OF DIRECT HYDROCARBON/AIR/HSPO
165         1 FUEL CELL BATTERY//36X,5HCASE ,I3//)
166      810 FORMAT(14X,3HW= ,E14.7,5X,4HY1= ,E14.7,5X,7HRHO 1= ,E14.7,
167         15X,7HRHO E= ,E14.7//14X,3HJ= ,E14.7,5X,4HY5= ,E14.7,5X,
168         27HRHO 2= ,E14.7,5X,7HRHO/I= ,E14.7//14X,3HI= ,E14.7,5X,
169         34HY6= ,E14.7,5X,7HRHO 3= ,E14.7,3X,9HV PRIME= ,E14.7/36X,4HYR= ,
170         4E14.7,5X,7HRHO 4= ,E14.7)
171      820 FORMAT(//5HA,3HL= ,E14.7,10X,6H2(H)= ,E14.7//8X,3HV= ,E14.7,
172         15X,10HI(UTIL)= ,E14.7,5X,13HI(PER CELL)= ,E14.7,12X,3HW= ,
173         2E14.7//8X,5HL-R1= ,E14.7,9X,6HL-R11= ,E14.7,12X,6HLR12= ,
174         3E14.7,9X,6HLR15= ,E14.7/8X,6HLR14= ,E14.7,11X,5HSWH= ,E14.7,
175         4-X,10HLR11/ R1= ,E14.7,5X,10HLR12/ R1= ,E14.7/30X,10HLR13/ R1= ,
176         5E14.7,8X,10HLR14/LR1= ,E14.7//)
177      910 FORMAT(1H1,11A,15HPLOT ERROR  NO= ,I3)
178      920 FORMAT(1H1,10A,15HPLOT ERROR  IX= ,I3)
179      930 FORMAT(1H1,11A,15HPLOT ERROR  NX= ,I3)
180     1000 FORMAT(1H1/15A,55HINPUT ERROR - SKIPPING TO NEXT CASE)
181          END
```

SPECIFIC WEIGHT OF DIRECT HYDROCARBON/AIR/H3PO FUEL CELL BATTERY

CASE 23

A=	0.6000000E 03	Y1=	0.5000000E 00	RHO 1=	0.6610000E 02	RHO E=	0.1650000E 01
D=	0.3000000E 02	Y5=	0.1250000E 00	RHO 2=	0.1300000E 00	RHO/T=	0.8300000E-02
T=	0.1500000E 03	Y6=	0.4250000E-01	RHO 3=	0.1000000E 00	VP=	0.3700000E 03
		Y8=	0.5000000E 00	RHO 4=	0.1060000E 03		

L= 0.5000000E 01 W= 0.4000000E 01

V=	0.3506648E 00	I(TOTAL)=	0.1668220E 04	I(PER CELL)=	0.4166667E 01	N=	0.4003728E 03
LB1=	0.1197055E 03	LB11=	0.4785996E 02	LB12=	0.2602423E 02	LB13=	0.1112147E 02
LB14=	0.3069988E 02	SWB=	0.1928426E 03	LB11/LB1=	0.4136358E 00	LB12/LB1=	0.2249178E 00
		LB13/LB1=	0.9611871E-01	LB14/LB1=	0.2853277E 00		

L= 0.1000000E 02 W= 0.4000000E 01

V=	0.3506648E 00	I(TOTAL)=	0.1668220E 04	I(PER CELL)=	0.8333333E 01	N=	0.2001864E 03
LB1=	0.1015719E 03	LB11=	0.3589497E 02	LB12=	0.2385555E 02	LB13=	0.1112147E 02
LB14=	0.3069988E 02	SWB=	0.1692864E 03	LB11/LB1=	0.3533948E 00	LB12/LB1=	0.2346637E 00
		LB13/LB1=	0.1094936E 00	LB14/LB1=	0.3022479E 00		

L= 0.1500000E 02 W= 0.4000000E 01

V=	0.3506648E 00	I(TOTAL)=	0.1668220E 04	I(PER CELL)=	0.1250000E 02	N=	0.1334576E 03
LB1=	0.9868064E 02	LB11=	0.3190664E 02	LB12=	0.2313265E 02	LB13=	0.1112147E 02
LB14=	0.3069988E 02	SWB=	0.1614344E 03	LB11/LB1=	0.3294077E 00	LB12/LB1=	0.2388241E 00
		LB13/LB1=	0.1148193E 00	LB14/LB1=	0.3169490E 00		

L= 0.2000000E 02 W= 0.4000000E 01

V=	0.3506648E 00	I(TOTAL)=	0.1668220E 04	I(PER CELL)=	0.1666667E 02	N=	0.1000932E 03
LB1=	0.9450503E 02	LB11=	0.2991247E 02	LB12=	0.2277120E 02	LB13=	0.1112147E 02
LB14=	0.3069988E 02	SWB=	0.1575084E 03	LB11/LB1=	0.3165173E 00	LB12/LB1=	0.2409523E 00
		LB13/LB1=	0.1176812E 00	LB14/LB1=	0.3248492E 00		

L= 0.2500000E 02 W= 0.4000000E 01

V=	0.3506648E 00	I(TOTAL)=	0.1668220E 04	I(PER CELL)=	0.2083333E 02	N=	0.8007456E 02
LB1=	0.9389166E 02	LB11=	0.2871597E 02	LB12=	0.2255433E 02	LB13=	0.1112147E 02
LB14=	0.3069988E 02	SWB=	0.1551592E 03	LB11/LB1=	0.3084699E 00	LB12/LB1=	0.2422809E 00
		LB13/LB1=	0.1194674E 00	LB14/LB1=	0.3297812E 00		

L= 0.5000000E 01 W= 0.6000000E 01

V=	0.3585829E 00	I(TOTAL)=	0.1673253E 04	I(PER CELL)=	0.6250000E 01	N=	0.2677205E 03
LB1=	0.1095535E 03	LB11=	0.3440349E 02	LB12=	0.2320245E 02	LB13=	0.1115502E 02
LB14=	0.3079251E 02	SWB=	0.1725891E 03	LB11/LB1=	0.3708546E 00	LB12/LB1=	0.2240625E 00
		LB13/LB1=	0.1077223E 00	LB14/LB1=	0.2973586E 00		

L= 0.1000000E 02 W= 0.6000000E 01

```
V=   0.3585829E 00    I( OTAL)=  0.1673253E 04    I(PER CELL)=  0.1250000E 02          N=  0.1538603E 03
LH1=  0.9041091E 02        LB11=  0.2720247E 02          LB12=  0.2126891E 02       LB13=  0.1115502E 02
LB14=  0.3079251E 02        SWB=  0.1506982E 03     LB11/LB1=  0.3008493E 00   LB12/LB1=  0.2352263E 00
                       LB13/LB1=  0.1233705E 00     LB14/LB1=  0.3405539E 00

                              L=  0.1500000E 02          H=  0.6000000E 01

V=   0.3585829E 00    I(TOTAL)=  0.1673253E 04    I(PER CELL)=  0.1875000E 02          N=  0.8924018E 02
LH1=  0.9604072E 02        LB11=  0.2346880E 02          LB12=  0.2062440E 02       LB13=  0.1115502E 02
LB14=  0.3079251E 02        SWB=  0.1434012E 03     LB11/LB1=  0.2727638E 00   LB12/LB1=  0.2397051E 00
                       LB13/LB1=  0.1296482E 00     LB14/LB1=  0.3578830E 00

                              L=  0.2000000E 02          H=  0.6000000E 01

V=   0.3585829E 00    I(TOTAL)=  0.1673253E 04    I(PER CELL)=  0.2500000E 02          N=  0.6693013E 02
LH1=  0.9359163E 02        LB11=  0.2140176E 02          LB12=  0.2030214E 02       LB13=  0.1115502E 02
LB14=  0.3079251E 02        SWB=  0.1397527E 03     LB11/LB1=  0.2576212E 00   LB12/LB1=  0.2421198E 00
                       LB13/LB1=  0.1330329E 00     LB14/LB1=  0.3672261E 00

                              L=  0.2500000E 02          H=  0.6000000E 01

V=   0.3585829E 00    I(TOTAL)=  0.1673253E 04    I(PER CELL)=  0.3125000E 02          N=  0.5354411E 02
LH1=  0.9253818E 02        LB11=  0.2048186E 02          LB12=  0.2018879E 02       LB13=  0.1115502E 02
LB14=  0.3079251E 02        SWB=  0.1375636E 03     LB11/LB1=  0.2481[illegible]E 00   LB12/LB1=  0.2436301E 00
                       LB13/LB1=  0.1351498E 00     LB14/LB1=  0.[illegible]30699E 00

                              L=  0.5000000E 01          H=  0.8000000E 01

V=   0.3570882E 00    I(TOTAL)=  0.1680351E 04    I(PER CELL)=  0.8333333E 01          N=  0.2016421E 03
LH1=  0.9771563E 02        LB11=  0.3374559E 02          LB12=  0.2164457E 02       LB13=  0.1120234E 02
LB14=  0.3092313E 02        SWB=  0.1628594E 03     LB11/LB1=  0.3453449E 00   LB12/LB1=  0.2235524E 00
                       LB13/LB1=  0.1146423E 00     LB14/LB1=  0.3164604E 00

                              L=  0.1000000E 02          H=  0.8000000E 01

V=   0.3570882E 00    I(TOTAL)=  0.1680351E 04    I(PER CELL)=  0.[illegible]66667E 02          N=  0.1008211E 03
LH1=  0.9548445E 02        LB11=  0.2289880E 02          LB12=  0.2[illegible]02419E 02       LB13=  0.1120234E 02
LB14=  0.3092313E 02        SWB=  0.1417474E 03     LB11/LB1=  0.2692441E 00   LB12/LB1=  0.2354444E 00
                       LB13/LB1=  0.1317172E 00     LB14/LB1=  0.3635943E 00

                              L=  0.1500000E 02          H=  0.8[illegible]00E 01

V=   0.3570882E 00    I(TOTAL)=  0.1680351E 04    I(PER CELL)=  0.[illegible]00000E 02          N=  0.6721405E 02
LH1=  0.9482606E 02        LB11=  0.1928620E 02          LB12=  0.1941739E 02       LB13=  0.1120234E 02
LB14=  0.3092313E 02        SWB=  0.1347101E 03     LB11/LB1=  0.2385765E 00   LB12/LB1=  0.2402369E 00
                       LB13/LB1=  0.1385981E 00     LB14/LB1=  0.3825836E 00

                              L=  0.2000000E 02          H=  0.8000000E 01

V=   0.3570882E 00    I(TOTAL)=  0.1680351E 04    [illegible]PER CELL)=  0.3333333E 02          N=  0.5041054E 02
LH1=  0.9371486E 02        LB11=  0.1767540E 02          LB12=  0.1911399E 02       LB13=  0.1120234E 02
LB14=  0.3092313E 02        SWB=  0.1311914E 03     LB11/LB1=  0.222[illegible]E 00   LB12/LB1=  0.2428257E 00
                       LB13/LB1=  0.1423155E 00     LB14/LB1=  0.392[illegible]99E 00
```

```
                    L=  0.2500000E 02          W=  0.8000000E 01

V=   0.3570682E 00   I(TOTAL)=  0.1680351E 04   I(PER CELL)=  0.4166667E 02      N=  0.4032843E 02
LB1=  0.7744014E 02      LB11=  0.1639072E 02        LB12=  0.1893196E 02     LB13=  0.1120234E 02
LB14=  0.3002513E 02      SWB=  0.1290802E 03   LB11/LB1=  0.2116347E 00 LB12/LB1=  0.2444469E 00
                     LB13/LB1=  0.1446431E 00   LB14/LB1=  0.3992753E 00

                    L=  0.5000000E 01          W=  0.1000000E 02

V=   0.3551208E 00   I(TOTAL)=  0.1689566E 04   I(PER CELL)=  0.1041667E 02      N=  0.1621983E 03
LB1=  0.9446457E 02      LB11=  0.3102231E 02        LB12=  0.2108578E 02     LB13=  0.1126377E 02
LB14=  0.3109271E 02      SWB=  0.1574410E 03   LB11/LB1=  0.3284015E 00 LB12/LB1=  0.2232137E 00
                     LB13/LB1=  0.1192381E 00   LB14/LB1=  0.3291468E 00

                    L=  0.1000000E 02          W=  0.1000000E 02

V=   0.3551208E 00   I(TOTAL)=  0.1689566E 04   I(PER CELL)=  0.2083333E 02      N=  0.8109917E 02
LB1=  0.8204350E 02      LB11=  0.2035839E 02        LB12=  0.1932863E 02     LB13=  0.1126377E 02
LB14=  0.3109271E 02      SWB=  0.1367392E 03   LB11/LB1=  0.2481414E 00 LB12/LB1=  0.2355901E 00
                     LB13/LB1=  0.1372902E 00   LB14/LB1=  0.3789783E 00

                    L=  0.1500000E 02          W=  0.1000000E 02

V=   0.3551208E 00   I(TOTAL)=  0.1689566E 04   I(PER CELL)=  0.3125000E 02      N=  0.5406611E 02
LB1=  0.7700315E 02      LB11=  0.1680375E 02        LB12=  0.1874292E 02     LB13=  0.1126377E 02
LB14=  0.3109271E 02      SWB=  0.1298386E 03   LB11/LB1=  0.2157085E 00 LB12/LB1=  0.2405926E 00
                     LB13/LB1=  0.1445869E 00   LB14/LB1=  0.3991200E 00

                    L=  0.2000000E 02          W=  0.1000000E 02

V=   0.3551208E 00   I(TOTAL)=  0.1689566E 04   I(PER CELL)=  0.4166667E 02      N=  0.4054958E 02
LB1=  0.7583297E 02      LB11=  0.1502643E 02        LB12=  0.1845000E 02     LB13=  0.1126377E 02
LB14=  0.3109271E 02      SWB=  0.1263883E 03   LB11/LB1=  0.1981517E 00 LB12/LB1=  0.2432987E 00
                     LB13/LB1=  0.1485340E 00   LB14/LB1=  0.4100157E 00

                    L=  0.2500000E 02          W=  0.1000000E 02

V=   0.3551208E 00   I(TOTAL)=  0.1689566E 04   I(PER CELL)=  0.5208333E 02      N=  0.3243967E 02
LB1=  0.7459086E 02      LB11=  0.1396004E 02        LB12=  0.1827435E 02     LB13=  0.1126377E 02
LB14=  0.3109271E 02      SWB=  0.1243181E 03   LB11/LB1=  0.1871548E 00 LB12/LB1=  0.2449944E 00
                     LB13/LB1=  0.1510074E 00   LB14/LB1=  0.4168434E 00

                    L=  0.5000000E 01          W=  0.1200000E 02

V=   0.3527406E 00   I(TOTAL)=  0.1700967E 04   I(PER CELL)=  0.1250000E 02      N=  0.1360773E 03
LB1=  0.9256034E 02      LB11=  0.2927966E 02        LB12=  0.2063840E 02     LB13=  0.1133978E 02
LB14=  0.3130251E 02      SWB=  0.1542672E 03   LB11/LB1=  0.3163385E 00 LB12/LB1=  0.2229723E 00
                     LB13/LB1=  0.1225123E 00   LB14/LB1=  0.3381849E 00

                    L=  0.1000000E 02          W=  0.1200000E 02

V=   0.3527406E 00   I(TOTAL)=  0.1700967E 04   I(PER CELL)=  0.2500000E 02      N=  0.6803867E 02
```

Case 23

```
LB1=   0.5026727E 02        LB11=   0.1870645E 02        LB12=   0.1891853E 02        LB13=   0.1133978E 02
LB14=  0.3130251E 02        SWB=    0.1337786E 03        LB11/LB1=  0.2358520E 00    LB12/LB1=  0.2356942E 00
                         LB13/LB1=  0.1412752E 00        LB14/LB1=  0.3899745E 00

                                L=   0.1500000E 02          W=   0.1200000E 02

V=     0.3527406E 00     I(TOTAL)=  0.1700967E 04    I(PER CELL)=  0.3750000E 02        N=   0.4535911E 02
LB1=   0.7416957E 02        LB11=   0.1518205E 02        LB12=   0.1834524E 02        LB13=   0.1133978E 02
LB14=  0.3130251E 02        SWB=    0.1269493E 03        LB11/LB1=  0.1993198E 00    LB12/LB1=  0.2408474E 00
                         LB13/LB1=  0.1488754E 00        LB14/LB1=  0.4189582E 00

                                L=   0.2000000E 02          W=   0.1200000E 02

V=     0.3527406E 00     I(TOTAL)=  0.1700967E 04    I(PER CELL)=  0.5000000E 02        N=   0.3401933E 02
LB1=   0.7412073E 02        LB11=   0.1341984E 02        LB12=   0.1805840E 02        LB13=   0.1133978E 02
LB14=  0.3130251E 02        SWB=    0.1235345E 03        LB11/LB1=  0.1810539E 00    LB12/LB1=  0.2436376E 00
                         LB13/LB1=  0.1529906E 00        LB14/LB1=  0.4223179E 00

                                L=   0.2500000E 02          W=   0.1200000E 02

V=     0.3527406E 00     I(TOTAL)=  0.1700967E 04    I(PER CELL)=  0.6250000E 02        N=   0.2721547E 02
LB1=   0.7289142E 02        LB11=   0.1236252E 02        LB12=   0.1788661E 02        LB13=   0.1133978E 02
LB14=  0.3130251E 02        SWB=    0.1214857E 03        LB11/LB1=  0.1696019E 00    LB12/LB1=  0.2453870E 00
                         LB13/LB1=  0.1555708E 00        LB14/LB1=  0.4294402E 00
```

4.6 DEFINITION OF SCREEN RESISTIVITY (OHM PER SQUARE) (P.J. Chludzinski, D.C. Shah)

"Ohm per square" is a conventional name for specific resistivity of objects whose geometries are complicated, with the result that resistance is difficult to predict from geometry and resistivity. For instance, take the case of a metal screen carrying current along its strands:

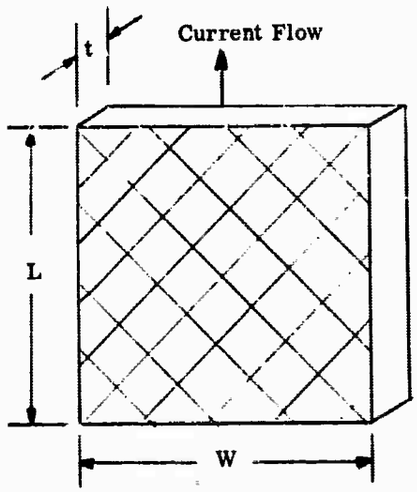

The resistance R, will be related to the metal resistivity, ρ, by:

$$R = \frac{\rho L}{Wt}$$

where t is a thickness parameter which accounts for the complication in geometry due to the strands in the screen. The parameter t is not the actual thickness of the screen. The parameter $\left(\frac{\rho}{t}\right)$ is factored out of the expression for resistance, and called:

$$\left(\frac{\rho}{t}\right) \quad \frac{\text{ohm-cm}}{\text{cm-thick}} \quad \text{or "ohm per square"}$$

The parameter $\left(\frac{\rho}{t}\right)$ is assigned as a specific resistivity of a particular screen geometry and is useful in predicting the resistance of any size rectangular screen, once (ρ/t) has been experimentally measured on one specific size. Notice that if an actual square (L = W) is considered, then the resistance $R = \left(\frac{\rho}{t}\right)$ remains constant regardless of the magnitude of L (hence the term "ohm per square").

4.7 DETAILED EQUATIONS FOR HEAT, MASS, AND ENERGY BALANCES, WEIGHT AND PARASITIC POWER (P.J. Chludzinski, D.C. Shah)

This set of equations is the continuation of optimization of the fuel cell system from Appendix 4.5. The system is divided into four different stations. The heat and mass balances are calculated separately for each station. The optimum values obtained from the previous program (Appendix 4.5) were fed to this set of equations, assuming that an optimum fuel cell stack would produce a correspondingly optimum system.

To obtain consistency in units each flow rate is presented as gram moles per hour. Heat units are in K Cal/hr and °C unless specified. Pressure is given in mm Hg (absolute), and percent composition as mole fraction.

4.7.1 Explanation for Notation

(E)	Electrolyte flow rate (gm mole/hr)	
(X)	Mole fraction H_2O	
(T)	Temperature (°C)	
(P)	Pressure (mm Hg absolute)	
(D)	O_2 flow rate (gm mole/hr) or air flow	
(G)	N_2 flow rate (gm mole/hr)	
(B)	H_2O (gm mole/hr)	(v) = vapor
		(l) = liquid
(F)	Fuel flow (gm mole/hr)	(v) = vapor
		(l) = liquid
(K)	CO_2 flow (gm mole/hr)	

Subscripts refer to Station No., Stream No., and inlet or outlet condition, respectively. For example:

(F132) Fuel flow rate in (gm mole/hr) at Station No. one, Stream No. three at the outlet.

4.7.2 Optimum System Values

The following optimum values were obtained for the Hydrocarbon/Air fuel cell system from Appendix 4.5:

(T100)	Temperature of system (°C)
(V)	Voltage per cell (volts)
2(H)	Height of the electrode (inch)
(L)	Length of the electrode (inch)

(ρ/t)	Screen resistivity (ohm per square)
(J)	Current density (amps per square foot)
(N)	Number of cells
(W)	Gross power (watt)
(ρ 2)	Weight of screen (lb/sq ft)
(I)	Total current (amp)
(i)	Current per cell (amp)
(Y1)	Width of frame (inch)
(Y2)	Air gap (inch)
(Y3)	Insulation thickness (inch)
(Y4)	Electrode thickness (inch)
(Y5)	Gas frame thickness (inch)
(Y6)	Electrolyte gap (inch)
(Y8)	Projected screen height from battery for bus bar connections (inch)
(M1)	Length of fuel cell stack (inch)
(M2)	Thickness of end plate (inch)
(T_a)	Ambient temperature (°F)
(T 101)	Temperature of insulation surface (°C)
(LB1)	Total weight of core (lb)
(LB11)	Weight of frames (lb)
(LB12)	Weight of screens (lb)
(LB13)	Weight of catalyst (lb)
(LB14)	Weight of electrolyte in Core (lb)
(ρ 1)	Density of frame material (lb/ft^3)
(ρ 3)	Average catalyst loading (lb/ft^2)
(ρ 4)	Density of electrolyte at 70°F (lb/ft^3)
(SWB)	Specific weight of the core (lb/KW)
(ρ e)	Electrical resistivity of electrolyte (ohm-cm)
(N)	Number of carbon atoms

4.7.3 Calculation Procedure

4.7.3.1 Fuel Cells (See Figure 4.7-1.)

A. Anode Mass Balance

$$\text{Theoretical fuel flow} = \frac{3600\ (I)}{96500\ \left(6\ (n) + 2\right)}$$

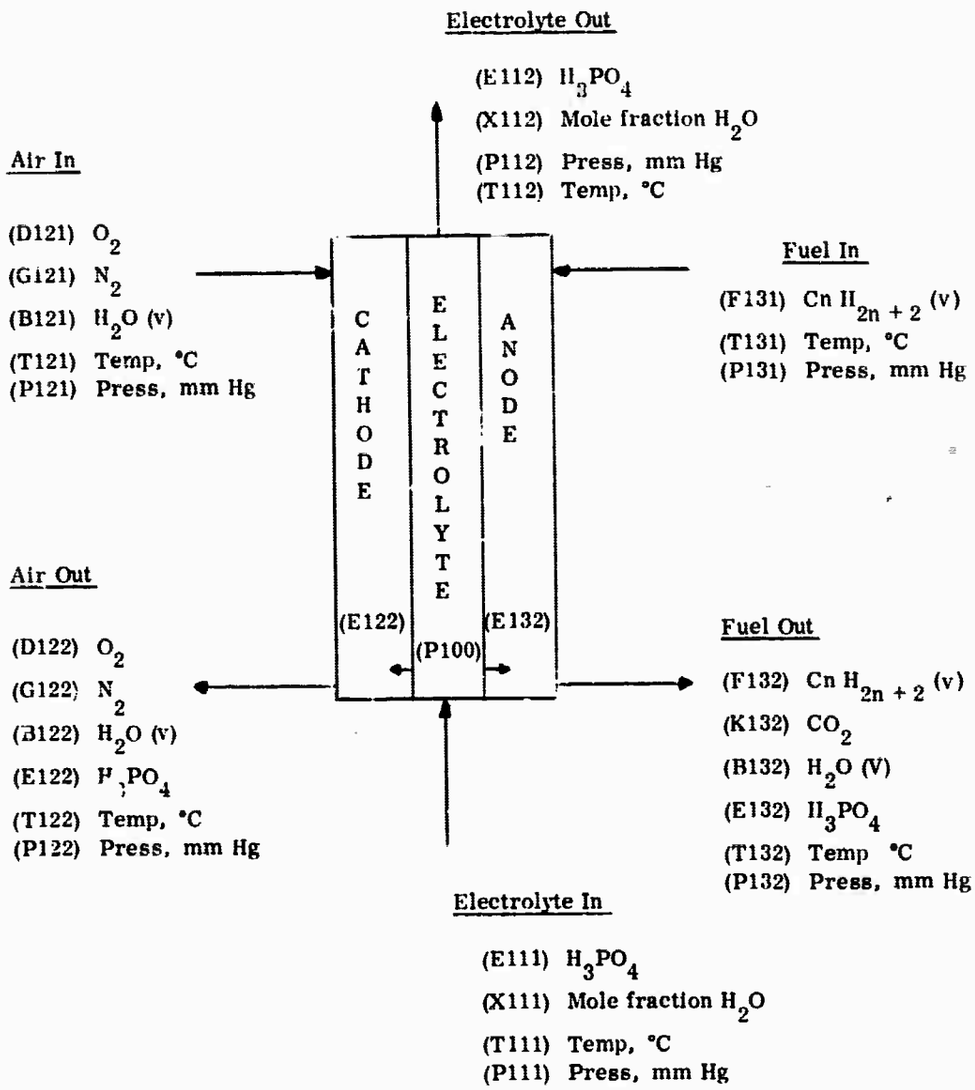

Figure 4.7-1. Process Streams for Heat and Mass Balance on Fuel Cells

$$(F131) = (SF)\left(\frac{3600\ (I)}{96500\ \left(6\ (n) + 2\right)}\right) \qquad (1)$$

(F131) Fuel feed rate (gm mole/hr)

(F132) Fuel exhaust (gm mole/hr)

( ) Fuel stoichiometry

( ) Total current (amp)

No of carbon atoms

$$(F132) = \left((SF) - 1\right)\left(\frac{3600\ (I)}{96500\ \left(6(n) + 2\right)}\right) \qquad (2)$$

$$(K132) = \frac{3600\ (I)\ (n)}{96500\ \left((n) + 2\right)} \qquad (3)$$

(K132) CO_2 exhaust from anode (gm mole/hr)

$$(B132) = \frac{(P100)\ \left((F132) + (K132)\right)}{(P132) - (P100)} \qquad (4)$$

(B132) Water vapor leaving anode (gm mole/hr)

(P100) Saturation vapor pressure of water at temperature (T100) over phosphoric acid (mm Hg)

(P132) Total pressure into the system (mm Hg)

$$(PE100) = \frac{1.7 \times 25.4\ \left(2\ (H)\right)}{13.6} + \frac{(PD100)}{2} + 760 \qquad (5)$$

(PE100) Average pressure in electrolyte chamber (mm Hg)

(PD100) Pressure drop at exhaust (mm Hg)

2 (H) Total height of the fuel cell (inch)

$$(PA100) = (P132) \qquad (6)$$

(PA100) Average pressure anode (mm Hg)

(P132) Pressure at anode exhaust

$$(PC100) = (P122) \qquad (7)$$

(PC100) Average pressure in cathode (mm Hg)

(P122) Pressure at cathode exhaust (mm Hg)

$$(\Delta PA) = (\Delta PC) = (PE100) - (PA100) = (PE100) - (PC100) \qquad (8)$$

(ΔPA) or

(ΔPC) Pressure drop across anode or cathode chamber with respect to electrolyte chamber (mm Hg)

$$(E132) = \frac{0.017\ (N)\ (L)\ (2\ (H))}{144} \left(\frac{13.6\ (\Delta PA) \times 1.67}{25.4} - 3.33 \right) \quad (9)$$

(E132) Electrolyte leakage to anode (gm mole/hr)

$$(E122) = (E132) \quad (10)$$

(E122) Electrolyte leakage to cathode (gm mole/hr)

B. Cathode Mass Balance

$$(D121) = \frac{3600\ (I)}{96500 \times 4} \left((SD) \right) \quad (11)$$

(D121) O_2 feed to cathode (gm mole/hr)

(SD) Air stoich

$$(G121) = \frac{79}{21}\ (D121) \quad (12)$$

(G121) N_2 feed to cathode corresponding to O_2 feed (D121) (gm mole/hr)

$$(B121) = \frac{20\ (RH)}{740} \left(\frac{100}{21} \right) (D121) \quad (13)$$

(RH) Relative humidity

(20) Partial pressure H_2O air at saturation with respect to 20°C (mm Hg)

(740) Partial pressure air (mm Hg)

$$(D122) = \left((SD) - 1 \right) \left(\frac{3600\ (I)}{96500 \times 4} \right) \quad (14)$$

(D122) O_2 exhaust from cathode (gm mole/hr)

$$(G122) = (G121) \quad (15)$$

(G122) Exhaust N_2 (gm mole/hr)

$$(B122) = \frac{\left((D122) + (G122) \right)\ (P100)}{(P122) - (P100)} \quad (16)$$

(B122) Equilibrium water content in exhaust stream from cathode in equilibrium to inlet concentration of H_3PO_4

$$(B100) = \left((n) + 1 \right) \left(\frac{3600\ (I)}{96500\ \left(3\ (n) + 2 \right)} \right) \quad (17)$$

(B100) Water produced into the system (gm mole/hr)

C. Heat Balance

Cathode

$$(H120) = \left[\begin{array}{l}(D122)\ (HD122) + (G122)\ (HG122) \\ +(B122)\ (HB122) + (E122)\ (HE122)\end{array}\right] - \left[\begin{array}{l}(D121)\ (HD121) + (G121)\ (HG\ 121) \\ (B121)\ (HB121) + (B100)\ (HB100) + (E122)\ (HB122)\end{array}\right] \quad (18)$$

(H120) Heat out by cathode exhaust (K cal/hr)

(HD122); (HG122); (HB122); (HE122) - Heat content of O_2, N_2, H_2O (vap.), Electrolyte at cathode exhaust and at (T122) (K cal/gm mole)

(HD121); (HG121); (HB121); (HB100); (HE122); Heat content of O_2, N_2, H_2O, and electrolyte inlet to cathode and at (T121) (K cal/gm mole)

Anode

$$(H130) = \left[\begin{array}{l}(F132)\ (HF132) + (K132)\ (HK132) + (B132)\ (HB132) \\ +(E132)\ (HE132)\end{array}\right] - \left[(F131)\ (HF131) + (E132)\ (HE131)\right] \quad (19)$$

(H130) = Heat rejection by anode exhaust (K Cal/hr)

(HF132); (HK132); (HB132); (HE132) heat content fuel (V); CO_2, H_2O(V) and electrolyte at anode exhaust and at (T132)

(HF131); (HE131) Heat content of fuel and electrolyte inlet to anode and at (T131)

$$(HR) = \frac{(W)\ (1 - (Z))}{(Z)} \times 3.412 \times 0.252 \quad (20)$$

(HR) Heat to be rejected from the fuel cell system (K Cal/hr)

(W) Gross power (watts)

(Z) Fuel cell efficiency

$$(M1) = (N)\left((Y5) + 2\ (Y4) + (Y6)\right) \quad (21)$$

(N) Number of cells

(M1) Length of the fuel cell stack (inch)

This is explained in Appendix 4.5.

$$(A101) = \frac{2}{144}\left(\left(2\ (H)\right) + 2(Y1) + 2\ (Y2) + 2(Y3)\right)\left(\left((M1) + 2\ (M2) + 2(Y3)\right) + \left((L) + 2(Y1) + 2(Y3)\right)\right) + \frac{\left((L) + 2(Y1) + 2(Y3)\right)\left((M1) + 2(M2) + 2(Y3)\right)}{144} \quad (22)$$

(A101) Skin surface area of the battery cell stack (sq ft)

See Figure 4.7-2.

$$(T101) = \frac{1/12(U)\ (T)\ (Y3) + (K1)\left((T100) \times 1.8 + 32\right)}{(U)\ \frac{(Y3)}{12} + (K1)} \tag{23}$$

(T101) Surface temperature of insulation in equilibrium with ambient temperature (°F)

(U) Heat transfer by free convection $\left(\frac{\text{Btu}}{\text{hr sq ft °F}}\right)$

(T) Ambient temperature (°F)

(T100) Operating temperature of the battery (°C)

(K_1) Thermal conductivity of insulation (Btu/hr sq ft °F/ft)

$$(Q1\ Loss) = \frac{1}{4}(U)\ (A101)\ \left((T101) - (T)\right) \tag{24}$$

(Q1 Loss) Heat loss by free convection and radiation (K Cal/hr)

$$(H110) = (HR) - \left((H120) + (H130) + (Q1\ Loss)\right) \tag{25}$$

(H110) Heat to be rejected by electrolyte (K Cal/hr)

D. Electrolyte Mass Balance

$$(F112) = \frac{(H110)}{(C_pE)\ (\Delta T)} \times 10^3\ \text{(gm mole/hr)} \tag{26}$$

(E112) Exhaust electrolyte flow rate (gm mole/hr)

(C_pE) Specific heat of phosphoric acid (Cal/gm mole °C)

(ΔT) Temperature rise, phosphoric acid (°C)

Phosphoric acid balance:

$$(E111)\left(1-(X111)\right) = (E112)\left(1-(X112)\right) + 2\,(E122)\left(1 - \frac{(X112)+(X111)}{2}\right)$$

Water balance:

$$(E112)\ (X112) = (E111)\ (X111) + (B100) - (B122) - (B132) - 2\,(E122)\left(\frac{(X122)+(X111)}{2}\right) \tag{27}$$

(E111) = Electrolyte flow rate to the fuel cell

(X111) Mole fraction (H_2O) at inlet electrolyte condition

(X112) Mole fraction (H_2O) in the electrolyte at the exhaust

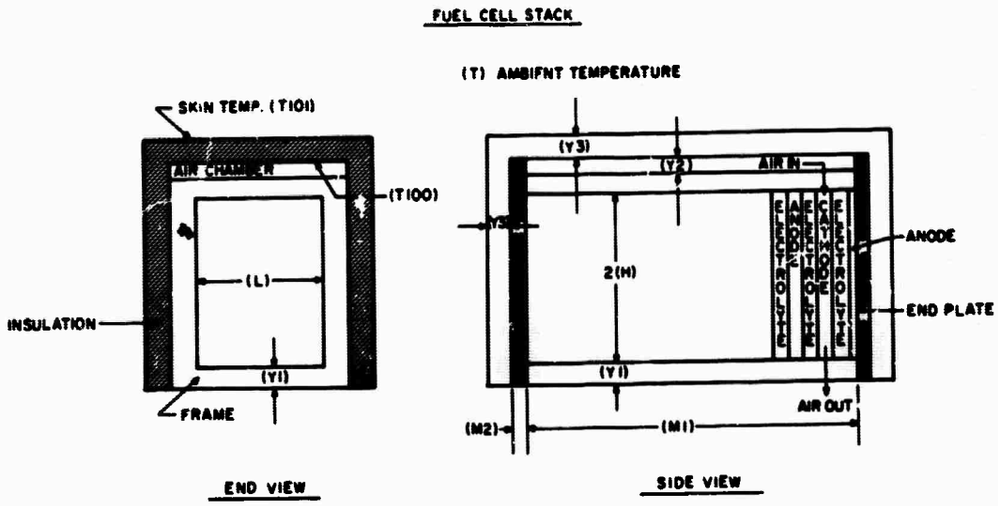

Figure 4.7-2. Cell Stack and Insulation for Heat and Mass Balance

Equation 27 is solved simultaneously for (E111) and (X111) by fixing the outlet concentration of the electrolyte.

4.7.3.2 Fuel Condenser (See Figure 4.7-3.)

A. Mass Balance

$$(F332) = \frac{(K132)\ (PF332)}{(P332) - (PF332) - (PB332)} \quad (28)$$

(F332) Fuel loss to stack (gm mole/hr)

(PF332) Fuel vapor pressure in equilibrium with liquid at temperature (T332) (mm Hg)

(PB332) Equilibrium water vapor pressure at temperature (T332) (mm Hg)

(P332) Atmosphere pressure (mm Hg)

$$(F322) = (F132) - (F332) \quad (29)$$

(F322) Fuel recovered by condensation

(F132) Fuel in (the anode exhaust)

$$(B332) = \frac{(K132)\ (PB332)}{(P332) - (PF332) - (PB332)} \quad (30)$$

(B332) Water loss to stack

$$(B312) = (B132) - (B332) \quad (31)$$

(B312) Water recovered from exhaust stream

B. Heat Balance

$$(H300) = (F132)\ (HF132) + (K132)\ (HK332) + (B132)(HB132)$$
$$-(F332)\ (HF332) + (K132)\ (HK132) - (B332)\ (HB332)$$
$$-(F332)\ (HFL332) - (B312)\ (HBL312) \quad (32)$$

(H300) Heat load on fuel condenser (K Cal/hr)

(HF132) = (HK132); (HB132) Heat content fuel, CO_2 and water in, inlet stream

(HF332); (HK132); (HB332), Heat content of exhaust stream (HFL332); (HB312)

Assuming surface temperature of feed condenser to be the same as condensation temperature of fuel:

Fuel vapor pressure (P300) (mm Hg)

$$(P300) = \frac{(F132) \times (P132)}{(K132) + (F132) + (B132)} \quad (33)$$

$$(T300) = f\ (P300) \quad (34)$$

(T300) Skin temperature of the fuel condenser

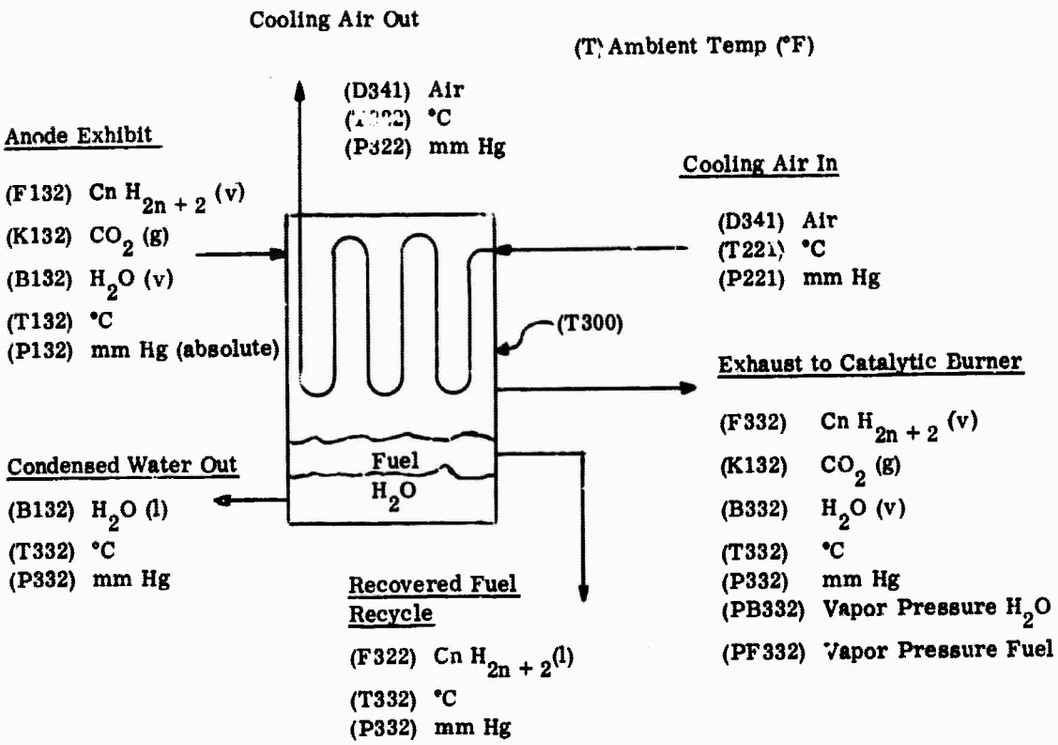

Figure 4.7-3. Process Streams for Heat and Mass Balance - Fuel Condenser

$$(TLM3) = \frac{\left((T132) - (T322)\right) - \left((T322) - (T221)\right)}{\ln \dfrac{(T132) - (T332)}{(T322) - (T221)}} \qquad (35)$$

(TLM3) Log mean temperature (°C)

$$(A300) = \frac{(H300) \times 4}{(U3)\ \left((TLM3) \times 1.8\right)} \qquad (36)$$

(A300) Heat transfer area required (sq ft)

(U3) Overall heat transfer coefficient for air to vapor system (Btu/hr sq ft °F) (assume approximately 4.0)

$$(A301) = 6\left(3\sqrt{\frac{A300}{200}}\right)^2 \qquad (37)$$

Assume fuel condenser to be of cubical shape.

(A301) Outside surface area (sq ft)

(T300) Surface temperature (°C)

$$(Q3\ Loss) = 1/4\ (U)\ (A301)\ \left((T300) \times 1.8 + 32\right) - (T) \qquad (38)$$

(Q3 Loss) Heat loss by free convection (K Cal/hr)

(U) Heat transfer coefficient for free convection $\left(\frac{Btu}{hr\ sq\ ft\ °F}\right)$

$$(D341) = \frac{(H300) - (Q3\ Loss)}{(HD322) - (HD221)} \qquad (39)$$

(D341) Air flow rate (gm mole/hr)

(HD322) Heat content air at exhaust and

(HD221) inlet to the condenser

$$(V300) = \left(\frac{A300}{200}\right) \qquad (40)$$

(V300) Volume (cu ft)

4.7.3.3 Exhaust Air Condenser (See Figure 4.7-4.)

A. Heat and Mass Balance

$$(B222) = \frac{(PB222)\ \left((D122) + (G122)\right)}{(P222) - (PB222)} \qquad (41)$$

(PB222) Water to stack from exhaust air condenser (gm mole/hr)

(PB222) Equilibrium water vapor pressure temperature (T222).

(P222) Pressure inside condenser (mm Hg)

(T222) Temperature of exhaust air assuming (15°F ≈ 9°C) approach with ambient temperature (T)

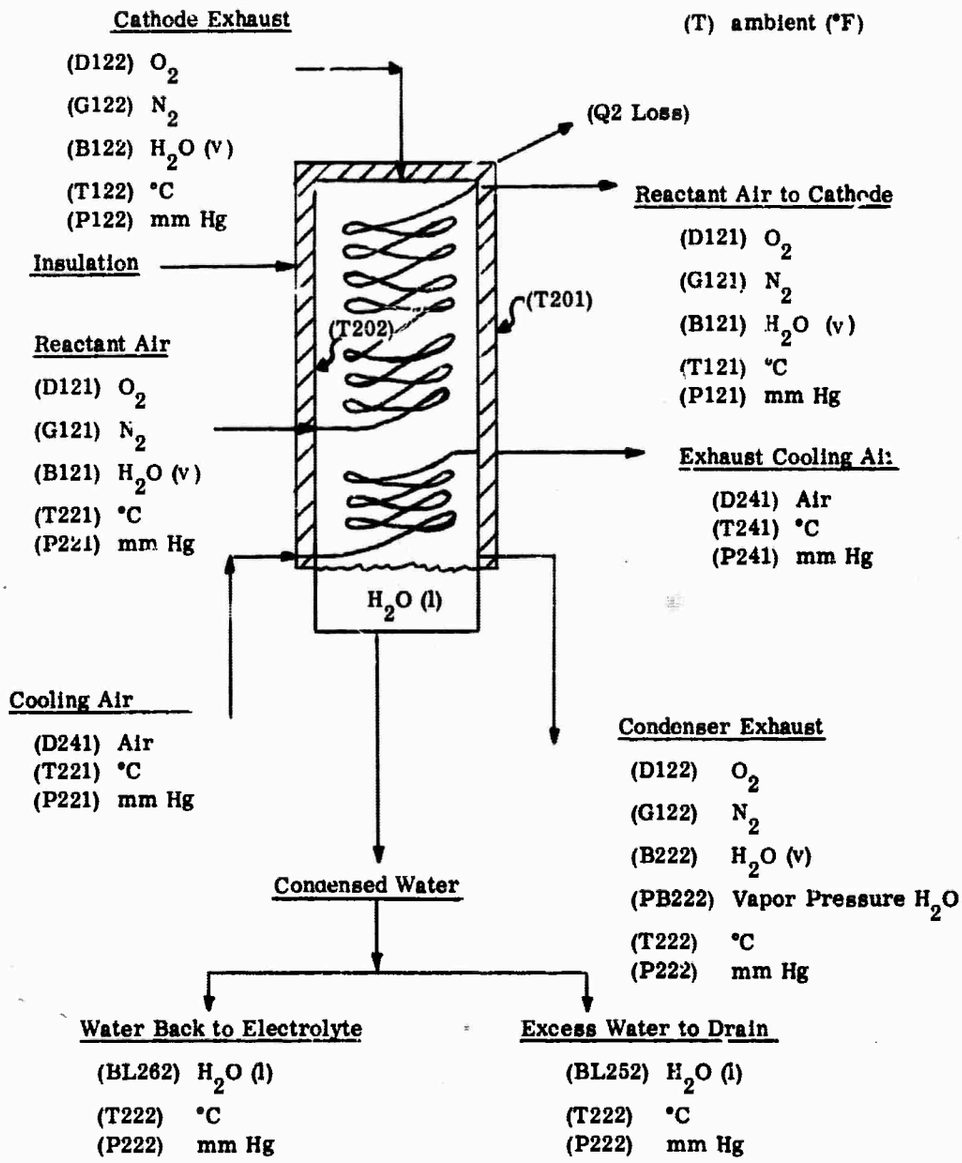

Figure 4.7-4. Process Streams for Heat and Mass Balance - Exhaust Air Condenser

$$\big((H121) - (H221)\big) = (D121)\ \big((HD121) - (HD221)\big) + (G121)\ \big((HG121) - (GH221)\big) + (B121)\ \big((HB121) - (HB221)\big) \quad (42)$$

$\big((H121) - (H221)\big)$ Heat required to preheat reaction air (K Cal/hr)

$$\big((BL252) + (B222)\big) = (B121) + (B100) - (B332) \quad (43)$$

(BL252) + (B222) <u>Total water to be rejected from the system</u>

(B121) Water into the fuel cell with air feed

(B332) Water to stack from fuel condenser

(B222) Water vapor to stack at assumed equilibrium exhaust temperature (T222)

(BL252) Water rejected as condensed water from exhaust air condenser

If it is desired to reject $\big((BL252) + (B222)\big)$ total amount of water as vapor in exhaust stream, V. P. of water in exhaust stream could be calculated as:

$$(P200) = \frac{\big((BL252) + (B222)\big)\ (P122)}{(D122) + (G122) + (BL252) + (B222)} \quad (44)$$

(P200) Vapor pressure H_2O in exhaust stream (mm Hg)

(D122) Exhaust oxygen to stack (gm mole/hr)

(G122) Exhaust nitrogen to stack (gm mole/hr)

(BL252) + (B222) Water to be rejected (gm mole/hr)

(T200) Is the dew point corresponding to (P200)

$$(T200) = f(P200) \quad (45)$$

(T200) Is the maximum allowable exhaust temperature (°C) to keep the system self-sustaining for water

$$(BL262) = (B122) - (B222) - (BL252) \quad (46)$$

(BL262) Amount of water to be recirculated to electrolyte chamber (gm moles/hr)

$$(H200) = (D122)\ \big((HD122) - (HD222)\big) + (G122)\ \big((HG122) - (HG222)\big) + (B122)\ (HG122) - \big((B222) + (BL252)\big)\ (HBL222) - (BL262)\ (HBL222) \quad (47)$$

(H200) Is the heat load (K Cal/hr) on exhaust air condenser

$$(T241) = (T121) \quad (48)$$

(T242) Exhaust air temperature (°C)

(T121) Reactant air inlet temperature (°C)

(T122) Exhaust temperature (°C) can be equated to (T200) or one may assume a 15°F approach to ambient temperature

$$(TLM2) = \frac{\left((T222) - (T221)\right) - \left((T122) - (T121)\right)}{\ln\left(\frac{(T222) - (T221)}{(T122) - (T121)}\right)} \quad (49)$$

(TLM2) Log mean temperature in exhaust air condenser

$$(A200) = \frac{(H200)}{(U2)\ (TLM2)} \quad (50)$$

(A200) Heat transfer area required (sq ft)

(U2) Heat transfer coefficient $\left(\frac{\text{Btu}}{\text{hr sq ft °F}}\right)$

$$(A201) = 6\left(3\sqrt{\frac{(A200)}{200}} + \frac{2(Y3)}{12}\right)^2 \quad (51)$$

(A201) Outside surface area (sq ft) of condenser considering thickness of insulation = (Y3) inch

$$(T201) = \frac{\frac{(U)\ (T)\ (Y3)}{12} + (K1)\left((T202) \times 1.8 + 32\right)}{(U)\ \frac{(Y3)}{12} + (K1)} \quad (52)$$

(T201) Skin temperature of insulation (°F)

$$(Q2\ Loss) = \frac{1}{4}\ (U)\ (A201)\ \left((T201) - (T)\right) \quad (53)$$

(Q2 Loss) Heat loss by free convection from the outside surface of condenser (K Cal/hr)

$$(D241) = \frac{(H200) - (Q2\ Loss) - \left((H121) - (H221)\right)}{(HD242) - (HD221)} \quad (54)_a$$

(D241) Supercooling air rate to condenser (gm mole/hr)

Reactant air = (D121) + (G121) + (B122) $(54)_b$

4.7.3.4 <u>Electrolyte Cooler</u> (See Figure 4.7-5.)

A. <u>Enthalpy Balance</u>

$$(H430) = (F131)\left((HF131) - (HFL431)\right) \quad (55)$$

(H430) Heat required to vaporize and superheat fuel feed from ambient temperature (T) (K Cal/hr)

(HF131) Heat content of superheated fuel to temperature (T131) in vapor phase (K Cal/gm mole)

$$(A401) = \frac{1}{144}\left((M1) + 2(Y3)\right)\left((L) + 2(Y3) + 2(Y1)\right) + \frac{2\left((Y7) + (Y3)\right)\left((L) + 2(Y1) + 4(Y3) + (M1)\right)}{144} \quad (56)$$

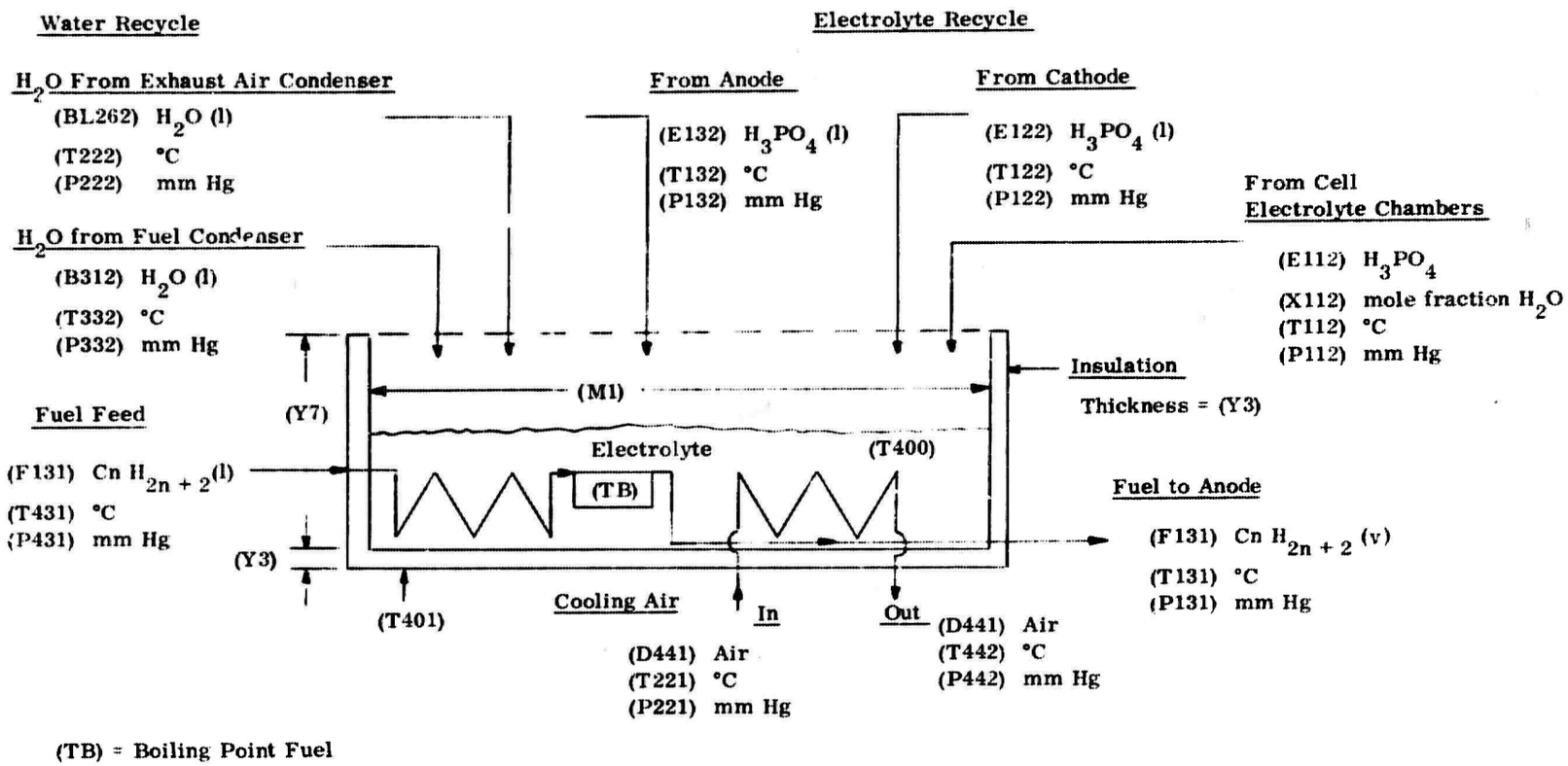

Figure 4.7-5. Process Streams for Heat and Mass Balance - Electrolyte Cooler and Fuel Vaporizer

(A401) Outside surface area of electrolyte cooler

$$(T401) = \frac{\frac{(U)\ (T)\ (Y3)}{12} + (K)\ \Big((T400) \times 1.8 + 32\Big)}{(U)\ \frac{(Y3)}{12} + (K)} \qquad (57)$$

(T401) Skin temperature (°F)

$$(Q4\ Loss) = \frac{1}{4}\ (U)\ (A401)\ \Big((T401) - (T)\Big) \qquad (58)$$

(Q4 Loss) Heat loss from electrolyte cooler surface by free convection (K Cal/hr)

$$(D441) = \frac{\left[\begin{array}{l}(E122)\ (HE122) + (E112)\ (HE112) + (E132)\ (HE132) \\ +(BL262)\ (HBL262) + (B312)\ (HBL312) \\ -(F131)\ \ (HFL431) - (HF131)\ \ -\ \ (Q4\ Loss) \\ -(E111)\ (HE111)\end{array}\right]}{(HD442) - (HD441)} \qquad (59)$$

(D441) Cooling air required to remove excess heat from electrolyte cooler (gm mole/hr)

(HE111) Heat content of electrolyte at temperature (TUW)

$$(TB) = f(P131) \qquad (60)$$

(TB) Boiling point of the fuel corresponding to the pressure (P131), could be calculated from V. P. vs. temperature chart (°C)

$$(Q402) = (F131)\ \Big((HBFL) - (HFL131)\Big) \qquad (61)$$

(Q402) Heat required to heat the fuel to boiling temperature (K Cal/hr)

$$(TLM402) = \frac{\Big((T400) - (T431)\Big) - \Big((T400) - (TB)\Big)}{\ln \frac{(T400) - (T431)}{T400 - (TB)}} \qquad (62)$$

(TLM 402) Log mean temperature for preheat surface area of fuel (°C)

(T400) Electrolyte temperature (°C)

$$(A402) = \frac{(Q402) \times 4}{(U402)\ \Big((TLM402) \times 1.8\Big)} \qquad (63)$$

(A402) Heat transfer area to preheat fuel to boiling point (sq ft)

$$(Q403) = (F131)\ (HVF) \qquad (64)$$

(Q403) Heat required to vaporize fuel (K Cal/hr)

(HVF) Heat of vaporization (K Cal/gm mole)

$$(A403) = \frac{(Q403) \times 4}{(U403)\left((T400) - (TB)\right) \times 1.8} \tag{65}$$

(A403) Surface area required to vaporize fuel (sq ft)

$$(TLM404) = \frac{\left((T400) - (T221)\right) - \left((T400) - (T442)\right)}{\ln \left(\frac{(T400) - (T221)}{T400 - (T442)}\right)} \tag{66}$$

(TLM 404) Log mean ΔT to cool the electrolyte to a required temperature

$$(A404) = \frac{(D441)\left((HD442) - (HD441)\right) \times 4}{(U404)\left((TLM404) \times 1.8\right)} \tag{67}$$

(A404) Heat transfer surface area required to cool the electrolyte to a desired temperature level

4.7.3.5 Water Balance

$$(B121) + (B100) = (B332) + (B222) + (BL252) \tag{68}$$

4.7.3.6 Fuel Balance

$$(F531) = \frac{3600\ (I)}{96500 \times 6(N) + 2} + (F332) \tag{69}$$

(F531) Fresh feed required per hr.

Total fuel tank capacity will depend on operation time.

4.7.3.7 Entire System (See Figure 4.7-6.)

(3) Heat Balance on Entire System

$$\begin{aligned}
&(F531)\ (HFL431) + \left((D241) + (D341) + (D441)\right)\ (HD221) \\
&+ (D121)\ (HD221) + (G121)\ (HG221) + (B121)\ (HB221) + HR \\
&= (F332)\ (HF332) + (K132)\ (HK332) + (B332)\ (HB332) \\
&(C122)\ (HD222) + (G122)\ (HG222) + (B222)\ (HB222) \\
&(BL252)\ (HBL222) + (D441)\ (HD442) + (D341)\ (HD322) \\
&(D241)\ (HD242) + (Q1\ Loss) + (Q2\ Loss) + (Q3\ Loss) \\
&+ (Q4\ Loss)
\end{aligned} \tag{70}$$

Equate two sides. If the right-hand side is higher than the left-hand side, then decrease air flow rate or decrease the temperature limit to equate both sides, or vice versa.

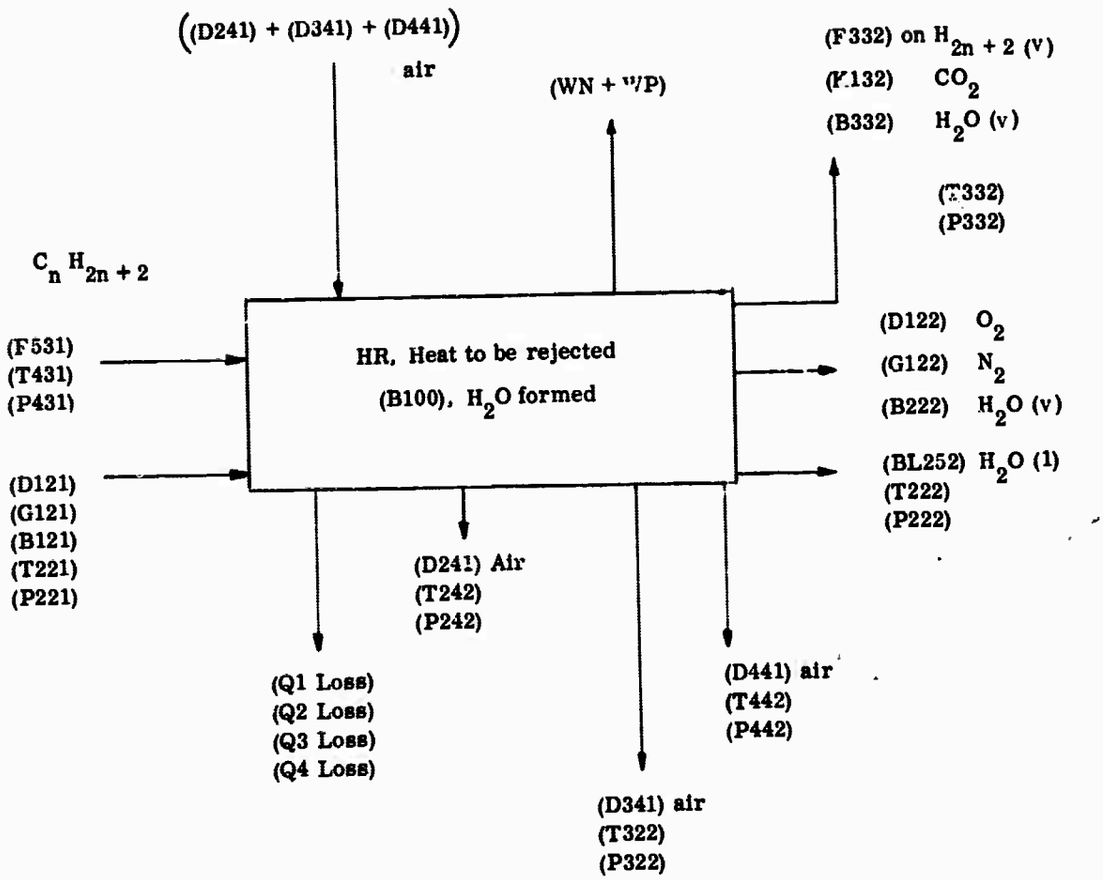

Figure 4.7-6. Process Streams for Heat and Mass Balance on Entire System

4.7.3.8 Parasitic Power

(i) To pump electrolyte

Amount of electrolyte pumped = (E111)

Pressure difference = (P111) - (P112) mm Hg

$$(WPE4) = 2.16 \times 10^{-6} (E111) \left((P111) - (P112)\right) \text{ watts} \quad (71)$$

(ii) Pump fuel

$$(WPE4) = 5.3 \times 10^{-8} (F131) \left((P431) - 760\right) \left(14(N) + 2\right) \text{ watts} \quad (72)$$

(iii) Pump air to cells

$$(WPD4) = 2.3 \times 10^{-3} \left((T221) + 273\right) \left(\ln \frac{(P121)}{760}\right) \left((D121) + (G121) + (B121)\right) \text{ watts} \quad (73)$$

(iv) Pump air to exhaust air condenser

$$(WPD5) = 2.3 \times 10^{-3} \left((T221) + 273\right) \left(\ln \frac{(P121)}{760}\right) (D241) \quad (74)$$

(v) Pump air to fuel condenser

$$(WPD6) = 2.3 \times 10^{-3} \left((T221) + 273\right) \left(\ln \frac{(P121)}{760}\right) (D341) \quad (75)$$

(vi) Pump air to electrolyte cooler

$$(WPD7) = 2.3 \times 10^{-3} \left((T221) + 273\right) \left(\ln \frac{(P121)}{760}\right) (D441) \quad (76)$$

(vii) Power supplied by the auxiliary battery

$$(WRB) = \left(\begin{matrix}(WPE4) + (WPF4) + (WPD4) \\ + (WPD5) + (WPD6) + (WPD7)\end{matrix}\right) (10) \quad (77)$$

here we assume the pump efficiency = 10%

(viii) Power required to recharge the battery

$$(RB) = \frac{(WRB)\ (START)}{(CHARGE)} \quad (78)$$

4.7.3.9 Weight of the System

(A) Exhaust Air Condenser

$$(LB2) = 4 \times 10^{-4} (A200) (\rho_5) \quad (79)$$

(ρ_5) = density of metal used lb/cu ft

0.08 = fraction of total volume as metal

200 = sq ft area/ft^3 of volume

(B) Fu xhaust Condenser

$$(LB3) = 4 \times 10^{-4} (A300) (\rho_5) \quad (80)$$

(C) Weight of electrolyte cooler and fuel vaporizer

$$(LB4) = 4 \times 10^{-4} \left((A402) + (A403) + (A404)\right) (\rho 6) \quad (81)$$

$(\rho 6)$ density of cooler material of construction most probably tantalum

(D) Weight of Electrolyte Pan

$$(LB51) = \frac{(\rho 6)\ (Y9)}{1728} \left(2(Y7)\ (M1) + \left(2(Y7) + (M1)\right)\left((L) + 2(Y1)\right)\right) \quad (82)$$

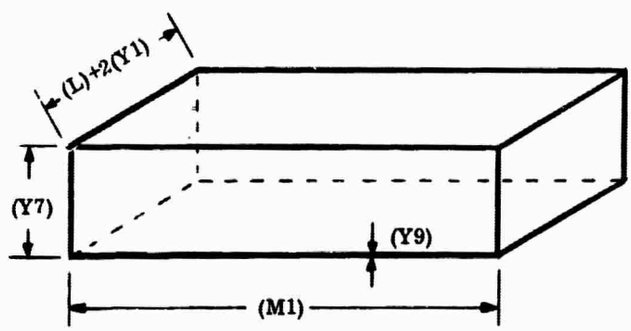

(E) Weight of Electrolyte in Pan

$$(LB14) = 2(H)\ (L)\ (Y6)\ (\rho 4)/1728 \quad \text{lb} \quad (83)$$

(F) Weight of Electrolyte Cooler

$$(LB5) = (LB14) + (LB51) \quad (84)$$

(G) Weight of Manifolds

$$(LB7) = 0.1\left((LB1) + (LB2) + (LB3) + (LB4) + (LB5) + (LB6)\right) \quad (85)$$

This is assuming manifolds average 10% of the weight of unit.

(W) Weight of Pump = LB8 = 15 lb (86)

(J) Total Weight of the System (LBT)

$$(LBT) = 1.1\left((LB1) + (LB2) + (LB3) + (LB4) + (LB5) + (LB6) + (LB8)\right) \quad (87)$$

4.7.3.10 Net Power Output

$$(WN) = \left((W) - (RB) - (WRB)\right) \quad (88)$$

Net power output per unit weight

$$(NPOPW) = \frac{(WN)}{(LBT)} \tag{89}$$

4.7.3.11 Overall Thermal Efficiency

(A) Based on higher heating value of the fuel

$$\eta_{HHV} = \frac{(WN) \quad watts}{(F531)\ (HHV)\ (1.164)} \tag{90}$$

(HHV) K Cal/gm mole

(F531) gm mole/hr

4.8 RESULTS OF DETAILED HEAT, MASS, AND ENERGY BALANCE FOR 0.5 KW SYSTEM

(P. J. Chludzinski, D. C. Shah)

Based on the set procedure for calculation of detailed heat and mass balance in Appendix 4.7, the following results were obtained for two optimum systems based on cell efficiency, battery core weight, and the electrolyte gap.

The optimum values of the fuel cell battery were obtained from a computer program set for Appendix 4.5. These values were used to calculate the entire system mass and heat balance, assuming that optimum core condition would result in an optimum overall system.

Heat content of different streams were obtained from Tables 4.8-1 thru 4.8-6 at the end of this appendix. Temperature conditions for the fluid streams were based on cell operating temperature for each system. For most cases 15°F approach was used, except where a lower temperature difference was necessary.

Results shown in parentheses are for forced convection cooling, otherwise results are for free convection cooling.

4.8.1 Optimum System Values

The following optimum values were obtained for the system from Appendix 4.5.

		Case 1	Case 2
(T100)	Temperature of system (°C)	150°C	180°C
(V)	Net voltage per cell (volts)	0.32	0.429
2(H)	Height of the cell (inch)	10	10
(L)	Length of the cell (inch)	15	15
(ρ/t)	Screen resistivity (ohm/square)	0.0053 (at room temp.) 0.0083 at 150°C	0.0053 (at room temp.) 25% 0.0088 at 180°C
(J)	Current density (ASF)	30	40
(N)	Number of cells	61	34
(W)	Gross power (watts)	600	600
(ρ_2)	Weight of screen (lb/sq ft)	0.13	0.13
(I)	Total current (amps)	1689.5	1400
(i)	Current per cell (amps)	31.25	41.7
(Y1)	Width of frame (inch)	0.5	0.5

		Case 1	Case 2
(Y2)	Air gap (inch)	0.0625	0.0625
(Y3)	Insulation thickness (inch)	2.0	2.0
(Y4)	Electrode thickness (inch)	0.012	0.012
(Y5)	Gas frame thickness (inch)	0.125	0.125
(Y6)	Electrolyte gap (inch)	0.0625	0.0625
(Y8)	Projected screen height from battery for bus bar connection (inch)	0.5	0.5
(M1)	Length of fuel cell stack (inch)	11.6	5.0
(M2)	Thickness of end plate (inch)	0.5	0.5
(T)	Ambient temperature (°F)	68 = 20°C	68 = 20°C
(T101)	Temperature of insulation surface (°C)	= 100°F	
(LB1)	Weight of stack (total) wet (lb)	87.19	48.41
(LB11)	Weight of frames (lb)	18.81	10.44
(LB12)	Weight of screens (lb)	20.98	11.65
(LB13)	Weight of catalyst (lb)	12.60	7.00
(LB14)	Weight of electrolyte in battery (lb)	34.80	19.32
(ρ_1)	Density of frame material (lb/ft^3)	66.1	66.1
(ρ_3)	Average catalyst loading (lb/ft^2)	0.1	0.1
(ρ_4)	Density of electrolyte at 70°F (lb/ft^3)	106	106
(SWB)	Specific weight of the battery (lb/KW)	129.83	50.5
(ρ_e)	Electrical resistivity of electrolyte (ohm-cm)	1.85	1.5
(N)	Number of carbon atoms	8	8
(SF)	Fuel stoichiometry	10	10
(SD)	Air stoichiometry	3	3
(RH)	Relative humidity (air)	50%	50%
(Z)	Fuel cell efficiency (%), (η_{LHV})	29.9	40.5
(U)	Overall heat transfer coefficient for free convection (Btu/hr sq ft °F)	1.0	1.0
(K1)	Thermal conductivity of insulation (Btu/hr sq ft °F/ft)	0.025	0.025
(CpE)	Specific heat phosphoric acid (Cal/gm mole °C)	42.1	42.1
(ΔT)	Electrolyte temperature rise in fuel cell (°C)	9	9

		Case 1	Case 2
(X112)	Water mole fraction in electrolyte at exhaust	0.144 (97 wt % H_3PO_4)	-0- (100 wt % H_3PO_4)
(U3)	Overall heat transfer coefficient for air to vapor system (Btu/hr sq ft °F)	4.0	4.0
(U2)	Overall heat transfer coefficient exhaust air condenser (Btu/hr sq ft °F)	1.5	1.5
(U402)	Overall heat transfer coefficient for liquid fuel electrolyte (Btu/hr sq ft °F)	5.0	5.0
(U404)	Heat transfer coefficient air to electrolyte (Btu/hr sq ft °F)	1.0	1.0

4.8.1.1 Temperature of Streams (°C)

		Case 1	Case 2
(T122)	Air exhaust from cathode	145.5	180
(T121)	Air inlet to cathode	142	172
(T131)	Inlet fuel feed to anode	142	172
(T132)	Anode exhaust fuel temperature	145.5	180
(T332)	Exhaust non-condensable gas from fuel condenser	29	29
(T322)	Exhaust cooling air from fuel condenser	142	-
(T221)	Inlet air temperature to exhaust air condenser	20	20
(T222)	Temperature of exhaust gases from air condenser	29	29
(T202)	Surface temperature exhaust air condenser	81.3	104
(T431)	Fuel feed temperature to vaporizer	20	20
(T400)	Electrolyte cooler surface temperature	145.5	180
(T442)	Exhaust air temperature from electrolyte cooling	80	80
(TB)	Boiling point of fuel	126.87	126.87
(T112)	Exhaust electrolyte from fuel cell	154.5	189
(T111)	Inlet electrolyte to fuel cell	145.5	180
(T300)	Fuel condenser surface temperature	98	102
(T242)	Reactant air temperature from air condenser	142	-

4.8.1.2 Pressure of Streams (mm Hg)

Pressure of different streams were assumed on the basis of pressure drops through the system, assuming atmospheric pressure of 760 mm Hg. All the streams from the system are exhausted to atmosphere.

		Case 1	Case 2
(P100)	Saturation vapor pressure of water over electrolyte	150 (97 wt %)	70 (100 wt %)
(P132)	Pressure at anode exhaust	780	780
(PD100)	Pressure drop at cathode exhaust	12	12
(P121)	Air pressure at cathode inlet	786	786
(P124)	Air pressure at cathode exhaust	780	780
(PF332)	Equilibrium fuel vapor pressure at (T332)	18.5	18.5
(PB332)	Equilibrium water vapor pressure at (T332)	30.8	30.8
(P332)	Pressure in fuel condenser	765	765
(PB222)	Equilibrium water vapor pressure at (T222)	30.8	30.8
(P112)	Electrolyte exhaust pressure	772	772
(P111)	Electrolyte inlet pressure to fuel cell	836	836
(P131)	Pressure in fuel vaporizer	786	786
(P322)	Exhaust pressure cooling air for fuel condenser	765	765
(P221)	Cooling air inlet pressure to fuel condenser	770	
(P222)	Exhaust air condenser exhaust pressure	765	765
(P442)	Exhaust air pressure for electrolyte cooling	765	765
(P431)	Fuel feed pressure	786	786

4.8.1.3 Specific Heat Content of Various Chemical Species

		Case 1		Case 2	
		Temp °C	K Cal/ gm mole	Temp °C	K Cal/ gm mole
(HD122)	Oxygen at (T122)	145.5	2.922	180	3.17
(HD121)	Oxygen at (T121)	142	2.900	172.0	3.12

		Case 1		Case 2	
		Temp °C	K Cal/ gm mole	Temp °C	K Cal/ gm mole
(HD322)	Air at (T322)	142	2.245		
(HD221)	Air at (T221)	20	2.03	20	2.03
(HD222)	Air at (T222)	29	2.10	29	2.10
(HD442)	Air (T442)	80	2.46	80	2.46
(HG122)	Nitrogen (T122)	145.5	2.910	180	3.125
(HG121)	Nitrogen (T121)	142	2.885	172.0	3.10
(HG221)	Nitrogen (T221)	20	2.03	20	2.03
(HG222)	Nitrogen (T222)	29	2.10	29	2.10
(HB122)	Water (v) (T122)	145.5	11.91	180.0	11.93
(HB121)	Water (v) (T121)	142	11.88	172.0	11.895
(HB100)	Water (v) (T100)	150	11.93	180.0	11.93
(HB132)	Water (v) (T132)	165.5	11.91	180.0	11.93
(HB221)	Water (v) (T221)	20	10.45	20	10.45
(HB332)	Water (v) (T332)	29	10.45	29	10.45
(HBL222)	Water (L) (T222)	29	0.522	29	0.522
(HBL262)	Water (L)	29	0.522	29	0.522
(HBL312)	Water (L) (T312)	29	0.52	29	0.52
(HF132)	Fuel (v) (T132)	145.5	24.14	180	26.23
(HF131)	Fuel (v) (T131)	142	23.82	172	25.75
(HF332)	Fuel (v) (T332)	29	17.87	29	17.87
(HFL332)	Fuel (L) (T332)	29	8.16	29	8.16
(HFL431)	Fuel (L) (T431)	20	7.607	20	7.607
(HVF)	Heat of vaporization of fuel	-	8.36	-	8.36
(HK132)	CO_2 (T132)	145.5	3.36	180	3.73
(HK332)	CO_2 (T332)	29	2.285	29	2.285

Calculations

4.8.2 Anode Mass Balance

Eq. No.			Case 1	Case 2
	Theoretical fuel consumption (gm mole/hr)		1.26	1.145
(1)	(F131)	Fuel feed (gm mole/hr)	12.6	11.45

Eq. No.			Case 1	Case 2
(2)	(F132)	Fuel exhaust from anode (gm mole/hr)	11.34	10.30
(3)	(K132)	CO_2 exhaust (anode)	10.08	9.16
(4)	(B132)	Water vapor leaving anode (gm mole/hr)	5.11	1.919
(5)	(PE100)	Average pressure in electrolyte chamber (mm Hg)	797.7	797.7
(6)	(PA100)	Average pressure (mm Hg)	780	780
(7)	(PC100)	Average pressure in cathode (mm Hg)	780	780
(8)	$(\Delta P_A) = (\Delta P_C)$	Pressure drop across anode or cathode chamber with respect to electrolyte chamber (mm Hg)	17.7	17.7
(9)	(E132)	Electrolyte leakage to anode (gm mole/hr)	11.62	4.55
(10)	(E122)	Electrolyte leakage to cathode (gm mole/hr)	11.62	4.55
(11)	(D121)	O_2 feed to cathode (gm mole/hr)	47.25	13.1
(12)	(G121)	N_2 feed to cathode (gm mole/hr)	178.0	162.0
(13)	(B121)	Water vapor feed to cathode with reactant air (gm mole/hr)	3.0	2.77
(14)	(D122)	O_2 exhaust from cathode (gm mole/hr)	31.50	28.7
(15)	(G122)	N_2 exhaust (gm mole/hr)	178.0	162.0
4.8.3	Cathode Mass Balance			
(16)	(B122)	Equilibrium water content in exhaust stream from cathode (in equilibrium with H_3PO_4)	49.9 (95 wt %)	28.9 (100 wt %)
(17)	(B100)	Product water	11.32	10.3
4.8.4	Heat Balance			
		Cathode		
(18)	(H120)	Heat out by cathode exhaust (K Cal/hr)	384.7	151
		Anode		
(19)	(H130)	Heat out by anode exhaust (K Cal/hr)	77.5	32.6
(20)	(HR)	Heat to be rejected from the fuel cell system (K Cal/hr)	1021	586
(21)	(M1)	Length of fuel cell stack (inch)	11.6	5.0
(22)	(A101)	Skin surface area of the battery cell (sq ft)	10.58	7.68
(23)	(T101)	Surface temperature of insulation in equilibrium with ambient temperature (°F)	100	177.5

Eq. No.			Case 1	Case 2
(24)	(R1 Loss)	Heat loss by free convection and radiation from battery surface (K Cal/hr)	79.3	206
(25)	(H110)	Heat to be rejected by electrolyte (K Cal/hr)	482.5	630.4
4.8.5	Electrolyte Mass Balance			
(26)	(E112)	Exhaust electrolyte flow rate (gm mole/hr)	1270.0	1660
(27)	(X111)	Mole fraction water at inlet (electrolyte)	0.167	0.0124
	(E111)	Inlet electrolyte flow rate (gm mole/hr)	1335	1690
4.8.6	Mass Balance on Fuel Condenser			
(28)	(F332)	Fuel loss to stack (gm mole/hr)	0.262	0.2365
(29)	(F322)	Fuel condensed (gm mole/hr)	11.078	10.063
(30)	(B332)	Water exhaust with non-condensable gases (gm mole/hr)	0.434	0.394
(31)	(B312)	Water recovered from anode exhaust (gm mole/hr)	4.676	1.525
4.8.7	Heat Balance on Fuel Condenser			
(32)	(H300)	Heat load on fuel condenser (K Cal/hr)	244.05	215.3
(33)	(P300)	Fuel vapor pressure in anode exhaust (mm Hg)	333	37.6
(34)	(T300)	Fuel dew point temperature (°C)	98	102.0
(35)	(TLM3)	Log mean temperature difference for fuel condenser (°C)	109.4	$\Delta T = 145.6$
(36)	(A300)	Heat transfer area required (sq ft)	2.130	7.4
(37)	(A301)	Skin surface area of fuel condenser (sq ft)	0.2904	-
(38)	(Q3 Loss)	Heat loss by free convection from fuel condenser surface (K Cal/hr)	11.55	-
(39)	(D341)	Airflow rate required to reject amount of heat from fuel condenser (gm mole/hr)	1080	-
(40)	(V300)	Volume of fuel condenser (cu ft)	1.066×10^{-2}	0.154
4.8.8	Heat and Mass Balance, Exhaust Air Condenser			
(41)	(B22)	Water vapor overboard from exhaust air condenser (gm mole/hr)	8.34	8.0
(42)	((H121) - (H221))	Heat required to preheat reaction air (K Cal/hr)	194.4	224.5

Eq. No.			Case 1	Case 2
(43)	((BL252) + (B222))	Total water to be rejected from the system (gm mole/hr)	13.886	12.676
	(BL252)	Water rejected as condensed water from exhaust air condenser (gm mole/hr)	5.546	4.676
	(B222)	Water vapor overboard at assumed equilibrium exhaust temperature (T222)	8.34	8.0
(44)	(P200)	Vapor pressure of water in cathode exhaust (mm Hg)	48.5	48.6
(45)	(T200)	Maximum allowable exhaust temperature to keep the system self-sustaining for water at 70°F assumed ambient temperature, 50% relative humidity (°C)	37.22	37.22
(46)	(BL262)	Amount of water to be recirculated to electrolyte (gm mole/hr)	36.014	16.224
(47)	(00)	Heat load exhaust air condenser (K Cal/hr)	739.15	526.1
(48)	(T242)	Exhaust air temperature (°C)	142	180
(49)	(TLM2)	Log mean temperature in exhaust air condenser (°C)	5.67	8.5
(50)	(A200)	Heat transfer area required, air condenser (sq ft)	(200)	39.1
(51)	(A201)	Outside surface area (sq ft)	(6.75)	5.58
(52)	(T201)	Skin temperature of insulation (°F)	(86)	89.5
(53)	(Q2 Loss)	Heat loss by free convection and radiation from condenser (K Cal/hr)	(27)	27.2
(54)a	(D241)	Air required to supercool exhaust (gm mole/hr)	(594)-	Used Free Convection
(54)b		Reactant air flow (gm mole/hr)	228.25	207.87
(55)	(H430)	Heat required to preheat, vaporize and superheat fuel feed to the system (K Cal/hr)	206	208
(56)	(A401)	Outside surface area of electrolyte cooler (sq ft)	6.13	4.85
(57)	(T401)	Skin temperature (°F)	99.4	107.5
(58)	(Q4 Loss)	Heat loss from electrolyte cooler surface by free convection (K Cal/hr)	45.1	45.5
(59)	(D441)	Cooling air required to remove excess heat assuming temperature rise of 60°C (gm mole/hr)	130	268

Eq. No.			Case 1	Case 2
(60)	(TB)	Boiling point of the fuel corresponding to the pressure (P131) (°C)	126.87	126.87
(61)	(Q402)	Heat required to bring fuel to boiling point (K Cal/hr)	68.5	80
(62)	(TLM402)	Log mean temperature for fuel preheater (°C)	56	97.3
(63)	(A402)	Heat transfer area required to preheat fuel (sq ft)	0.54	1.22
(64)	(Q403)	Heat required to vaporize fuel (K Cal/hr)	105.3	87.5
(65,	(A403)	Heat transfer area required to vaporize fuel (sq ft)	0.525	0.777
(66)	(TLM404)	Log mean temperature for electrolyte cooling by air (°C)	92	128
(67)	(A404)	Heat transfer area required to cool electrolyte (sq ft)	1.31	3.89

4.8.9 Overall Heat and Mass Balance

(68) Water Balance

IN = OUT

(B121) + (B100) = (B332) + (B222) + (BL252)

3.0 + 11.32 = 0.434 + 8.34 + 5.546

14.32 = 14.32

(69) Fuel Balance

(F531) fuel feed gm mole/hr 1.522

(F531) = ((F131) - (F132)) + (F332)

1.522 = 1.26 + 0.262 = 1.522

(70) Heat Balance

IN

1.522 x 7.607 + (594 + 1080 + 130) x 2.03 + 47.25 x 2.03

+ 178 x 2.885 + 3.0 x 10.45 + 1024

= 11.58 + 3600 + 96.0 + 514 + 31.4 + 1024

= 5276.98

OUT

0.262 x 17.87 + 10.08 x 2.285 + 0.434 x 10.45

+ 31.50 x 2.095 + 178 x 2.10 + 8.34 x 10.45

$+ 5\ 546 \times 0.522 + 130 \times 2.45 + 1080 \times 2.245$

$+ 594 \times 2.90 + 79.3 + 27.0 + 11.55 + 45.1$

$= 4.58 + 23.05 + 4.54 + 66 + 374 +$

$87.10 + 2.885 + 320 + 2435 + 1720$

$+ 79.3 + 27.0 + 11.55 + 45.1$

$= 5200.20$

4.8.10 Parasitic Power (watts)

Eq. No.				Case 1	Case 2
(71)	(WPE4)	To pump electrolyte	0.1845	(0.1845)	0.233
(72)	(WPF4)	To pump fuel	0.002	(0.002)	.0005
(73)	(WPD4)	Pump air to cells	5.31	(5.31)	4.80
(74)	(WPD5)	Pump air to exhaust air condenser	-	(5.55)	-
(75)	(WPD6)	Pump air to fuel condenser	-	(10.1)	-
(76)	(WPD7)	Pump air to electrolyte cooler	-	(1.22)	-
(77)	(WRB)	Power aupplied by auxiliary battery (assuming 10% pumping efficiency)	55	(223.64)	50.33
(78)	(RB)	Power required to recharge auxiliary battery 8 hr operation	2	(7)	2
Total Parasitic Power			57	(231)	52

The main portion of parasitic power requirement is a result of forcing air through heat exchangers. If these heat exchangers are constructed to use free convection as a means of heat loss, it is possible to save considerable amount of power requirements.

(1) Fuel Condenser

Heat to be rejected = 244.05 K Cal/hr

Temperature of the surface will vary according to condensation of fuel. We assume the arithmetic mean average temperature based on inlet and exhaust conditions:

$$T_{ave} = \frac{288 + 85}{2} = 186.5°F$$

$\Delta T = 186.5 - 70 = 116.5°F$

Overall heat transfer coefficient = 0.9 Btu/hr sq ft °F

Surface area required

$$= \frac{Q}{U \times T} = \frac{244 \times 4}{0.8 \times 116.5}$$

$$= 10.48$$

$$\approx 10.5 \text{ sq ft}$$

Assuming we can build 50 sq ft of surface area per cu ft:

$$\text{Total volume} = \frac{10.5}{50} = 0.21 \text{ cu ft}$$

(LB3) Weight of fuel condensor = $4 \times 10^{-4} \times 10.5 \quad 168.5 = .718$ lb

(2) <u>Exhaust Air Condenser</u>

Heat to be rejected = 517.7 K Cal/hr

$$\Delta T = \frac{288 + 8.[illegible]}{2} - 70 = 116.5°F$$

$Q = U\ A\ T \qquad U = 0.8$ Btu/hr sq ft °F

$$A = \frac{517.7 \times 4}{0.8 \times 116.5} = 22.20 \text{ sq ft}$$

(LB2) (1) = $4 \times 10^{-4} \times 22.2 \times 168.5 = 1.5$ lb

(LB2) (2) = Reactant air preheater

Amount of heat exchange = 739.15 - 517.7

= 221.45 K Cal/hr

(TLM2) = 10.22°F

(A200) = $\frac{221.45 \times 4}{1.5 \times 10.22} = 57.6$ sq ft

$(LB2)_2$ = $U \times 10^{-4} \times 57.6 \times 168.5$

= 3.88

(LB2) = 1.5 + 3.88

= 5.38 lb

Therefore, volume of the

Exhaust Air Condenser = $\frac{21.18}{50} = 0.423$

Reaction Air Preheater = $\frac{57.6}{200} = 0.288$

(3) <u>Electrolyte Cooler</u>

$\Delta T = 295 - 70 = 225°F$

$U = 0.8$ Btu/hr sq ft °F

Heat to reject = Q = 54 K Cal/hr

$$(A404) = \frac{54 \times 4}{0.8 \times 225}$$

$$= 1.2 \text{ sq ft}$$

$$\text{Volume} = \frac{1.2}{50} = 0.024 \text{ cu ft}$$

(LB4) $= 4 \times 10^{-4} \times 1035\ (0.54 + 0.525 + 1.2)$

$= 0.94$ lb

The calculations show that about 169 watts of parasitic power can be saved by using free convection. The same argument holds true for the case of 180°C operating temperature.

Total parasitic power requirements

= 223.64 - 168.7

= 54.94 watts

≈ 55 watts

As some of the units are changed, total weight of the system will change.

(LBT) $= 1.1\ \big((LB1) + (LB\ \ \ (LB3) + (LB4) + (LB5) + (LB8)\big)$

$= 1.1\ (77.9 + 5.38 + 0.72 + 0.94 + 73.70 + 15)$

$= 191.7$ lb

	New Power Output		Case 1	Case 2
(88)	(WN)	Net power out (watt)	543	548
(89)	(NPOPW)	Net power out per unit weight of the system (watts/lb)	3.14	4.88
(90)	(η_{HHV})	Overall efficiency based on higher heating value of the fuel (%)	23.25	25.8

Table 4.8-1

Heat of Vaporization of n. parafins

Compound	At 25°C			At Normal Boiling Point		
	K Cal / gm mole	Cal / gm	Btu / lb	K Cal / gm mole	Cal / gm	Btu / lb
1 n-Pentane	6.316	87.54	157.15	6.16	85.38	153.6
2 n-Hexane	7.54	87.50	157.4	6.896	80.03	143.96
3 n-Heptane	8.735	87.18	156.82	7.575	75.[illegible]	136
4 n-Octane	9.915	86.80	156.14	8.36	73.19	131.65

Table 4.8-2

Specific Enthalpies for Normal Parafins

Temp, °C	n - octane Mole wt = 114 Enthalpy Liquid, K Cal / gm mole h_L	Vapor, K Cal / gm mole h_V	n - heptane 100.2 h_L	h_V	n - hexane 86.2 h_L	h_V	n - pentane 72.1 h_L	h_V
10.0	6.98	17.0	6.28	15.24	5.65	13.40	4.88	11.53
20	7.607	17.44	6.84	15.64	6.1	13.71	5.31	11.82
23.89	7.85	17.61	7.06	15.80	6.27	13.83	5.48	11.93
29	8.16	17.87	7.32	16.00	6.53	14.00	5.7	12.16
37.78	8.69	18.32	7.79	16.35	6.99	14.31	6.08	12.33
51.67	9.57	18.95	8.62	16.96	7.66	14.78	6.68	12.73
65.56		19.65		17.58		15.31		13.17
93.33		21.10		18.80		16.41		14.09
121.1		22.61		20.13		17.61		15.05
148.9		24.35		21.58		18.80		16.09
176.7		26.0		23.03		20.14		17.17
180		26.23		23.22		20.3		17.3
204.4		27.87		24.64		21.53		18.29

Table 4.8-3

Vapor Pressures and B. P. for Liquid Hydrocarbons

V. P., mm Hg	n-octane B. P., °C	n-heptane B. P., °C	n-hexane B. P., °C	n-pentane B. P., °C
10	19.2	-2.1	-25.0	-50.1
20	31.5	+9.49	-14.3	-40.2
30	39.28	16.84	-7.4	-33.93
40	45.13	22.35	-2.3	-29.22
50	49.85	26.81	+1.85	-25.41
60	53.84	30.57	5.36	-22.81
80	60.39	36.76	11.13	-16.89
100	65.70	41.77	15.81	-12.59
150	75.91	54.41	24.81	-4.33
200	83.63	58.69	31.61	1.92
250	89.90	64.62	37.15	7.01
300	95.24	69.66	41.85	11.34
400	104.05	77.99	49.63	18.49
500	111.24	84.79	55.99	24.34
600	117.37	90.58	61.40	29.32
700	122.73	95.65	66.15	33.68
760	125.67	98.43	88.74	36.074
800	127.53	100.18	70.38	37.59
1000	135.85	108.06	77.75	44.37
1200	142.96	114.79	84.05	50.17
1500	152.10	123.41	92.1	57.6

Table 4.8-4

Mole Fraction H_3PO_4 at Different Concentrations

H_3PO_4 % by weight	Mole Fraction H_3PO_4	Mole Fraction H_2O
93	0.71	0 29
94	0.743	0.257
95	0.777	0.223
96	0.815	0.185
97	0.856	0.144
98	0.90	0.10
99	0.948	0.052
100	1.00	0.0

Table 4.8-5

Specific Heat Content of Water
Enthalpy

Temp, °F	Temp, °C	Liquid, K Cal/gm mole	Heat of Vaporization, K Cal/gm mole	Vapor, K Cal/gm mole
68	20	0.360	10.54	10.90
78	25.6	0.460	10.48	10.94
84.2	29.0	0.522	10.45	10.972
88	31.1	0.560	10.43	10.99
98	36.7	0.659	10.37	11.029
110	43.3	0.779	10.31	11.089
120	48.9	0.879	10.25	11.129
140	60.0	1.078	10.14	11.218
160	71.1	1.278	10.02	11.298
180	82.2	1.479	9.898	11.377
200	93.3	1.679	9.777	11.456
220	104.4	1.880	9.651	11.531
240	115.6	2.083	9.520	11.603
260	126.7	2.285	9.384	11.669
302	150.0	2.715	9.081	11.796
338	170.0	3.091	8.795	11.886
356	180.0	3.279	8.652	11.931
374	190.0	3.475	8.487	11.962
400	204.4	3.750	8.255	12.005

Table 4.8-6

Heat Content of Different Chemical Species, Vapor Phase

Temperature		Heat Content, Cal/gm mole °K			
°C	°K	O_2	H_2	N_2	CO_2
-273	0	0	0	0	0
-23	250	6.93	6.78	6.95	-
20	293	6.94	-	6.95	7.5
25.16	298.16	6.94	6.790	6.95	7.51
27	300	6.942	6.790	6.95	7.52
29	302	6.943	6.791	6.95	7.529
50	323	6.951	6.799	6.952	7.628
100	373	6.971	6.819	6.957	7.867
127	400	6.98	6.83	6.960	7.99
150	423	7.0	6.83	6.960	8.07
180	453	7.0[illegible]	6.84	6.965	8.22
200	473	7.033	6.848	6.967	8.318
227	500	7.05	6.86	6.97	8.45
327	600	7.13	6.88	7.00	8.87
427	700	7.22	6.90	7.03	9.26

Security Classification

DOCUMENT CONTROL DATA - R&D

(Security classification of title, body of abstract and indexing annotation must be entered when the overall report is classified)

1. ORIGINATING ACTIVITY *(Corporate author)* General Electric Company, Direct Energy Conversion Operation, Lynn, Massachusetts	2a. REPORT SECURITY CLASSIFICATION Unclassified 2b. GROUP None

3. REPORT TITLE

Hydrocarbon - Air Fuel Cell

4. DESCRIPTIVE NOTES *(Type of report and inclusive dates)*

Semi-Annual Report No. 10 (1 July-31 December 1966)

5. AUTHOR(S) *(Last name, first name, initial)*

None

6. REPORT DATE 31 December 1966	7a. TOTAL NO. OF PAGES 235	7b. NO. OF REFS 35

8a. CONTRACT OR GRANT NO. DA44-009-AMC-479(T) b. PROJECT NO. c. d.	9a. ORIGINATOR'S REPORT NUMBER(S) SAR-10 9b. OTHER REPORT NO(S) *(Any other numbers that may be assigned this report)* None

10. AVAILABILITY/LIMITATION NOTICES

U[redacted]ies may obtain copies of this report [redacted]her [redacted] Fort Belvoir, Va., [redacted]

11. SUPPL[redacted]TARY NOTES	12. SPONSORING MILITARY ACTIVITY U.S. Army, Engineer Research and Development Laboratories, Fort Belvoir, Va.

13. ABSTRACT

Detailed information is presented on a continuing research and development program to develop a direct hydrocarbon oxidation-air fuel cell technology. Current work included research on electrocatalysts, multi-component fuels, and investigations with alternate acid electrolytes. An analysis of a direct hydrocarbon/air fuel cell system for liquid fuels is presented. The system represents a view of the upper limit in performance now attainable, based on data assembled under this and previous government contracts.

DD FORM 1 JAN 64 1473

Unclassified

Security Classification

14 KEY WORDS	LINK A ROLE	LINK A WT	LINK B ROLE	LINK B WT	LINK C ROLE	LINK C WT

INSTRUCTIONS

1. ORIGINATING ACTIVITY: Enter the name and address of the contractor, subcontractor, grantee, Department of Defense activity or other organization *(corporate author)* issuing the report.

2a. REPORT SECURITY CLASSIFICATION: Enter the overall security classification of the report. Indicate whether "Restricted Data" is included. Marking is to be in accordance with appropriate security regulations.

2b. GROUP: Automatic downgrading is specified in DoD Directive 5200.10 and Armed Forces Industrial Manual. Enter the group number. Also, when applicable, show that optional markings have been used for Group 3 and Group 4 as authorized.

3. REPORT TITLE: Enter the complete report title in all capital letters. Titles in all cases should be unclassified. If a meaningful title cannot be selected without classification, show title classification in all capitals in parenthesis immediately following the title.

4. DESCRIPTIVE NOTES: If appropriate, enter the type of report, e.g., interim, progress, summary, annual, or final. Give the inclusive dates when a specific reporting period is covered.

5. AUTHOR(S): Enter the name(s) of author(s) as shown on or in the report. Enter last name, first name, middle initial. If military, show rank and branch of service. The name of the principal author is an absolute minimum requirement.

6. REPORT DATE: Enter the date of the report as day, month, year; or month, year. If more than one date appears on the report, use date of publication.

7a. TOTAL NUMBER OF PAGES: The total page count should follow normal pagination procedures, i.e., enter the number of pages containing information.

7b. NUMBER OF REFERENCES: Enter the total number of references cited in the report.

8a. CONTRACT OR GRANT NUMBER: If appropriate, enter the applicable number of the contract or grant under which the report was written.

8b, 8c, & 8d. PROJECT NUMBER: Enter the appropriate military department identification, such as project number, subproject number, system numbers, task number, etc.

9a. ORIGINATOR'S REPORT NUMBER(S): Enter the official report number by which the document will be identified and controlled by the originating activity. This number must be unique to this report.

9b. OTHER REPORT NUMBER(S): If the report has been assigned any other report numbers *(either by the originator or by the sponsor)*, also enter this number(s).

10. AVAILABILITY/LIMITATION NOTICES: Enter any limitations on further dissemination of the report, other than those imposed by security classification, using standard statements such as:

(1) "Qualified requesters may obtain copies of this report from DDC."

(2) "Foreign announcement and dissemination of this report by DDC is not authorized."

(3) "U. S. Government agencies may obtain copies of this report directly from DDC. Other qualified DDC users shall request through _____."

(4) "U. S. military agencies may obtain copies of this report directly from DDC. Other qualified users shall request through _____."

(5) "All distribution of this report is controlled. Qualified DDC users shall request through _____."

If the report has been furnished to the Office of Technical Services, Department of Commerce, for sale to the public, indicate this fact and enter the price, if known.

11. SUPPLEMENTARY NOTES: Use for additional explanatory notes.

12. SPONSORING MILITARY ACTIVITY: Enter the name of the departmental project office or laboratory sponsoring *(paying for)* the research and development. Include address.

13. ABSTRACT: Enter an abstract giving a brief and factual summary of the document indicative of the report, even though it may also appear elsewhere in the body of the technical report. If additional space is required, a continuation sheet shall be attached.

It is highly desirable that the abstract of classified reports be unclassified. Each paragraph of the abstract shall end with an indication of the military security classification of the information in the paragraph, represented as *(TS)*, *(S)*, *(C)*, or *(U)*.

There is no limitation on the length of the abstract. However, the suggested length is from 150 to 225 words.

14. KEY WORDS: Key words are technically meaningful terms or short phrases that characterize a report and may be used as index entries for cataloging the report. Key words must be selected so that no security classification is required. Identifiers, such as equipment model designation, trade name, military project code name, geographic location, may be used as key words but will be followed by an indication of technical context. The assignment of links, roles, and weights is optional.